

1993

Solution-State Proton Nuclear Magnetic Resonance (NMR) Spectroscopic Studies of the Active Site of Myoglobins in Various Ligated States: Models for Macromolecule-Substrate Binding and Advancement of Paramagnetic NMR Techniques

Sidney Yee

Portland State University

Follow this and additional works at: https://pdxscholar.library.pdx.edu/open_access_etds

Let us know how access to this document benefits you.

Recommended Citation

Yee, Sidney, "Solution-State Proton Nuclear Magnetic Resonance (NMR) Spectroscopic Studies of the Active Site of Myoglobins in Various Ligated States: Models for Macromolecule-Substrate Binding and Advancement of Paramagnetic NMR Techniques" (1993). *Dissertations and Theses*. Paper 1253.

<https://doi.org/10.15760/etd.1252>

This Dissertation is brought to you for free and open access. It has been accepted for inclusion in Dissertations and Theses by an authorized administrator of PDXScholar. Please contact us if we can make this document more accessible: pdxscholar@pdx.edu.

**SOLUTION-STATE PROTON NUCLEAR MAGNETIC RESONANCE (NMR)
SPECTROSCOPIC STUDIES OF THE ACTIVE SITE OF MYOGLOBINS IN
VARIOUS LIGATED STATES: MODELS FOR MACROMOLECULE-SUBSTRATE
BINDING AND ADVANCEMENT OF PARAMAGNETIC NMR TECHNIQUES**

by

SIDNEY YEE

A dissertation submitted in partial fulfillment of the requirements for the degree of

**DOCTOR OF PHILOSOPHY
in
ENVIRONMENTAL SCIENCES AND RESOURCES:
CHEMISTRY**

**Portland State University
©1993**

TO THE OFFICE OF GRADUATE STUDIES:

The members of the Committee approve the dissertation of Sidney Yee
presented April 26, 1993.


David H. Peyton, Chair


Gordon L. Kilgour


Raymond P. Lutz


Robert L. Millette


David T. Clark


Pavel K. Smejtek

APPROVED:


Robert O. Tinnin, Acting Dean, College of Liberal Arts and Sciences


Roy W. Koch, Vice Provost for Graduate Studies and Research

AN ABSTRACT OF THE DISSERTATION OF Sidney Yee for the Doctor of
Philosophy in Environmental Sciences and Resources: Chemistry presented April 26,
1993.

Title: Solution-State Proton Nuclear Magnetic Resonance (NMR) Spectroscopic
Studies of the Active Site of Myoglobins in Various Ligated States: Models for
Macromolecule-Substrate Binding and Advancement of Paramagnetic NMR
Techniques.

APPROVED BY THE MEMBERS OF THE DISSERTATION COMMITTEE:


David H. Peyton, Chair


Gordon L. Kilgour


Raymond P. Lutz


Robert L. Millette


David T. Clark


Pavel K. Smejtek

This work focuses on pigmy sperm whale and horse myoglobins (Mbs),
which are distinguished by a single heme pocket residue variant in the CD3 position,

when the heme iron is in the +3 oxidation state (i.e. the met form). The strategy employed is as follows: (i) assign heme peripheral protons; (ii) assign the amino acid residues from the heme cavity; (iii) assess the dynamics of ligand binding in the active site by means of hydrogen lability, solvent isotope effects, and heme-insertion isomer trapping, all by ^1H NMR methods. The results of these studies portray a dynamic solution structure of the Mb ligand binding site, and provide a set of standard parameters for the studies of larger hemoproteins. The findings are also important for understanding protein-ligand interactions in general.

My research investigates the mixed spin metazido and metimidazole complexes of Mbs for the following reasons. First, the allosteric properties of hemoglobin arise mainly from the transition between its two possible quaternary structures. This can be studied by paramagnetic NMR because it is one of the most sensitive tools in terms of changes in the molecular and/or electronic structure of the heme. Second, both the N_3^- and imidazole (Im^-) complexes are good compromises, in terms of sizes, between the small diatomic oxygen or CN^- molecules and the bulky phenyl group. Thus, we can determine the influence of ligand size on structural perturbation of the heme crevice by comparison among the different size groups. Third, the saturation-transfer phenomenon between metMbIm and metMbH_2O provides a route to assignments in metMbH_2O by using assignments of metMbIm . This is crucial because metMbH_2O is the basis of theoretical calculations of the isotropic shift due to axial ligand field in pure high-spin hemoproteins. Finally, the importance of the metMbIm is underscored by the fact that it is a bis-imidazolium complex, which can then serve as a model other bis-histidyl proteins.

Most of the heme peripheral resonances of metEqMbIm and metEqMbN_3 were identified by means of two-dimensional NOESY, COSY, and EXSY spectroscopy. The strongly relaxed upfield protons in metMbIm were assigned based

on steady-state 1D NOE and T_1 experiments. Based on the results from metMbIm, in which saturation transfer of one upfield resonance led to two different free ligand peaks, bound Im equilibration was envisioned and proven by the divergence of broad downfield heme methyl peaks into two peaks each, showing distinctive population preference of each isomer. Dicyanoheme probe, as well as hydrogen lability comparison studies between pigmy sperm whale Mb and horse Mb in the azido and imidazole states, asserts that single variant pocket residue CD3 is crucial in gating the ligand mobility into and out of the active site.

The assignments of heme peripheral and upfield resonances enabled the subsequent assignments of some heme pocket amino acid residues. The facile exchange of bound Im with solvent H_2O lays the ground work for identification of heme pocket residues in metMb H_2O . Furthermore, while deuterated heme previously allowed only assignment of the non-diastereomeric specific heme 2-vinyl β proton, saturation-transfer from horse imidazole Mb affords the specific identification of $2H_{\beta t}$.

DEDICATION

**To my beloved father, Yee Oy Chong, and mother, Pang Chau, who are my
idols and inspirations.**

ACKNOWLEDGEMENTS

These past four years have given me some totally new perspectives on graduate school. It has definitely not been a ball. As reflected by the stark contrast to the four-year-old picture posted at the Chemistry office, my noticeable aging can attest to that. To survive graduate school training requires perseverance, determination, and tolerance to work with the same faces more than eight hours a day without bloodshed. I had little of those abilities four years ago, but have since acquired some with the help of a few very notable individuals. I cannot express enough gratitude for my mentor, Dr. David H. Peyton. He is a dear friend, a big brother, and an understanding adviser. I have made countless academic mistakes, but having worked for Dr. Peyton was one of the most intellectual choice I have ever made. No word can do justice to Dr. Peyton's incredible kindness. I am indebted to my parents, my sister Jenny, my grandmother, and my two brothers for their constant encouragement, endless confidence in me, and unconditional love. They provided the initial spark that ignited my quest for higher education, and stayed with me throughout the process. The love of my family carried me through the sometimes unbearably inevitable facts of life. My dearest friend, Derek C.S. Ho, has been most supportive and respectful of my every decision. He keeps me from going insane. I am also grateful for having the opportunity and for all the fun and joy of working with Ruba S. Deeb, Elisar (Elsie) J. Barbar, and Dietmar Leitner. I would like to thank Dr. Gordon L. Kilgour, Dr. David T. Clark, Dr. Robert L. Millette, Dr. Raymond, P. Lutz, and Dr. Pavel K. Smejtek for serving on my committee, and critically reviewing my dissertation. I am especially grateful to Dr. Kilgour for having always been there to listen (and to tell stories). The completion of

the doctorate program was not a child's play, and the help of many other friends was pertinent. Among those are my colleagues Hong Mu-Moulton, Esther E. Luo, Clary B. Clish, and friends Michelle M. Hay, Ching L. Hay, Andy C.P. Wong, Yen L. Lau, and Ruben Torres. This achievement is only the beginning of a new chapter of my life. As Dr. Peyton once said, " A doctorate degree is the passport, hopefully allowing you to go places." I will go somewhere with this degree -- my way of paying tribute to all those who believed in me.

TABLE OF CONTENTS

	PAGE
ACKNOWLEDGEMENTS.....	iii
LIST OF TABLES	viii
LIST OF FIGURES	x
ABBREVIATIONS AND DEFINITIONS.....	xviii
CHAPTER	
I INTRODUCTION.....	1
General	1
Significance To Environmental Sciences and Resources	3
Background.....	7
II MATERIALS AND METHODS.....	17
Sample Preparation.....	17
General NMR Experiments	20
Acknowledgements	24
III ASSIGNMENTS OF HEME PERIPHERAL RESONANCES IN AZIDO AND IMIDAZOLE MYOGLOBINS BY MULTI-DIMENSIONAL PROTON NUCLEAR MAGNETIC RESONANCE	25
Results.....	27
Discussion.....	34

IV	PROTON NUCLEAR MAGNETIC ASSIGNMENTS OF PROTONS FROM Fe-COORDINATED LIGANDS FOR VARIOUS IMIDAZOLATE MYOGLOBINS	54
	Results and Discussion	55
	Conclusions	69
V	PROTON NMR INVESTIGATION OF THE RECONSTITUTION OF EQUINE MYOGLOBIN WITH HEMIN DICYANIDE	103
	Results	104
	Discussion	105
	Conclusions	107
VI	STUDY OF HEME BINDING TO THE PROTEIN MATRIX BY ¹ H NMR AND OPTICAL ABSORPTION SPECSTROSCOPY	113
	Methods	115
	Results and Discussion	117
	Conclusions	122
VII	LABILITIES OF THE EXCHANGEABLE PROTONS OF IMIDAZOLE AND AZIDO MYOGLOBINS	133
	General	133
	Results and Discussion	137
VIII	ASSIGNMENTS OF THE HEME POCKET RESIDUES IN IMIDAZOLE HORSE HEART MYOGLOBIN	172
	Results and Discussion	173
IX	CONCLUSIONS	183

REFERENCES	187	vii
------------------	-----	-----

APPENDICES

A	CHEMICAL MODIFICATIONS OF PIGMY SPERM WHALE MYOGLOBIN	193
B	PRELIMINARY STUDIES ON THE MYOGLOBIN AND HEMOGLOBIN OF <i>BIOMPHALARIA GLABRATA</i>	200

LIST OF TABLES

TABLE	PAGE
I Iron complexes at different oxidation states with various sixth ligands.....	9
II Chemical shifts for minor-insertion isomer of metEqMbN ₃ at 25°C and pH 7.0.....	30
III Chemical shifts for metEqMbIm at at 50°C and pH 6.2.....	31
IV Assignments of heme peripherals for metEqMb1CH ₃ Im at 25°C, otherwise parenthesized, and pH 7.....	32
V Assignments of heme peripherals for metEqMb4CH ₃ Im at 323 K and pH 7	33
VI T ₁ s for 5CH ₃ s and 1CH ₃ s of the indicated myoglobin species in N ₃ and Im ligated states at 25°C; included is also the literature T ₁ s for metSwMbCN.....	35
VII Upfield resonance assignments for imidazolate bound to pigmy sperm whale and horse heart myoglobins.....	70
VIII Heme reorientational rates, k _f , at pH 6.7 and 25°C in 1:1 concentration ratio of heme to apoEqMb.....	118

IX	Rate constants of reorientational of EqMb reconstituted from 5:1 apo to heme concentration by optical spectroscopy with column chromatography at pH 8.38-8.50 and various temperatures	121
X	Activation free energies for heme reorientational disorder in EqMb and heme insertion in human Mb.....	121
XI.	Assignments of the exchangeable protons for metEqMbN ₃ . at 298 K	137
XII	Saturation factors for G1 (ring NH of His FG3) at the slowest- exchanged pH for various Mbs in different ligated states	142
XIII	Assignments for some heme pocket residues in metEqMbIm. and metEqMbH ₂ O, as indicated at pH 6.8-7.0, 308 K. The numbers after the residues indicate the corresponding positions on the helix of protein.....	177
XIV	Amino acid analysis of band III (Figure 91) as compared to that of native PSwMb.....	198

LIST OF FIGURES

FIGURE	PAGE
1. Proposed mechanism for the formation of the altered heme products, hemes <u>1</u> , <u>2</u> , <u>3</u> , and <u>4</u> , a His F8 (93) bound adduct (Osawa et al., 1991).	13
2. A. Redox cycle of MbO ₂ in myocytes (Galaris et al., 1989).....	14
3. ¹ H NMR spectrum of the nearly 1:1 mixture of heme-insertion isomers formed by reconstitution, then quenched with CN ⁻	15
4. Arrangement of proximal and distal residues in myoglobin, showing the hydrogen bond between the distal His and the bound sixth ligand - oxygen (Phillips, 1978).....	16
5. COSY/NOESY in a nut shell.....	42
6. The numberings and labels of peaks correspond directly to all the NMR spectra hereafter	43
7. Phase-sensitive NOESY (left) and magnitude COSY (right) for native metEqMbN ₃ in ² H ₂ O at 25°C and pH7.0.....	44
8. Phase-sensitive NOESY (left) and magnitude COSY (right) for reconstituted metEqMbN ₃ in ² H ₂ O at 25°C and pH7.0.....	45
9. Phase-sensitive NOESY (left) and magnitude COSY (right) for metEqMbIm in ² H ₂ O at 35°C and pH 7.....	46
10. Phase-sensitive NOESY (left) and magnitude COSY (right) for metEqMb1CH ₃ Im in ² H ₂ O at 25°C and pH 7.....	47

11.	400-MHz ^1H NMR 1-D difference spectra of metEqMbH ₂ O : metEqMbIm at 308K and pH 6.2.....	48
12.	Phase-sensitive NOESY for 1:1 metEqMbH ₂ O:Im at 50°C and pH 6.2.....	49
13.	Phase-sensitive NOESY for 1:1 metEqMbH ₂ O:1CH ₃ Im at 50°C and pH 6.75.....	50
14.	Phase-sensitive NOESY for 1:1 metEqMbH ₂ O:4CH ₃ Im at 50°C and pH 6.2..	51
15.	T ₁ plot (ln{int(infinity)-int(t)} vs time in ms) of some resonances, as indicated, of metEqMbX, where X is indicated in the parentheses on the plot.....	52
16.	Energy level diagram for saturation-transfer	53
17.	Comparison of upfield regions in metEqMbIm (left), and metPSwMbIm (right) at pH 6.9.....	72
18.	400MHz ^1H NMR 1D NOE of metEqMbIm at 298K, and pH 8.2.....	73
19.	Schematics showing A. the pseudo C ₂ axis of bound imidazole, B, C, the geometries and labelings of free and bound Im, 1-CH ₃ Im and 4-CH ₃ Im, respectively.....	74
20.	Free Im which has been incubated in $^2\text{H}_2\text{O}$ at 25°C and pH 10; spectra were taken at different time periods, shown correspondingly	75
21.	Free 4CH ₃ Im which has been incubated in $^2\text{H}_2\text{O}$ at 65°C; spectra were taken at different time periods, shown correspondingly	76
22.	Free 1CH ₃ Im which has been incubated in $^2\text{H}_2\text{O}$ at 65°C; spectra were taken at different time periods, shown correspondingly	77
23.	MetEqMbIm at 298K and pH 8.0.....	78

24.	MetEqMbIm reconstituted with deuterated Im at 298K and pH 8.0.....	79
25.	1D NOE of metEqMbIm, reconstituted with deuterated Im at the C ₂ H position at pH 7 and 298K.....	80
26.	400MHz ¹ H NMR 1D NOE of metPSwMbIm at pH 6.9 and 313K.....	81
27.	400MHz ¹ H NMR 1D NOE of metPSwMbIm at pH 6.9 and 303K.....	82
28.	400MHz ¹ H NMR 1D NOE of metPSwMbIm at pH 9.05 and 303 K.....	83
29.	MetPSwMbIm at 303K and pH 6.9, after Im has been deuterated	84
30.	MetPSwMbIm at 313K and pH 6.9, after Im has been deuterated	85
31.	400MHz ¹ H NMR 1D NOE of metPSwMb1CH ₃ Im at pH 8.0 and 313K.....	86
32.	400MHz ¹ H NMR 1D WEFTNOE of metPSwMb1CH ₃ Im (1CH ₃ Im has been deuterated) at pH8.0 and 313K.....	87
33.	pH dependence of the methyl linewidths in metPSwMb4CH ₃ Im at 298K and various pHs of A. 6.5, B. 7.5, C. 9.0.....	88
34.	MetPSwMb1CH ₃ Im at 313K and pH 8.0, after 1CH ₃ Im has been deuterated..	89
35.	metPSwMb4CH ₃ Im (4CH ₃ Im has not been deuterated) at 313K and pH 7.1....	90
36.	metPSwMb4CH ₃ Im (4CH ₃ Im has not been deuterated) at 313K and pH 7.1....	91
37.	MetPSwMb4CH ₃ Im at 313K and pH 7.11, after 4CH ₃ Im has been deuterated	92
38.	Comparison of the downfield regions among the imidazolate PSwMbs at 298K.....	93
39.	1D NOE hit of the methyl peak, j, of metEqMb1CH ₃ Im at 298K and pH 8.....	94
40.	1D NOE hit of the methyl peak, k, of metPSwMb4CH ₃ Im at 313K and pH 7.1.....	95

41.	Imidazole titration of EqMb and PSwMb at 298K in 10% $^2\text{H}_2\text{O}$ (A and B), and 100% $^2\text{H}_2\text{O}$ (C) at pH 7.0.....	96
42.	Comparison of pH dependence between metEqMbIm and metPSwMbIm at 298K and pHs 9 (top) and 7 (bottom).....	97
43.	^1H NMR spectra of MetPSwMbIm at pH 6.9, A. 298K, and B. 278 K.....	98
44.	^1H NMR spectra of metPSwMbIm in $^2\text{H}_2\text{O}$, at pH 9.05 and A. 298 K, B. 278 K.....	99
45.	^1H NMR spectra of metEqMbIm in $^2\text{H}_2\text{O}$, at pH 9.17 and A. 298 K, and B. 278 K.....	100
46.	Comparison of the proposed energy diagrams for equilibration of bound Im in metPSwMbIm (solid line) and metEqMbIm (dashed line).....	101
47.	A. ^1H NMR comparison of EqMb4CH ₃ Im (left) and PSwMb4CH ₃ Im (right) at 313K (top) and 298K (bottom) pH 9.....	102
48.	Products of reconstitution reactions at pH 9.2 and 25°C in $^2\text{H}_2\text{O}$	108
49.	Products of reconstitution reactions for metPSwMbCN at pH 9.2 and 25°C in $^2\text{H}_2\text{O}$	109
50.	^1H NMR of the product of reconstitution of apoSwMb with heme(CN) ₂ , at pH 9 and 25°C.....	110
51.	^1H NMR of the products of reconstitution reactions at pH 7.0 and 25°C in $^2\text{H}_2\text{O}$: A. Product of heme(CN) ₂ + apoEqMb; B.....	111
52.	Kinetics for the formation of metEqMbCN from heme(CN) ₂ and apoEqMb at pH 9.2 and 25°C, acquired within 0.5 hour after reconstitution.....	112

53. **TOP.** The top-down view of the major, and minor insertion-
isomers on the right and left, respectively.....124
54. Low field portion of 400-MHz ^1H NMR spectrum of the reaction
product immediately after the reconstitution of
1 equivalence each of apoEqMb and heme at pH 6.72
and 25°C, with the use of column chromatography.....125
55. UV-VIS spectrum of the Soret region of the reconstituted EqMb at
pH 6.71 and 26.5°C.....126
56. Low field portion of the 400-MHz ^1H NMR spectra of the reconstitution of
1 equivalence each of apoEqMb and heme at pH 6.72
in $^2\text{H}_2\text{O}$ with the use of chromatography; the elapsed times
are indicated on the right.....127
57. Low field portion of the 400-MHz ^1H NMR spectra of the reconstitution of
1 equivalence each of apoEqMb and heme at pH 6.72
in $^2\text{H}_2\text{O}$ without the use of chromatography; the elapsed times
are indicated on the right.....128
58. Optical spectroscopy difference spectra of the reconstitution of
1 equivalence each of apoEqMb and heme at pH 6.72
in $^2\text{H}_2\text{O}$ with the use of chromatography; the elapsed times
are indicated on the right.....129
59. Plots of $\ln(A_e - A_t)$ vs. time for the equilibration of metEqMbH₂O..... 130
60. Arrhenius plot for heme redistribution process.....131

61.	Free energy diagram of the reversible, completely dissociative pathway for the reorientation of metEqMbH ₂ O based on the mechanism by Gibson and Antonini (1960).....	132
62.	Proposed H-bonding between an A. iron-bound H ₂ O and His E7 at acidic pH, where a neutral H ₂ O acts as a H-donor to the imidazole.....	148
63.	Presented here is one of the possible protonation scheme; other schemes have also been proposed.....	149
64.	Selective excitation (p11 or jump-return) saturation-transfer spectra of metEqMbN ₃ in 10% ² H ₂ O at 25°C and pH 7.4.....	150
65.	Selective excitation (p11 or jump-return) saturation-transfer spectra of P2 of metEqMbN ₃ in 10% ² H ₂ O at 25°C and pH 7.3.....	151
66.	Selective excitation (p11 or jump-return) saturation-transfer spectra of metEqMbN ₃ in 10% ² H ₂ O at 25°C and pH 8.....	152
67.	Selective excitation (p11 or jump-return) saturation-transfer spectra of metEqMbN ₃ in 10% ² H ₂ O at 25°C and pH 9.....	153
68.	pH profiles metEqMbN ₃ at 298 K.....	154
69.	Selective excitation (p11 or jump-return) saturation-transfer spectra of saturating G1 of metEqMbN ₃ at pH 9.02 and 298 K in 10% ² H ₂ O.....	155
70.	Selective excitation (p11 or jump-return) saturation-transfer spectra of saturating G2 of metEqMbN ₃ at pH 9.02 and 298 K in 10% ² H ₂ O.....	156
71.	Magic angle rotation diagram.	157

72.	Selective excitation (p11 or jump-return) saturation-transfer spectra of metEqMbIm at pH 9.02 and 298 K.....	158
73.	pH profiles of metEqMbIm at 298 K.....	159
74.	Selective excitation with jump-return saturation of G1 of metEqMb4CH3Im at pH 9 and 298 K in 10% $^2\text{H}_2\text{O}$	160
75.	Comparison of pH titration with the NOE from saturation the C β H of His F8 of metMb4CH3Im.....	161
76.	pH titration of metEqMb1CH3Im at pH 9.32 and 298 K.....	162
77.	pH titration of metEqMb4CH3Im at pH 8.30 and 298 K.....	163
78.	A, B. pH profiles of metPSwMbN $_3$, and metPSwMbIm, respectively at 298 K.....	164
79.	Movement involved in modulating ligand entry into the heme pocket	165
80.	Comparison among the methyl linewidths of metEqMbN $_3$ at 298 K and pH 9 in different ratios of $^2\text{H}_2\text{O}$: $^1\text{H}_2\text{O}$	166
81.	Comparison among the methyl linewidths of metEqMbN $_3$ at 298 K and pH 6.2 in different ratios $^2\text{H}_2\text{O}$: $^1\text{H}_2\text{O}$	167
82.	Comparison among the methyl linewidths of metEqMbN $_3$ at 298 K and different pHs in 1:1 ratio $^2\text{H}_2\text{O}$: $^1\text{H}_2\text{O}$	168
83.	Comparison of metEqMbIm in different ratios of $^2\text{H}_2\text{O}$: $^1\text{H}_2\text{O}$ at pH 9.12.....	169
84.	Comparison of metEqMb1CH3Im in different ratios of $^2\text{H}_2\text{O}$: $^1\text{H}_2\text{O}$ at pH 7.....	170

85.	Comparison of metPSwMbIm in different ratios of $^2\text{H}_2\text{O}:$ $^1\text{H}_2\text{O}$ at pH 9 and 298K	171
86.	Schematic representation of the spatial disposition of amino acid side chains in the heme pocket of SwMb, from its X-ray coordinates in CO form (Kuriyan et al., 1986).....	178
87.	400-MHz 2D ^1H phase-sensitive NOESY spectrum of metEqMbIm in $^2\text{H}_2\text{O}$ at pH 7.0, 308 K.....	179
88.	C. 400-MHz 2D ^1H magnitude COSY spectrum of metEqMbIm at pH 7.0 and 308 K.	180
89.	1D NOE saturation of $\text{C}_\gamma\text{H}_3$ Val E11 (marked by arrows) in metEqMbH $_2\text{O}$ at pH 6.8 and 323 K.....	181
90.	400-MHz 2D ^1H NMR phase-sensitive EXSY spectrum of metEqMbH $_2\text{O}$:Im at pH 6.8 and 308 K, compared with NOESY spectrum of metEqMbIm in Figure 87.....	182
91.	DEAE-Cellulose anion exchange chromatogram, expanded at 0.1 absorbance scale, of Arg-modified apoPSwMb, detected at 254 nm and 298 K on ISCO monitor, with pump speed set at 18.....	199
92.	^1H NMR spectral comparison of metBgMbN $_3$ at pH 7.5 (A) with metEqMbN $_3$ (B) at pH 7.0 and 298 K.....	206
93.	^1H NMR spectral comparison of metEqMbCN at pH 9 (A) with metBgMbCN (B) at 298 K and pH 8.1	207
94.	^1H NMR of metBgHb in various ligated states and temperatures at pH 11.20, as indicated on respective traces.....	208

ABBREVIATIONS AND DEFINITIONS

apo:	protein without the prosthetic group, heme in this document
Arg:	arginine
Asp:	aspartate
CAMb:	Canine myoglobin
CN ⁻ :	cyanide
CO:	carbonmonoxy
COSY:	COrrrelation SpectroscopY
DQF:	double-quantum-filtered
EqMb:	Horse myoglobin
EXSY:	EXchange SpectroscopY
H ₂ O:	aquo
Hb:	hemoglobin
His:	histidine
Ile:	isoleucine
Im ⁻ :	imidazole
Lys:	lysine
Mb:	myoglobin
metMb:	myoglobin in iron(III) state
N ₃ ⁻ :	azide
NOE:	Nuclear Overhauser Effect
NOESY:	Nuclear Overhauser Effect SpectroscopY
O ₂ :	oxy

Phe:	phenylalanine
PSwMb:	Pigmy Sperm whale myoglobin
SwMb:	Sperm whale myoglobin
T₁:	spin-lattice relaxation time
T₂:	spin-spin relaxation time
TOCSY:	T_Otal C_Orrelated S_Pectroscop_Y
TPPI:	t_ime-p_roportional p_hase i_ncrementing
Val:	valine

CHAPTER I

INTRODUCTION

GENERAL

Vertebrate hemoglobin (Hb) is a tetrameric protein that transports oxygen from the lungs, gills, or skin of an animal to the blood for respiration. It is an allosteric protein that is made up of four myoglobin-like subunits of ~17 kDa each. Each subunit, as well as myoglobin (Mb), is noncovalently bound to a heme group. The iron atom of the heme group normally remains in the Fe(II) oxidation state to function as oxygen carrier. The interaction of globin and ferrous heme is crucial because free ferrous hemes are readily oxidized by oxygen to the Fe(III) state; globin keeps iron in the ferrous state which is necessary for reversible binding of oxygen. Despite the enormous amount of effort made to understand the structure and function of Hb, many of the heme-globin interactions are still not well understood because of both its size and cooperative intersubunit interactions.

Myoglobin is the classical model for Hb. Made up of eight right-handed α -helical segments interrupted by bends, Mb is an oxygen-binding protein found in muscle cells. The helices are identified alphabetically from the N-terminus. Mb serves to store oxygen and to enhance oxygen transport to the mitochondria during oxidation of cell nutrients. Because it is monomeric and non-allosteric, Mb is more easily studied by nuclear magnetic resonance (NMR) than is Hb. The relatively small size of Mb exhibits less complex NMR spectra, thus increasing spectral resolution. Even though the protein sequences of vertebrate Mb and HbA (human adult Hb) are not strictly homologous (for instance, the sequence similarity between human Mb and α -subunit of HbA is only 25%, Dayhoff,

1972), their ligand binding sites are largely conserved. Therefore, the study of ligand binding to Mb would facilitate better understanding of heme-globin interactions in HbA. A less well-known role of Mb is the involvement of its oxidized form in a redox cycle in the presence of a reducing agent, acting as a peroxidase. This is of great chemical and clinical interest because of the implication of an altered protein structure (Osawa & Korzekwa, 1991), and the potential for improvement in reperfusion following ischemia (hypoxia) and myocardial surgery (see below).

This work also serves to provide experimental results to verify and aid in theoretical calculations of magnetic axes in paramagnetic systems. When the first detailed X-ray crystal structures of Mb were reported in the early 1960's (Kendrew et al., 1960; Stryer et al., 1964; Perutz & Matthews, 1966), the structures showed a protein matrix too compact to allow any ligand traffic. Yet, Mb not only binds small diatomic molecules like O₂ and CO, but also ligands as large as imidazole and phenyl. Therefore, there must exist a passageway (perhaps more than one) which involves transient movements of amino acids that lie around the binding pocket. More recently, Mb has been the subject of numerous experimental and theoretical molecular dynamics simulation studies (Kuriyan et al., 1986; Case & Karplus; 1979, Kottalam & Case, 1988).

Solution state ¹H NMR studies of Mbs in various ligated states such as MbCO (Dalvitt & Wright, 1987; Mabbutt & Wright, 1985) and metMbCN (Emerson & La Mar, 1990) have also proven invaluable in providing basis sets for NMR spectroscopy to advance to solution structure elucidations of larger and more complex proteins like cytochrome c peroxidase (Satterlee et al. 1991; Satterlee & Erman, 1991), horseradish peroxidase (Thanabal et al., 1987a, b; 1988), and chloroperoxidase (Dugad et al., 1992). These three enzymes are hemoproteins that range between 34 to 42 kDa in sizes, and are responsible for critical oxidation/reduction reactions. Studies by NMR of paramagnetic

Mbs are relevant to these proteins, because their active sites consist of paramagnetic iron-porphyrin,

This dissertation investigates horse heart Mb (EqMb) and pigmy sperm whale Mb (PSwMb) in different ligated states; sperm whale Mb (SwMb) and dog Mb (CAMb) were also occasionally used for comparison. The focus is on paramagnetic forms of Mb, when its iron atom has at least one unpaired electron. In this form, the proximity of the electrons and nuclei yields hyperfine-shifting interactions that allows resolution of the resonances from protons at the active site. Therefore, the conformations and dynamics of the residues at the binding site can be investigated without regard for the spectral crowding by the nuclei from the main body of globin. The strategy employed is as follows: (i) assign heme peripheral protons; (ii) assign the amino acid residues from the heme cavity; (iii) assess the dynamics of ligand binding in the active site by means of hydrogen lability, solvent isotope effects, and heme-insertion isomer trapping, all by ^1H NMR methods. The results portray a dynamic solution structure of the Mb ligand binding site, and provide a set of standard parameters for studies of Hb. They also provide lessons for protein-ligand interactions in general. While X-ray crystallography offers a global picture of the species in its crystalline form, NMR affords a dynamic view in solution state, as is more relevant to living systems.

SIGNIFICANCE TO ENVIRONMENTAL SCIENCES AND RESOURCES

In addition to the above biophysiological motivations, these studies of Mb contribute significantly to environmental issues. There are numerous species that live in oxygen (O_2) deprived and/or atmospherically contaminated environments (deep-diving Sperm Whale, and humans in polluted metropolitan areas being among the most prominent examples). In order to understand how these species are able to sustain life under such conditions, one has to investigate the mechanism of O_2 -binding in Hb (Han et al. 1988, Jue

et al. 1984, Han & La Mar, 1986), and Mb (Antonini & Brunori, 1971). Also, mechanics of ligand binding, and even the binding of heme to the protein globin matrix can be viewed as a model for metal-poisoning in the blood stream because even free heme in the blood is toxic by promoting the formation of hydroxyl free radicals which in turn consume lipids (Morgan & Muller-Eberhard, 1976 and references therein). This may help formulate mechanisms for detoxification.

Direct interactions of environmentally hazardous organic molecules like CCl_4 , BrCCl_3 , enflurane ($\text{CHF}_2\text{OCF}_2\text{CHClF}$, a common inhalant anaesthetic), and CHCl_3 have also been shown to adversely affect the functions of hemoproteins both *in vitro* and *in vivo* (Osawa et al., 1992; Rice et al., 1983; Prasad et al., 1989). For example, enflurane is oxidatively metabolized by cytochrome P-450 to form inorganic fluoride, which is responsible for its nephrotoxicity (Burke et al., 1980). The hepatotoxicity of CCl_4 and BrCCl_3 is traced to its formation of $\cdot\text{CCl}_3$ radical, which inactivates Cyt P-450 in the liver (Levin et al., 1972). Similar reactions with MbO_2 have been found, in which altered hemes, as well as cross-linked protein adducts were formed (Osawa et al., 1989, 1990). Figure 1 illustrates a proposed mechanism for the formation of the altered heme and protein adducts from the reaction of BrCCl_3 with MbO_2 (Osawa & Korzekwa, 1991). The cross-linked Mb is found to be redox active, in which it reduces O_2 rapidly to form superoxide anion $\text{O}_2^{\cdot-}$ (or hydrogen peroxide from rapid dismutation), which in turn enhances the autoxidation of this altered Mb to form more superoxide anions, as well as other radicals like $\cdot\text{CCl}_3$. Superoxide anion, and the subsequent formation of hydroxyl radicals, are notorious for their damaging power to membranes and cellular proteins, which lead to chronic pathological conditions including cancer, cardiovascular diseases, aging, and myocardium injury during reperfusion. Studies (Metzler & McLachlan, 1978; Rogan et al., 1979) also showed that the peroxidase function of hemoproteins is capable of catalyzing the covalent linkage of organic molecules to nucleic acids, suggesting possibilities of cellular

genetic damage from the interactions of hemoproteins and organic molecules.

Understanding the structures of these altered adducts is important in formulating remedies to radical destructions. However, only the structure of the $\cdot\text{CCl}_3$ -modified Mb has been elucidated fully at its active site by ^{13}C and ^1H NMR (Osawa et al., 1991). Therefore, studies aimed at structural perturbation of the binding site of Mb by various ligands are highly relevant as model systems. This has become especially important in light of the implication by computer simulation that such cross-linked Mb undergoes a 'histidine-shuffle' (Osawa et al., 1991), in which the heme Fe^{2+} becomes axially bis-histidyl coordinated to His FG3 and His E7. Involvement of exogenous imidazole in such a bis-histidyl complex might allow NMR study of this altered Mb in its paramagnetic Fe^{3+} form. This is highly analogous to the metMbIm system under study in this research, and it has the advantages of spectral resolution inherent in paramagnetic hemoproteins.

Involvement of the oxidative modification of Mb in Fe^{3+} (i.e. metMb) states by H_2O_2 has also been documented (Osawa & Korzekwa, 1991; Galaris et al., 1989a) that suggested the possibility of metMb as a H_2O_2 scavenger in the prevention and treatment of myocardial infarction. Figure 2A shows the redox cycle of Mb. Normally, only traces of deoxyMb $^{2+}$ are present in myocytes when supply of O_2 is abundant. This is an evolutionary defense mechanism that prevents the facile oxidation of deoxyMb $^{2+}$ by oxidants that are continuously generated by various cellular metabolisms. However, in the case of ischemia, the accumulation of deoxyMb $^{2+}$ leads to a cascade of damages, which is extremely relevant during reoxygenation that accompanies reperfusion. The oxidized Mb $^{4+}$, which is readily formed from the interactions of deoxyMb $^{2+}$ and metMb with H_2O_2 , can be easily reduced by a one-electron donor such as ascorbate (Galaris et al., 1989b), while metMb reduction to the physiologically functional MbO $_2$ is slower. The slow reduction of metMb potentiates its reaction with H_2O_2 , in which metMb is modified to a protein-bound heme adduct that catalyzes the reduction of O_2 to H_2O_2 by NADH (as

depicted in Figure 2B; Osawa & Korzekwa, 1991). Because the exact nature of this cross-linked protein is unknown, the mechanism of its oxidation, as well as the following degradative activities are still speculative. Presumably, the protein-bound heme adduct, when reduced to the ferrous deoxy complex, is oxidized by the molecular O_2 (Osawa & Pohl, 1989). This is unlike the native ferrous deoxy Mb, which forms a stable, reversible ferrous- O_2 complex upon introduction of molecular O_2 . Studying the structure of the active site of this modified Mb will not only facilitate better estimation of its toxicity, but more importantly, it will clarify its potential as a H_2O_2 scavenger, in which the modification scheme (Figure 2B) stops at the Mb^{4+} state which can be readily reduced. The studies of autoxidation of MbO_2 (Tajima & Shikama, 1987; Satoh & Shikama, 1981; Shikama, 1984) have also implied a role for metMb in eliminating the production of H_2O_2 , formed by dismutation from $O_2^{\cdot -}$ that is produced from nucleophilic displacement of MbO_2 by H_2O or OH^- .

Another ligated metMb, metMbphenyl, is also an important system to study because phenylhydrazine inactivates hemoglobin *in vivo* and triggers its precipitation in the form of Heinz bodies (French et al., 1978; Goldberg et al., 1976). Mb reacts similarly with phenylhydrazine to form metMbphenyl, although without precipitation (Augusto et al., 1982). Dynamics and orientation of the binding of phenylhydrazine to Mb hence lend direct support to understanding metal or organic poisoning of blood stream.

In my research, ligands other than O_2 are used for these purposes because Mb in the ferric form, which is investigated more extensively, does not bind O_2 , and MbO_2 is not paramagnetic. In this regard, there is a protein, hemopexin (Hx), which appears to be responsible for clearing free heme from the blood and shutting down its ability to catalyze many unwanted oxidation reactions (Wochner et al., 1974; Muller-Eberhard & Nikkila, 1989). Hx is a glycoprotein of ~60 kDa, whose complex glycosylation pattern and large molecular weight have deterred its characterization by X-ray crystallography. So far, it is

known that the binding site of Hx consists of two axial His residues coordinated to the heme iron (Nikkila et al., 1991; Morgan & Muller-Eberhard, 1976; Morgan et al., 1988). Imidazole-bound Mb is therefore a model for the heme-hemopexin system, and much effort was spent in this research to determine the dynamics and geometry of its binding site.

BACKGROUND

Application of Paramagnetism to NMR

Since the 1950's, the investigation of paramagnetic species by NMR has proven to be a powerful research tool in the field of biological sciences. In spite of the insufficiently rigorous theoretical treatment of the physical principles, the paramagnetic phenomenon provides invaluable utility as a structural probe. Paramagnetic probes are useful in these studies because of large induced shifts and short relaxation times of nearby nuclei. The paramagnetic shift arises from either direct (Fermi contact) or indirect (pseudocontact) couplings between nuclear magnetic moments and unpaired electrons (La Mar, 1973; Satterlee, 1990a, b). These interactions can result in the hyperfine shifting of resonances from the crowded diamagnetic envelope of resonances. This is particularly helpful for studying biological macromolecules such as Mb and Hb because the active site contains a potential paramagnetic center Fe; the hyperfine shift provides resolved resonances for nuclei in the vicinity of the active site. Paramagnetic line broadening is another result of direct interaction between an electron and a nucleus of interest. This line-broadening is a function of the spin-lattice and spin-spin relaxation times, T_1 and T_2 , respectively, which can be immensely shortened by the effective relaxation mechanism of nearby unpaired electron. The shortened spin-lattice relaxation time, T_1 , allows fast signal-averaging during NMR experiments, hence enhances signal-to-noise ratios.

Historical Information about Proton NMR Studies of Mb

While X-ray studies of SwMb show a single orientation for the heme within the holoprotein (Takano, 1977), ^1H NMR in solution reveals that freshly reconstituted Mb yields a 1:1 mixture of two heme-insertion isomers that are readily distinguishable by NMR (Jue et al., 1983) as shown in Figure 3. Peyton and coworkers (Gebe et al., 1989) were also able to differentiate the isomers by visible spectroscopy. The isomers differ by a 180° rotation about the α,γ -*meso* axis, as shown in the inset in Figure 3.

For easier reading and understanding of this dissertation, Figure 4 is included to depict the general environment of heme with respect to a few amino acid residues from the protein matrix. In the holoprotein, heme iron is linked to N_ϵ of His F8 (i.e. the eighth residue on helix F) on the proximal side. On the opposite or distal side, heme faces His E7, Val E11 and Phe CD1.

When the iron atom of heme in Mb is in the (III) state, ligands such as water, azide (N_3^-), cyanide (CN^-), imidazole (Im^-), and phenyl can be bound at the Fe 6th coordination site (i.e. replacing O_2 in Figure 4). In the presence of intermediate-field ligands like N_3^- and Im^- , the five electrons of Fe(III) are in mixed spin states of $S = 1/2$ and $S = 5/2$. Otherwise, the electrons are in low spin state of $S = 1/2$, or high spin state of $S = 5/2$ when complexed to strong-field CN^- or weak-field water, respectively (see Table I).

Both high-spin and low-spin Mbs have been well characterized by solution state NMR. Most of the work has been done on metMbCN and metMbH₂O, while little effort has been invested in the metMbIm and metMbN₃ systems. MetMbH₂O was first studied by NMR by isotopic-labeling (La Mar et al., 1980), when its crystal structure was available (Takano, 1977); only the heme methyls were identified. Because of the high-spin ($S = 5/2$)

character which was thought to diminish the magnitude of nuclear Overhauser effect (NOE) (Noggle & Shirmer, 1971; Freeman et al., 1971), the utility of NOEs for this system was not realized until the mid 1980's (Unger et al., 1985). The application of NOE techniques allowed the semiquantitative interpretation of the magnitude of NOE to characterize the nature of relaxation for the pure high-spin system, based on Equations (1) and (2) in Chapter II. However, practical difficulties allowed identification of only a handful of

TABLE I
IRON COMPLEXES AT DIFFERENT OXIDATION STATES WITH
VARIOUS SIXTH LIGANDS

Species	Fe^{2+}	Fe^{2+}	Fe^{3+}	Fe^{3+}	Fe^{3+}
Ligands	deoxy	O_2 , CO	N_3 , Im	H_2O , OH^-	CN^-
Spin	2	0	5/2; 1/2	5 / 2	1 / 2
Spin State	high-spin	low-spin	mixed-spin	high-spin	low-spin

resonances, including heme peripheral protons, and protons from Val E11 and His F8 in metSwMbH₂O (La Mar et al., 1980; Unger et al., 1985). Detection of low-intensity peaks, relative to a large diamagnetic mass, constitutes large demands on the dynamic range of the receiver and the digitizer. Saturation of broad peaks in NOE studies, on the other hand, requires strong radio-frequency (rf) power, which inevitably induces off-resonance artifacts.

MetMbCN, thus far, is the most extensively studied system by NMR. The single unpaired electron in MetMbCN renders the system paramagnetic, which helps resolve the residues in the binding site from the diamagnetic range; yet, the relaxation of the resonances

by the electron is not efficient enough to cause tremendous decreases in T_1 and T_2 , which alleviates the problems encountered in metMbH₂O. The relaxation behavior and kinetic lability of exchangeable protons in the heme pockets of various metMbCNs (Cutnell et al., 1981; Lecomte & La Mar, 1985, 1986) were investigated to probe possible ligand entry passageway through a trajectory involving mainly distal amino acids side chains of Arg CD3 (or Lys CD3), His E7, Val E11, and the heme 6-propionate (Case & Karplus, 1979). By probing the exchange rate constant of the labile ring NH of His E7, it was found that the distal side has higher solvent accessibility in Mbs that bear Lys CD3 (for instance EqMb and CAMb) than SwMb that has Arg CD3. The usefulness of multi-dimensional NMR techniques in paramagnetic systems was demonstrated by Emerson and La Mar (1990) in elucidating the solution structure of the heme pocket of metSwMbCN.

MetMbCN and metMbH₂O are two extreme limits of paramagnetic systems. Although studies of the low-spin metMbCN have been fruitful, difficulties encountered in metMbH₂O system inhibited efforts in NOE studies of high- and mixed-spin systems until the demonstration of heme resonance assignments on metEqMbN₃, which is mixed-spin, by 2D NOESY/COSY NMR (Peyton, 1991). Mixed-spin systems such as metMbIm and metMbN₃ are even less investigated by NMR methodologies than the high-spin case in terms of their potential to obtain assignments in high-spin systems like metMbH₂O from saturation transfer (see Chapter III). This is important because experimental data from the pure low-spin metMbCN has allowed verification of its electronic structure based on quantum mechanical model calculations (Shulman et al., 1971), but insufficient high-spin data is available to do the same.

MetMbphenyl is an interesting low-spin case, in that although its X-ray crystal structure has been determined (Ringe, 1984), only the o-, p-, and m-protons on the phenyl ring have been identified by NMR (Kunze & Ortiz de Montellano, 1983). The phenyl ring is covalently bonded to the iron, and the heme pocket was shown to adopt a dramatically

different geometry from the other ligands (Ringe, 1984). Although not included in this document, preliminary studies with metMbphenyl showed remarkably distinctive spectral properties from low-spin metMbCN as well as all other systems mentioned previously, and warrant the need for further, more detailed investigations. One of the most striking features of metMbphenyl is the absence of hyperfine-shifted heme methyls, as evidenced from the lack of downfield 3-proton resonances. Reconstitution of apoEqMb with heme deuterated at the heme $2H_{\alpha}$ position, followed by the addition of phenyl, allowed the assignment of this peak at 10.35 ppm. 2D 1H NMR methods identified the $2H_{\beta c}$, and $2H_{\beta t}$ at -2.80 ppm, and -3.55 ppm, respectively, at pH 6.0 and 298 K. The preliminary results instills confidence in the potential usefulness of the solution-state 1H NMR methodologies to investigate this system.

My research focuses on studying the mixed spin metazido and metimidazole complexes of Mbs for the following reasons. First, the allosteric properties of Hb arise mainly from the transition between its two possible quaternary structures, namely, the R or high affinity (for example, low-spin Fe(II)- or Fe(III)Hb) and the T or low-affinity state (deoxyHb) (Yamamoto & La Mar, 1989). Paramagnetic NMR is one of the most sensitive tools to study this in terms of changes in the molecular and/or electronic structure of the heme. The metazido form, because of the thermal equilibrium between high-spin and low-spin states, is inherently a more sensitive probe than the metcyano form toward changes in the axial field strength. MetHbN₃ is also an optimal species to study due to a set of well-resolved resonances downfield of the diamagnetic envelope (La Mar et al., 1988, Yamamoto & La Mar, 1986; Peyton, 1991). Second, both the N₃⁻ and Im⁻ complexes are good compromises, in terms of sizes, between the small diatomic oxygen or CN⁻ molecules and the bulky phenyl group. This is important because distal His E7 has been suggested to modulate the activities of binding by acting as a doorstep to incoming ligands (Olson, 1988). Thus, we can determine the influence of ligand size on structural

perturbation of the heme crevice by comparison among the different size groups. The X-ray crystal structure has distal His E7 of SwMb partially swung out from the binding pocket towards the protein surface in the imidazole complex (Lionetti et al., 1991). On the other hand, in metMbphenyl, His E7 is totally swung-out to accommodate the bulky size of the phenyl ring (Ringe et al., 1984). While metMbIm provides a transient state model in the binding dynamics, the wide-open metMbphenyl system is an extreme limit to gauge the direct influence of distal residues on ligand-binding. Third, the saturation-transfer phenomenon between metMbIm and metMbH₂O promises of assignments in metMbH₂O by using assignments of metMbIm. Extensive assignments of metMbH₂O, which is electronically isotropic due to 5 unpaired electrons, is crucial because it is the basis of theoretical calculation of the isotropic shift due to axial ligand field in pure high-spin hemoproteins. Fourth and finally is the importance of metMbIm as a bis-imidazolium complex, which can then serve as a model for hemopexin, cytochrome b₅, and other bis-histidyl proteins (Bertini & Luchinat, 1986; Lecomte & Moore, 1991).

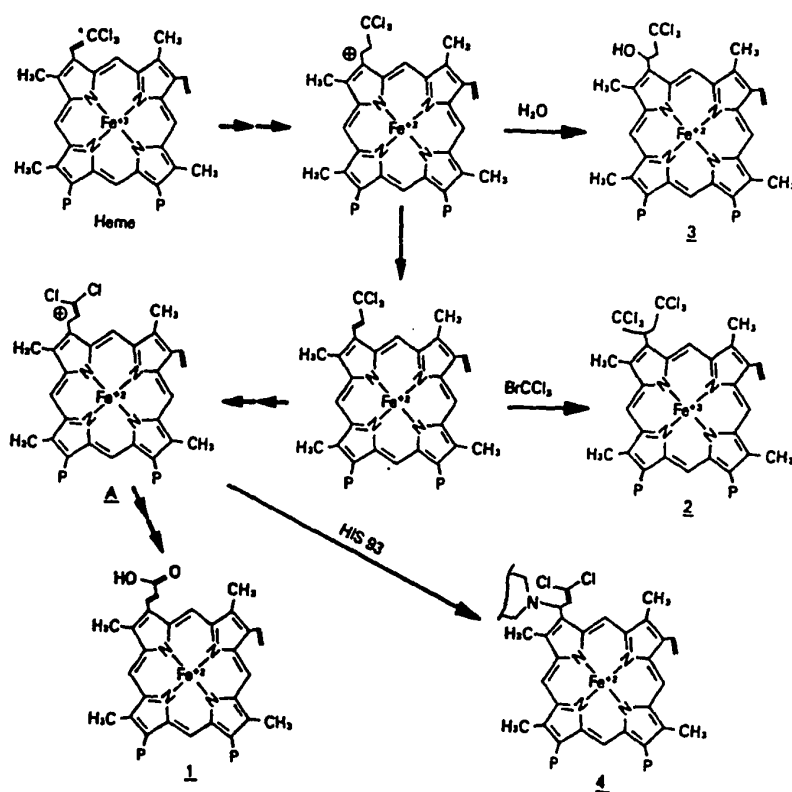


Figure 1. Proposed mechanism for the formation of the altered heme products, hemes 1, 2, 3, and 4, a His F8 (93) bound adduct (Osawa et al., 1991).

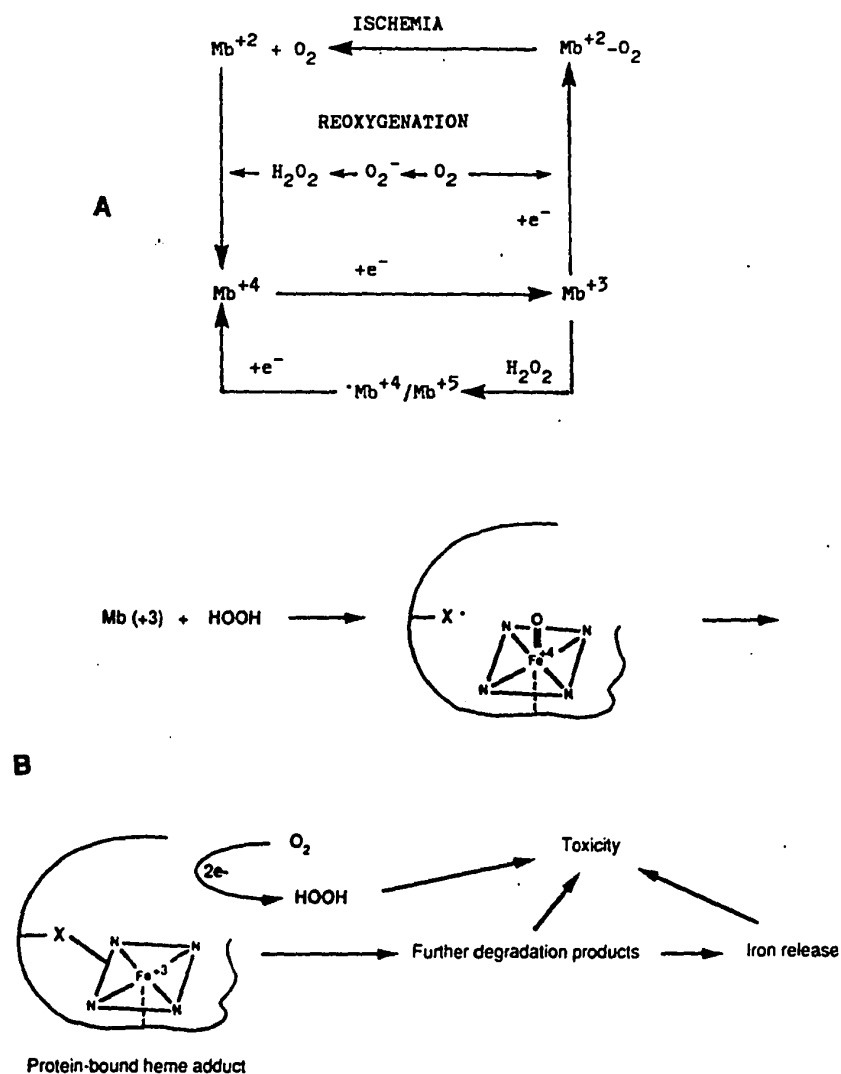


Figure 2. A. Redox cycle of MbO_2 in myocytes (Galaris et al., 1989). B. Proposed mechanism for the reaction of metMb with H_2O_2 (Osawa & Korzekwa, 1991). The reduction of O_2 to H_2O_2 depicted here is an oversimplification. It is the protein-bound Mb in the ferric state that catalyzes the reduction of O_2 to H_2O_2 by NADH.

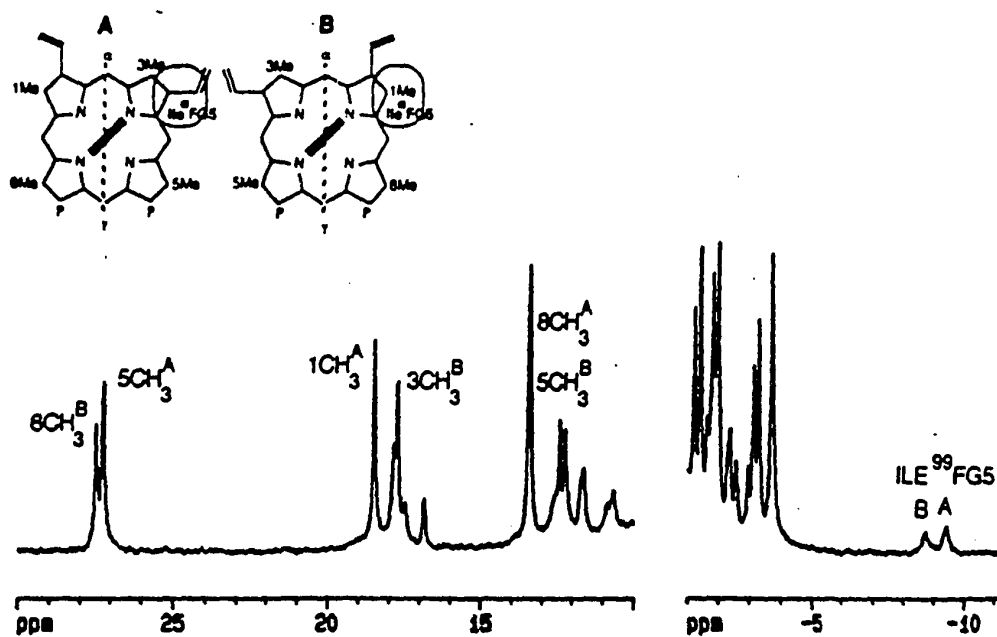


Figure 3. ^1H NMR spectrum of the nearly 1:1 mixture of heme-insertion isomers formed by reconstitution, then quenched with CN^- . Inset: the two heme-insertion isomers in SwMb (A is the major form).

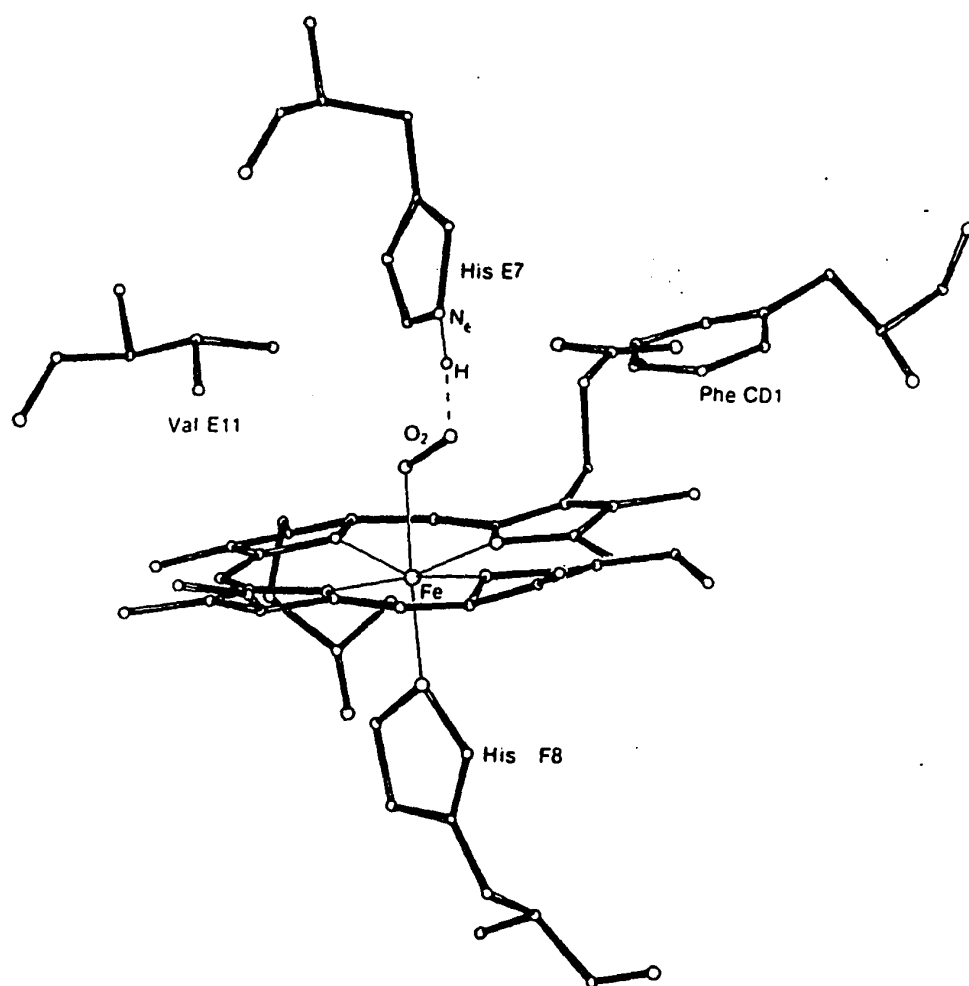


Figure 4. Arrangement of proximal and distal residues in myoglobin, showing the hydrogen bond between the distal His and the bound sixth ligand - oxygen (Phillips, 1978).

CHAPTER II

MATERIALS AND METHODS

Other than procedures specific to the corresponding chapter, all experimental procedures are included here. The appropriate pulse-sequence parameters and sample conditions are incorporated into the figure captions.

SAMPLE PREPARATION

General

Horse heart myoglobin was purchased from Sigma as a salt-free lyophilized powder. The protein was used without further purification. The solutions were 1.5-2 mM in protein in either 99.8% $^2\text{H}_2\text{O}$ or 90% H_2O /10% $^2\text{H}_2\text{O}$ solvent for 1D NMR experiments. For 2D NMR experiments, the solutions were 3-6 mM. The metazido and metimidazole forms were prepared by adding ~10-fold molar excess NaN_3 crystals and imidazole, respectively; the pH was adjusted with 10% NaOH or HCl (in 99.8% $^2\text{H}_2\text{O}$ or 90% H_2O /10% $^2\text{H}_2\text{O}$, based on the experiments). The pH values used were not corrected for isotope effect. All ^1H NMR experiments were performed on a Bruker AMX-400, at 9.4 T magnetic field strength. Chemical shifts are referenced to DSS (2,2-dimethyl-2-silapentane-5-sulfonate) through the residual water signal at 4.76 ppm.

For the $\text{heme}(\text{CN})_2$ reconstitution experiments, the following is employed. Reconstitutions with heme required dissolving the heme with a minimum amount of NaO^2H , which resulted in a pH of at least 11. $\text{Heme}(\text{CN})_2$ was generated by adding ~5-fold excess of KCN to the heme, then adjusting the pH to 9.0-9.2 (higher pH values result in significant displacement of CN^- by OH^- , McGrath, 1979). The apoMb solution pH was

adjusted before adding the heme or heme(CN)₂. In each case the apoMb was in ~20% excess, as determined by optical titration of an aliquot against the heme solution. After reconstitution the sample pH was checked, resulting in the uncorrected value of 9.2.

Protein Isolation

Pigmy Sperm whale myoglobin was isolated from the back muscle of whales donated by the Biology department of Portland State University. The protein was isolated according to the method of Yamazaki et al (1964). The isolated protein was inspected for integrity of tertiary fold by conventional ¹H 1D NMR, 2D COSY (COrelated SpectroscopY), NOESY (Nuclear Overhauser Effect SpectroscopY), and TOCSY (TOtal Correlated SpectroscopY) (Equations (2), (3), and (4), respectively) in the diamagnetic MbCO and MbO₂ forms. The spectra compare strongly with those of SwMb counterparts (Mabbutt et al., 1985; Dalvitt & Wright, 1987). 2D COSY of diamagnetic samples were processed with phase-sensitive implementation, as opposed to the magnitude processing done on paramagnetic metMbs, because diamagnetic species have sharp linewidths that can offer scalar coupling information.

Sample Preparation for Kinetics Determinations

Kinetics determination for the heme reorientational disorder within the protein matrix in Chapter VI required careful consideration of pH, concentration, temperature, and column chromatography to prevent complications from competitive reactions.

For optical spectroscopy, hemin solutions were prepared fresh for each reconstitution by adding 5 μ L of 5% NaOH and 3.6 μ L of 5 mM ferricyanide to a H₂O suspension of hemin (~0.5 mg) to make a final volume of 200 μ L. ApoMb solution was made by dissolving ~5 mg apoMb in 100 μ L of desired buffer at desired pH. The buffer systems employed were 40-50 mM Tris, 100-200 mM NaCl at pH 8.4-8.5; or 50 mM phosphate, 100-200 mM NaCl at pH 6.7-6.8; and 50 mM borate, 100 mM NaCl at pH 7.5.

Reconstitutions were performed by adding 20 μ L of the hemin stocks to 100 ml of the apoMb solutions. The mixtures were immediately eluted through a Sephadex G-25 column at 5°C, pre-equilibrated with the same buffer. Aliquots of the effluents were added to the sample cell, with equivalent amounts of ferricyanide added to the reference. When no column was used, the hemin stock was directly added to the apoMb solution; and then an aliquot of the mixture was immediately added to the sample cell.

The optical spectrophotometer was a Cary 16; the cells were 1 cm pathlength, unless otherwise stated, and were maintained at desired temperature with circulating antifreeze. A Macintosh Plus computer was employed to collect data via a Keithley model 195A digital voltmeter as the ADC and Mac 488A bus controller from IOTech. Each run consisted of 2000 data points acquired over the range 470 to 337 nm in three minutes (0.067nm digital resolution). The software was a gift of Professor J.H.Golbeck.

For NMR spectroscopy, ~2.5 mg hemin was dissolved in 5 μ L NaOH, 120 μ L of 5 mM ferricyanide and H₂O to make a final volume of 1 mL. 16-23 mg of apoMb was dissolved in 500 μ L of desired buffer at the desired pH. For each reconstitution, 220 μ L of hemin stock was added to the apoMb solution. The mixture was eluted in a Sephadex G-25 column at 5°C, pre-equilibrated with the same buffer. The effluent was collected, ultrafiltered and exchanged with D₂O of the same buffer at 5°C down to ~0.5 mL; the solution was then transferred to a 5 mm nmr tube. The final concentrations of the hemin and apoMb were ~1.2-1.5 mM.

Chromatography of protein from isolation and modification preparations was performed on ISCO UA-5 Absorbance/Fluorescence Detector , set at 254 nm; a WIZ Peristaltic Pump for controlling speed of elution; a Model 1133 Multiplexer-Expander to scale size of transient, and a Retriever IV fraction collector. For isolation of highly colored heme proteins, the Gilson micro fractionator without the use of a UV/fluorescence detector was employed.

GENERAL NMR EXPERIMENTS

Standard 1D ^1H NMR experiments were run with the zgpr pulse sequence as shown in Equation (1), unless otherwise indicated, in which water resonance was suppressed with a low power, long pulse during the relaxation delay (RD). Standard 2D ^1H NMR experiments for this work include COSY, NOESY, and TOCSY as described in Equations (2), (3), and (4), respectively. 2D EXSY utilizes the same pulse sequence as NOESY in Equation (3).

$$\text{RD} - 90^\circ - \text{FID} \quad (1)$$

$$\text{RD} - 90^\circ - t_1 - 90^\circ - \text{FID} (t_2) \quad (2)$$

$$\text{RD} - 90^\circ - t_1 - 90^\circ - t_m - 90^\circ - \text{FID} (t_2) \quad (3)$$

$$\text{RD} - 90^\circ - t_1 - 90^\circ - \text{mlev17} - 90^\circ - \text{FID} (t_2) \quad (4)$$

where 90° is the pulse length (typically $\sim 8\text{-}9$ ms), t_1 is the incremental time, t_m is the mixing time, FID is the sampled free induction decay during t_2 , and mlev17 is a train of 16 composite pulses and 2 trim pulses. The mixing time is required in NOESY for build-up of coherence between spins; therefore, an appropriate choice of this time-period is crucial to the detection of NOE signals. If too long a mixing time is employed, resonances of short T_1 s will have completely relaxed and no coherence is observed. On the other hand, if a short t_m is used, not enough coherence is accumulated for resonances of long T_1 s. Typically, a t_m of 2-4 ms, 5-20 ms, or 30-50 ms was utilized for high-spin, mixed-spin, or low-spin paramagnetic samples, respectively. Typically, for paramagnetic high- and mixed-spin samples with broad resonances, 512 and 300 data points were required in the f_2 and f_1 dimensions, respectively. 2D EXSY was collected identically to NOESY (Equation (3)), except that the cross peaks represent magnetization transfer, instead of dipolar or through-space interaction, between exchanging species. Phase sensitive detection by TPPI

(time-proportional phase incrementing) was employed for all 2D NOESY, TOCSY, and EXSY (Wuthrich, 1986; Mabbutt & Wright, 1985). In 2D COSY, on the other hand, because of the broad linewidths of these paramagnetic samples, not only is the determination of coupling constants immaterial, but two adjacent cross peaks may cancel out each other rendering no cross peak observed; therefore, absolute value detection (magnitude COSY) is sufficient for the processing. Furthermore, to increase the signal-to-noise without introducing proportional noise, zero-filling to at least twice the size of data points collected was implemented before Fourier transformation of data.

Rates of exchange between labile protons and water solvent, as well as between exchanging resonances, were measured by the 1D saturation transfer method. The extent of saturation transferred from the irradiated water resonance to an exchangeable proton was determined by Cutnell et al. (1981) as follows:

$$k_{\text{exch}} = [T_1^{-1}(1-F)]/F \quad (5)$$

where T_1^{-1} is the intrinsic spin-lattice relaxation rate, and F is the saturation factor, which is the ratio between the intensity of the involved resonance with and without irradiation. The non-selective spin-lattice relaxation times, T_1 's, of the methyls were determined by the conventional inversion-recovery method, illustrated in Equation (6).

$$\text{RD} - 180^\circ - t_D - 90^\circ - \text{FID} \quad (6)$$

where t_D is a delay time under the control of the operator. T_1 s for resonances close to the paramagnetic center such as heme methyls can be determined through a non-selective, hard 180° inversion pulse. For these resonances, relaxation by the unpaired electron(s) overwhelms all other mechanisms, so that the T_1 s obtained through either selective or non-selective inversion pulse are approximately the same (La Mar, 1973).

Labile protons were detected in pH titrations, performed by ^1H NMR with p11noedif pulse sequence as outlined in Equation (7).

$$\text{saturate/miss H}_2\text{O (decoupler)} - 90^\circ_{(x)} - t_D - 90^\circ_{(-x)} - \text{FID} \quad (7)$$

where the first and second 90° pulses are exactly out of phase by x . t_D is the delay time between the two pulses, and is usually in the range of 30-80 μs . The transmitter frequency is always set on the solvent (i.e. H_2O), so the ADC would not be overfilled by the giant solvent signal, decreasing the dynamic range. Because t_D is much shorter than T_1 of H_2O (~ 1 s), there is no net excitation of H_2O , while resonances offset from the transmitter frequency precess between the two pulses. Null point of the pulse sequence is determined by $1/(2t_D)$ from the transmitter frequency. Resonances that are on the high and low side of the transmitter frequency are 180° out of phase. Saturation factor was obtained from alternatingly saturating and missing the water signal with a decoupler. Resonances in exchange with the solvent water will be attenuated in intensity while the decoupler is on water.

Selective irradiation of resonances (Chapter IV) were done with the pulse sequence 'zgh2pr' -- zg decoupling with relaxation delay, outlined as in Equation (8).

$$\text{RD} - \text{d1 (dl0)} - 90^\circ - \text{FID} \quad (8)$$

The parameters used in this sequence are the relaxation delay, the saturation time, and dl0 (the saturation power). The irradiation is thus performed by a selective low-power, long-pulse decoupler. Relaxation delays employed are on the order of T_1 of the resonances. The saturation time is inversely proportional to the accuracy of the irradiation, based on Heisenberg Uncertainty Principle; therefore, a precise frequency selection for saturation requires a longer saturation time than that of a broad one. However, a saturation time that

is too long can induce spin diffusion, especially in macromolecule like Mb. Spin diffusion occurs when the energy of saturation has time to diffuse throughout the protein; in such a case, some of the peaks detected in the difference spectrum may be caused by indirect interaction -- a situation that could lead to misassignment. On the other hand, very short saturation time with high power can lead to direct off-resonance saturation artifacts. Thus, a balance is achieved by only ~30% - 50% saturation of the peak with appropriate power and saturation time. For a methyl peak of metSwMbH₂O (with T₁ of 4.7 ms and T₂ of 1.1 ms), 50% saturation induces 5% off-resonance effect achieved at approximately 700 Hz (Lecomte et al., 1991). In this document, resonances to be decoupled are designated in reference spectra; and the decoupler power is varied to achieve the desired saturation effect.

A variation of the zgh2pr sequence is wefnoedif, as in Equation (9).

$$\text{RD} - 180^\circ - \tau - \text{SAT} - 90^\circ - \text{FID} \quad (9)$$

A 180° pulse hard pulse is used to invert all peaks in the spectrum. τ is the delay time for a particular peak to relax back just to zero intensity. This sequence is advantageous in that it allows the undesiredly huge resonances (for example: bulk H₂O solvent) that cause dispersive effect on the difference spectrum and/or overfilling the ADC to be tuned to a null. The faster-relaxing protein peaks have positive intensity and can be observed. In Chapter IV, because the upfield resonances that are inverted all have T₁s on the order of ms, as compared to s for the diamagnetic peaks including the residual water and artifacts from free ligand peaks, a short τ can strongly reduce the magnitudes of the undesired resonances in the spectrum.

ACKNOWLEDGEMENTS

I am most grateful to Professor Gordon Kilgour (Portland State University Chemistry Department) for his advice and guidance in modification of literature protein isolation preparation, supply of glassware and the Gilson micro fractionator.

CHAPTER III

ASSIGNMENTS OF HEME PERIPHERAL RESONANCES IN AZIDO AND IMIDAZOLE MYOGLOBINS BY MULTI-DIMENSIONAL PROTON NUCLEAR MAGNETIC RESONANCE

Heme resonance assignments in the past have been made using deuterium isotope-labeling (Satterlee, 1985; La Mar et al., 1980). Even though this method provides unambiguous assignments, it is extremely labor-intensive and uninformative of any other NMR parameters. Alternatively, a combination of NOESY and COSY ^1H NMR experiments has been successfully done on metMbN₃ allowing assignment of the majority of the heme peripheral resonances (Peyton, 1991) to supplement the results from isotope-labeling. The NMR-only method is by far more desirable because it not only allows easier assignments, albeit in a less straight-forward manner, but also offers structural and dynamic information based on lineshape, chemical-shift and relaxation analyses by ^1H NMR. In this research, the NMR-only protocol is employed.

Saturation transfer between the metMbH₂O and metMbIm complexes is used as an alternative assignment method if the resonances are assigned for one of the species. In this case, because many heme resonances from metMbH₂O have been well assigned (Unger et al., 1985; La Mar et al., 1980), saturation-transfer is used to supplement the assignments of metMbIm resonances; during this work, however, a mistake in the literature (Unger et al., 1985) regarding metMbH₂O resonance assignments is found. Saturation transfer between the aquo, imidazole, and methylated imidazole complexes is possible because the exchange rate is slow relative to the chemical shift difference between the exchanging resonances, yet comparable to the spin-lattice relaxation rates, $R_1s = T_1^{-1}s$, of the

resonances of interest (see Utility of Saturation Transfer below). 2D Exchange spectroscopy (EXSY) experiments were done on ~ 1:1 complex of metMbIm : metMbH₂O at various temperatures, with increasing cross peaks intensities at higher temperatures -- confirming the saturation transfer phenomenon. Because the exchange rate is faster at a higher temperature, while intrinsic R₁ decreases, experiments performed at higher temperatures produce increased saturation transfer.

The proximities of nearby heme pocket residues are manifested by their through-space dipolar interaction with the heme resonances, and to the paramagnetic center by their relaxation rates, as related by Equations (9) and (10), respectively. Thus, assignment of the heme peripheral resonances is the stepping stone to the deconvolution of the amino acid residues in the heme crevice.

$$\eta_{a \rightarrow b} = [-(g_H^4 h^2 \tau_c)(T_{1b})]/(10r_{ab}^6) = \sigma_{ab} T_{1b} \quad (9)$$

$$T_{1a}/T_{1b} = (r_{Fe-a})^{-6}/(r_{Fe-b})^{-6} \quad (10)$$

In these equations, $\eta_{a \rightarrow b}$ is the observed NOE to b upon irradiation of a, σ_{ab} is the cross relaxation (or spin exchange rate) between spins a and b, g_H is the gyromagnetic ratio of a proton, τ_c is the correlation time of the ab vector, and r is the distance between the points indicated at the subscripts. Usually one of the parameters is a methyl group, whose T₁ is determined, and r ~ 6.1 Å from the crystal structure of MbCO (Kuriyan et al., 1986).

Scalar-coupling, or through-bond interaction, between protons fewer than three bonds apart is detected by 2D COSY and TOCSY experiments, both of which bear spatial implication by the size of cross peak, which depends on the dihedral angle between the adjacent carbons. For example, geminal protons in the "anti" conformation (dihedral angle = 180° has a much larger scalar coupling than if the dihedral angle = 90°). TOCSY allows the detection of indirect scalar coupling beyond three bonds through coherence relayed

through a mutually scalar coupled proton. Figure 5 illustrates the manifestation of both dipolar and scalar interaction isoleucine.

RESULTS

Assignments of the Heme-Insertion Isomer Resonances of MetEqMbN₃

Figure 5 demonstrates the utilities of 2D COSY and NOESY in a nut-shell, to aid understand the more complex protein spectra. Figure 6 gives the labeling system for the peripheral resonances in both heme insertion-isomers, including arrows that demonstrate the kind of interactions expected of the resonances. ¹H NMR 2D COSY and NOESY spectra of native and freshly reconstituted metEqMbN₃ species were analyzed, as shown in Figures 7, and 8, respectively. Using metMbN₃ as an example (Peyton, 1991), the assignment process is made starting from the 8CH₃ and 1CH₃ NOE, the only heme methyls with an NOE between them. Heme methyls are first recognized by their integrals of three protons and tremendous hyperfine-shifted positions due to contact with the iron center. The 8CH₃ and 1CH₃ are distinguishable by the 8CH₃ to 7H_α and the 1CH₃ to 2H_{βc,t} NOEs. The 2- and 4-vinyl spin systems are identified by their characteristic COSY/NOESY patterns, and distinguished from each other by their NOEs to 1CH₃ and 3CH₃, respectively. In NOESY, which is based on dipolar connectivity, H_α is nearer in space to H_{βc} than to H_{βt}, and so is of greater intensity. COSY, on the other hand, detects scalar couplings between these two sets of protons, therefore shows a larger cross peak for the trans interaction (coupling constants are ~ 16 Hz for trans vs ~ 6 Hz for cis). The propionates have similar spin systems in NOESY and COSY; i.e. H_α to H_{α'}, as well as H_β to H_{β'}, produces both sizable COSY and NOESY cross peaks due to geminal coupling and close proximity, respectively, and H_α to H_β incurs bigger NOESY and smaller COSY intensities as compared to H_α to H_{β'}. The 3CH₃ and 5CH₃ are differentiated by the 3CH₃ to 4H_{α,βt} and 5CH₃ to 6H_α NOEs. Because strong COSY cross peaks are from

no more than three-bond scalar coupling, they are used mainly for identifying spin systems. The *meso* protons, being extremely close to the paramagnetic center, are unable to be identified by the 2D protocols, due to fast-relaxation (T_1 , T_2) and because are not strongly J-coupled to any proton.

The assignments of the heme peripheral protons in the reversed isomer of metEqMbN₃, however, do not follow the above method exactly because the $8\text{CH}_3^{\text{B}} \leftrightarrow 1\text{CH}_3^{\text{B}}$ cross peak could not be observed. From Figure 6, it is possible to speculate the shifts of the resonances in the minor insertion isomer through pairwise exchange to their corresponding positions on the heme. For instance, 5CH_3^{A} and 8CH_3^{B} are in identical heme position and same environment in the protein matrix, therefore, their chemical shifts should be similar. Figure 8 shows two methyl peaks around 33 ppm in the freshly reconstituted metEqMbN₃, as compared to one in the native form (5CH_3 in Figure 7). The smaller intensity of the two was assigned to 8CH_3^{B} on the premise that the ratio of major to minor insertion isomer is always 1:<1 in practice because of the redistribution to the native form during preparation time, although when extrapolated to time zero, the ratio should be 1:1. The identical protein environment is reflected through their parallel cross peaks to other heme and protein resonances. One of the cross peaks to 8CH_3^{B} at 15.4 ppm, exhibits familiar propionate spin system (as discussed above), and is assigned to $7\text{H}_\alpha^{\text{B}}$. This is also consistent with the exchanged position of $7\text{H}_\alpha^{\text{B}}$ with $6\text{H}_\alpha^{\text{A}}$ because their chemical shifts are similar.

Assignments of MetEqMbXIm, where X is H, 1CH_3 , and 4CH_3

The assignments of metEqMbIm, metEqMb 1CH_3 Im and metEqMb 4CH_3 Im follow a similar routine as that described above for the native azido species. The 2D NOESY/COSY spectra are as shown in Figures 9 and 10. Possible overlapping NOESY and COSY cross peaks around ~15 ppm at 298 K was evident (not shown), indicating that

there are two overlapping peaks; hence, same experiment was performed at 308 K (figure 9), which resolved the peaks and showed distinctive propionate and geminal coupling characteristics. Those peaks were assigned to be heme $6H_{\alpha}'$ and $C_{\beta}H$ of His F8, as listed in Tables III, IV, and V. Heme $6H_{\alpha}'$ was assigned not only from its connectivity to $6H_{\alpha}$ and $6H_{\beta,\beta'}$, but also from the verification from 2D TOCSY (not shown). $C_{\beta}H$ of His F8 was identified from its exchange with its counterpart in metEqMbH₂O from 2D EXSY (see below). Because the 3CH₃ and the 4-vinyl protons were buried in the crowded diamagnetic region, and so could not be identified by 2D COSY/NOESY method, the saturation-transfer technique was utilized. Saturation-transfer experiments at various temperatures were employed between metMbH₂O and all three metMbXIm's; Figure 11 presents the 1-D saturation-transfer by selectively perturbing a selected resonance, in this case the 3CH₃ of metEqMbH₂O. This gave the 3CH₃ assignment for metEqMbIm. In 2D EXSY experiments, because all spins are perturbed at the same time, and because in this case the exchange rate comparable to the T_1 -1s of the exchanging peaks, the effect of saturation transfer, instead of dipolar interaction, is observed as the off-diagonal cross peaks (see Figures 12, 13, and 14). During this work, a mistake in the literature assignments of the vinyl systems of metSwMbH₂O was found (see asterisks in Figure 12) (Unger et al., 1985), demonstrating the power of saturation-transfer technique not only in making but also in verifying assignments (see Discussion). The assignments of the heme peripheral protons for the azido and imidzolate complexes are listed in Tables II, III, IV, and V.

Figure 11 shows examples of 1D NOE saturation-transfer experiments involving metEqMbH₂O : Im. As shown in the figures, the irradiated methyl peak of metEqMbH₂O is strongly relaxed; therefore, the use of high rf power, possibly inducing off-resonance effects, is necessary to saturate the peak. To alleviate the problem, lower power irradiation of the methyl was attempted. However, to determine k_{ex} from Equation (5) normally

TABLE II

CHEMICAL SHIFTS FOR MINOR-INSERTION ISOMER OF
MetEqMbN₃ AT 25°C AND pH 7.0

<u>Assignments</u>	<u>Chemical Shift (ppm)</u>
1CH ₃	18.3
3CH ₃	17.3
5CH ₃	25.2
8CH ₃	33.4
2H _α	--
2H _{βc}	--
2H _{βt}	--
4H _α	28.3
4H _{βc}	0.7
4H _{βt}	-2.3
6H _α	11.0
6H _α '	6.9
6H _β	--
6H _β '	--
7H _α	15.4
7H _α '	12.0
7H _β	--
7H _β '	--

TABLE III
CHEMICAL SHIFTS FOR MetEqMbIm AT 50°C AND pH 6.2

<u>Assignments</u>	<u>Chemical Shifts (ppm)</u>
1CH ₃	25.0
3CH ₃	8.0
5CH ₃	36.8
8CH ₃	18.3
2H _α	23.0
2H _{βc}	-1.6
2H _{βt}	-3.0
4H _α	8.3
4H _{βc}	--
4H _{βt}	--
6H _α	15.4
6H _α '	13.5
6H _β	2.5
6H _β '	2.3
7H _α	6.2
7H _α '	2.6
7H _β	2.5
7H _β '	--
F8 His C _β H	13.5

TABLE IV

ASSIGNMENTS OF HEME PERIPHERALS FOR METE_qMb1CH₃Im
AT 25°C, UNLESS OTHERWISE PARENTHESESIZED, AND pH 7

<u>Assignments</u>	<u>Chemical Shifts (ppm)</u>
1CH ₃	24.1
3CH ₃ (323 K)	4.7
5CH ₃	31.1
8CH ₃	16.9
2H _α	22.9
2H _{βc}	-1.0
2H _{βt}	-2.3
4H _α (323 K)	7.5
4H _{βc}	-
4H _{βt}	-
6H _α	11.8
6H _α '	10.4
6H _β	2.2
6H _β '	3.2
7H _α (323 K)	3.6
7H _α ' (323 K)	1.4
7H _β (323 K)	1.9
7H _β '	-
F8 His C _β H	-

TABLE V
 ASSIGNMENTS FOR HEME PERIPHERALS OF MetEqMb4CH₃Im AT
 323 K AND pH 7

<u>Assignments</u>	<u>Chemical Shifts (ppm)</u>
1CH ₃	23.5
3CH ₃	4.0
5CH ₃	34.1
8CH ₃	13.8
2H _α	22.1
2H _{βc}	-
2H _{βt}	-
4H _α	6.8
4H _{βc}	-
4H _{βt}	-
6H _α	13.3
6H _α '	12.0
6H _β	-
6H _β '	-
7H _α	3.3
7H _α '	1.2
7H _β	1.33
7H _β '	-
F8 His C _β H	12.7

requires that magnetization of the irradiated peak be reduced to zero (Sandstrom, 1982), i.e. the peak has to be completely saturated. Fortunately, it is possible to use the area ratio of the effected to irradiated methyl peak determined directly from the difference spectra as presented in Figures 10 and 11 to yield the fraction, f , of the effected peak diminished from saturation transfer, and then saturation factor, F , obtained from $1-f$. The exchange rate, k_{ex} , calculated in this manner from Equation (5) yields rate-constant of $\sim 3 \text{ s}^{-1}$ with determined T_1 of 31 ms for the 5 CH_3 of metEqMbIm at 298 K; while k_{ex} at 308 K is determined to be $\sim 53 \text{ s}^{-1}$. These rate constants correlate well with the effected peak height as presented in Figures 10 and 11. At 298 K, k_{ex} is relatively slow, so that the saturation transfer is only $\sim 6\%$. At 308 K, nevertheless, the effected metEqMbIm methyl peak is more than 50% reduced in intensity, with k_{ex} comparable to its R_1 . The non-selective T_1 of the 5 CH_3 of metEqMbIm is fitted to data obtained by inversion recovery experiment by the method of Harris (1989), Sanders (1988), and Sandstrom (1982), using pulse sequence as shown in Equation (6). Figure 15 illustrates the plot of $\ln(\text{int(at infinity)} - \text{int(time } t))$ vs delay time (t_D in Equation (8)) to determine T_1 s for the 5 CH_3 s of metMbN₃ and metMbXIm (where X is 1- CH_3 , 4- CH_3 , or H). The slope extracted from such a plot is $1/T_1$. T_1 s obtained are listed in Table VI.

DISCUSSION

The Scope and Limitations of 2D NMR Experiments

The 2D NOESY/COSY experiments allow assignments of most of the heme resonances of the various paramagnetic species examined above. Similar results can also be obtained with numerous steady-state 1D NOE irradiations in conjunction with a COSY map. The major advantage of 2D NOESY is the ability to exhibit all the observable dipolar connectivities in one experiment as cross peaks, saving instrument time. Failure to

TABLE VI

T_1 S FOR 5CH₃S AND 1CH₃S OF THE INDICATED MYOGLOBIN SPECIES IN N₃ AND Im LIGATED STATES AT 25°C; INCLUDED IS ALSO THE LITERATURE T_1 S FOR MetSwMbCN

Species	T_1 of 5CH ₃ (ms)	T_1 of 1CH ₃ (ms)
metEqMbN ₃	14.4	14.5
metEqMbIm	43.7	57.1
metEqMb1CH ₃ Im	31.0	73.0
metPSwMb4CH ₃ Im	42.6	63.4
metSwMbCN (Cutnell et al., 1981)	81.6	115

observe certain cross peaks in the 2D maps are attributed to a few reasons. Because the unpaired electron from the iron center has gyromagnetic ratio that is 658 times greater than that of a proton (La Mar, 1973), resonances that are closer to the Fe than ~ 5 Å can be strongly relaxed ($T_1 < 1$ ms) and broadened ($\nu_{1/2} > 600$ Hz) by electron. Resonances in high-spin systems (for example, metMbH₂O) are more severely influenced than those in low-spin systems (for instance, metMbCN). 2D experiments, in order to collect optimum dipolar connectivities for the majority of the protein resonances, often require mixing times that are too long for the coherences of the strongly relaxed nuclei to linger enough to permit build-up of cross peaks. Also, because a 2D data set requires a large amount of computer memory (for example, to process a 512 x 512 data point NOESY requires 4 X 512 X 512 X 32/8 = 4 Mbytes), availability of data processing disk space constitutes limitation on data resolution, especially for sharp lines for protons relatively far from the paramagnetic center. In some cases, when a resolved peak can be selectively irradiated, a 1D NOE may take precedence over a 2D data set because the difference spectrum eliminates peaks that are not affected, and yet retains high digital resolution.

Utility of Saturation Transfer

As introduced earlier, saturation transfer is manifested when the rate of chemical exchange is comparable with or larger than that of the spin-lattice relaxation, R_1 , but smaller than the chemical shift difference between the exchanging resonances. When the rates are comparable, the chemical exchange rate can, in principle, be determined by this method (Sanders & Hunter, 1986). There are many chemical processes, such as conformational isomerization of cyclohexane at 298 K, that occur much faster than the chemical shift timescale; in those cases, the exchange broadening of the peaks may render the technique useless, although low temperature may slow the process sufficiently to allow resolution of individual resonances.

The exchanging species studied in this work have chemical shift timescales of $> 10^4$ Hz, which is much greater than the exchange rate between them. Therefore, this system not only permits this technique, but also avoids off-resonance effects in steady-state 1D difference experiments, and allows easy identification in 2D NOESY experiments. To demonstrate the importance of k_{ex} relative to R_1 , consider the energy level diagram shown in Figure 16. For a representative spin exchanging between two species, metMbH₂O and metMbIm, we must consider the first-order exchange rate constants k_{H_2O} and k_{Im} , and spin lattice relaxation rates of each species, R_{H_2O} and R_{Im} . The diagram also assumes that the spin exchanges without changing its quantum mechanical spin state, hence possesses two independent exchange processes. If we saturate the spin in metMbH₂O, i.e. equilibrizing the spin populations of the higher and lower energy states of metMbH₂O, the effect will be transferred to metMbIm by feeding more population to its higher energy state through k_{Im} . However, if k_{Im} is much slower than R_{Im} , the spin population of metMbIm will have approached Boltzmann's distribution, i.e. equilibrium, thus providing no net perturbation to metMbIm. On the other hand, if k_{Im} is compatible to or much faster than R_{Im} , metMbIm will be saturated significantly or almost completely, respectively. Exchange rates obtained

through this method range from 10^3 s^{-1} to 10^{-2} s^{-1} , with the metMbH₂O : Im system, k_{ex} is 3 s^{-1} to 53 s^{-1} , depending on the temperatures. It should be mentioned that the lower boundary is not accessible by another popular rate-constant determination method based on lineshape fit. At such low rate, lineshape analysis, as an alternative method for determining k_{ex} , becomes highly insensitive.

Status of Assignments

For the minor heme-insertion isomer of metEqMbN₃, 11 out of 22 possible heme ¹H NMR resonances are now assigned. Heme-insertion isomer redistribution of the reconstituted metEqMbN₃ is too rapid to allow detection of the 8CH₃^B to 1CH₃^B cross peak, which is usually the starting point to 'walk' around the porphyrin ring. Nevertheless, NOE patterns to the diamagnetic region and pairwise-exchange between heme-insertion isomer resonances are self-consistent and allow solid assignments.

On the other hand, for the major isomer of metEqMbIm, 15 of the heme peripheral resonances, and one C_βH of His F8 are assigned. In addition, literature assignments for metMbH₂O (Unger et al., 1985) are verified and one was corrected. Figures 12, 13, and 14 all showed connectivities between the literature 4H_α of metEqMbH₂O and 2H_α of metEqMbIm. Either the literature or the metEqMbIm assignment of the proton must be wrong. In the 2D NOESY of metEqMbIm (Figure 9), the 1CH₃ <--> 8CH₃ cross peak, the only one between methyls, is identified; the assignment of 2H_α is then ascertained by its dipolar connectivity to 1CH₃. For the saturation transfer profile in Figure 12 to be valid, the literature assignment of the vinyls must have been reversed. Unger et al. (1985) identified the 4H_α by its characteristic vinyl spin system (as discussed in the Result section), but did not detect the diagnostic vinyl <--> methyl cross peaks.

For the metEqMb1CH₃Im and metEqMb4CH₃Im systems, identical assignments to metEqMbIm are determined from 2D EXSY (Figures 13 and 14) and NOESY/COSY

experiments (Figure 10 shows an example for metEqMb1CH₃Im). Interestingly, although performed and processed under similar conditions, the EXSY cross peaks in the methylated imidazole systems are stronger than their imidazole counterpart. This increase in saturation transfer is attributed to the increase in either k_{ex} (i.e. k_{Im} and k_{H_2O} in Figure 16) or R_1 (i.e. R_{Im} in Figure 16). Since R_1 of protein is governed mainly by the resonance's distance to the paramagnetic center and the protein's tumbling rate (see Equations 1 and 2), both of which are invariant for all three imidazolate systems of Mbs (compare T_1 s in Table VI), increased k_{ex} is the most likely difference between the methylated imidazole and imidazole systems. This can be explained by the extra methyl group on the imidazole ring, introducing steric hindrance in the binding pocket, and increasing the dissociation constant k_{H_2O} . This illustrates the utility of saturation transfer in providing evidence for ligand dynamics in proteins.

Comparison of Spin-States of metMbN₃ and metMbIm

T_1 values in Table VI present an interesting question regarding the estimation of spin-states from the hyperfine shifts of the heme methyls. ¹H NMR spectra of metEqMbIm clearly indicates broader linewidths for the methyls than those of the metEqMbN₃ counterpart (compare, for example, Figures 5 and 7). Literature (La Mar et al., 1980) suggested similar high-spin character (~30%) in both metSwMbN₃ and metSwMbIm, which are in thermal equilibrium of $S = 1/2 \leftrightarrow S = 5/2$. Although the 5CH₃ of metEqMbIm is much more downfield shifted and broader than the metEqMbN₃ counterpart, the averages of methyl chemical shifts at pH 7 and 298 K for both species are quite compatible, at 22.4 ppm and 23.1 ppm for metEqMbIm and metEqMbN₃, respectively -- supporting evidence that they are nearly spin equivalent. Nevertheless, comparison of their T_1 s from Table VI suggests that metMbIm is in a much lower spin-state than metMbN₃. Spin-lattice relaxation rates, T_1 s, like hyperfine shifts, are sensitive

indicators of the heme pocket geometry based on the interactions of individual heme pocket residues with the heme moiety, as well as the spin density of the heme peripheral protons (La Mar, 1979). Increasing high-spin character allows more efficient relaxation mechanism of the affected protons through higher electron density. However, even in similar spin states, for instance, metMbH₂O and metMbSCN -- both of which are purely high-spin, differential hyperfine shifts are observed which imply that the nature of the axial ligand in a given spin-state can modulate the extent of equatorial spin transfer (La Mar et al., 1978). Hence, T₁s of heme pocket resonances, including those of the heme methyls, are probably more reflective of the spin state of the ligand. The fact that metMbIm is lower spin than metMbN₃ is surprising because metMbIm exhibits generally broader linewidths and has higher dissociation rate than metMbN₃, from the ability of the former but not the latter to involve in saturation-transfer with metMbH₂O. As demonstrated in Chapter IV, the line-broadening effect, especially that of the 5CH₃ and 1CH₃ of metMbIm, is a consequence of orientational disorder of the exogenous ligand; this influence may be the predominant factor in governing the methyl linewidths in metMbIm, thus masking the fact that it is mostly low-spin. Traditionally, SwMb has been the species to study in various ligated states (metSwMbIm was the only species studied by ¹H NMR, Budd et al., 1979), which explains the inconsistency between the linewidths of heme methyls and T₁s in the case of metMbIm, because metSwMbIm stabilizes orientationally disordered intermediate more than metEqMbIm (Chapter V), which does not exhibit as severe methyl line-broadenings.

The revelation that Im is a stronger-field ligand than N₃⁻ raises question as to why Im dissociates much more readily from the heme pocket. The discrepancy must result from the differential interactions between the ligands and the protein matrix. Perturbations inflicted on predominantly and purely low-spin Mbs by the protein matrix include magnetic anisotropy and rhombic nature of heme from the coordination of Fe to proximal His F8 (La Mar, 1979). Although models have shown that the dipolar shifts of rhombic origin are

insignificant in mostly and purely low-spin systems (La Mar et al., 1978), the transfer of π spin density from the axial ligand or protein residues to heme is pivotal in the manifestation of electron-nuclear interaction (Budd, 1979). X-ray crystal structure of metMbN₃ (Stryer et al., 1964) found that N (of azide)-Fe bond angle is approximately 111°, close to what is expected for a covalent bond for azido compounds (Hughes, 1935; Pauling & Brockway, 1937). Donation of one of the lone-pair electrons from N₃⁻ to Fe lends the formation of a σ covalent bond of the sort (Pauling, 1960): $\text{Fe}-\text{N}=\overset{+}{\text{N}}=\overset{-}{\text{N}} \leftrightarrow \text{Fe}-\overset{-}{\text{N}}-\overset{+}{\text{N}}\equiv\text{N}$. N₃⁻ is also showed in its crystal structure to adopt a conformation such that hydrogen-bonding with the ring NH of distal His E7 occurs with the same nitrogen on N₃⁻ that is covalently bonded to Fe, to optimize binding and reduce steric hindrance. Both the covalent and the hydrogen-bonding characteristics contribute to the tight binding of N₃⁻, while the lack of π spin density contribution from N₃⁻ results in the high spin nature of metMbN₃, as demonstrated by the short T₁s of heme methyls.

The X-ray crystal structure of metSwMbIm (Lionetti, 1991) revealed that the exogenous Im exerts steric strain to the distal pocket by causing the partially 'open' conformation of distal His E7. This conformation allows the facile exchange of Im with the bulk solvent, a criterion for saturation-transfer. On the other hand, the interaction of the Im π orbital with the partially filled d π orbital of Fe contributes to the more low spin character of metMbIm, despite its broader linewidths, than metMbN₃. Because the proximal His F8 is also capable of such π electron transfer, the larger hyperfine shift of the 5CH₃ in metMbIm may be attributed to the orientation of His F8 relative to the heme plane, which is essentially independent of the bond length between the heme Fe and His F8 (Peyton et al., 1989). The g-tensors of His F8 have frequently been used to quantify the influence of an axial ligand on the in-plane asymmetry of the heme electronic structure (Soltis & Strouse, 1988), which underscores the involvement of His F8 in modulating the electron-nuclear interaction. In the crystal structure of metSwMbIm, the angle ϕ , defined

as that between the projection of His F8 imidazole plane onto the heme plane and the N_{II} -Fe- N_{IV} axis (see also Figure 4), is 47° (Lionetti, 1991), as compared to 19° for metSwMbCN (Phillips, 1978). The difference in the angles ϕ is significant enough to cause an anomaly in the respective hyperfine interactions; therefore, even though T_1 s of some heme methyls of metMbIm are almost compatible to those of metSwMbCN (~ 100 ms), the spread and average chemical shifts of heme methyls are indicative of the latter being pure low spin.

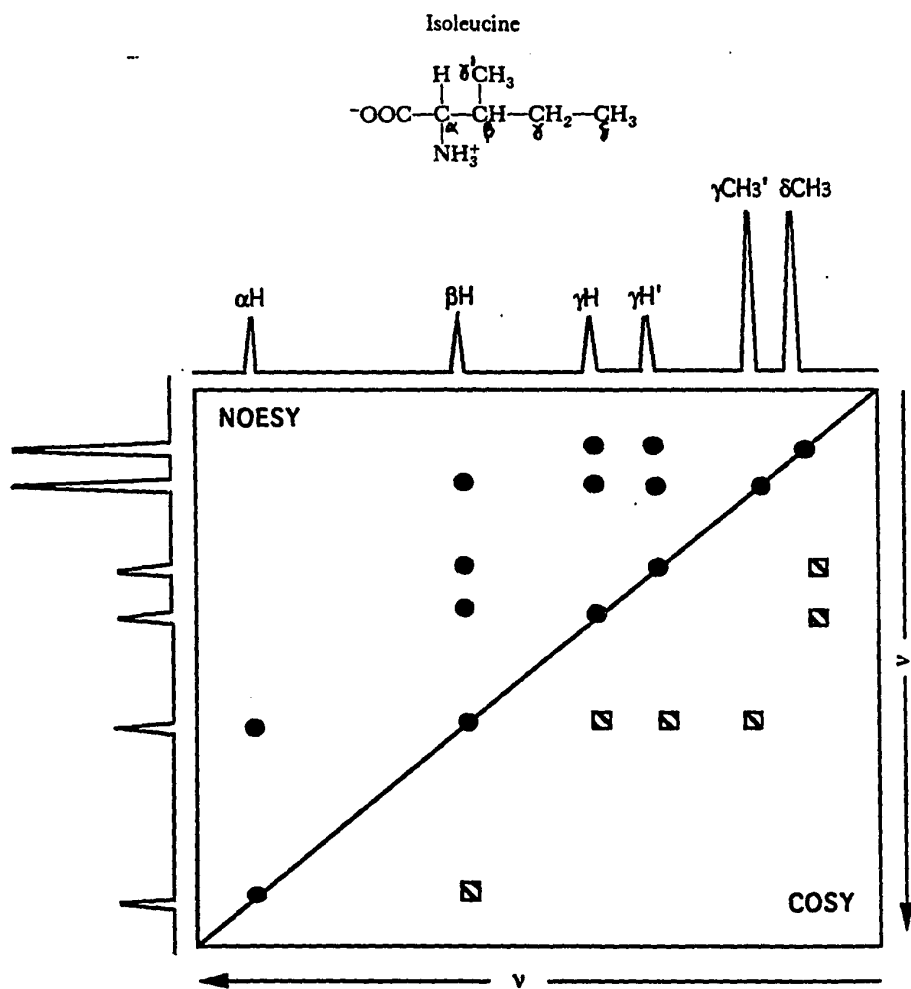


Figure 5. COSY/NOESY in a nut shell. Dashed squares, and solid circles represent COSY, and NOESY cross peaks, respectively, between the indicated resonances from Ile.

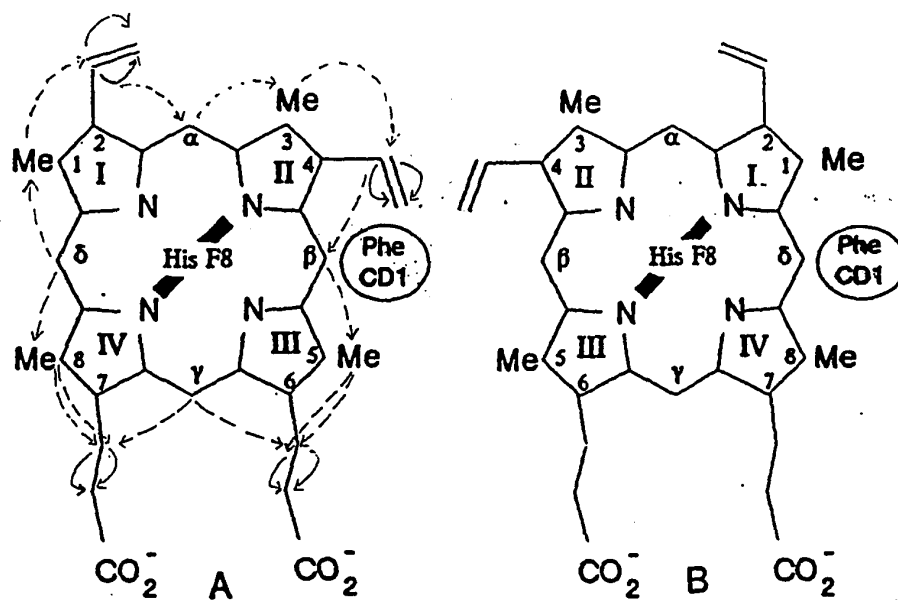


Figure 6. The numberings and labels of peaks correspond directly to all the NMR spectra hereafter. A and B are the major and minor heme insertion-isomers, respectively. The dashed, solid, and wavy arrows denote dipolar and scalar interactions, expected between the protons.

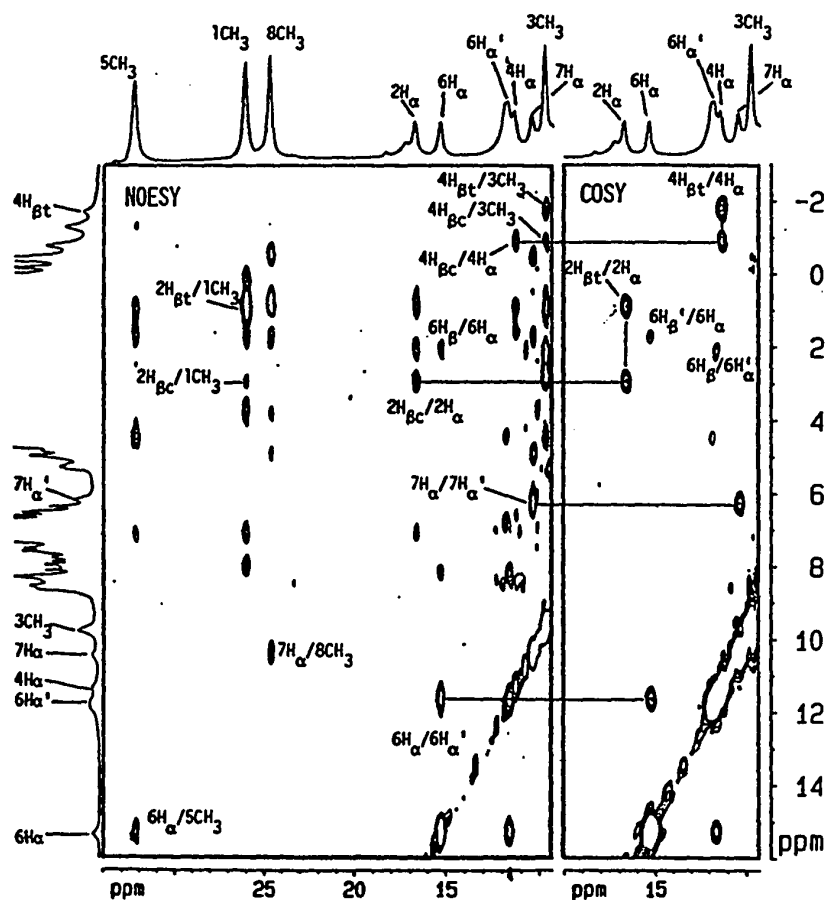


Figure 7. Phase-sensitive NOESY (left) and magnitude COSY (right) for native metEqMbN₃ in ²H₂O at 25°C and pH7.0. The correlations indicated by the horizontal lines between the two data sets show cross peaks which are superimposable, arising from interactions between identical proton sets. The vertical line connects cross peaks from the 4-vinyl H_{Bc,t} (Peyton, 1991).

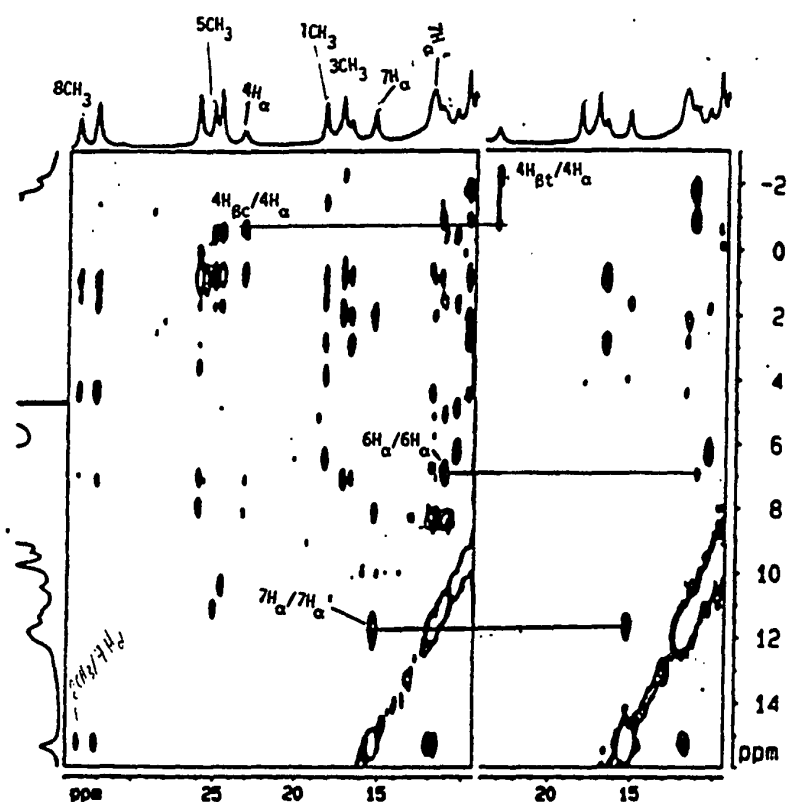


Figure 8. Phase-sensitive NOESY (left) and magnitude COSY (right) for reconstituted metEqMbN₃ in ²H₂O at 25°C and pH7.0. The correlations indicated by the horizontal lines between the two data sets show cross peaks which are superimposable, arising from interactions between identical proton sets. The vertical line connects cross peaks from the 4-vinyl H_{βc,t}.

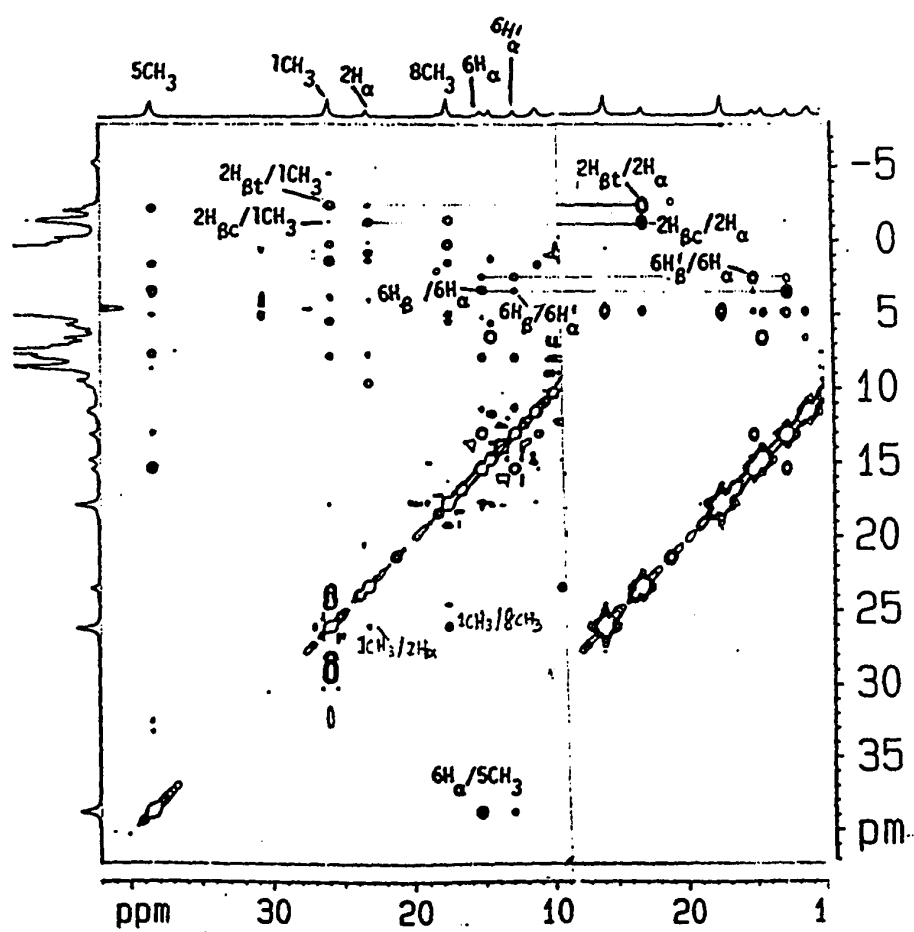


Figure 9. Phase-sensitive NOESY (left) and magnitude COSY (right) for metEqMbIm in $^2\text{H}_2\text{O}$ at 35°C and pH 7. The correlations indicated by the horizontal and vertical lines are as identified.

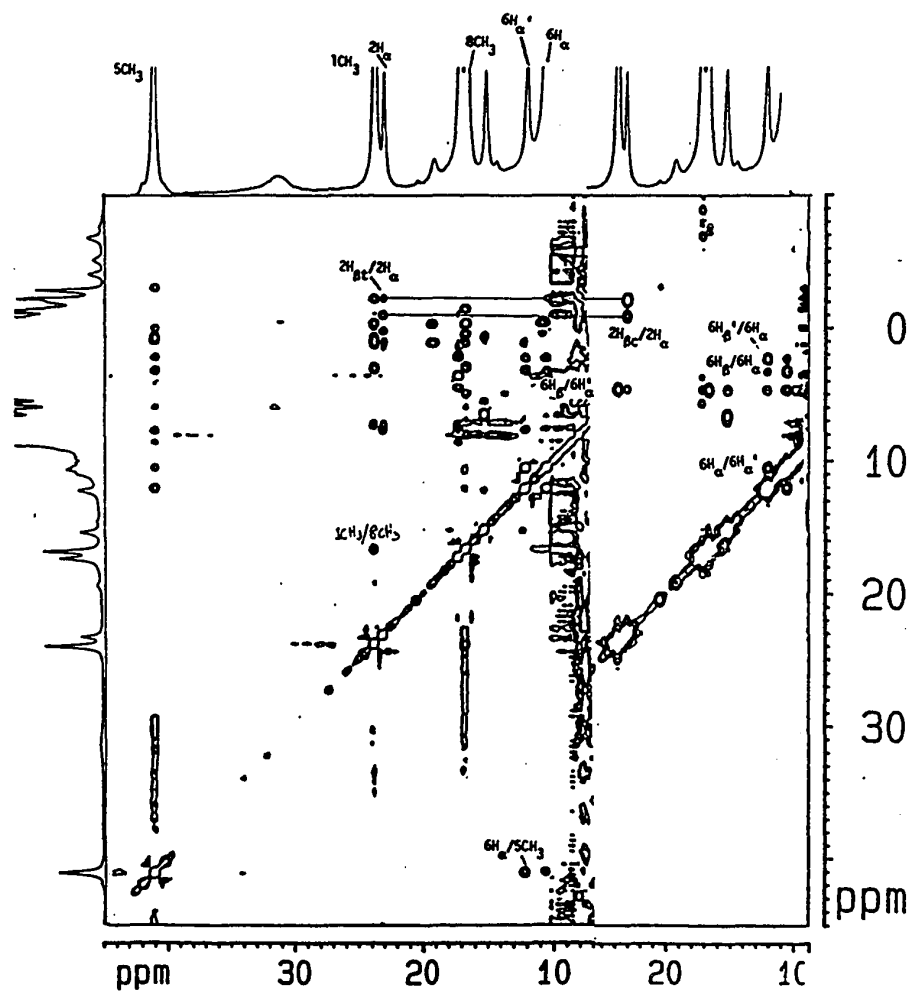


Figure 10. Phase-sensitive NOESY (left) and magnitude COSY (right) for metEqMb1CH₃Im in ²H₂O at 25°C and pH 7. The correlations indicated by the horizontal and vertical lines are as identified.

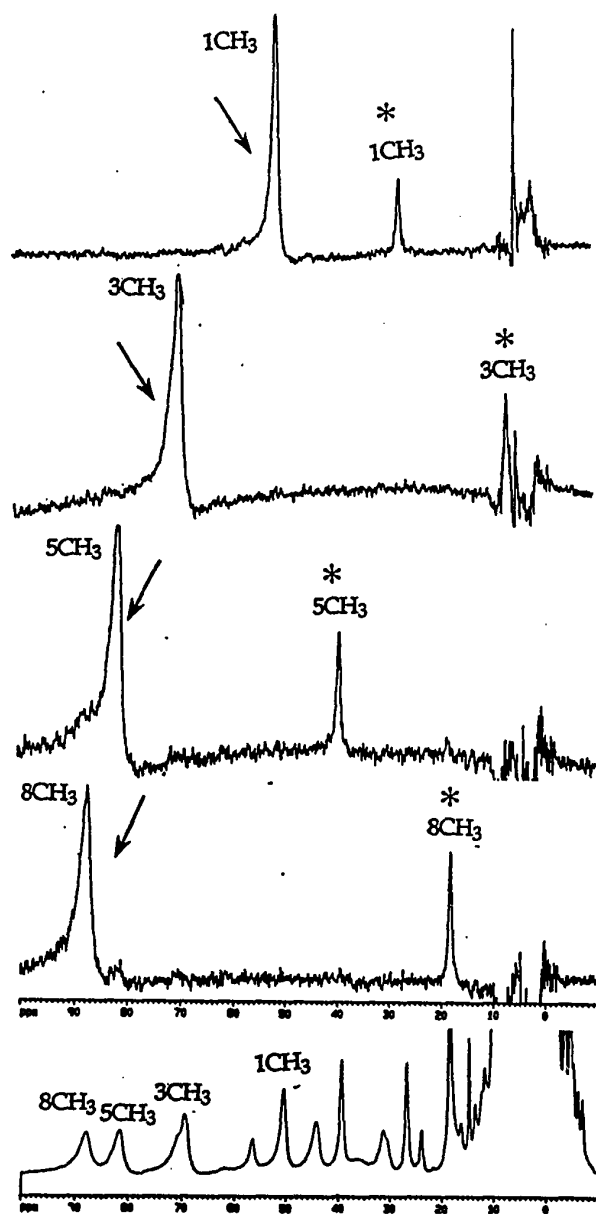


Figure 11. 400-MHz ^1H NMR 1-D difference spectra of metEqMbH₂O : metEqMbIm at 308K and pH 6.2. A. Reference spectrum of 1:1 metEqMbH₂O:Im. B-E Difference traces between one where a selected resonance is saturated and the reference trace. On a given difference trace, the arrow indicates the resonances that was saturated, and the asterisk shows the resonance that exchanges with the saturated peak.

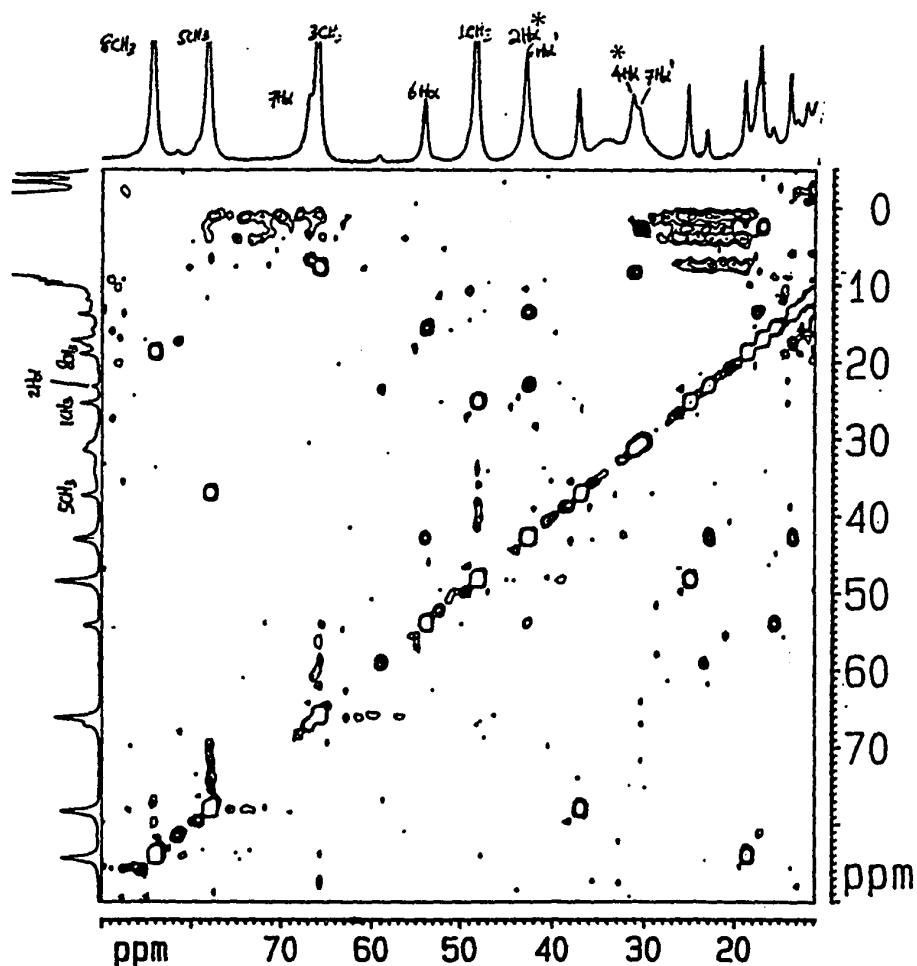


Figure 12. Phase-sensitive NOESY for 1:1 metEqMbH₂O:Im at 50°C and pH 6.2. The assignments on the horizontal and vertical axes are those of the metEqMbH₂O and metEqMbIm, respectively. The sample was made by titrating metEqH₂O with aliquots of Im by NMR, until the correlated peaks are comparable in sizes. Asterisks marked the previously incorrectly assigned peaks; labeled here are assignments made from this work.

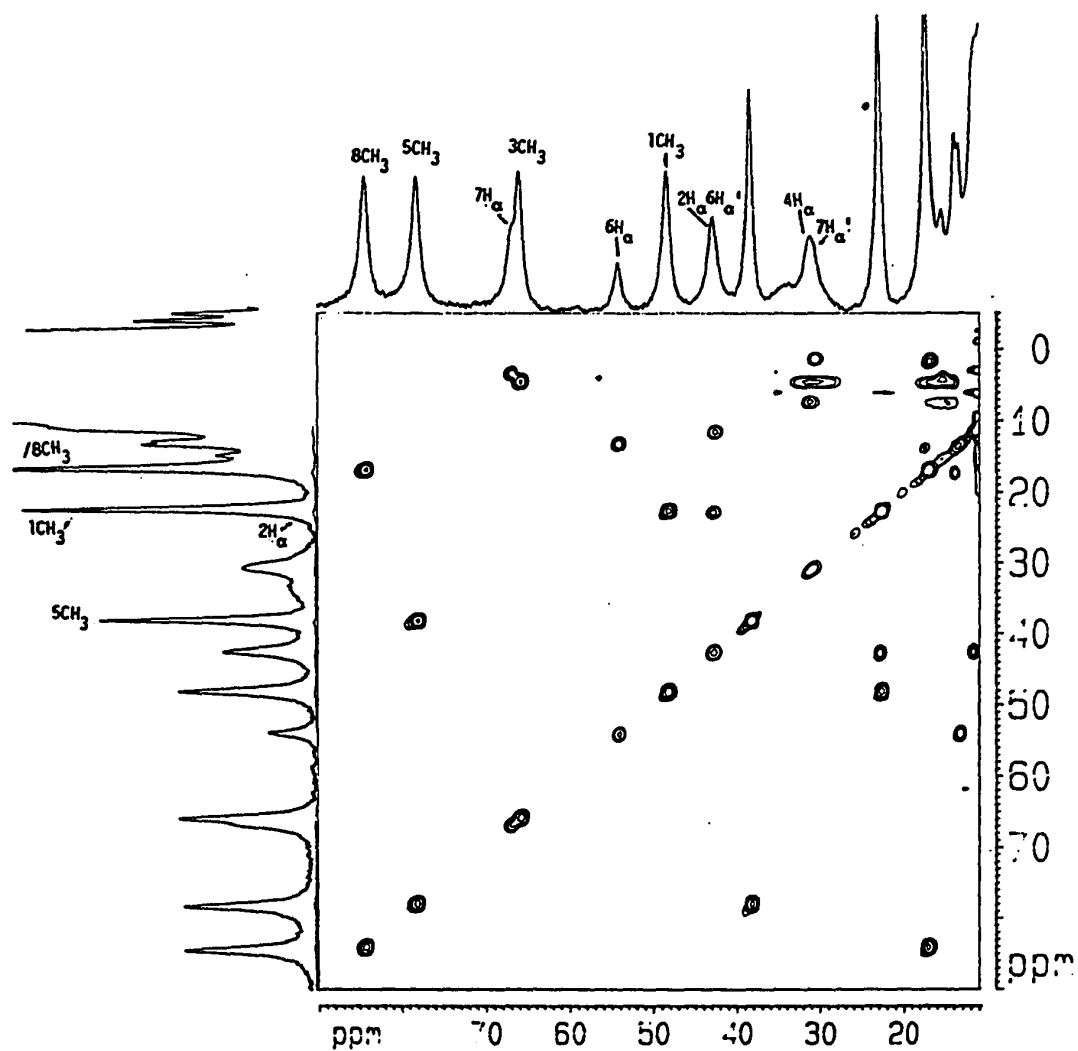


Figure 13. Phase-sensitive NOESY for 1:1 metEqMbH₂O:1CH₃Im at 50°C and pH 6.75. The assignments on the horizontal and vertical axes are those of the metEqMbH₂O and metEqMbIm, respectively.

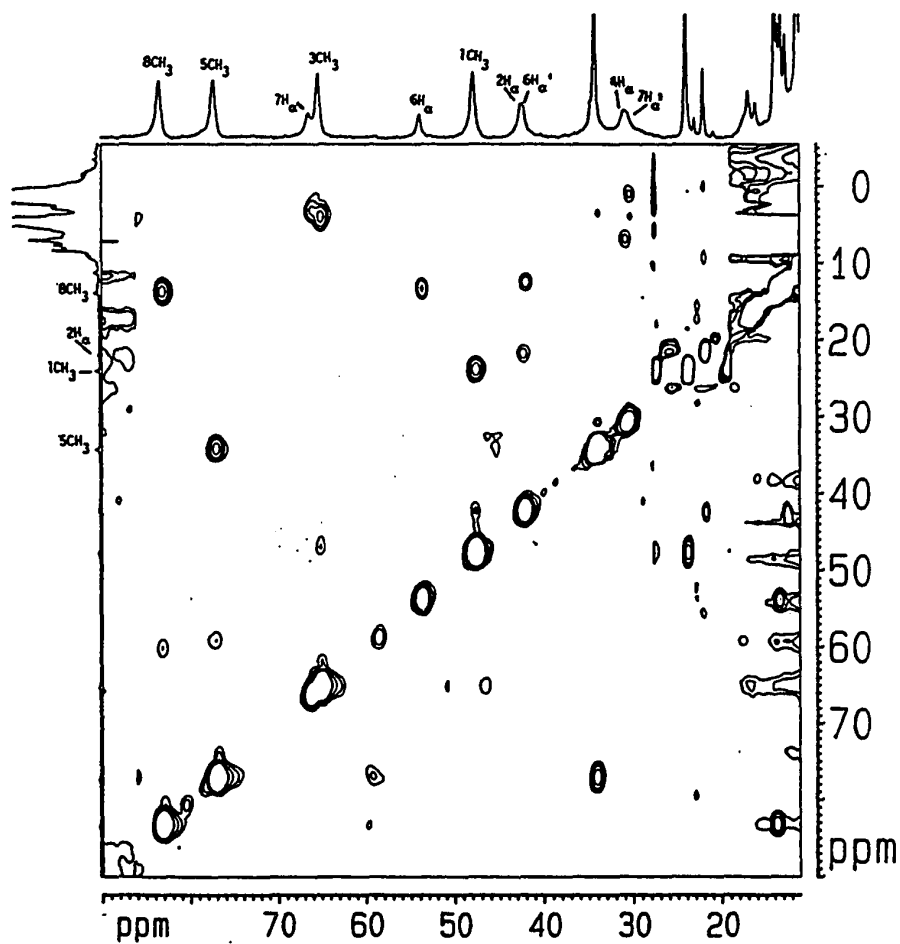


Figure 14. Phase-sensitive NOESY for 1:1 metEqMbH₂O:4CH₃Im at 50°C and pH 6.2. The assignments on the horizontal and vertical axes are those of the metEqMbH₂O and metEqMbIm, respectively.

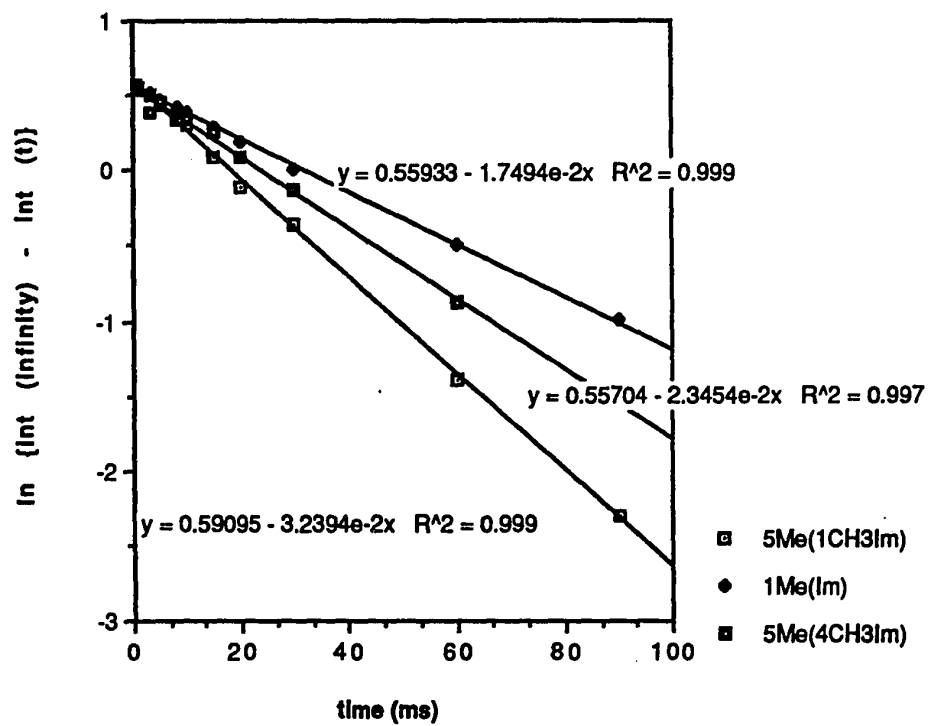


Figure 15. T_1 plot ($\ln\{\text{int}(\infty)-\text{int}(t)\}$ vs time in ms) of some resonances, as indicated, of metEqMbX, where X is indicated in the parentheses on the plot. Inverse of the slope of each line corresponds to the respective T_1 in ms.

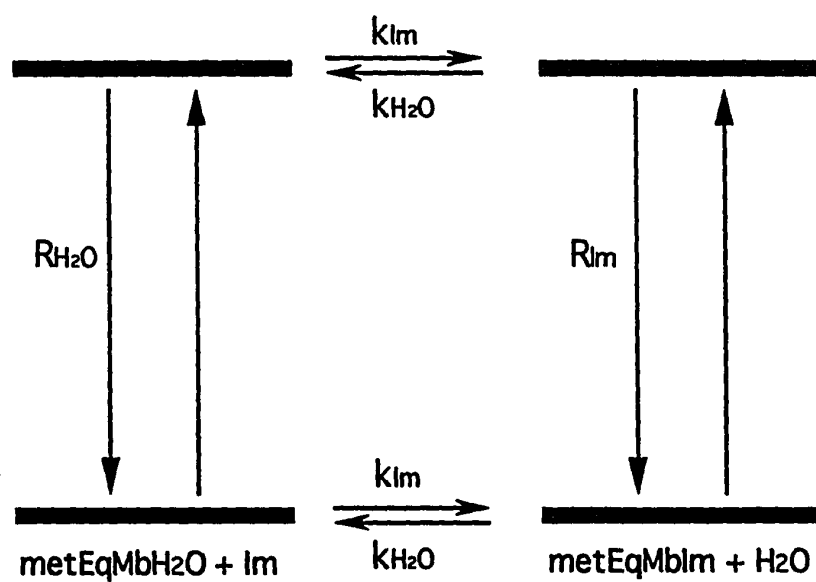


Figure 16. Energy level diagram for saturation-transfer. The ground states in both species are equivalent when their concentrations are equal.

CHAPTER IV

PROTON NUCLEAR MAGNETIC ASSIGNMENTS OF PROTONS FROM Fe-COORDINATED LIGANDS FOR VARIOUS IMIDAZOLATE MYOGLOBINS

In this chapter, the binding sites of bis-imidazolate Mb systems are characterized. In nature, there are numerous biological hemoproteins, such as hemopexin and cytochrome b₅, which have bis-imidazole coordination to a heme iron. Hemopexin is the strongest heme-binding protein known so far, and possibly plays significant role in detoxification by scavenging excess heme in the serum (Vincent et al., 1988). Excess heme in the human serum is ultimately broken down to biliverdin, then excreted.

Myoglobin (Mb) bound with imidazole (Im), or an Im-derivative, as the exogenous ligand makes a good model for bis-histidinyI coordinated heme proteins because Mb has an invariant coordination of heme iron to the proximal His F8, and is among the most extensively studied proteins by X-ray crystallography. For hemoproteins that cannot be successfully crystallized for X-ray analysis, or are too large for complete solution state elucidation by NMR (so far, NMR technology by protons only allows structural elucidation of proteins up to only ~10 kDa), structural determination of the active site seems the most logical stepping stone to understanding the protein. ¹H NMR studies of metMbCN (Emerson & La Mar, 1990) have revealed an upfield peak that corresponds to the ring C₄H of proximal F8 His. Our work on metMbIm has shown broad upfield resonances, similar to those of the CN⁻ counterpart, that presumably correspond to the resonances of the axial ligands. Using different methyl imidazoles as probes, various geometries in which bis-imidazolate heme exists are suggested.

Lineshape analysis simulation of the 5CH_3 resonances of metEqMbIm and metPSwMbIm at low temperatures allowed the determination of the rates of ring equilibration of bound Im. Intrinsic structural differences between the binding cavities of the two species were implicated. This chapter illustrates that much can be learned from the ^1H NMR studies of the binding sites of macromolecules.

RESULTS AND DISCUSSION

Investigation of Upfield Peak(s) in the Imidazole Complexes

Both metPSwMbIm and metEqMbIm show broad upfield resonance(s). At 298K, while the EqMb complex exhibits only one broad upfield peak, *f*, the PSwMb counterpart shows two, *a* and *b*. To verify this difference between the species, variable temperature NMR experiments were performed. Within the temperature range of 298 K to 313 K, there is no divergence of broad peaks in both cases. The two broad resonances of metPSwMbIm become more apparent at 303 K (see Figure 17). Included in Figure 17 are asterisked peaks that arise from the high-spin metMbH₂O, the presence of which is unavoidable at $\text{pH} < 7$.

Irradiation of the single upfield peak, *f*, in metEqMbIm shows a strong effect to two sharp peaks, *x* and *y*, in the diamagnetic envelope, as shown in Figure 18; other broad peaks in Figure 18C may be NOEs. Peaks *x* and *y* are so sharp that they must come from a small molecule, and their chemical shifts correspond to those of ring CHs of free imidazole (Figures 18 and 20, respectively). Therefore, the irradiated upfield resonance is identified as one of the ring CHs on the bound ligand. By virtue of the fast on/off rate of imidazole (see Utility of Saturation Transfer in Chapter III), irradiation of the bound ring CH induces saturation transfer to the free ligand. Because saturation transfer is observed to both the C₂ and C_{4,5} (two-proton integral at identical chemical shift) Hs of free imidazole, no specific assignment is possible at this point. However, it is interesting to note that even

though y ($C_{4,5}H$ of free ligand) is a two-proton peak, its effect is smaller than the one-proton x (C_2H of free ligand); also, integration of the broad peak, albeit highly uncertain because of its broadness, gives about two protons with respect to the three-proton methyls. It is therefore possible that f is a fortuitous chemical shift convergence of ring CH on His F8, and/or fractional populations of x and y (predominantly x). To differentiate between these postulates, experiments were performed in which variable sites on f were irradiated (not shown); no apparent difference was detected when compared to Figure 18, which argues for the fractional population of two conformations. Rapid equilibration of the bound imidazole ring about the pseudo C_2 axis can account for the saturation transfer to both x and y (as in Figure 19A). However, from the ratio of saturation transfer to x and y , one conformation must be favored. To verify this postulate, more experiments on metEqMbIm, formed with deuterated Im were performed, as discussed below. In addition to saturation transfer, through space correlation NOEs to the protein matrix are also apparent. Nevertheless, because extremely high decoupler power was required to irradiate the broad upfield peak, and the NOEs to the diamagnetic region are so close in chemical shift to the irradiated resonance, deconvoluting real from off-resonance artifacts is a difficult task. On the other hand, NOEs to the paramagnetic region helps identify the irradiated peak. Direct evidence for two conformations for the bound imidazole can also be obtained from the broadenings, or even splittings, of heme peripheral protons (most apparently of heme methyls because of intensity).

In light of the fact that the ring C_2H of free imidazoles exchanges rather rapidly with solvent protons, selective deuteration can be achieved by incubating the ligands in deuterium oxide before addition to Mbs. In this experiment, samples of excess imidazole, 1-methylimidazole, and 4-methylimidazole in deuterium oxide, all at $pH > 10$, were equilibrated in temperature bath of $25^\circ C$ for Im, and $67^\circ C$ for 1- and 4- CH_3 Im. Spectra at different times were recorded to verify the exchange (time intervals are shown on the

spectra in Figures 20 to 22). The following simple but extremely illuminating experiments identify, as well as confirm, some assignments.

MetEqMbIm- C_2^*H gives the spectrum shown in Figure 23B. Upon close inspection, the ratio of the upfield peak f' to methyl peak is smaller than in metEqMbIm, with an integral of about 1, as opposed to 2 in the metEqMbIm (non-deuterated). Figure 24 shows the saturation transfer profile on irradiating f' with various delay times. Even at the longest delay time (Figure 24E), when the induced effect on x and y should be greatest, there is no significant saturation transfer to x . Possible assignments for f' include the ring $C_{4,5}H_s$ (y) of the bound Im, ring CHs of His F8 and *meso* Hs. Figure 24E shows saturation transfer of f' to y , which confirms its likely identity to be the $C_{4,5}H$ of Im. Furthermore, no noticeable NOEs to any heme peripheral or other hyperfine-shifted resonance was induced (Figure 25). More compelling evidence for this assignment is the Fe-H distance, calculated based on the non-selective T_1 , determined to be ~ 1 ms by t_{null} method (Harris, 1989; Sanders, 1988), of f' by inversion recovery (Equation (6)) experiment. From the structural coordinates of MbCO (Kuriyan et al., 1986), the distance from the heme methyls to Fe is approximated at 6.1 Å. The T_1 experiment of Figure 15 (Table VI) determined the T_1 of $5CH_3$ of metEqMbIm to be 31 ms; correlation as outlined by Equation (11) thus extracted the distance of Fe- H_f at 3.4 Å. Comparison of the data to the crystal coordinates of heme pocket residues dictates that this distance is analogous to that of the Fe to C_2H of His F8 (at 3.42 Å), which is compatible to the number of bonds away from Fe to C_5H of the bound Im. The assignments of f and f' are likely those of the two conformational isomers of the bound Im as a result of the rapid ring equilibration. Due to the orbital symmetry of the bound ligand relative to the heme plane, and by analogy to metSwMbCN (Lecomte & La Mar, 1990), two ring protons from the same residue should be hyperfine-shifted in the opposite direction, i.e. one upfield and the other downfield. Both the ring C_2H and C_5H of the bound Im are shifted upfield; therefore, they must be

from different conformers. From the larger peak size of the saturation transfer from **f** to **x**, as compared to **y** (Figure 18), the major isomer is most probably when the upfield resonance is the ring C₂H of the bound Im.

For metPSwMbIm, one possible scenario is that one of its two broad upfield resonances is from one His F8 ring CH, while the other arises from the bound imidazole. Thus, similar saturation experiments can not only shed more light on the binding model of imidazole complexes, but also compare the heme pocket geometry in both proteins.

Results from irradiation of the two upfield peaks of metPSwMbIm at 313K and 303K with different parameters (as indicated in the legend) are compared in Figures 26-28. Because saturation transfer is a function of both the exchange rate and T₁, a longer relaxation delay will allow the resonances with long T₁s to relax to nearer full intensity; also, because the free ligand peaks are in excess, lower power with possibly longer saturation time (thus more selective saturation) may help reduce the overall contribution of dispersive effects that arise from the Bloch-Siegert effect (Sanders, 1988). At 313 K (Figures 26), the most upfield peak at -9.0 ppm, labeled **a**, shows strong saturation transfer to both kinds of free imidazole peaks, designated **x** (C₂H) and **y** (C_{4,5}Hs), whereas the resonance at -6.7 ppm, labeled **b**, has a preferential effect on **y**. Peak **a** most likely is a result of rapid equilibration between **x** and **y**, therefore both of which are affected. On the other hand, **b** correlates much stronger to **y**, dictating its identity to be C_{4,5}Hs. Because a residual effect from **b** to **x** is visible, further experiments with a longer relaxation delay and lower saturation power were performed at 303 K. If the saturation transfer to the free ligand is real, then a stronger effect to **x** should result because small molecules have longer T₁s. In all, this saturation data at 313 K helps provide more evidence for the rapid equilibration of the bound ligand in metMbIm, although it offers no additional information on the specific identities of these resonances.

At 303 K (Figures 27, 28), peaks **a** and **b** of metPSwMbIm became more resolved. Figure 27 presents data from experiment repeated with lower saturating power to reduce off-resonance effects. It is apparent that **a** induces stronger saturation transfer to **x**. The weaker effect by **b** is inevitable from its extreme broadness which spans over both **a** and the metMbH₂O peaks. Because **b** is so broad, higher saturating power and more nonspecific saturation pulse may be necessary to observe its saturation transfer effect; however, in doing so, severe artifacts would be generated from off-resonance effects to nearby resonances. From lability studies of these species (Chapter VII), it was found that the slowest bound ligand equilibration occurs at pH ~9, judging from the broadest methyl linewidths. Therefore, saturation experiment was repeated at pH 9 and 303 K, as shown in Figure 28, with lower saturating power, longer relaxation delay, and more specific saturation. These parameters should optimize the saturation transfer effects by increasing saturation to **x** and **y**, if any, and reducing off-resonance effects. At pH 9, because there is only one broad upfield peak, several irradiations were applied across the broad overlapping resonances, assuming that **a** and **b** converged. Figure 28C shows the saturation to **y** from irradiating slightly off-center of the upfield peak, which justified the assumption that there are both **a** and **b** under the peak. Below, selective isotope-labeling of the ring CH of free imidazole allows confirmation and extension of the assignments of the resonances.

Figure 29 shows the most upfield peak, **a**, of MetPSwMbIm decreased significantly in intensity upon deuteration, which assigns the peak to ring C₂H of bound imidazole. Comparing this and earlier saturation-transfer results at 303K (Figures 27, 28), **b** can be confidently assigned to ring C_{4,5}H of bound imidazole. In the earlier saturation-transfer experiment shown in Figure 27, although both upfield peaks show considerable transfer to both types of ring CHs on the ligand, **a** shows the strongest effect to free C₂H. This is consistent with the deuteration study shown in Figure 29, where **b** shows strongest effect to C_{4,5}H. The spectrum at 313K also shows the most upfield peak to be ring C₂H

of the bound Im (Figure 30). As in the case with metEqMbIm, **a** and **b** are the ring CHs of the conformational isomers of the bound ligand. From the bigger peak size of **a** than **b**, it is likely that the major isomer is when the upfield resonance is the ring C₂H of the bound Imidazole.

Investigation of upfield peak(s) in the 1- and 4-methylimidazole complexes

Unlike imidazole, the methylated imidazole complexes of both EqMb and PSwMb exhibit similar features in the upfield region. MetMb1CH₃Im complex shows one apparent broad upfield peak, while metMb4CH₃Im complex gives rise to two broad peaks in the temperature range studied, i.e. 298 K to 313 K (not shown). The results presented below pertains to the PSwMb species only, although the same trend follows for EqMb.

As illustrated in Figure 31, irradiation of the upfield peak, **g**, of metPSwMb1CH₃Im at 313K gives rise to two sets of saturation transfers. The free ligand has three distinct ring protons, designated **x** at 7.9 ppm (C₂H), **y'** at 7.3 ppm (C₅H), **y''** at 7.25 ppm (C₄H), and one aliphatic resonance, **w** at 3.8 ppm (1-CH₃) (compare with the spectrum of free 1CH₃Im in Figure 22; however, ring C₄ and C₅H of the excess free ligand appear to coincide when Mb is the sample because processing of the spectrum was optimized for broad paramagnetic peaks at line-broadening of 20 Hz, which is on the order of the chemical shift difference between the peaks observed if the data is processed with a line-broadening of 0.2 Hz). Only off-resonance effects were observed in Figure 31, possibly because of the large sizes of **y'**, **y''**. These peaks are sizable and close to the resonance irradiated, which causes the dispersive appearance of the peaks in the difference spectrum due to the Bloch-Siegert effect (Sanders, 1988). Experiments done at various relaxation delays with SUPERWEFT pulse sequence (Equation (9)) are shown in Figures 31 and 32. These experiments were performed on metPSwMb1CH₃Im formed from deuterated 1CH₃Im at C₂H position (see Figure 22) to reduce the off-resonance effect from

x. A delay time of 100 ms used in Figure 32 produced slight effect from residual C_2H ; more importantly, distinctive saturation transfers to y' and y'' were also observed. Other than reducing the off-resonance effect from the excess free ligand, this saturation profile implies exchange between multiple conformations of the bound ligand.

The bound ligand in metMb1CH₃Im may undergo bound-Im ring-flip despite steric hindrance from its extra methyl group (as illustrated by its slight methyl broadening in Figure 47). Figure 19 shows that the geometries of 1- and 4-methylimidazoles might be similar with respect to the location of the extra methyl group in the protein matrix, especially in light of the lack of line-broadening of the heme methyls in both of these species as compared to imidazole Mb complexes. Nevertheless, the non-coordinating ring N of metPSwMb1CH₃Im is positively charged regardless of pH, while that of metPSwMb4CH₃Im can be protonated at pH ~ 6 (assuming the pK_as of bound imidazoles are similar to that of distal histidine at ~pK 5.5).

This electrostatic property of metPSwMb1CH₃Im may dictate the orientation of the ring such that the charged group can participate in salt-bridge interaction with nearby residues in the protein crevice. From the X-ray crystal structure of metSwMbIm (Lionetti et al., 1991), the carboxylate of Asp E3 is hydrogen bonded to the N_εH of Arg CD3, which is involved in salt-bridging with heme 6-propionate; this triad interaction, and the size of the 1CH₃ imidazole ligand may bring the other carboxylate of Asp E3 to the vicinity of the positive charge of ligand for electrostatic interaction. There is no other distal pocket residue capable of such interaction. In this respect, there may be a difference in the conformation of the ligand, or in whether there are two conformations, rather than in metPSwMb4CH₃Im. If this scenario is true, then metMb1CH₃Im should be pH-independent, i.e. no change in heme methyl linewidths; whereas metMb4CH₃Im will be pH-dependent as the ring NH on the bound 4CH₃Im is protonated/deprotonated at appropriate pHs. Figures 33 clearly demonstrates the variance of the methyl linewidths of

metMb4CH₃Im at different pHs. Figure 33 shows that at pH 6.5, metMb4CH₃Im shows sharper 5CH₃ and 1CH₃ peaks, as noted by the decrease in their heights as well as linewidths at half-height. This result verifies the postulate of electrostatic interaction of the bound ligands with nearby pocket residue, because at lower pH, the non-coordinating ring N of metPSwMb4CH₃Im is protonated and thus positively charged, like metPSwMb1CH₃Im. More saturation-transfer experiments at 313 K with lower power and/or different sequence were performed on deuterium exchanged metPSwMb1CH₃Im in an attempt to verify the assignment.

MetPSwMb1CH₃Im formed from reconstitution with deuterated ligand in the C₂H position (Figure 22) was indistinguishable from that formed with non-deuterated ligand (see Figure 34). Therefore, other than asserting that *g* is not the C₂H of the bound ligand, not much more information is offered. Although because of the overlap of *g* with another peak, assigned to be C₇H of Ile FG5 in Chapter VIII, the T₁ obtained is highly uncertain, the determination of T₁ for *g* at ~0.5 ms extracted $r_{\text{Fe-Hg}} \sim 3.8 \text{ \AA}$ by Equation (11), which limits the option for possible candidates of *g*. Comparison of the distances with those of heme *meso* protons (4.5 Å), ring C₂H (3.42 Å), and C₄H (3.33 Å) of His F8 from MbCO crystal coordinates (Kuriyan, 1986), and also the fact that no paramagnetic NOE was observed from saturating *g* (not shown), suggest that *g* is most likely the ring C_{4,5}H the bound ligand, which is also supported by the saturation-transfer profile observed in Figure 32.

Irradiation of the two upfield peaks of 4-methylimidazole complex is probably the most instructive of all the imidazolate studies. The saturation transfer trends are compared between two experiments done with different irradiating powers. With high-power irradiation, significant saturation transfer is detected to one single ring CH, *x*, of the free ligand from the resonance at -13.7 ppm, labeled *h*. On the other hand, the peak at -9.2 ppm, labeled *i*, shows little effect to both free ring CHs (Figures 35C, 36C). Postulating

that the little effect may have arisen from off-resonance effect, less power was then used. In this experiment (Figure 35), peak **h** exhibits similar saturation transfer pattern, while **i** shows no effect at all. Figure 36 further verifies **i** to have no saturation transfer at longer relaxation delay.

This data clearly demonstrates not only that there is one dominant conformation to the bound ligand in the 4-methylimidazole system because only one dominant saturation transfer was observed, but also identifies peak **h** as the ligand ring C₂H; this is further supported by selective deuteration data below (**x** is assigned ring C₂H of the ligand in the free ligand spectrum in Figure 21), and peak **i** as His F8 ring CH (may be C₄H because in metSwMbCN (Lecomte & La Mar, 1991), the upfield peak was found to be His F8 ring C₄H). Additionally, the T₁ of **i** was determined to be 0.72 ms (Table VI) at 308K, which places it at a distance 3.37 Å from Fe, most closely correlated to His F8 ring C₄H in metSwMbCN (3.33 Å). This complex is especially important because 4-methylimidazole, among the imidazolate choices, most closely resembles the structure of histidine.

Reconstitution to form ligand-deuterated metPSwMb4CH₃Im merely confirmed the earlier finding that peak **h** corresponds to the ring C₂H of bound ligand, because this resonance is totally gone after deuteration. Figure 37 demonstrates clearly the power of this deuteration experiment in giving direct assignments.

Assignment of an additional downfield methyl peak in metPSwMbXCH₃Im, where X=1,4

Figure 38 displays the spectra for the various imidazolate PSwMbs. In comparing the downfield region of various imidazolate species, metPSwMb-1CH₃ and -4CH₃Im exhibit an extra 3-proton downfield peak in the 10-to-20 ppm region relative to the imidazole adduct. By correlation to the assignments metEqMbIm in Chapter III, one of the methyls is the heme 8CH₃, whereas the other one can be either the 3CH₃ of heme, or the

methylys from the bound ligand. By selectively saturating the two adjacent methyl peaks, Figures 39 and 40 clearly identify the peaks, **j** and **k** as the 1- and 4CH₃ on the ligand, respectively. According to Equation (12), this translates to a paramagnetic shifts of ~13.8 ppm and 9.8 ppm for metPSwMb-1CH₃ and 4CH₃Im, respectively. The following analysis of this shifts apply to both species.

$$\delta_h = \delta_{para} + \delta_{dia} \quad (12)$$

Where δ_h is the observed hyperfine shift, δ_{para} and δ_{dia} are the paramagnetic and diamagnetic shifts, respectively. The diamagnetic shift is obtained from the spectrum of the free ligand; this is only an approximation because the chemical shift of the resonance can vary in the protein matrix due to hydrogen-bonding, van-der-Waals, and hydrophobic interactions, and especially ring current effects (Swift, 1973; La Mar, 1979).

This shift is quite similar to that of its C β H of His F8, which is calculated to receive more dipolar than contact interaction from the paramagnetic Fe (Bertini & Luchinat, 1986). In this same reference, however, it was calculated that the contact contribution is larger than the dipolar contribution to the hyperfine shifts of the methyl groups on the heme, even though the methylys are the same number of bonds away from the Fe as the 4-methyl of the ligand, as well as the C β H of His F8. Presumably, because 1- and 4CH₃Im, like His F8, is axially coordinated to Fe, orbital overlap with the unpaired electrons on Fe ought to be similar; hence, the paramagnetic shift observed for the methyl groups of the bound ligands can be attributed largely to dipolar interaction. For metPSwMb4CH₃Im, although when in the free form, nomenclature of the 4(5)CH₃Im is arbitrary, the position of the methyl group is fixed once coordinated to the Fe in the protein matrix. Peak **k** is assigned on the 4- instead of the 5-position of the bound ligand based on the following reason. First, if **k** is on the imidazole 5-position, it will be as close to the Fe as the ring CHs of His F8, which

are strongly relaxed (as characterized by ρ in Figures 36A and 37A). The sharp appearance of κ argues against it being the 5-CH₃. The T_1 of κ (Table VI) enables the extraction of $r_{Fe-\kappa}$ of ~ 5.66 Å, which places the methyl in the 4-position.

The similar binding fashion depicted in Figure 19 based on similar geometries in the free ligand forms of 4CH₃Im and 1CH₃Im is justified by both the presence of electrostatic interaction at low pH in metPSwMb4CH₃Im and the downfield shifts of the methyls on the ligands. However, illustrated by the differential paramagnetic shifts of ring CHs and methyls of the ligands, and on the larger spread of chemical shifts in metPSwMb1CH₃Im, their coordinations to Fe are not identical. Comparison of both in the bound forms (Figure 19C) also provides insight to the absence of ring C₂H of ligand in metPSwMb1CH₃Im. This proton is orientated, relative to Fe, at a position opposite to that in metPSwMb4CH₃Im; therefore, its effect may be that of a downfield shift.

Comparison of the methyl linewidths between PSwMb and EqMb

Direct comparison was made between metEqMbIm and metPSwMbIm in H₂O at 298K, similar pH, protein and imidazole concentrations. The heme 5- and 1- methyl linewidths are consistently broader in PSwMb (see Figure 41A, B) (more pronouncedly, the 8CH₃ is taller with respect to 5CH₃ and 1CH₃). This may be a result of comparable population of the two conformations of imidazole in PSwMb, in contrast to a single dominant conformation in EqMb. To ascertain that this is not an effect from possible hydrogen-bonding interaction with distal His E7 in PSwMb (Lecomte & La Mar, 1987; Chapter VII), Figure 41C compares both species in ²H₂O, showing a pattern. The broader methyl linewidths dictate that rate of ring-flip must be slower in PSwMb, or that both conformations are allowed only in PSwMb. A distinctive difference between the Mbs in the active site is the Lys CD3 --> Arg CD3 substitution in PSwMb. It has been shown that Arg CD3 stabilizes the heme-insertion reorientationally disordered isomers in the binding

pocket by ~ 0.6 kcal/mol over Lys CD3 due to better salt-bridging with heme-6-propionate (Hauksson et al. 1990; La Mar et al. 1991), and that Arg CD3 increases the outer barrier to escape of the ligand by ~ 1 kcal/mol over Lys CD3 by flash photolysis on CO geminate recombination in Mb mutated at CD3 position (Balasubramanian et al., 1993).

Furthermore, Chapter V (Yee & Peyton, 1991) provides evidence that the single substitution is responsible for the slower dicyanoheme reorientation rate within the binding pocket of SwMb. In addition, X-ray crystal structures of SwMb and its Arg CD3 \rightarrow Lys CD3 mutated counterpart (Oldfield et al., 1992) revealed that Lys side chain is shorter than that of Arg, rendering a more flexible binding pocket. As shall be seen in Chapter VII, hydrogen-bonding interaction between Im and His E7, as predicted by crystal structure of metSwMbIm, is detected in metPSwMbIm but is absent in metEqMbIm -- providing yet more reason to believe that the longer Arg CD3 not only has a direct influence on the prosthetic group by electrostatic interaction, but also restricts the ligand access trajectory by an indirect influence on His E7. Therefore, the answer to the comparable population of both ligand conformations in PSwMb relative to EqMb may be that the longer side-chain of Arg CD3 deters the rapid flipping of the ligand by hydrogen-bonding interaction, thus slowing it to the extent where the rate is comparable on NMR time-scale for the peaks to be detected as averaged broad signals.

Perhaps the most compelling evidence for the energetics difference between EqMb and PSwMb in their binding pockets comes from their respective pH behaviors shown in Figure 42 for metMbIm. There are two factors that contribute to line-broadening of methyls, namely the rapid equilibration of the ligand, and isotope-exchange due to hydrogen-bonding with His E7 in 50/50 $^2\text{H}_2\text{O}/^1\text{H}_2\text{O}$ solvent (Chapter VII). The effects are separable because the extent of line-broadening differs. For broadening arising from ring equilibration, 5CH_3 and 1CH_3 peaks experience the greatest impact; while 8CH_3 is unaffected on the NMR time-scale. It seems that the chemical shifts of 8CH_3 in both

conformations coincide. On the other hand, hydrogen interaction produces more severe line-broadening in 5CH₃ and 8CH₃ of metEqMbN₃ (Figure 82 in Chapter VII). As demonstrated in Chapter VII, hydrogen-bonding with His E7 is absent in metMbIm, therefore, the major source of broadening observed in this chapter must be attributed to the ring-equilibration of the bound ligand.

A spectrum was run on metPSwMbIm at pH 6.9 and 278 K, in the hope of slowing the imidazole flipping sufficiently so that the methyls would resolve on NMR time-scale, showing distinct conformations and populations. The peaks merely broaden without splitting at this pH (see Figure 43). However, pH dependence studies on metPSwMbIm indicated increase in line broadening effect on the methyls as pH was raised, suggesting slower ring-flip at higher pH. A similar experiment was therefore performed on metPSwMbIm at pH 9, because at this high pH, the peak broadening is greater at room temperature. From Figure 44, splitting of the methyls occurs at 278 K, most notably 5- and 1CH₃'s. This phenomenon is a direct demonstration that there are two bound forms in metPSwMbIm, as hypothesized earlier, as well as provided sufficient resolution of the splitting to allow determination of kinetics and activation energy parameters for this equilibration based on two-site exchange model by complete bandshape simulation (CBS) (Sandström, 1982). The simulation parameters were based on those of the major peak, hence the activation energy data reflect the transition from the major to the minor form. Figure 44 also shows the population ratio of the major to minor conformations of the bound Im, which is approximated at 4 to 1. The CBS analysis yielded k_{exch} of 125 s⁻¹ at 278 K, and activation free-energy of 13.6 kcal/mol for the ring equilibration. MetEqMbIm, on the other hand, although showing splitting of methyls, has a population ratio of 22 to 1 for the major to minor form, and a larger linewidth for the minor form. There are two factors that contribute to the broader lines, which are a result of either intrinsically smaller chemical shift difference, or faster exchange. Saturation of the minor 5CH₃ peak in both

species under identical conditions at 278 K shows larger saturation transfer effect in metEqMbIm than in metPSwMbIm, showing that the rate constant for interconversion is greater. Furthermore, simulation of the splitting in metPSwMbIm at 278 K, with the population ratio of 22:1, required that k_{exch} be increased 4-fold. Therefore, a combination of population difference and faster exchange contributes to the broad lines in the low temperature spectrum of metEqMbIm. CBS of metEqMbIm, although more inaccurate because a slow-exchange spectrum could not be optimized, was also performed to approximate the activation energy perhaps 1 kcal/mol less than the metPSwMbIm case. Figure 46 illustrates the proposed energy diagrams comparing bound Im equilibration for EqMb and PSwMb, with the major form energies arbitrarily set to the same energy for both species.

Similar comparisons of methyl linewidths were also done on metMb- 4CH₃Im and 1CH₃Im (Figure 47). Relatively sharp methyl peaks were observed in metPSwMb- and metEqMb1CH₃Im at both 298 K and 313 K; while those of the 4CH₃Im counterparts are only intermediately sharp. It appears that in metMb4CH₃Im, some alternate conformation of the bound ligand is present despite the extra methyl group. Nevertheless, from the relative sharpness of the peaks in both forms, the energy barrier imposed by the extra methyl for the ligand to reorient is possibly less than compensated by the flexibility afforded by Lys CD3 in EqMb, so the methyl linewidths between the two species are indistinguishable. Alternatively, the population of the minor form may be very small, which can also lead to sharp lines.

The effects of imidazole ring reorientation are more pronounced in all cases for metPSwMbIm, as reflected by the distinctive proposed energy diagrams in Figure 46, suggesting that the only amino acid residue substitution in the binding pocket, in CD3, is responsible for this discrepancy. The decrease in bound ligand ring-flip, marked by splitting of methyls at low temperature and high pH (pH > 9), suggests deprotonation of

the ring NH on the bound ligand, enabling it to involve in hydrogen bonding interaction with any nearby proton donor. Reference to Figure 78 in Chapter VII reveals possible distal proton donors as Arg CD3 (Lys CD3 in metEqMbIm) and His E7. For reasons given in Chapter VII, it is unlikely that His E7 is involved in hydrogen bonding, therefore, the CD3 residue may play a more important role. Free Arg has a guanidinium side chain with pK of >12, and so is protonated throughout the stable pH range of the protein, assuming its similar pK in the protein environment; although free Lys side-chain also remains protonated, it has a lower pK of ~11. At acidic pH, the bound Im is protonated, thus the sharper methyls in both species are attributed to fast exchange arising from destabilization of the minor conformation due to electrostatic repulsion against the positive charges on the CD3 residue. At basic pH, on the other hand, the minor conformers in both proteins are stabilized, retarding the exchange to the extent that is detected on the NMR time scale. Lys CD3, because of shorter side-chain (which was found to cause a lower barrier for ligand escape by 1 kcal/mol than Arg CD3 in Balasubramanian et al., 1993), may not participate in hydrogen bonding interaction as efficiently as Arg CD3. Rajarathnam et al. (1992) also showed that the positively charged side chain of Arg CD3 stabilizes the swung-out conformation of His E7, which is necessary to accommodate imidazole ring-flip, by ~0.2 kcal/mol over Lys CD3. Both factors, the hydrogen-bonding between the Im and Arg CD3, and the electrostatic interactions between His E7 and Arg CD3, clearly contributed to the stabilization energy for the minor form in metPSwMbIm.

The assignments derived in this chapter for all the imidazolate complexes are tabulated in Table VII.

CONCLUSIONS

This work shows the assignments of the broad upfield resonances to be those of the ring CH of His F8, and/or the ring CHs of the exogenous ligand. Comparison of the heme

TABLE VII

UPFIELD RESONANCE ASSIGNMENTS FOR IMIDAZOLATE
BOUND TO PIGMY SPERM WHALE AND HORSE HEART
MYOGLOBINS

<u>Species</u>	<u>Peak Labels</u>	<u>Chemical Shifts</u>	<u>Assignments</u>
MetPSwMb Imidazole (303 K)	b a	-8.2 ppm -10.1 ppm	C _{4,5} H of Im C ₂ H of Im
4CH ₃ Im (313 K)	i h k	-9.2 ppm -13.7 ppm 12.2 ppm	C _{2,4} H of His F8 C ₂ H of 4CH ₃ Im 4CH ₃ of 4CH ₃ Im
1CH ₃ Im (313 K)	g j	-7.3 ppm 17.4 ppm	C _{4,5} H of Im 1CH ₃ of 1CH ₃ Im
MetEqMbIm (298 K)	f	-9.3 ppm	C ₂ H of Im
MetEqMbIm (308 K)	f'	-8.9 ppm	C ₅ H of Im

methyl linewidths between the imidazolate complexes of PSwMb and EqMb reveals an intrinsic structural difference at their active sites. In the imidazole complex, the Lys CD3 -- > Arg CD3 substitution in the binding site of PSwMb contributes to a greater stabilization for the conformational isomers of bound imidazole. Therefore, the minor conformation is more populated in metPSwMbIm. The linewidths of the heme methyl resonances are used as probes for the determination of the bound imidazole ring equilibration kinetics. Hence, at temperatures where this equilibration is fast compared to the chemical shift difference induced by the isomers, the heme methyls (especially 5CH₃ and 1CH₃) are broader in metPSwMbIm than in metEqMbIm. Possible electrostatic interaction is also implicated in metMb1CH₃Im between the positively charged ring N of bound 1CH₃Im to a nearby negatively charged amino acid in the binding pocket.

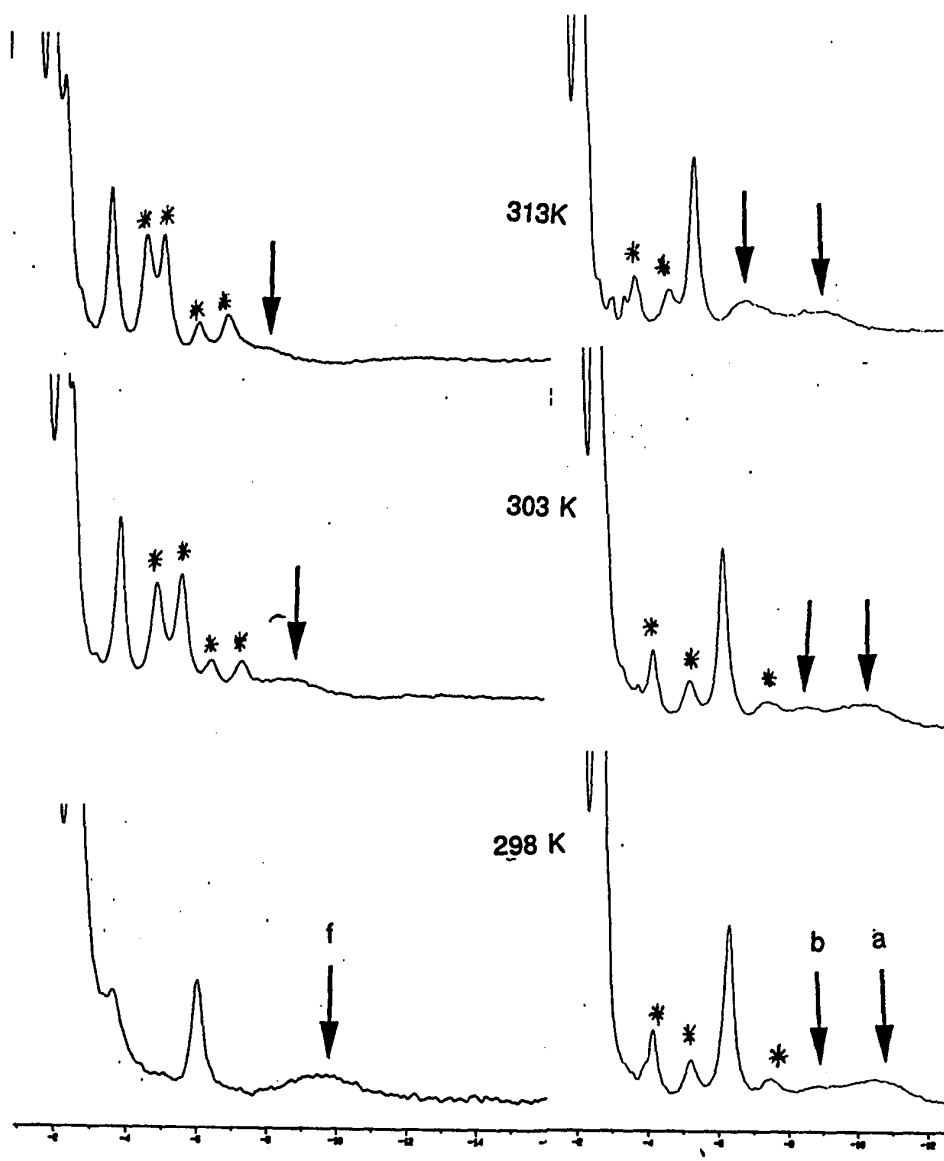


Figure 17. Comparison of upfield regions in metEqMbIm (left), and metPSwMbIm (right) at pH 6.9. Bottom to top: 298 K to 313 K, respectively. Peaks of interest are as labeled; the asterisks denote peaks from residual metMbH₂O. For a reference upfield region of metEqMbH₂O at 323 K, please refer to Figure 89.

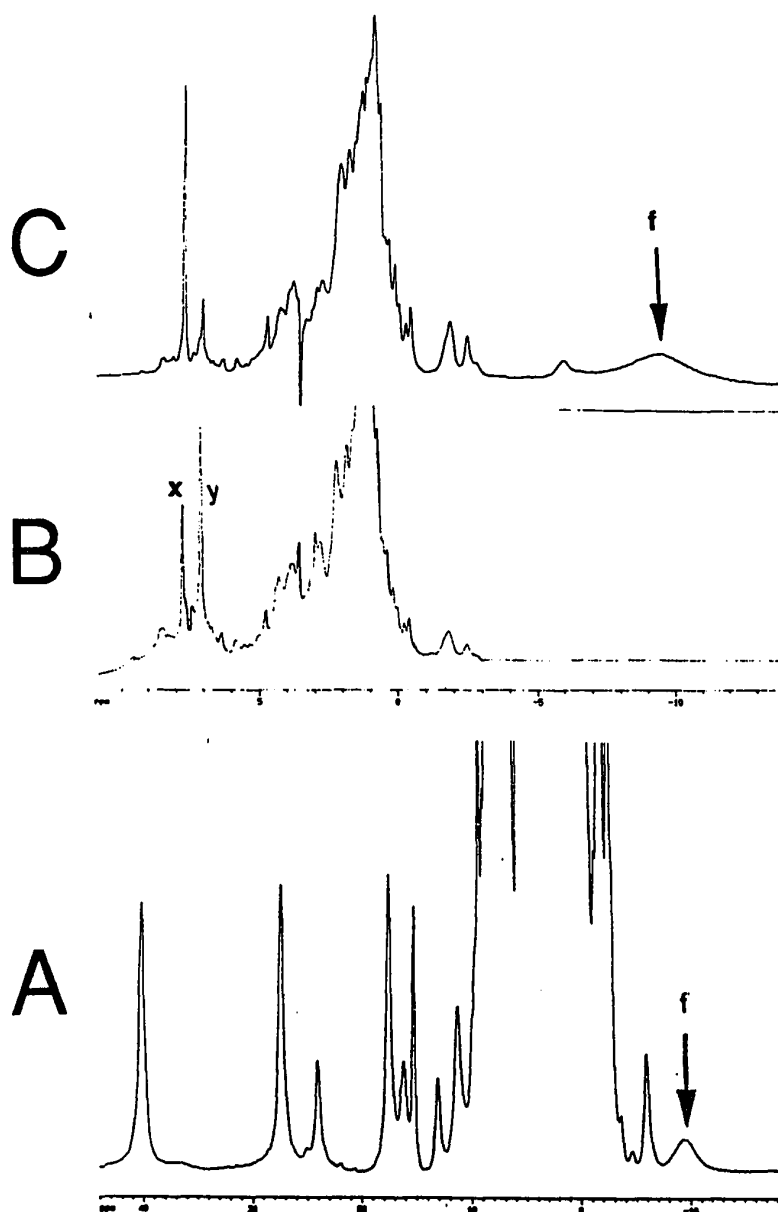


Figure 18. 400MHz ^1H NMR 1D NOE of metEqMbIm at 298K, and pH 8.2. **A,B** Reference spectra of metEqMbIm, with A showing the hyperfine-shifted, while B the diamagnetic region; **C** Difference spectrum after irradiation at peak shown by the arrow.

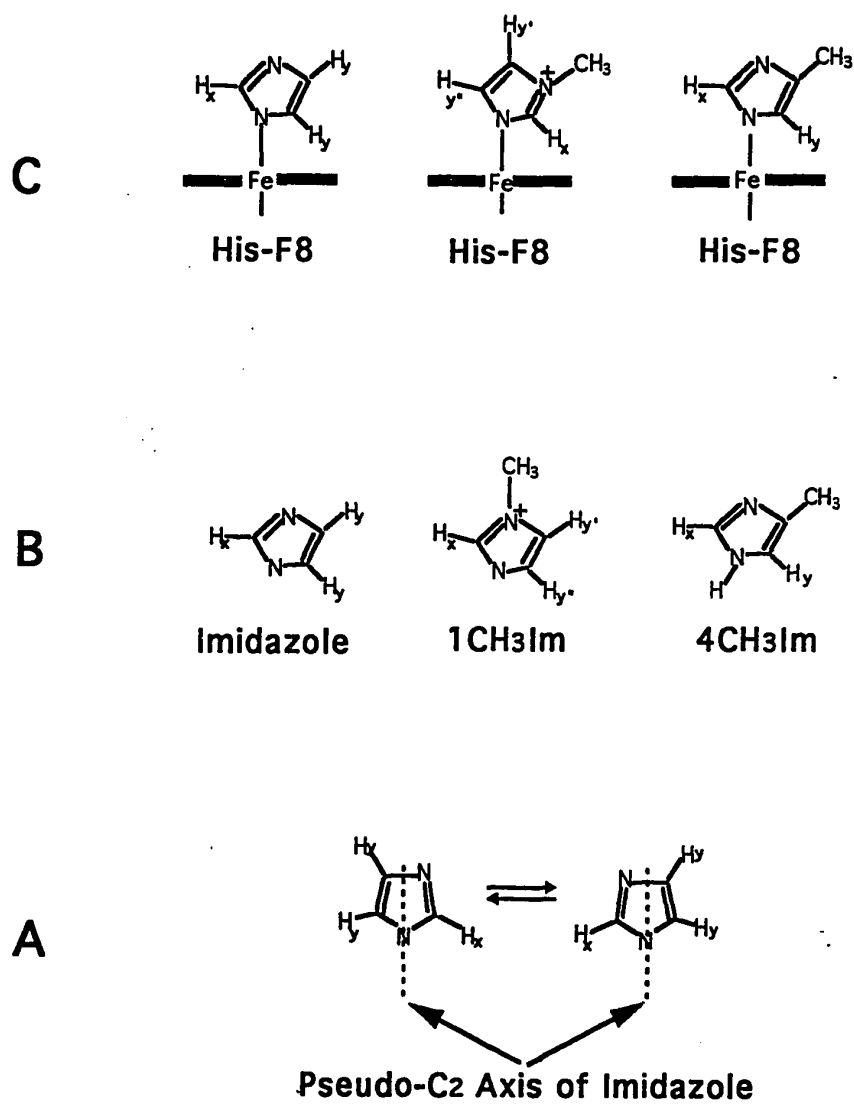


Figure 19. Schematics showing A. the pseudo C₂ axis of bound imidazole, B, C, the geometries and labelings of free and bound Im, 1-CH₃Im and 4-CH₃Im, respectively.

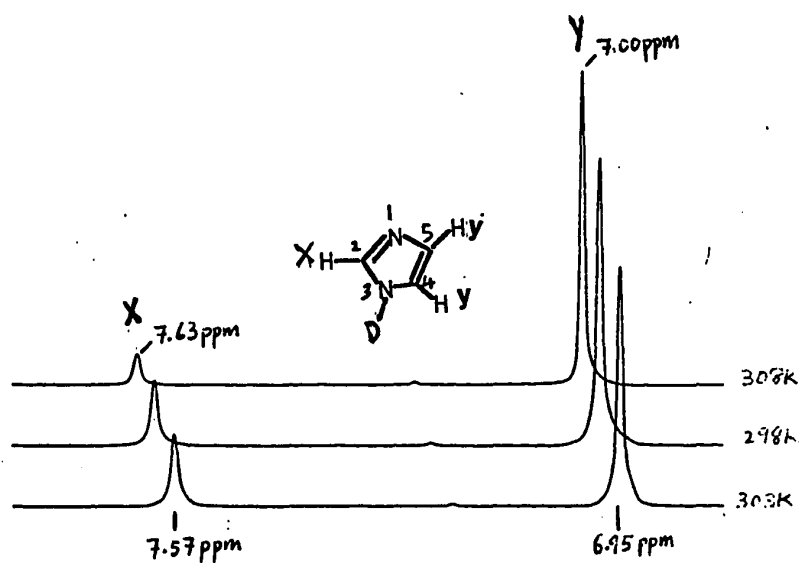


Figure 20. Free Im which has been incubated in $^2\text{H}_2\text{O}$ at 25°C and pH 10; spectra were taken at different time periods, shown correspondingly. Note that C_2H (other than N_3H) also exchanged with time. The accepted mechanism for the chemical exchange of C_2H is *via* the limiting-step formation of an ylide intermediate by extraction of the C_2H from the cationic imidazole by OH^- , which is then protonated by the isotope (Vaughan et al., 1970).

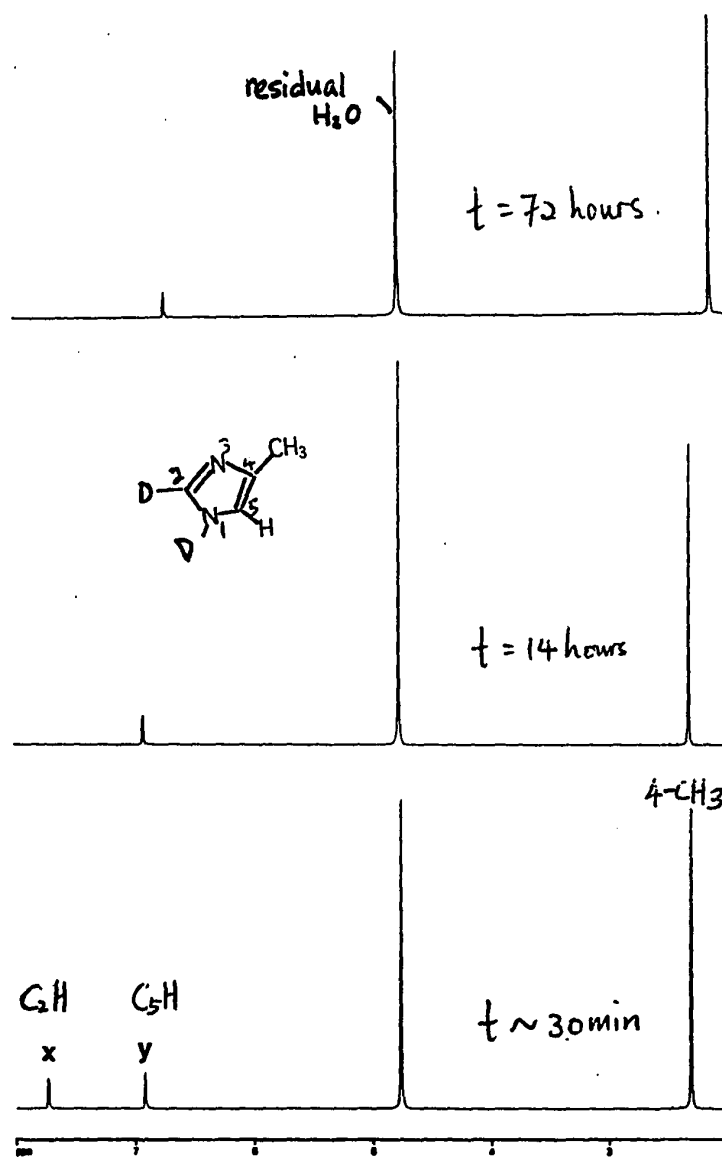


Figure 21. Free 4CH₃Im which has been incubated in ²H₂O at 65°C; spectra were taken at different time periods, shown correspondingly. Note that C₂H (other than N₁H) also exchanged with time. The accepted mechanism for the chemical exchange of C₂H is *via* the limiting-step formation of an ylide intermediate by extraction of the C₂H from the cationic imidazole by OH⁻, which is then protonated by the isotope (Vaughan et al., 1970).

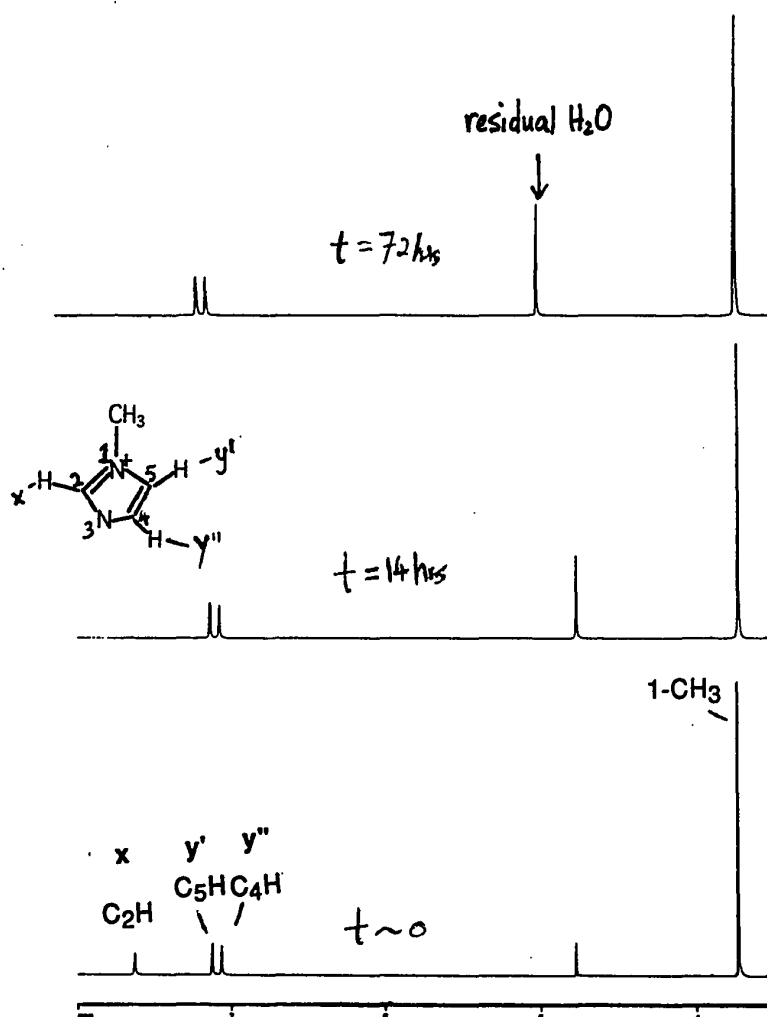


Figure 22. Free 1CH₃Im which has been incubated in ²H₂O at 65°C; spectra were taken at different time periods, shown correspondingly. Note that C₂H (other than N₃H) also exchanged with time. The accepted mechanism for the chemical exchange of C₂H is *via* the limiting-step formation of an ylide intermediate by extraction of the C₂H from the cationic imidazole by OH⁻, which is then protonated by the isotope (Vaughan et al., 1970).

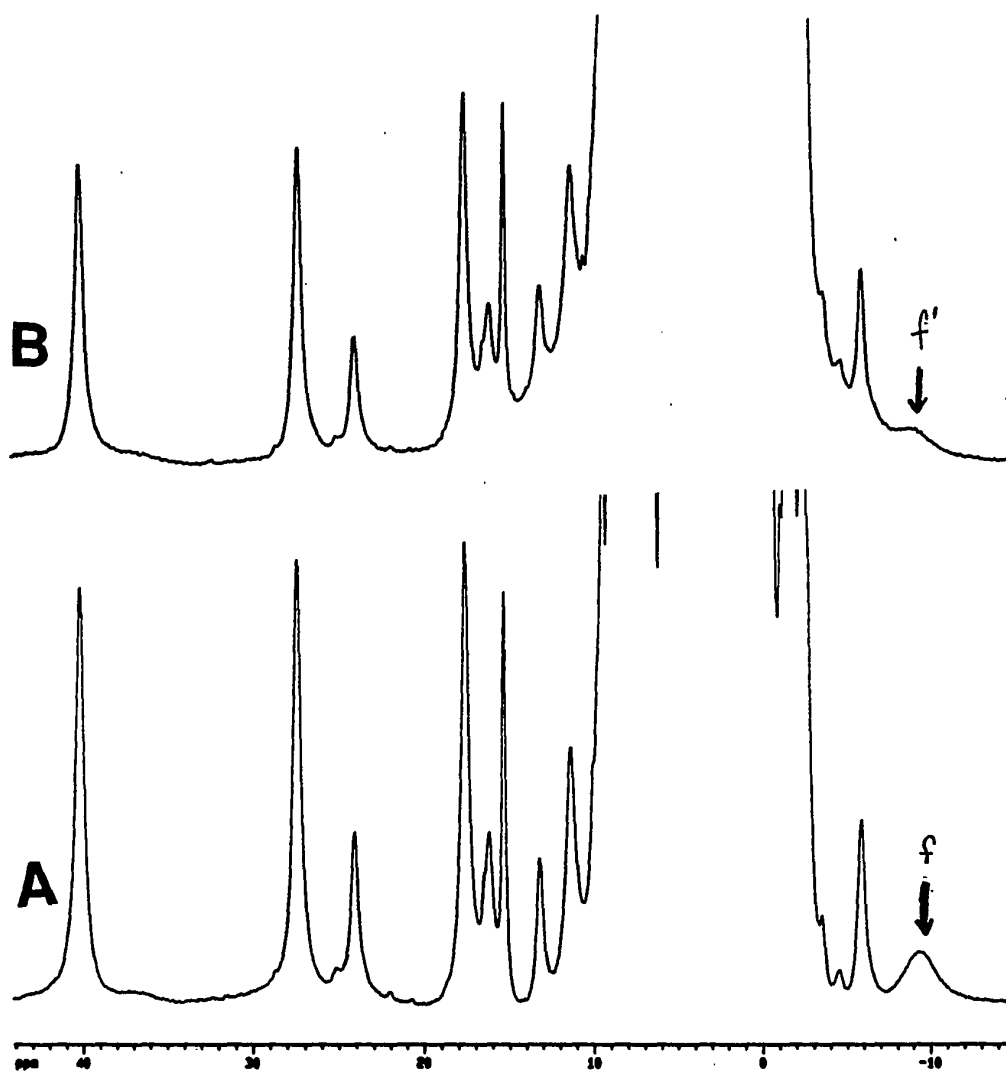


Figure 23. MetEqMbIm at 298K and pH 8.0. A Reference spectrum . B metEqMbIm reconstituted with deuterated Im.

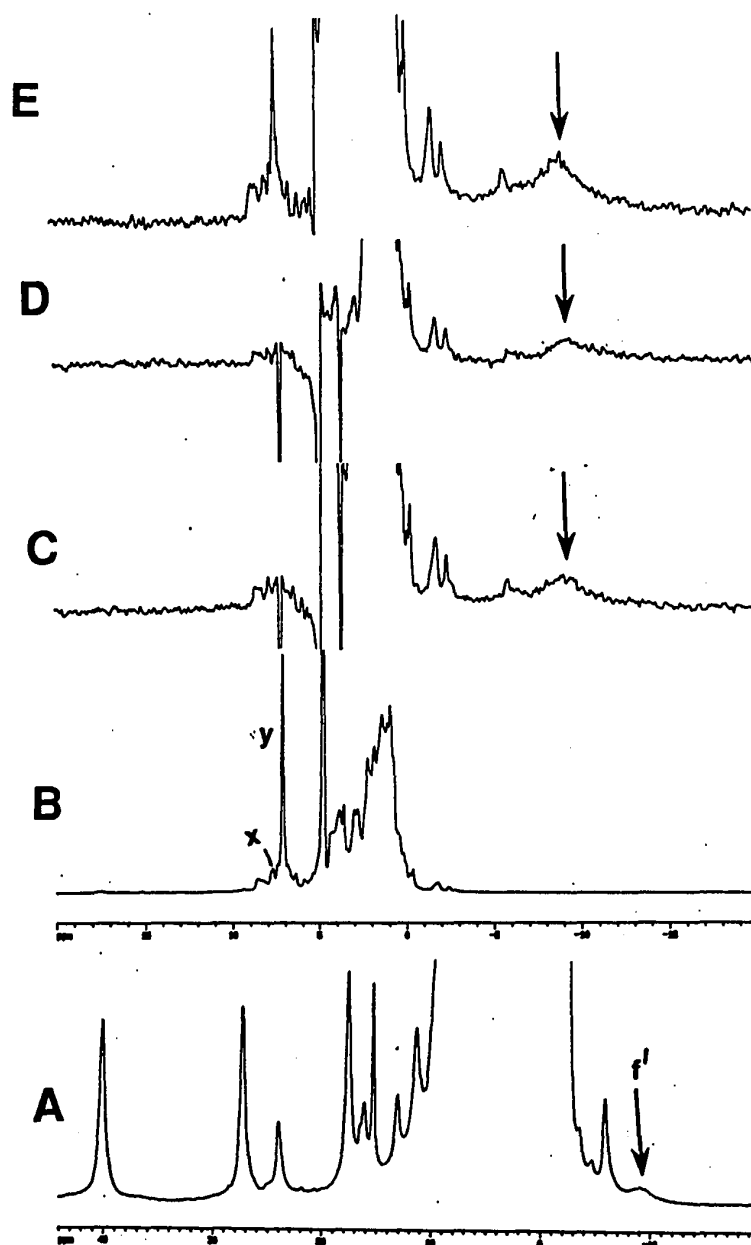


Figure 24. MetEqMbIm reconstituted with deuterated Im at 298K and pH 8.0. **A, B.** Reference spectra showing the paramagnetic and diamagnetic regions, respectively. **C-E.** Difference traces between the reference and irradiation of peak f' with the indicated parameters, saturation time of 70 ms.

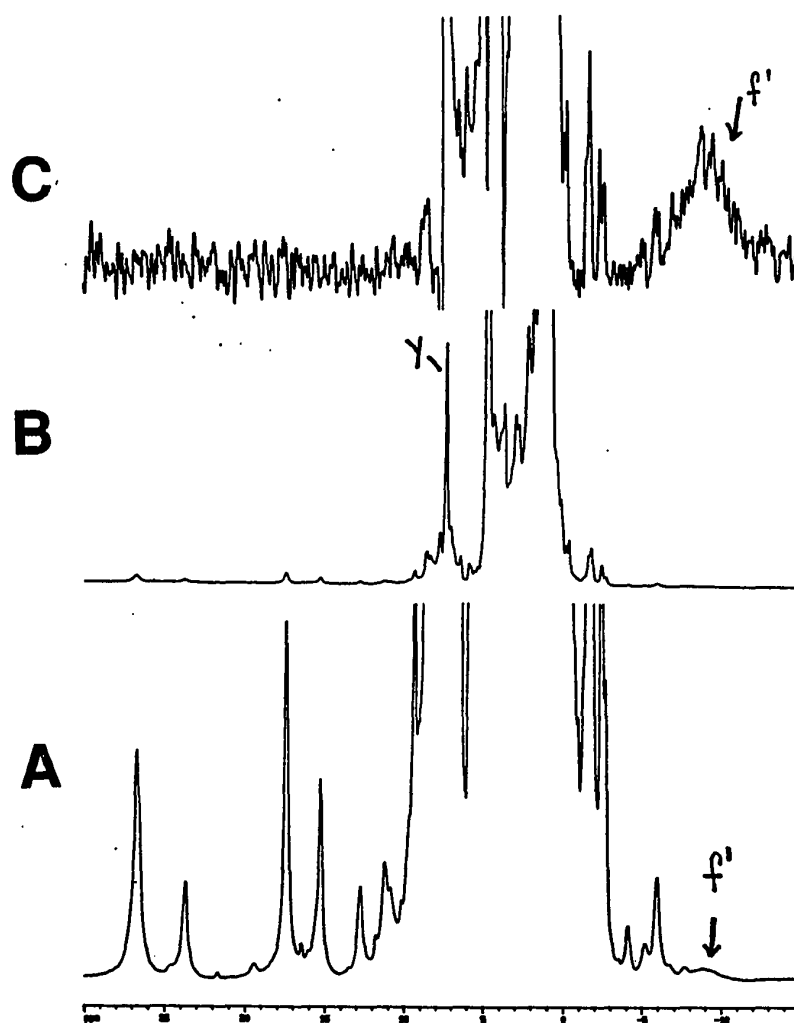


Figure 25. 1D NOE of metEqMbIm, reconstituted with deuterated Im at the C_2H position at pH 7 and 298K. Saturation parameters are: relaxation delay of 100ms, saturation power of 35, and saturation time of 70ms. **A.**, **B** Reference spectra of the expanded paramagnetic and diamagnetic regions, respectively. **C.** difference trace after irradiation of f' , showing no NOE to the paramagnetic region.

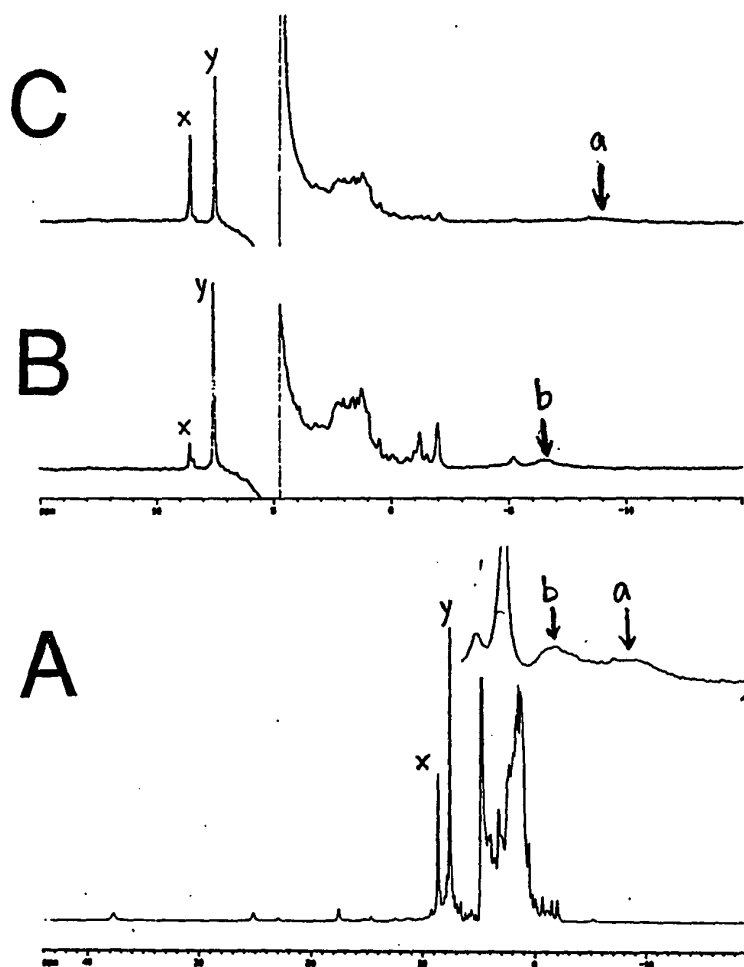


Figure 26. 400MHz ^1H NMR 1D NOE of metPSwMbIm at pH 6.9 and 313K **A.** Reference spectrum, *inset shows the expanded upfield region*; **B, C.** difference traces at relaxation delay of 100ms, saturation power of 28, and saturation time of 70ms, resonances irradiated are indicated with arrows.

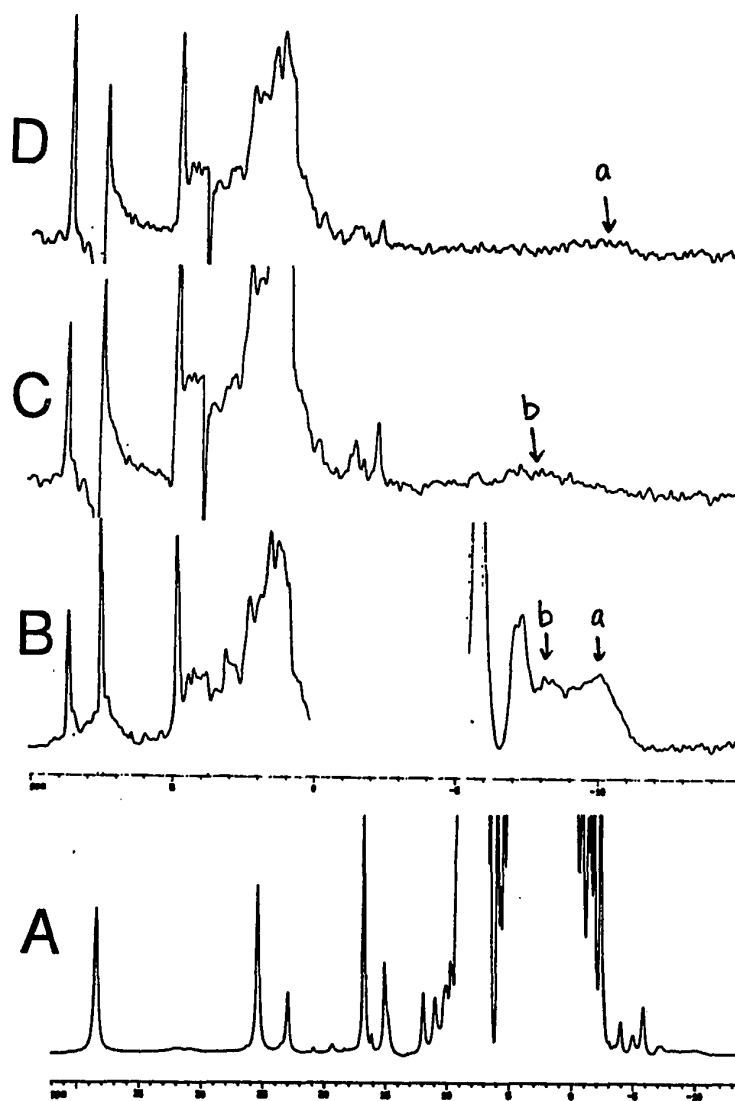


Figure 27. 400MHz ^1H NMR 1D NOE of metPSwMbIm at pH 6.9 and 303K **A, B** References showing the paramagnetic and diamagnetic regions, respectively, *inset shows expanded upfield region*; **C, D** difference traces at relaxation delay of 100ms, saturation power of 33, and saturation time of 70ms, resonances irradiated are indicated with arrows.

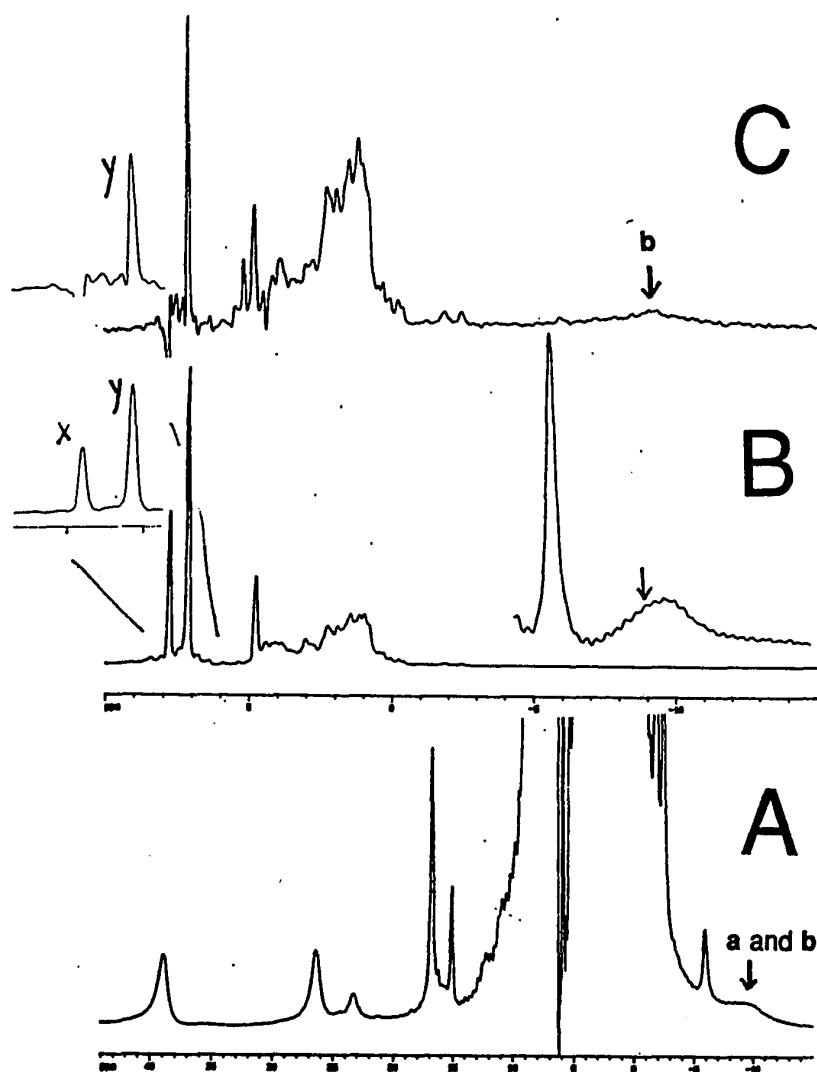


Figure 28. 400MHz ^1H NMR 1D NOE of metPSwMbIm at pH 9.05 and 303K. **A, B** Reference spectra showing diamagnetic and expanded upfield regions, respectively, *inset shows expanded upfield region*; **C** Difference traces at relaxation delay of 1s, saturation power of 34, and saturation time of 80ms, resonances irradiated are indicated with arrows.

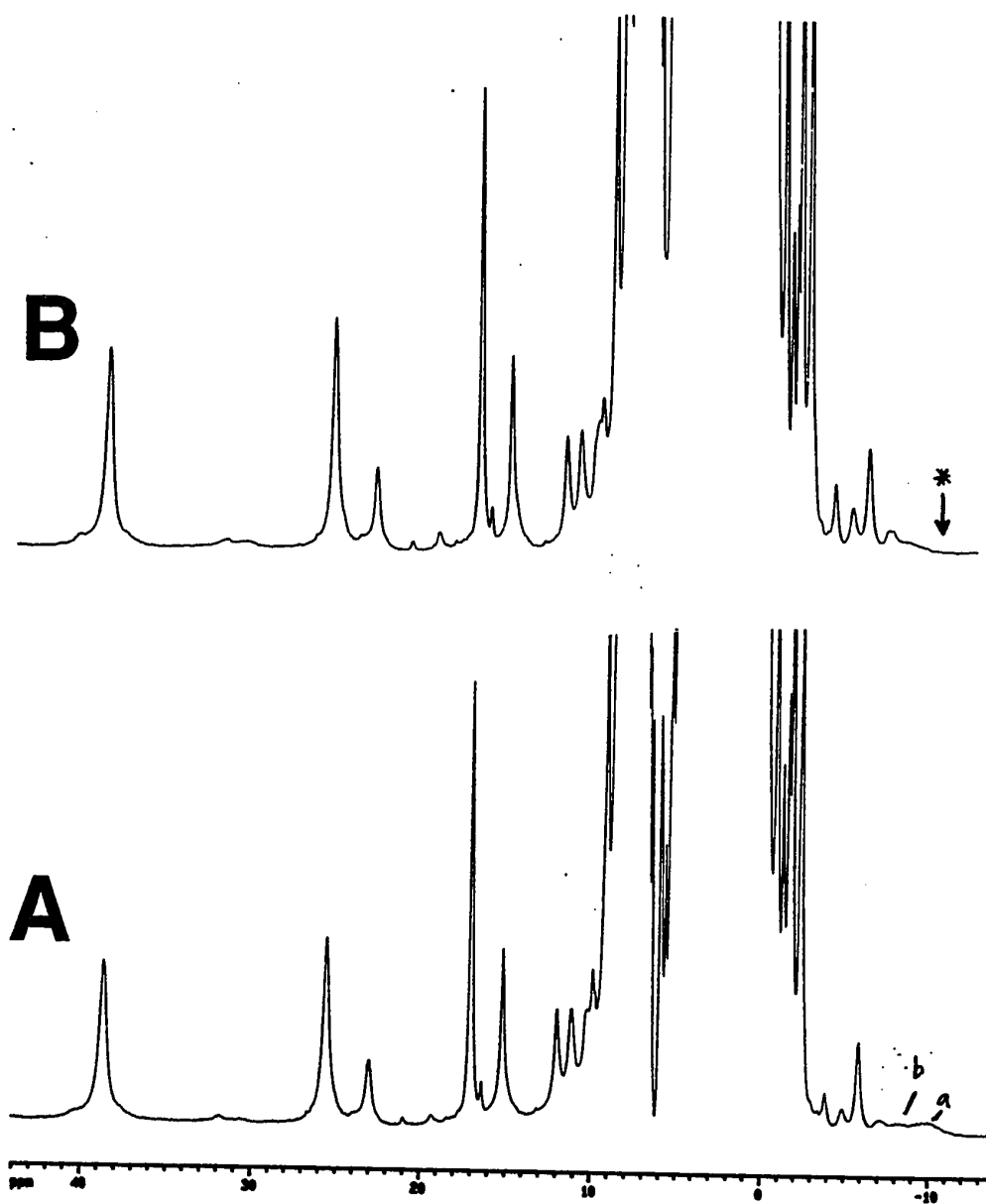


Figure 29. MetPSwMbIm at 303K and pH 6.9, after Im has been deuterated. **A** Reference spectrum, **B** metPSwMbIm reconstituted with deuterated Im. Peaks are as labeled.

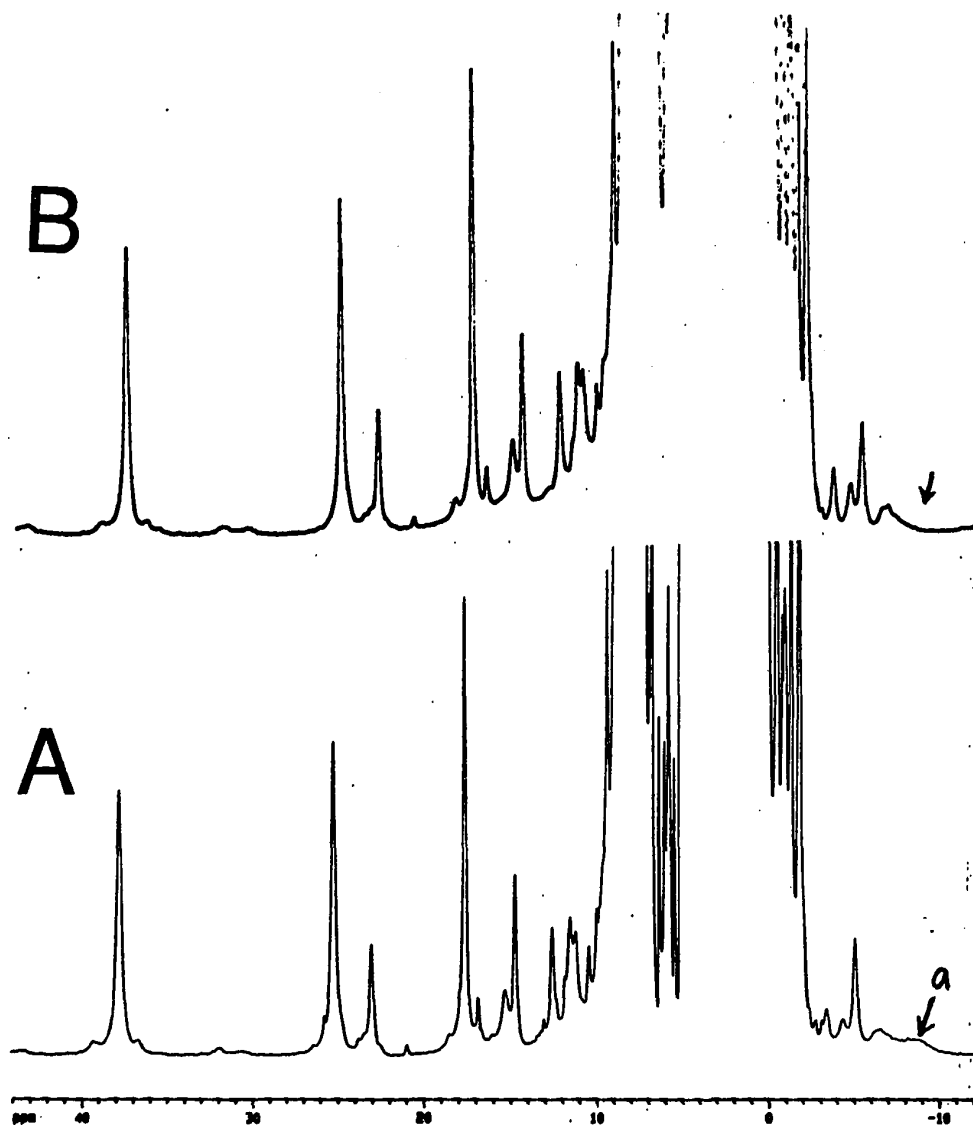


Figure 30. MetPSwMbIm at 313K and pH 6.9, after Im has been deuterated. **A** Reference spectrum, **B** metPSwMbIm reconstituted with deuterated Im. Peaks are as labeled.

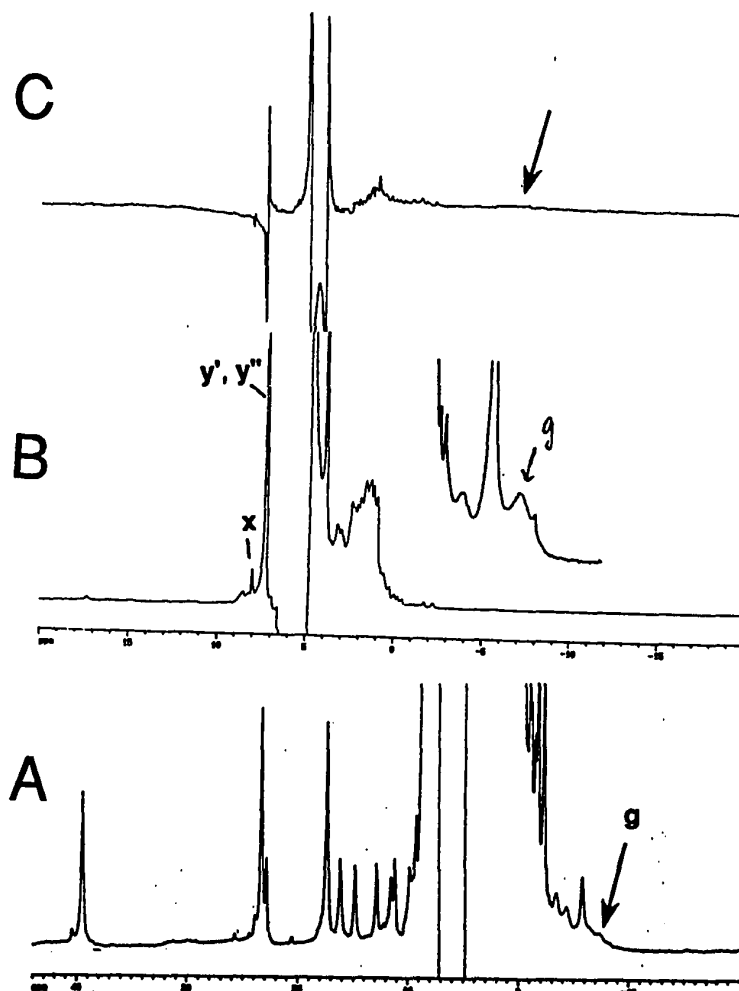


Figure 31. 400MHz ^1H NMR 1D NOE of metPSwMb1CH₃Im at pH 8.0 and 313K. **A, B** Reference spectra showing both the hyperfine-shifted and diamagnetic regions, respectively (*inset shows the expanded upfield region*); **C** Difference spectrum with relaxation delay of 1s, saturation power of 33, and saturation time of 70ms, peaks saturated are indicated by arrows.

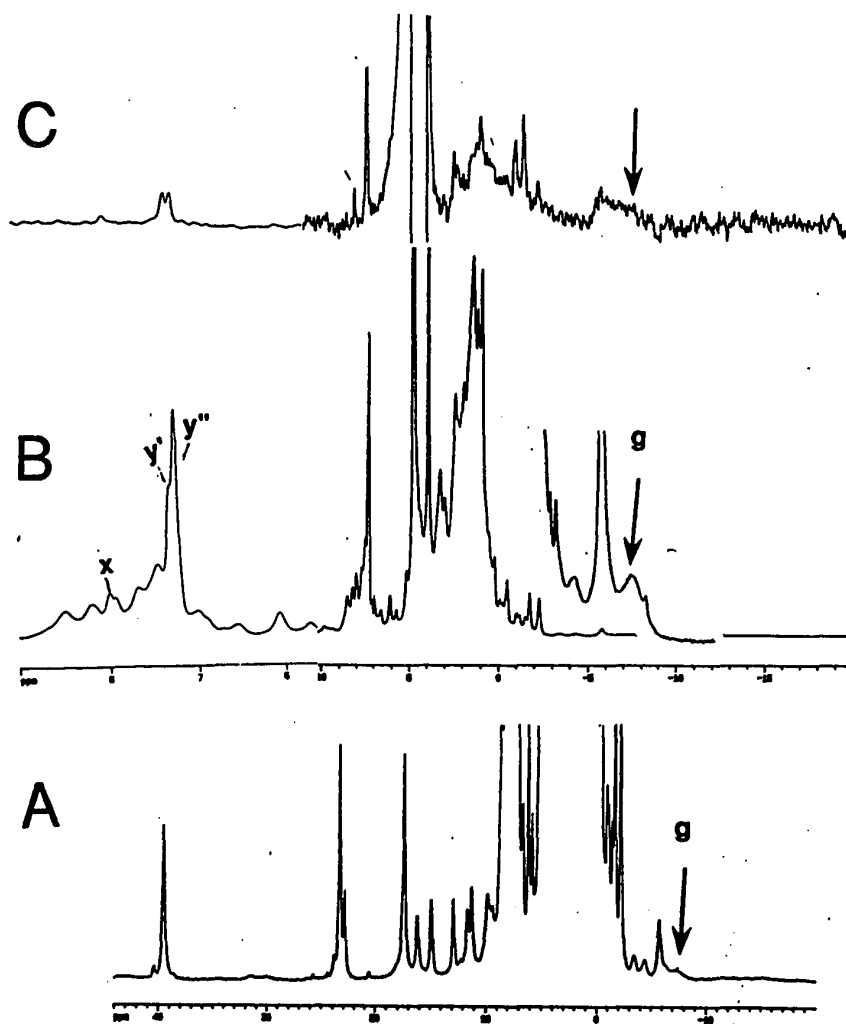


Figure 32. 400MHz ^1H NMR 1D WEFTNOE of metPSwMb1CH₃Im (1CH₃Im has been deuterated) at pH8.0 and 313K. **A,B** Reference spectra showing the expanded upfield and diamagnetic regions, respectively (*inset* shows the expanded upfield region). **C** Difference trace of saturating the peaks indicated by arrows, with relaxation delay of 100 ms, delay time of 100 ms, saturation time of 70 ms, and saturation power of 33. Regions of interests are expanded to the left of **B** and **C**.

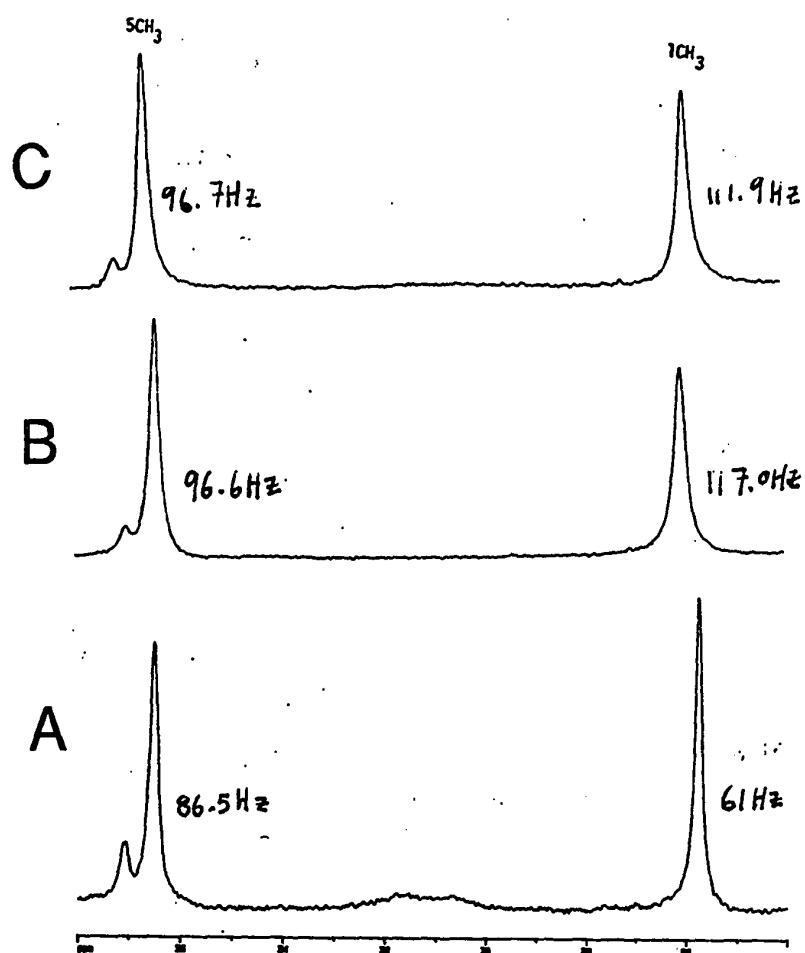


Figure 33. pH dependence of the methyl linewidths in metPSwMb4CH₃Im at 298K and various pHs of A. 6.5, B. 7.5, C. 9.0. The widths at half-height for each pH is marked correspondingly to show the disparity of linewidths. Respective methyl peaks were normalized to the same areas.

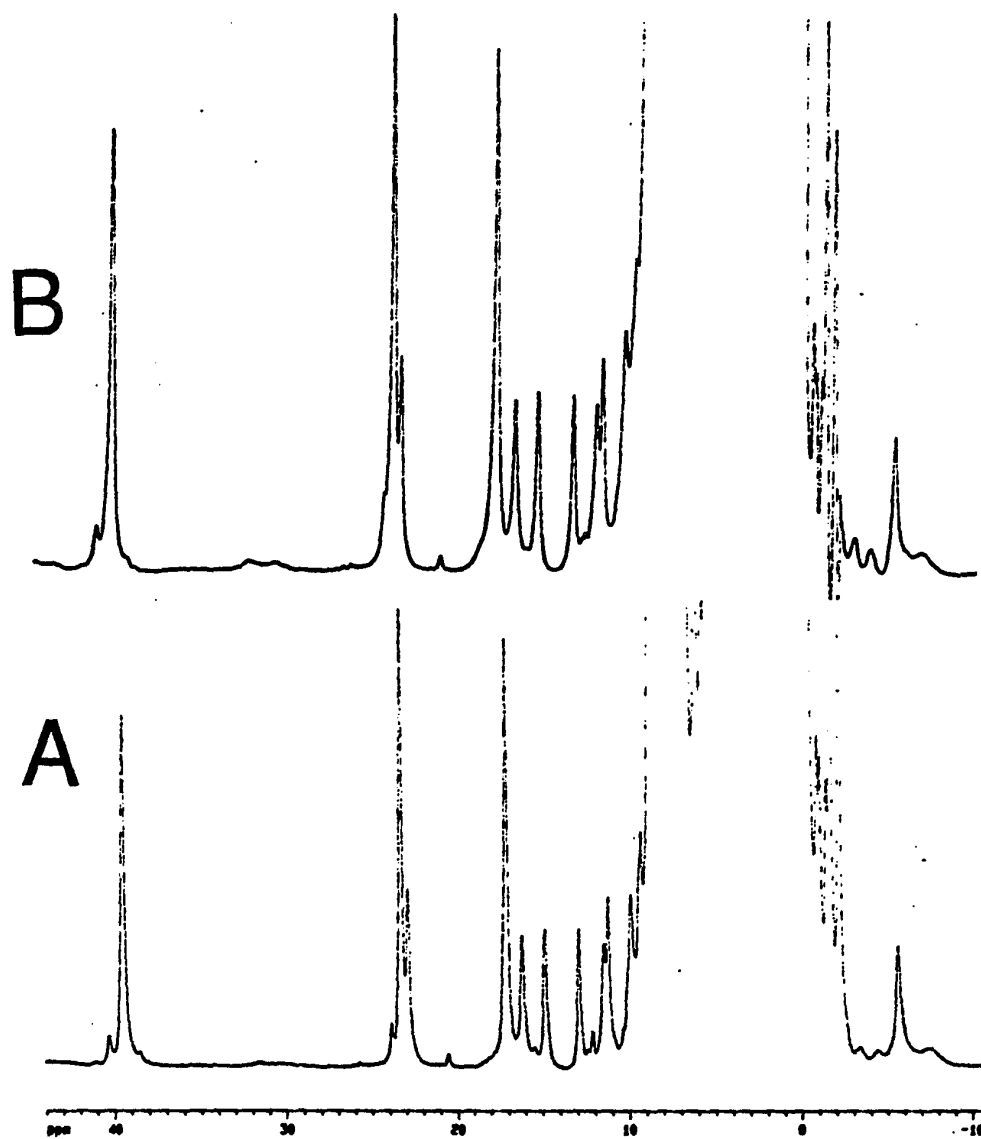


Figure 34. MetPSwMb $1\text{CH}_3\text{Im}$ at 313K and pH 8.0, after $1\text{CH}_3\text{Im}$ has been deuterated. **A** Reference spectrum at pH 8.0 and 313K. **B** corresponding spectra with deuterated $1\text{CH}_3\text{Im}$.

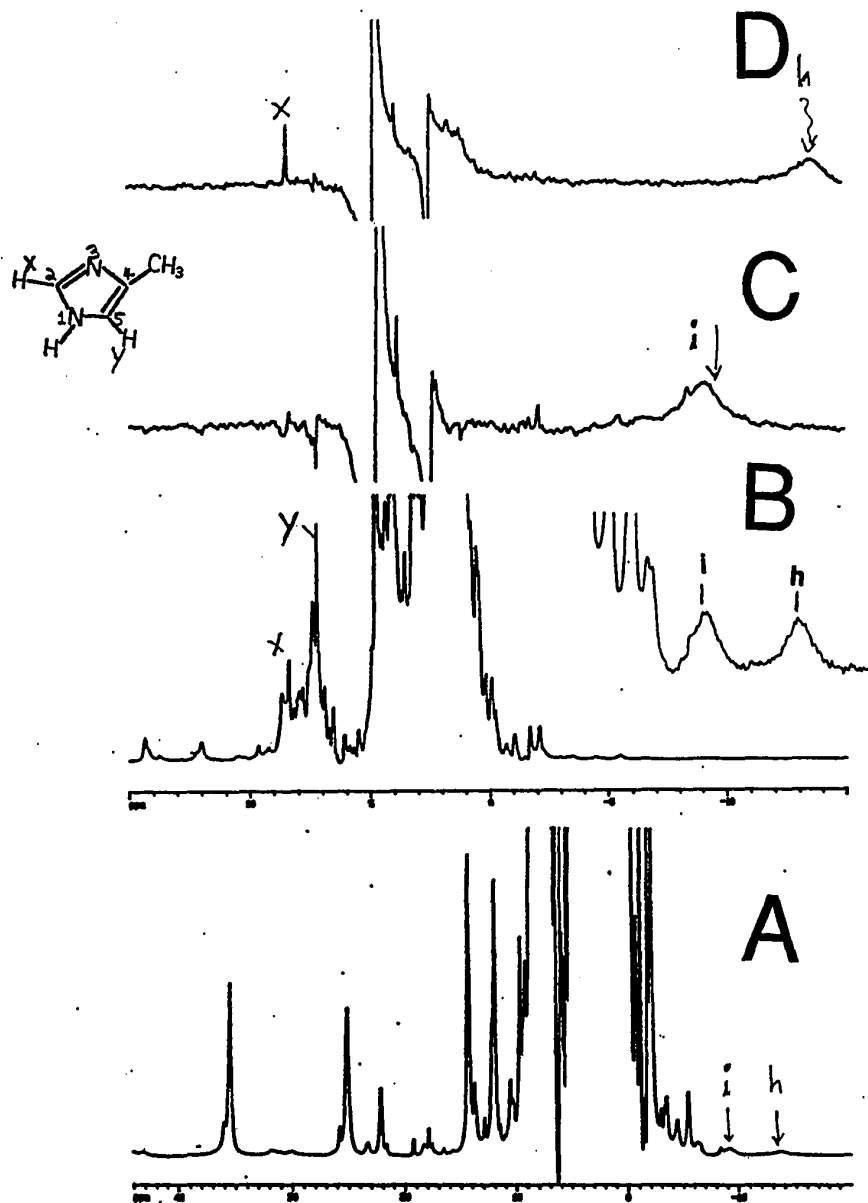


Figure 35. metPSwMb4CH₃Im (4CH₃Im has not been deuterated) at 313K and pH 7.1. **A, B** Reference spectra showing the the hyperfine-shifted, and diamagnetic regions, respectively; **C, D** Difference traces between the reference and irradiated peaks as indicated by arrows with parameters: relaxation delay of 100 ms, saturation time of 50 ms, and saturation power of 30 (Inset shows the labelings of the free ligand).

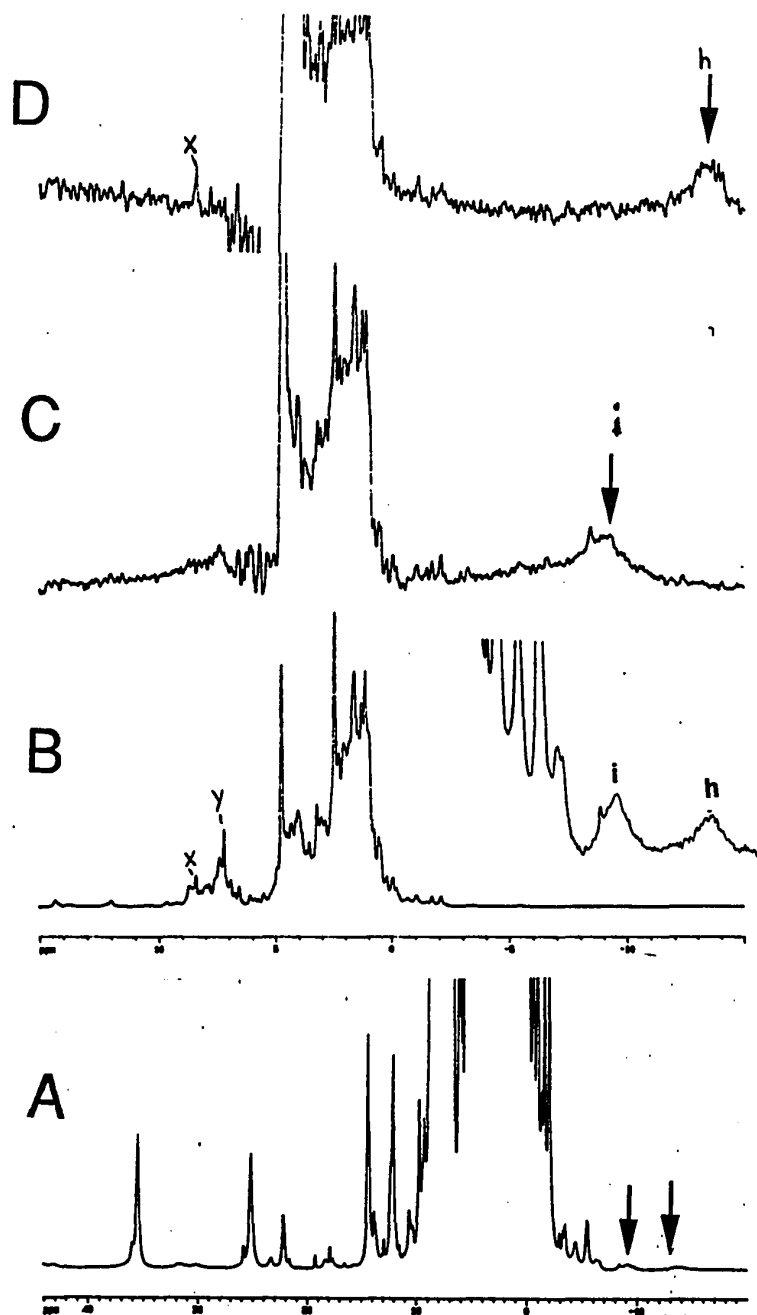


Figure 36. metPSwMb4CH₃Im (4CH₃Im has not been deuterated) at 313K and pH 7.1. A, B Reference spectra showing the the hyperfine-shifted, and diamagnetic regions, respectively; C, D Difference traces between the reference and irradiated peaks as indicated by arrows with parameters: relaxation delay of 1 s, saturation time of 50 ms, and saturation power of 30

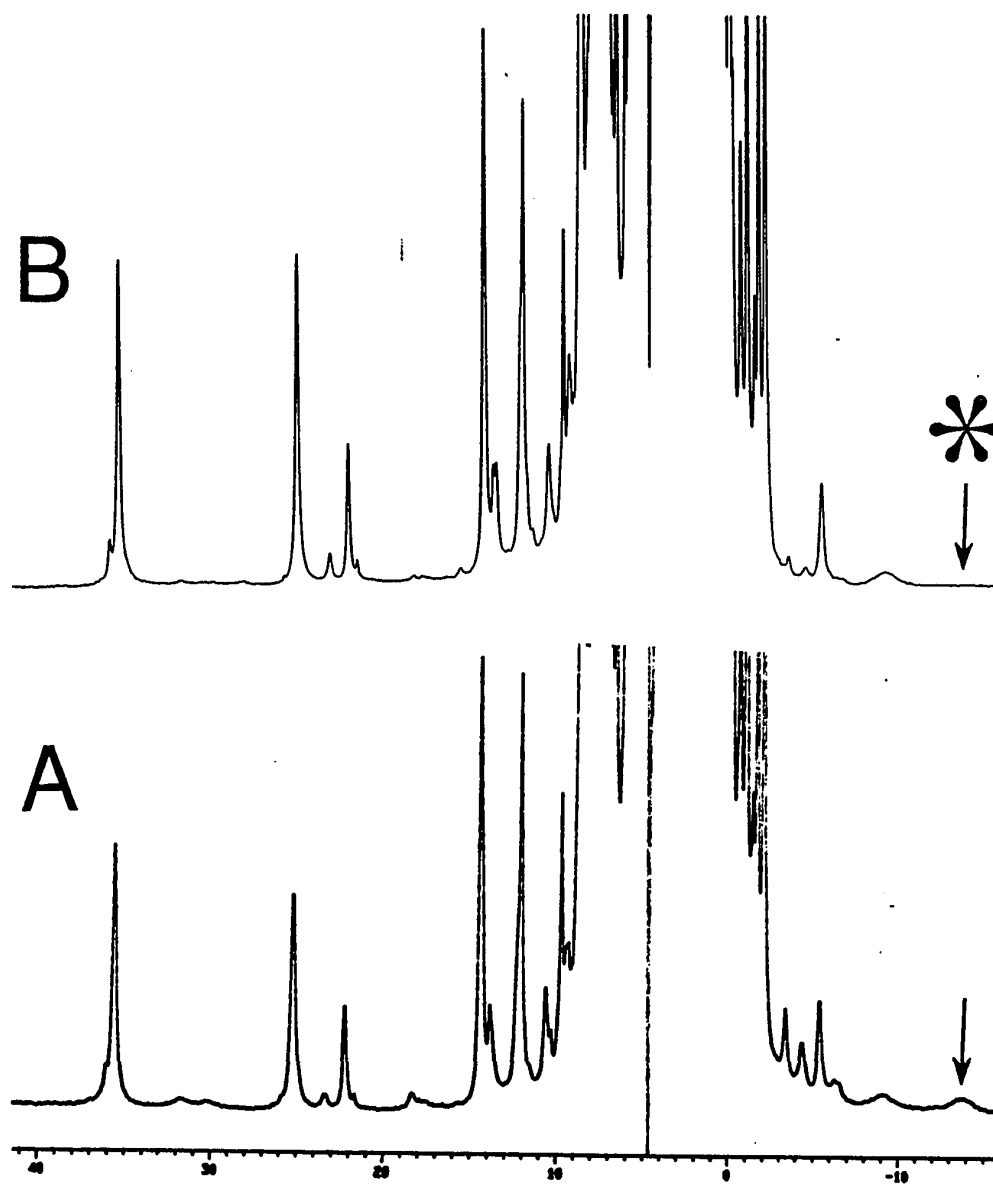


Figure 37. MetPSwMb4CH₃Im at 313K and pH 7.11, after 4CH₃Im has been deuterated. A Reference spectrum at pH 7.11 and 313K. B corresponding spectra with deuterated 4CH₃Im.

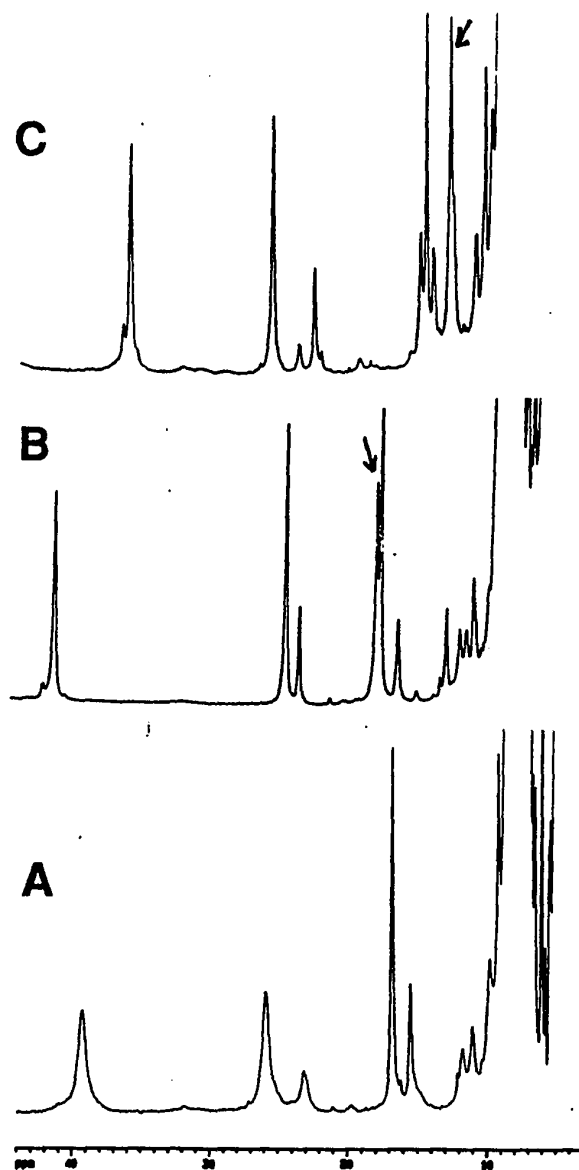


Figure 38. Comparison of the downfield regions among the imidazolate PSwMbs at 298K. **A.** MetPSwMbIm at pH 6.9. **B.** metPSwMb1CH₃Im at pH 7.9. **C.** MetPSwMb4CH₃Im at pH 7.1. The arrows denote extra methyl peaks in the corresponding complexes.

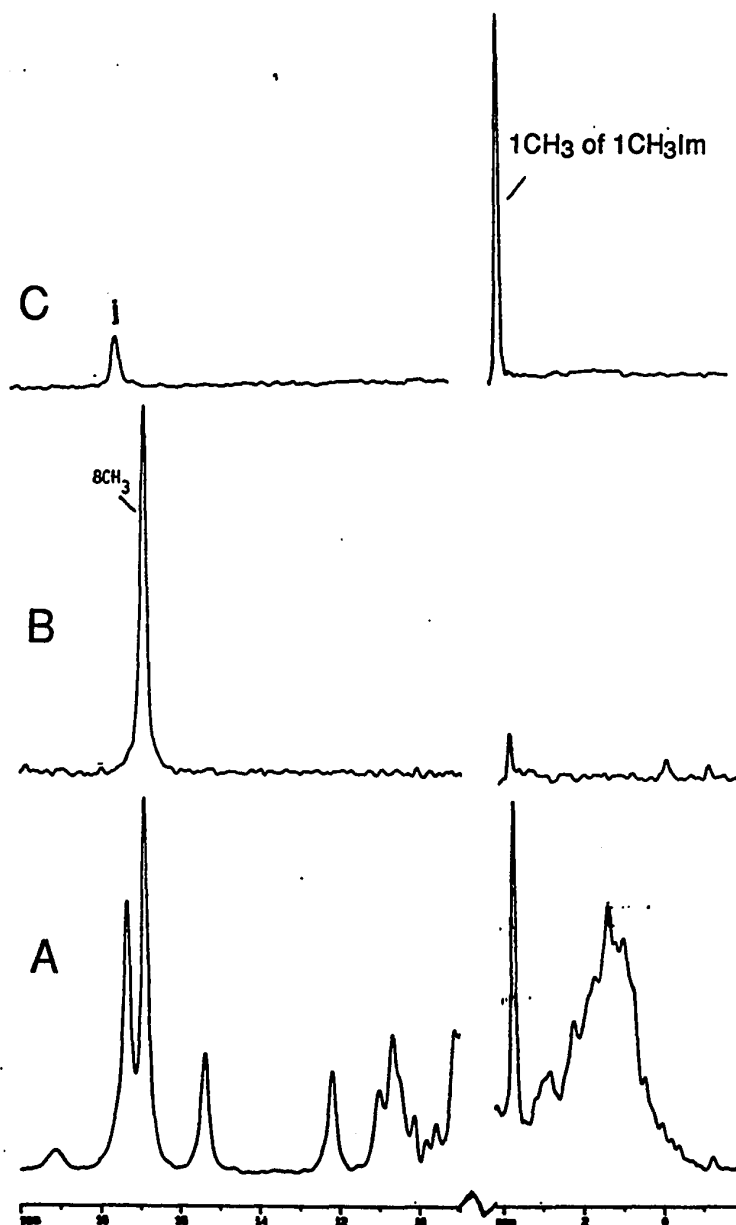


Figure 39. 1D NOE hit of the methyl peak, *j*, of metEqMb1CH₃Im at 298K and pH 8. **A.** Reference spectra showing the hyperfine-shifted and diamagnetic regions. **B, C.** Difference traces between the reference and the 8CH₃ peak; and peak *j*, respectively. Saturation parameters used are: relaxation delay of 200 ms, saturation time of 100 ms, and saturation power of 60.

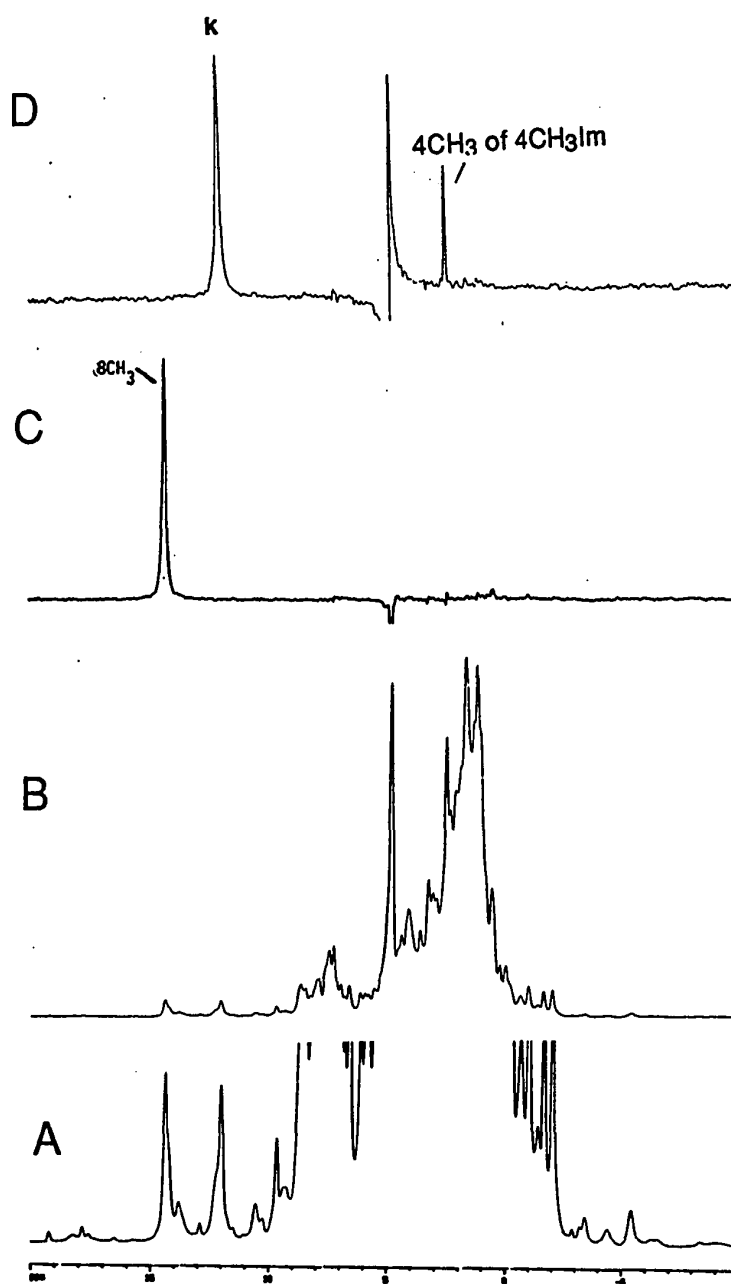


Figure 40. 1D NOE hit of the methyl peak, k, of metPSwMb4CH₃Im at 313K and pH 7.1. **A, B.** Reference spectra showing the hyperfine-shifted and diamagnetic regions, respectively. **C, D.** Difference traces between the reference and the 8CH₃ peak; and peak k, respectively. Saturation parameters used are: relaxation delay of 300 ms, saturation time of 100 ms, and saturation power of 60.

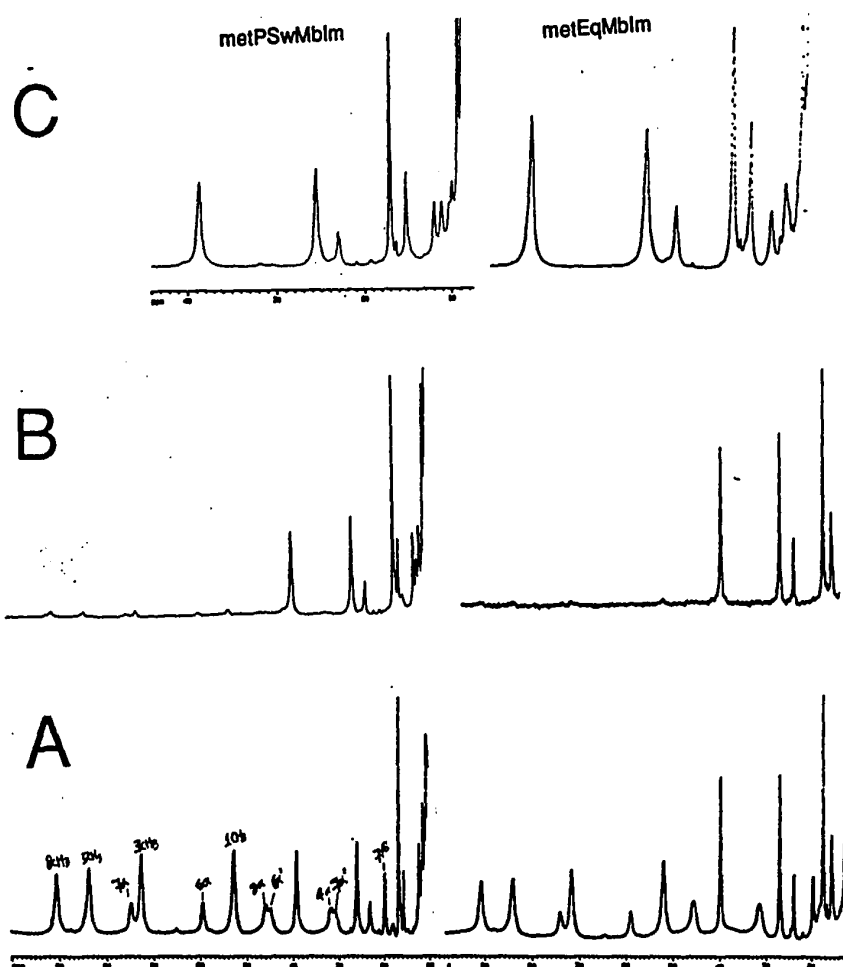


Figure 41. Imidazole titration of EqMb and PSwMb at 298K in 10% $^2\text{H}_2\text{O}$ (A and B), and 100% $^2\text{H}_2\text{O}$ (C) at pH 7.0. Right: metEqMbIm, and left: metPSwMbIm. Concentrations of Im used were 8 mM, and 120 mM in A and B, respectively (protein concentrations started at 2 mM). Identities of metPSwMbIm peaks are labeled..

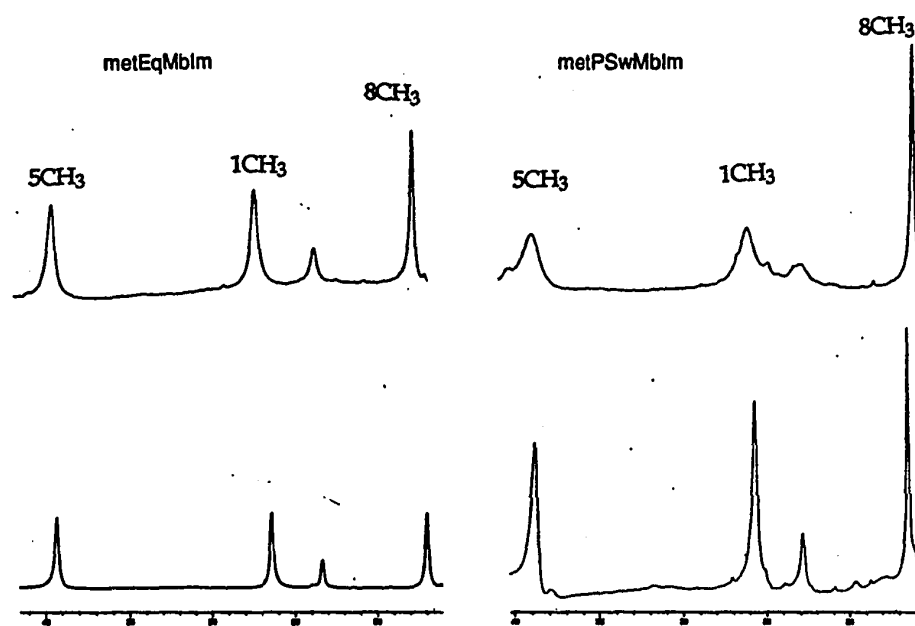


Figure 42. Comparison of pH dependence between metEqMbIm and metPSwMbIm at 298K and pHs 9 (top) and 7 (bottom). Left. metEqMbIm; right. metPSwMbIm.

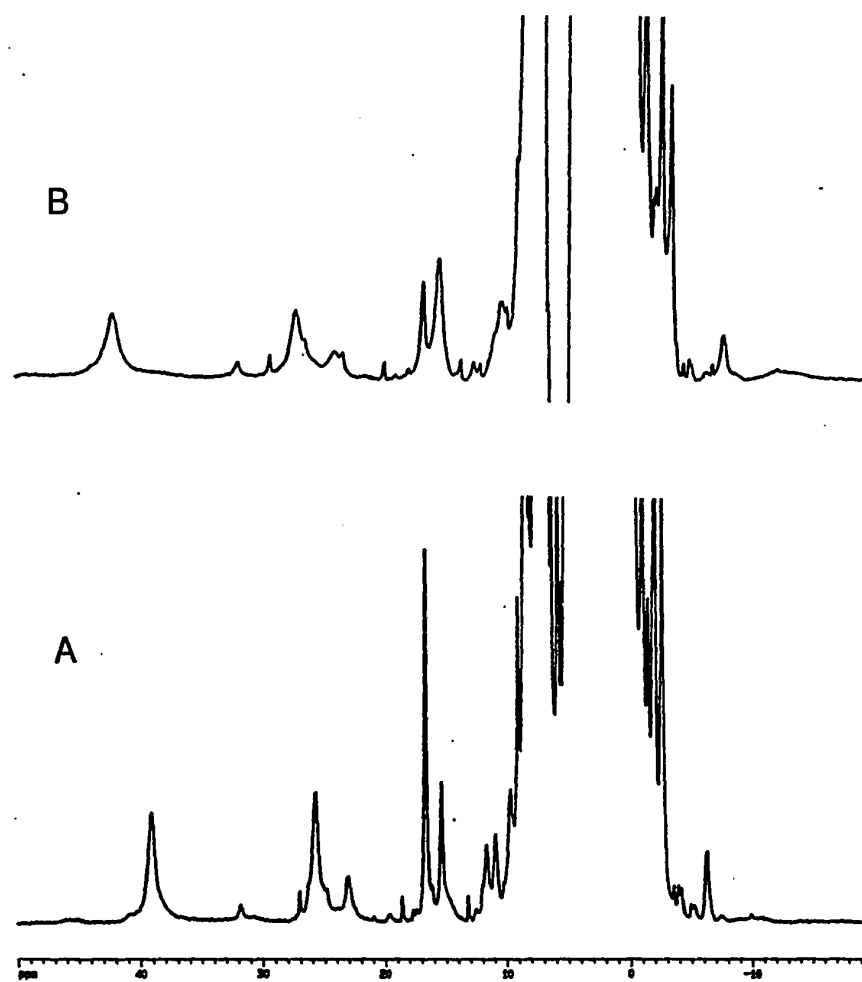


Figure 43. ^1H NMR spectra of MetPSwMbIm at pH 6.9, A. 298K, and B. 278K

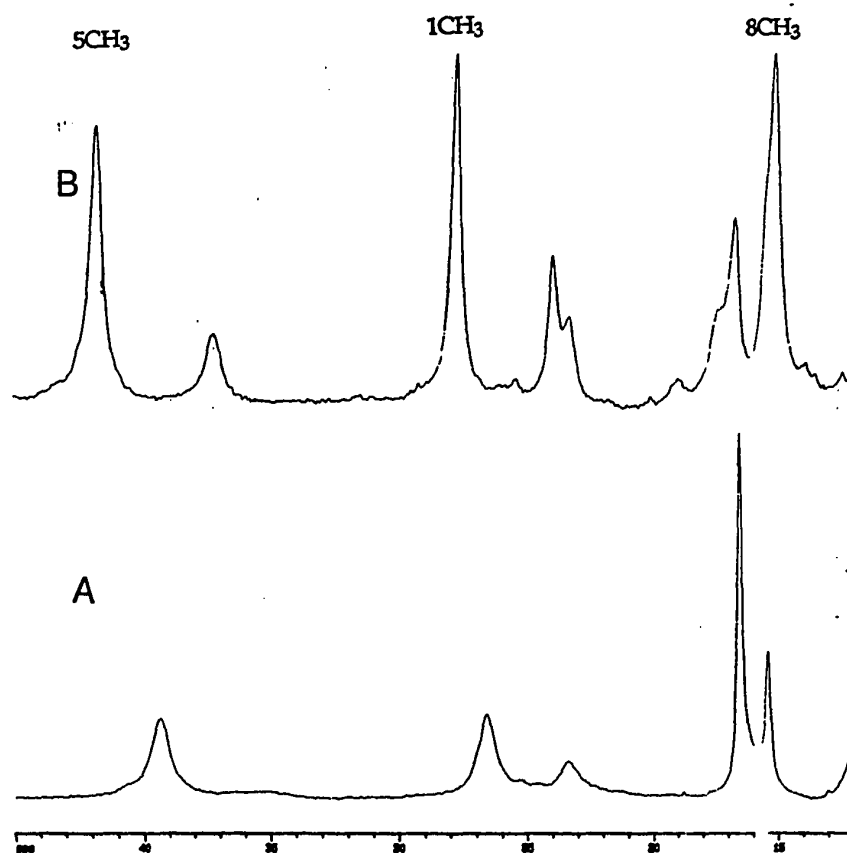


Figure 44. ^1H NMR spectra of metPSwMbIm in $^2\text{H}_2\text{O}$, at pH 9.05 and A. 298 K, B. 278 K.

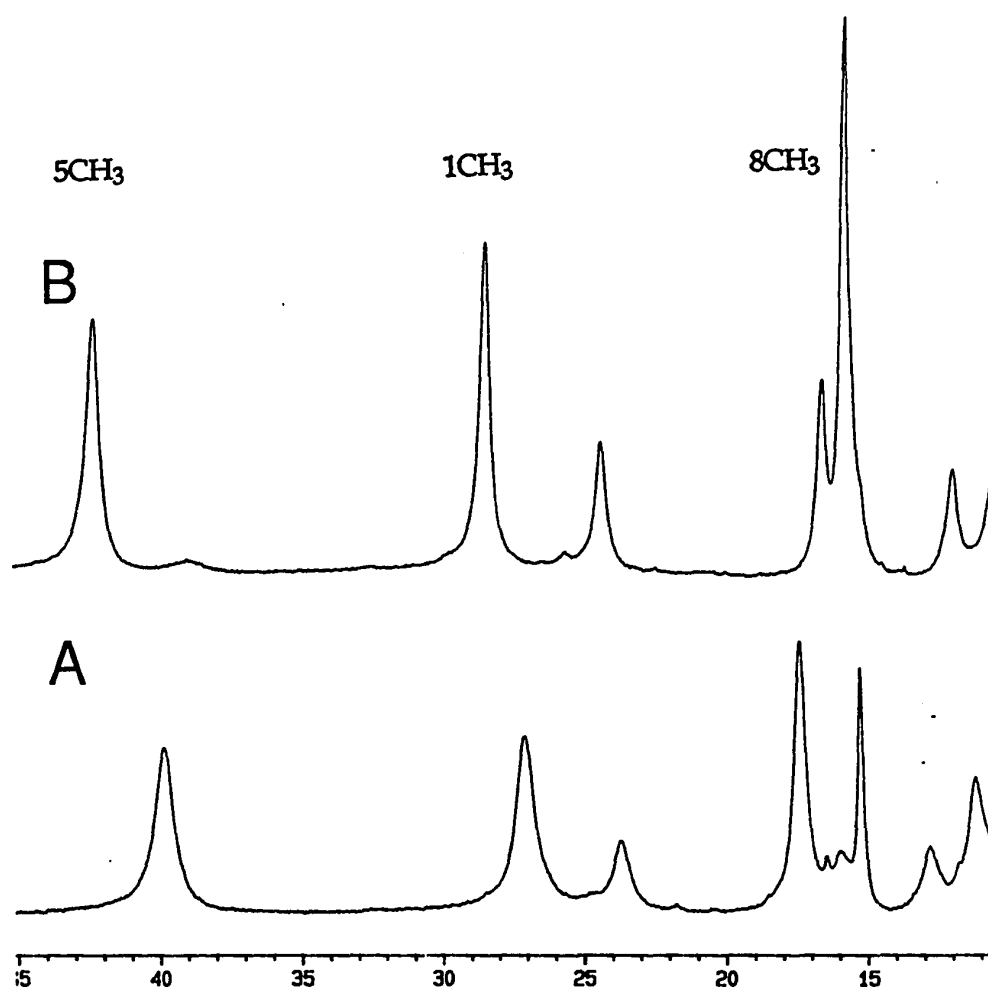


Figure 45. ^1H NMR spectra of metEqMbIm in $^2\text{H}_2\text{O}$, at pH 9.17 and A. 298 K, and B. 278 K.

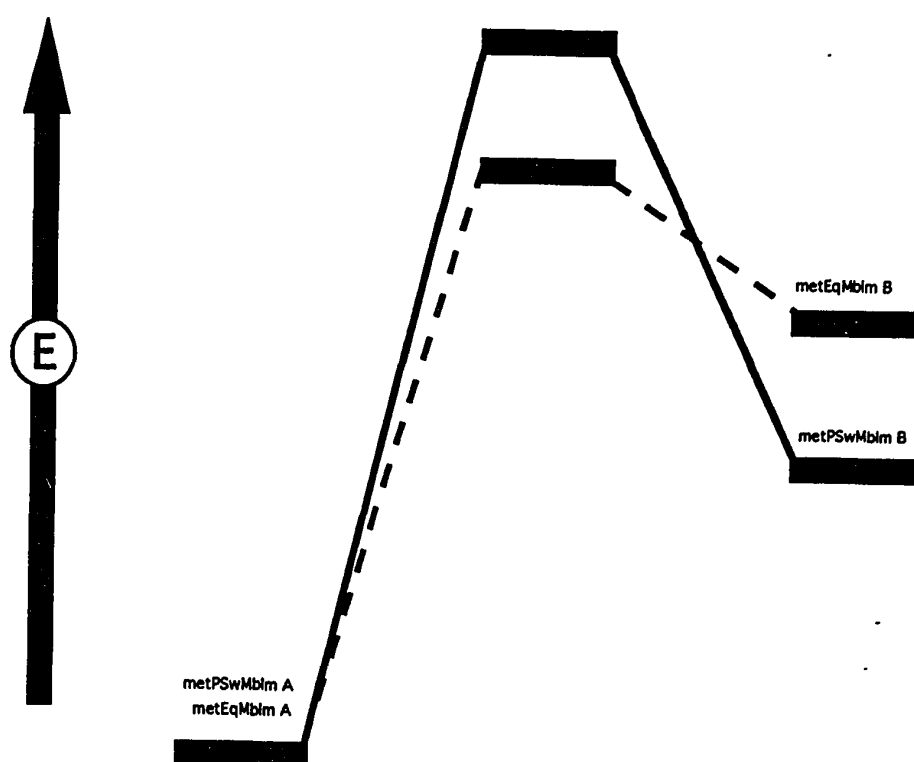


Figure 46. Comparison of the proposed energy diagrams for equilibration of bound Im in metPSwMbIm (solid line) and metEqMbIm (dashed line). Major conformations in both species are arbitrarily set at the same energy level.

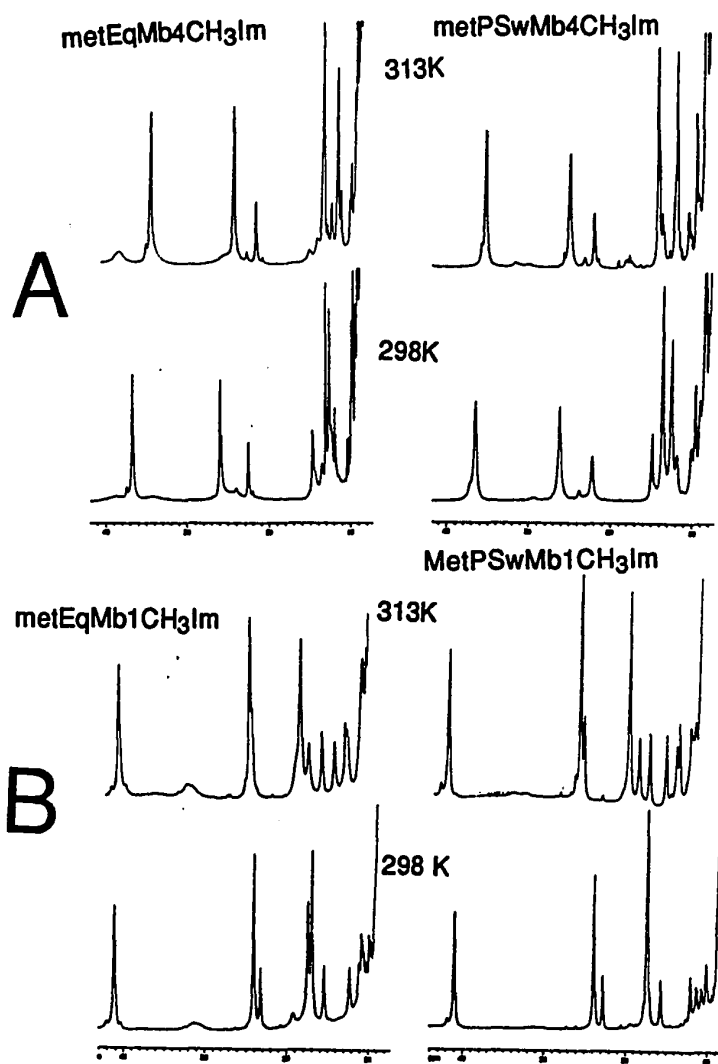


Figure 47. A. ^1H NMR comparison of EqMb4CH₃Im (left) and PSwMb4CH₃Im (right) at 313K (top) and 298K (bottom) pH 9, B. ^1H NMR comparison of EqMb1CH₃Im (left) and PSwMb1CH₃Im (right) at 313K (top) and 298K (bottom) at pH 8.0.

CHAPTER V

PROTON NMR INVESTIGATION OF THE RECONSTITUTION OF EQUINE MYOGLOBIN WITH HEMIN DICYANIDE

Over the past 3-4 decades, efforts have been made by means of optical absorbance (Gibson & Antonini, 1960), circular dichroism (Aojula et al., 1986), and NMR (La Mar et al., 1984) spectroscopic techniques to elucidate the pathway by which heme is reinserted into the globin. Kawamura-Konishi and coworkers (Kawamura-Konishi et al., 1988) reported four independent processes in the reconstitution of dicyanohemin (heme(CN)₂) with apoEqMb. Their study is of special interest because at least one of the proposed processes appears to be slow enough to be monitored by NMR. Others have found, by NMR, that upon reconstitution of apoSwMb with heme(CN)₂, a final 1:1 mixture of heme-insertion isomers, which differs from one another by a 180° rotation about the α,γ -*meso* axis (Lecomte et al., 1985). This is in disagreement with my data, as shown below (Yee & Peyton, 1991). This discrepancy may result from different relative amounts of OH⁻ and CN⁻ ligands complexed to the iron of the heme stock solutions. If the heme(CN)₂ solution pH were very high (>10), then the reconstitution would more resemble addition of heme only to apoMb, followed by quenching with CN⁻. This does lead to 1:1 ratio of heme-insertion isomers (Yee & Peyton, 1991). The degree to which the reorientation reaches equilibrium is conveniently followed by NMR, using the relative intensities of the methyl resonances from each insertion isomer. Again, the paramagnetic nature of metMbCN simplifies the task because three of the four heme methyls are hyperfine-shifted and resolved in metEqMbCN.

Findings from other research in our group (Deeb & Peyton, 1992) stimulated the thought that a slower step in the pathways proposed by Kawamura-Konishi could have corresponded to the breaking of a heme-cyanide bond, and the eventual forming of the proximal Fe-His F8 bond. If the slowest step is indeed found to be the formation of the heme-His F8 bond, the ultimate ratio of the insertion isomers in the metMbCN product would then signify the flexibility of the heme crevice and stability of an initial product, Mb-heme(CN)₂, with respect to reorientation of heme(CN)₂ *prior to iron-cyanide bond breakage*. This chapter compares apoEqMb to apoSwMb with heme(CN)₂ as a probe to test this postulate.

The material presented in this chapter resulted in the publication: Yee, S., and Peyton, D.H., "*Proton NMR investigation of the reconstitution of equine myoglobin with hemin dicyanide: evidence for late formation of the His⁹³F8-iron bond.*" FEBS letters, 290, 119-122, (1991).

RESULTS

Figures 48, 49, and 50 present a comparison of products from the two reconstitution protocols for generating metEqMbCN, metPSwMbCN, and metSwMbCN, respectively. In contrast to ~1:1 ratio of heme-insertion isomers upon cyanide-quenching of the freshly reconstituted myoglobins, heme(CN)₂ generates ~4.5:1 and ~2.5:1 ratios for EqMb and SwMb (also PSwMb), respectively. The same trend between the two reconstitution protocols also exists at pH 7 for EqMb (Figure 51). Possible reasons for observing >1:1 ratio of heme-insertion isomers in Figures 48A, 49A, and 51A include progress toward the native state of 9:1 ratio before quenching with CN⁻, and incomplete incorporation of heme which would then be converted to heme(CN)₂ before insertion. Figure 49 shows an anomaly in the upfield Ile FG5 (~9 ppm) in both cases for metPSwMbCN. This anomaly is reproducible when lyophilized apoPSwMb is used; and

is less severe when non-lyophilized apoPSwMb was used (not shown). Therefore, lyophilization seems to disrupt the integrity of the pocket residues in apoPSwMb, but not apoEqMb and apoSwMb.

Kinetics for the formation of metEqMbCN from heme(CN)₂ and apoEqMb at pH 9.2 and 298 K were done by following the time dependence for formation of the 5CH₃ resonance (of the major insertion isomer); the rate constant $k_{\text{obs}} \sim 3 \times 10^{-2} \text{ s}^{-1}$ was extracted. Figure 52 presents the time-dependence of the resonances by ¹H NMR and the corresponding kinetics plot. This rate corresponds most closely to the longest process reported by Kawamura-Konishi and coworkers with $k_{\text{obs}} \sim 5 \times 10^{-3} \text{ s}^{-1}$ (Kawamura-Konishi et al., 1988). The factor of ~10 difference may be due to the differences in the conditions of the experiments (for example, my reconstitution was performed at 25°C as opposed to theirs at 15°C). The heme-insertion isomer ratio did not change during the course of reconstitution, and no resonance other than from the two heme-insertion isomers were observed in the hyperfine-shifted regions of the spectrum.

DISCUSSION

The following mechanism attempts to account for the results presented.

Heme(CN)₂ is assumed to insert into the heme pocket, giving a 1:1 ratio of heme-insertion isomers of an intermediate, 'Heme(CN)₂·EqMb'. Equilibration toward the native heme-insertion isomer ratio would then occur before proximal CN⁻ is displaced by F8 His. Comparison between EqMb and SwMb (and PSwMb) (compare Figures 48 to 51) clearly reflects a fundamental difference between the two species in the heme pocket -- most likely the difference in Arg/Lys CD3 residue. Distal Arg/Lys CD3 is a surface residue that play a direct role in the mechanism of oxygen diffusion into and out of the heme pocket mainly because the side-chain of Arg/Lys CD3 is salt-bridged to the heme 6-propionate. The salt bridge involving Arg CD3 in SwMb has been reported to be more stable than that involving

Lys CD3 in EqMb by ~ 0.6 kcal/mol (Lecomte & La Mar, 1985; La Mar et al., 1991). Therefore, a "closed" conformation of the heme pocket is favored in SwMb, thus reducing the flexibility of the heme crevice. More probably, because the Arg salt-bridge is more stable, this strength may hold each isomer stronger so displacement of CN⁻ by His F8 in the reverse isomer is more likely. This is directly reflected by the ratio of heme insertion-isomer in SwMb relative to EqMb. Cyanide is unique for this method because it is, by far, the strongest-field ligand that binds to hemoproteins; this is pertinent to NMR spectroscopy because not only is longer time required to break the heme-CN bond, but also that heme reorientation may require the distal bond to be broken. Hence, these conditions allow the formation of metMbCN to be followed on the NMR time-scale.

All other processes than the one reported here seen by optical spectroscopic methods (Kawamura-Konishi et al., 1988) are much too fast to observe by our NMR measurements. Because heme(CN)₂ is supposed to insert into the heme pocket within 1 s, it appears that there is at least one intermediate species which is not observed in the hyperfine-shifted regions of the spectra. The reasons for not observing this may be that more than one initial set of products is formed. Kawamura-Konishi et al. (1988) reported four steps, and that there is exchange between at least two of these. If exchange were to be faster than the chemical shift difference of the exchanging peaks, we would not be able to distinguish the broadened peaks from the baseline (Sandström, 1982). This problem is very important for ¹H NMR of paramagnetic systems. On the other hand, it may be that peaks for the intermediates are very broad and/or heterogeneous, so as not to be observed. Should the isomer ratio shown in Figures 48-51 reflect the equilibrium ratio for 'heme(CN)₂Mb', it is likely that an intermediate would have a different isomer distribution than the native Mb because at least the proximal side of the heme pocket would be considerably distorted in 'heme(CN)₂Mb'.

CONCLUSIONS

Even though the only process we can observe directly by NMR using the methods as reported is formation of the heme-insertion mixture, the product ratio permits us to probe the mechanism of reconstitution. Furthermore, based on these results, caution must be advised when studying reconstitutions with heme ligands which might be slow to dissociate. Reconstitution with stock solutions hemin dicyanide at very high pH may be used, but only if the metMbOH system is to be studied, because at high pH, insertion of the heme and displacement of OH⁻ by His F8 is fast relative to displacement of OH⁻ by CN⁻ (McGrath & La Mar., 1978).

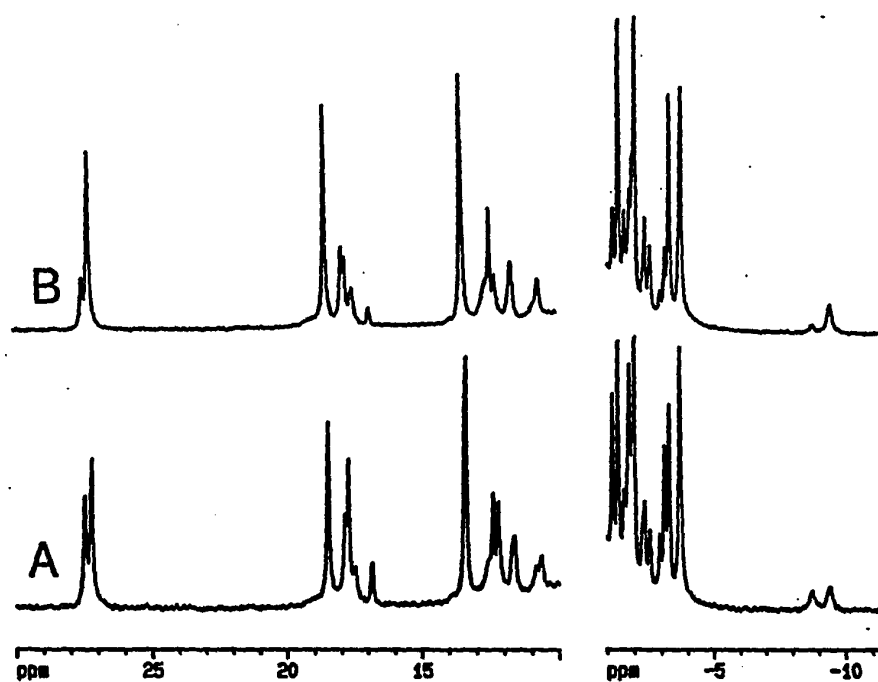


Figure 48. Products of reconstitution reactions at pH 9.2 and 25°C in $^2\text{H}_2\text{O}$. **A.** Product of heme + apoEqMb, then CN^- added; **B.** Product of heme(CN) $_2$ + apoEqMb. Data were collected at 1024 transients with a repetition rate of 1 s^{-1} employing quadrature. The acquisitions are initiated 0.5 hr after mixing the heme and apoMb. The difference in the ratio of heme insertion-isomers between these two protocols at pH 7.0 is not as obvious as in pH 9, shown in the following figures.

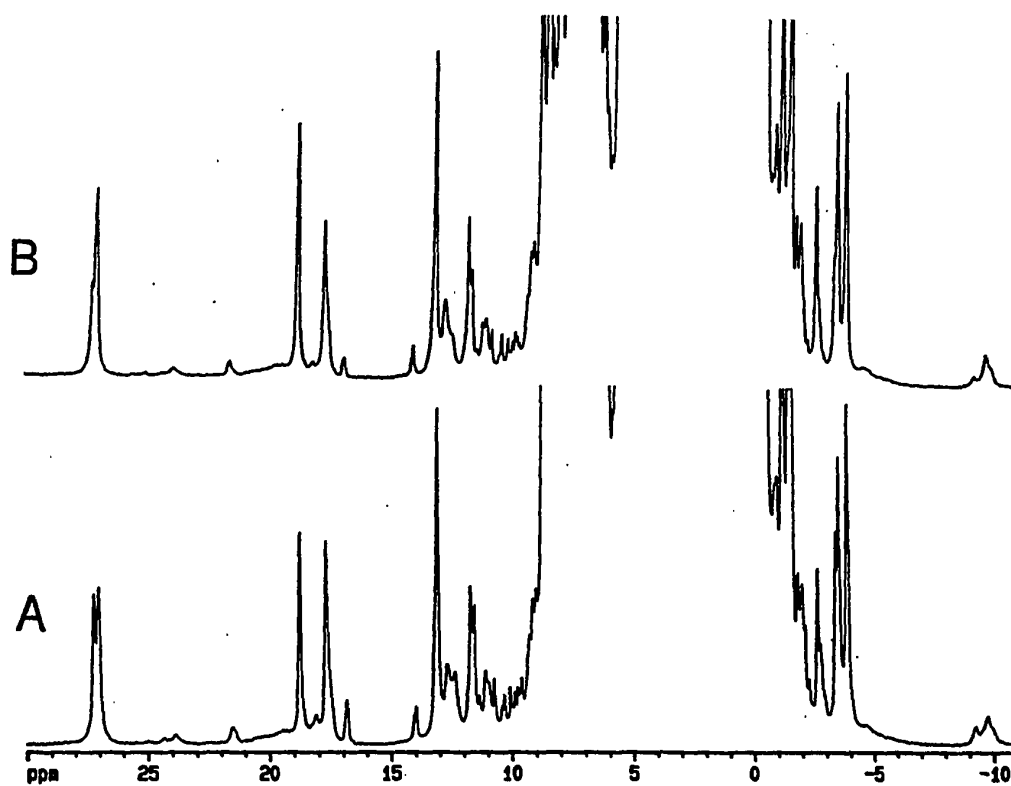


Figure 49. Products of reconstitution reactions for metPSwMbCN at pH 9.2 and 25°C in $^2\text{H}_2\text{O}$. **A.** Product of recon heme+ apoPSwMb, then + CN^- ; **B.** Product of heme(CN) $_2$ + apoPSwMb. Data were collected at 1024 transients with a repetition rate of 1 s^{-1} employing quadrature. The acquisitions are initiated 0.5 hr after mixing the heme and apoMb.

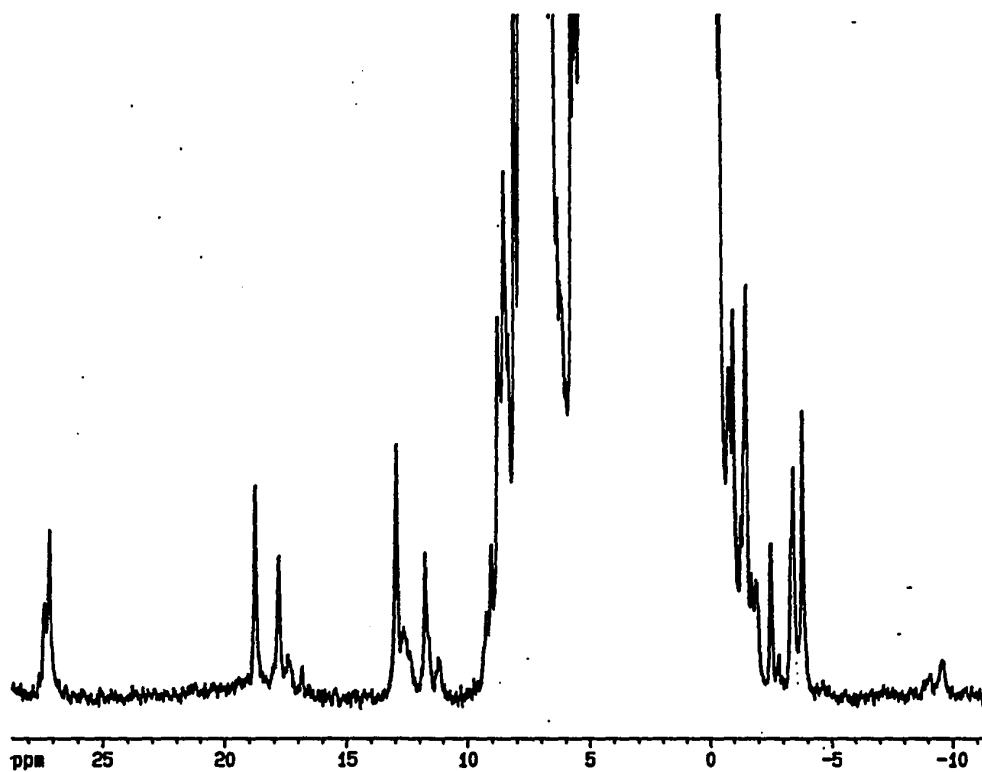


Figure 50. ^1H NMR of the product of reconstitution of apoSwMb with heme(CN) $_2$, at pH 9 and 25°C. Data were collected at 1024 transients with a repetition rate of 1 s $^{-1}$ employing quadrature. The acquisitions are initiated 0.5 hr after mixing the heme and apoMb.

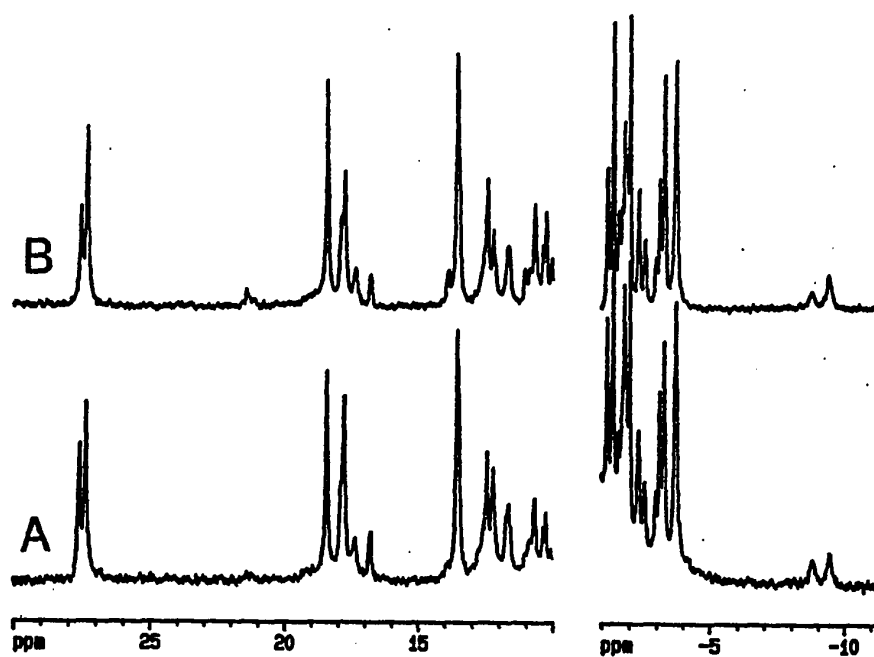


Figure 51. ^1H NMR of the products of reconstitution reactions at pH 7.0 and 25°C in $^2\text{H}_2\text{O}$. A. Product of heme(CN) $_2$ + apoEqMb; B. Product of heme(CN) $_2$ + apoEqMb. Data were collected at 1024 transients with a repetition rate of 1 s^{-1} employing quadrature. The acquisitions are initiated 0.5 hr after mixing the heme and apoMb.

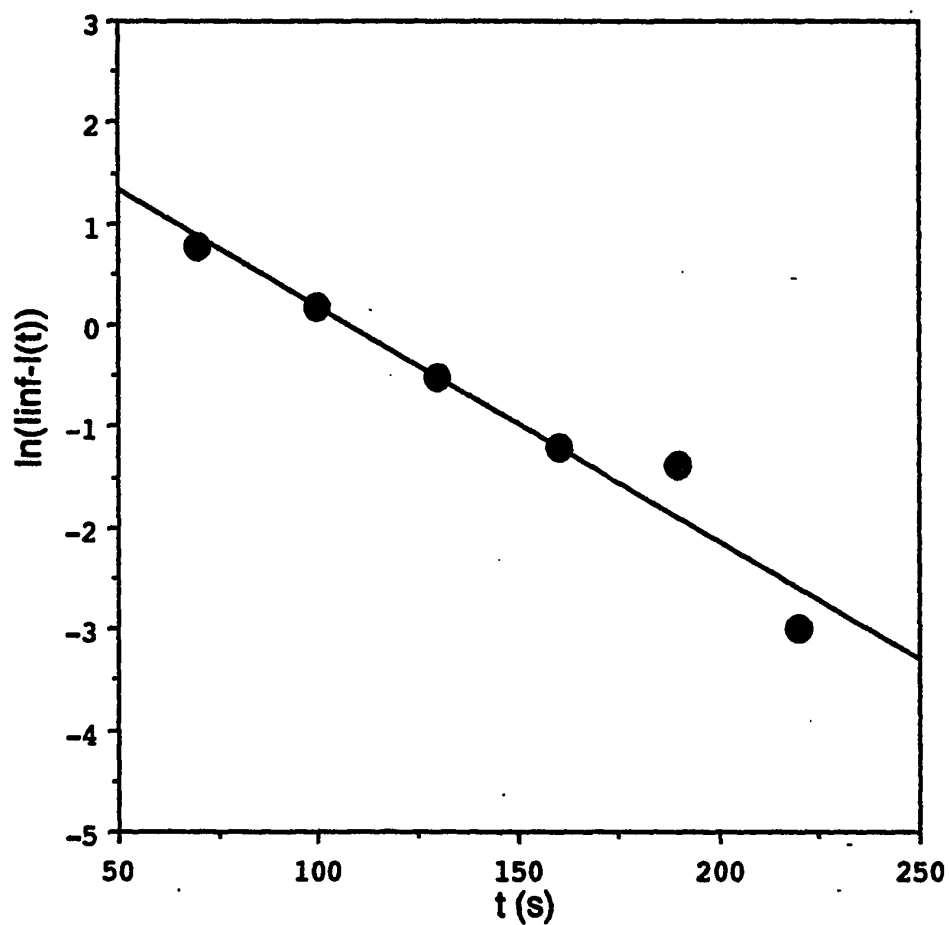


Figure 52. Kinetics for the formation of metEqMbCN from heme(CN)₂ and apoEqMb at pH 9.2 and 25°C, acquired within 0.5 hour after reconstitution. Each data point represents the time when a spectrum was recorded, which required ~0.25 min. Each time value required accumulation of 16 transients.

CHAPTER VI

STUDY OF HEME BINDING TO THE PROTEIN MATRIX BY ^1H NMR AND OPTICAL ABSORPTION SPECTROSCOPY

As a further effort to understand oxygen affinity and metal-toxication processes, this chapter evaluates the mechanism of heme binding to the protein matrix. Controversial work (Livinston et al., 1984; Light et al., 1986) has been done which asserted significantly different oxygen affinity for the two heme orientations, to illustrate the insight one can gain by studying heme reconstitution. High-resolution ^1H NMR has provided a general scheme in which the heme incorporated into the protein matrix as a 1:1 ratio of isomers which differ by a 180° rotation about the α,γ -*meso* axis. When equilibrium is reached, the dominant component ($\sim 90\%$ of the total isomer) has the same orientation as found in X-ray crystal structure (Takano, 1977). The highly similar ^1H NMR and optical spectra suggest that overall protein folding is essentially the same for both conformations. Heme reconstitution has long been pictured as in Figure 53 (La Mar et al., 1984), where bimolecular reaction occurs between the heme and apoprotein with association rate, k_2 . Dissociation is assumed to be first order reaction with rate of k_1 . Superscripts designate the heme insertion isomer, as labeled in the inset of Figure 53. k_2^A and k_2^B are taken to be the same because heme inserts in an initial 1:1 ratio. k_b and k_f are the reorientation rate constants.

The equilibration of the isomers, characterized by k_f and k_b , can be envisioned to occur by one of two mechanisms, both of which require the rupture of the heme-protein bond, i.e. the iron-His F8 bond. One pathway is reversible dissociation, where heme dissociates completely from the protein matrix, flips 180° , and re-inserts ($A \rightleftharpoons C \rightleftharpoons B$ in Figure 53). The other is an intramolecular rearrangement, where the Fe-His F8 bond

dissociates, the heme flips within the protein crevice, and the F8-Fe bond reforms ($A \rightleftharpoons B$ in Figure 53).

La Mar and coworkers (La Mar et al., 1984) have done competition studies of this system by ^1H NMR spectroscopy with a variety of iron-porphyrin derivatives, and concluded that the latter mechanism correlates most appropriately with their results. The extremely small heme-dissociation constant from Mb is indicative of the implausibility of the complete-dissociative pathway. Especially in light of the extraordinary protein flexibility which allows the myoglobin heme-binding pocket to accommodate double-decked Sn-protoporphyrin dimer (Deeb & Peyton, 1991), the intramolecular model seems likely. La Mar and coworkers' efforts also included pH dependence of heme reorientation. Upon close examination of their work, however, it was realized that the use of chromatography to eliminate artifacts due to heme dimerization was neglected. They essentially assumed that effects caused by heme-dimerization are minimal.

This chapter provides more supporting evidence to the intramolecular model by determining activated free energies of heme rotational disorder through temperature study. In addition, it presents the results of both NMR and optical studies of the reorientation EqMb with the inclusion of size-exclusion chromatography to demonstrate the significance of heme self-association to the reconstitution process. In a variable temperature study, the rate constant for interconversion between heme-insertion isomers at each temperature was determined. The Arrhenius and Eyring equations are used to extract activation energy parameters for the reorientation. The free-energy diagram obtained from this work did not rule out the possibility of a total dissociative mechanism. Nevertheless, it depicts a better picture for the heme redistribution process, in which the heme crevice sustains a sizable disruption.

METHODS

Determination of the heme reorientation kinetics

The time courses of the reconstitutions were all followed in the metMbH₂O form, by the development of the heme methyls peaks and the shift in the Soret band by ¹H NMR and optical spectroscopy, respectively. The ¹H NMR heme methyl peaks of metSwMbH₂O have been assigned previously (La Mar et al., 1980; Davis, 1982); similar NMR heme resonances to those of metEqMbH₂O and metPSwMbH₂O were expected because of homologous sequences and compatible heme pocket residues (Carver et al., 1991). Heme methyl-peak areas, M₁ and m₁ for the 'native' and the 'reversed' isomers (Figure 54), respectively, were used in Equation (13). The peak-areas were monitored over a period of time until the protein reached equilibrium, and k_{obs}'s were determined with the Equation (14) (La Mar et al., 1984):

$$A_i = [M_1]_i / [M_1 + m_1]_i \quad (13)$$

$$\ln(A_t - A_e / A_0 - A_e) = -k_{obs} t = \ln(A_e - A_t) \quad (14)$$

where A₀, A_t, and A_e are the mole fractions of the native protein at i = time zero, t, and at equilibrium, respectively; M₁ and m₁ are the peak areas of the methyls at time i. t is time in minute. A correction factor for heme rotational disorder was considered with the introduction of K_D, and the desired k_f was found to be

$$k_f = k_{obs} K_D / (K_D + 1) \quad (15)$$

K_D is the ratio of the intensities of major to minor peak at equilibrium, which is characteristic of the individual Mbs, the heme species, as well as possibly the ligated states. K_D used here is 12 for metEqMbH₂O.

For UV-VIS determination, the change in absorbances of the spectra were measured. The difference spectra were all taken by subtracting the runs at time t from the equilibrated one, $A_e - A_t$ (Gebe et al., 1989) (Figure 55). k_{obs} 's were then obtained from plots of $\ln(A_e - A_t)$ vs time according to Equation (14). The same correction factor was used to determine k_f 's.

Determination of Activated Energy Parameters

Temperature dependence studies were carried out to gain activation parameters. At each temperature, k_f for reorientation was extracted based on Equation (14). A combination of Arrhenius and Eyring Equations (Equations (16) and (17), respectively) were then employed to determine the activated change of enthalpy, entropy, and free energy for the process of heme redistribution.

$$k = Ae^{-E_a/RT} \quad (16)$$

$$k = (KRT/N_A h)e^{-\Delta G^\ddagger/RT} = (KRT/N_A h)e^{+\Delta S^\ddagger/R} \cdot e^{-\Delta H^\ddagger/RT} \quad (17)$$

where k is the rate constant, A is the Arrhenius constant, E_a is the activated energy, K is the transmission coefficient (here, the assumption is that all of the reactant at the transition state goes to product, so $K = 1$), R is the gas constant (which is 8.314 J/mol/ $^\circ$ K, or 2.0 cal/mol/ $^\circ$ K), T is the temperature, N_A is the Avogadro's number, h is the Planck's constant, ΔG^\ddagger is Gibbs free energy, ΔS^\ddagger the entropy, and ΔH^\ddagger the enthalpy of activation. Taking natural logarithm of Equation (16) allows the derivation of E_a from Equations (18) and (19); and natural logarithm of Equation (17) leads to Equations (20), (21), and (22).

$$\ln k = \ln A - E_a/RT \quad (18)$$

$$\partial \ln k / \partial (T^{-1}) = -E_a/R \quad (19)$$

$$\ln k = \ln R + \ln T - \ln N_A - \ln h + \Delta S^\ddagger/R - \Delta H^\ddagger/RT \quad (20)$$

$$\partial \ln k / \partial (T^{-1}) = (\partial \ln k / \partial T) (\partial T / \partial T^{-1}) = (1/T + \Delta H^\ddagger/RT^2)(-T^2) \quad (21)$$

$$\partial \ln k / \partial (T^{-1}) = -(\Delta H^\ddagger + RT)/R \quad (22)$$

Equations (19) and (22) thus combine to yield Equation (23):

$$\Delta H^\ddagger = E_a - RT \quad (23)$$

Therefore, an Arrhenius plot (Equation (19)) obtained from k 's at variable temperatures leads directly to ΔH^\ddagger . The entropy term can be derived either directly from Equation (21), or from the intercept off the Arrhenius plot. Finally, the Gibbs free energy of activation is extracted from Equation (24):

$$\Delta G^\ddagger = \Delta H^\ddagger - T\Delta S^\ddagger \quad (24)$$

RESULTS AND DISCUSSION

Effects of Size Exclusion Chromatography

Chapter II outlines the details of the experiments. The data obtained with and without size-exclusion column chromatography by ^1H NMR and UV-VIS spectroscopy at different pHs and concentrations is presented in Table VIII (see also Figures 56-58).

The results dictate that there is an obvious discrepancy that can be traced to the use of the column. While the reorientational rate constants are within uncertainty range between the two spectroscopic methods, the reconstitution performed without column elution consistently yielded rate constant of ~1.5 fold lower. Because NMR experiments were done at a concentration of mM levels for better signal resolution, while UV-VIS experiments required that only at μM levels, reconstitution of EqMb at ~5 fold the

TABLE VIII

HEME REORIENTATION RATES, k_f , AT pH 6.7 AND 25°C IN 1:1
CONCENTRATION RATIO OF HEME TO APOEqMb

<u>Conditions</u>	<u>Rate Constants ($\times 10^3 \text{ min}^{-1}$)</u>
Without gel filtration (by NMR)	0.97
With gel filtration (by NMR)	1.8
(by UV-Vis) ^a	1.6
(by UV-Vis) ^b	1.7

a. Concentration of the final reconstituted Mb is on the order of 0.1 mM.

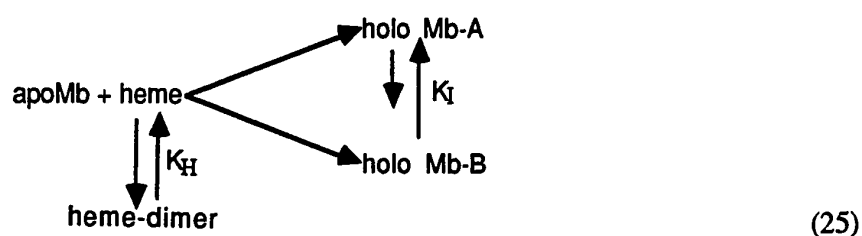
b. 5-fold the concentration in a.

usual spectrophotometric concentration was also performed (with a 0.5 cm pathlength cell) to assess the concentration dependence (data also included in Table VIII). The result paralleled that shown by previous study on SwMb (La Mar et al, 1984), that the process is clearly independent of concentration. This is significant because it justified the direct comparison of the results between these two methods.

The discrepancy is best explained by the presence of more than one process at comparable rates, escaping earlier scrutiny. The most compelling evidence for this rationale, though, comes from the ^1H NMR spectra themselves (Figures 56, 57). When integration of each of the methyl resonances was determined for both with and without chromatography, the former (Figure 56) gave the expected shift of intensity ratio from an initial ~1:1 to the final ~10:1 ratio; on the other hand, the latter (Figure 57) showed a constant increase in integrals of both the major and the minor forms. Kinetics plots of $\ln(A_e - A_t)$ vs time obtained as a result of Figures 56 and 57 clearly distinguishes the two protocols (Figure 59).

The results presented underscore the importance of experimental details involved in kinetics analysis. In the absence of chromatography, dimerization of excess heme occurs readily in solution (Blauer & Silfen, 1982). When that happens, reconstitution of

apoMb with heme becomes a competitive process. Heme-dimer association competes against heme insertion into the apo; while heme-dimer dissociation competes against holo Mb-A to holo Mb-B interconversion. These interacting reactions can be represented as in Equation (25):



where holo Mb-A and holo Mb-B are the major and minor heme insertion isomers, respectively, and the postulate here is that $K_H \sim K_I$. These intervening reactions will slow the reorientational disorder apparent rate (Blauer & Silfen, 1982). Above neutral pH, OH^- becomes more prevalent, and can compete favorably (McGrath et al., 1978) with H_2O to form metMbOH, instead of metMbH₂O -- the system being studied. To avoid that complication, the data and discussion are limited to interactions at $\text{pH} < 7$.

The crucial question arises as to whether the findings nullified the previous kinetics work done on heme reorientational disorder. It has been shown that at pH's between ~ 8.5 and ~ 6 , heme flipping occurs an order of magnitude slower than at other pH's (La Mar et al., 1984). Since it is demonstrated here that heme dimerization competes with the reconstitution process at pH 6.72, where the reorientation rate constant is expected to be low, the interacting dimerization process must also be on a similar time-scale. Therefore, at higher pH's, the competing processes observed will be at a much lower rate to be successfully affecting measure of the reinsertion process. Hence, negligible discrepancies for kinetics studies done at pH's below 6.5 and above 8.5 is expected. At the pH region of concern (pH 6.7 - 8.4), on the other hand, even though the rate constants obtained were

lower than they should have been (for example, compare k_{fs} with and without gel filtration in Table VIII), kinetics plots of $\ln(A_e - A_t)$ vs time appeared linear under both conditions (Figure 59). This explained why previous workers were oblivious to the significance of chromatography. The time-scale of the interacting heme aggregation must be sufficiently close to that of the heme insertion and reorientation; or one would expect to see deviation of the kinetics plots from linear relationship. Therefore, it is reasonable to conclude that while the use of size-exclusion chromatography is indeed indispensable for kinetics analysis of heme-apo reconstitution, especially when done at pH region of slow insertion rate, it does not nullify the conclusions made by previous workers. However, with the intervention of heme-dimerization, depending on the extent of excess heme used, the range of rate constants obtained may be greater than expected between two independent reconstitutions at the same pH, which may explain the sizable error bars found in referenced work (La Mar et al., 1984).

The most significant conclusion from this work is the fact that kinetics determination by optical spectroscopy is quantitatively compatible with the results by NMR. Earlier work by Gebe et al. (1989) found discrepancy between the reorientational rate constant obtained by optical and NMR methods (La Mar et al., 1984), casting unnecessary doubts on the validity of optical spectroscopy, when in fact, it was the NMR work that was performed inadequately, i.e. size-exclusion chromatography was neglected. This is important because it validates the following determination of activation energies by optical methods, saves on NMR time (which is often competitive and expensive), and minimized the amount of protein used.

Temperature Dependence of heme redistribution in EqMb

Table IX presents k_{fs} obtained, based on Equation (14) (see also Figure 59) at various temperatures for the reorientation at pH 8.3-8.5, as indicated. Table X lists

activation energy parameters. Also included on Table X are activated free energy parameters found for carboxyheme insertion into apohumanMb at pH 9.1 from previous work (Gibson & Antonini, 1960). Figure 60 shows the Arrhenius plot that resulted from Table IX.

TABLE IX

RATE CONSTANTS OF REORIENTATION OF EqMb
RECONSTITUTED FROM 5:1 APO TO HEME CONCENTRATION BY
OPTICAL SPECTROSCOPY WITH COLUMN CHROMATOGRAPHY
AT pH 8.38-8.50 AND VARIOUS TEMPERATURES

Rate Constants, k_f ($\times 10^3 \text{ min}^{-1}$)	Temperatures (K)
0.51	283.0
2.2	294.4
5.8 ^a	295.2
7.3	301.1
11	305.0
54	312.2
130	314.5
180	316.2

a. 1:1 concentration ratio of apoEqMb:heme.

TABLE X

ACTIVATION FREE ENERGIES FOR HEME REORIENTATIONAL
DISORDER IN EqMb AND HEME INSERTION IN HUMAN Mb^a

	ΔH^\ddagger (kcal/mol)	ΔS^\ddagger (cal/mol/K)	ΔG^\ddagger (kcal/mol)
Heme Reorientation (294.4 K)	30.6	33.7	20.7
Heme Insertion (293 K) ^b (Figure 61)			22.6

a. Parameters were determined from fitting data in Table IX to Equation (19).

b. Data was obtained from Antonini & Gibson, 1960.

A free energy diagram of the proposed mechanism for heme insertion into human Mb (Antonini & Gibson, 1960) is presented in Figure 61, to compare with the activation Gibbs free energy from this work. The diagram assumes that redistribution of heme follows a reversibly, and completely dissociative route, with the assumption that both the dissociated and the free (heme + apoMb) are at the same energy level. Only one heme-insertion isomer is shown in Figure 61.

Scientific intuition of the heme reorientation pathway is that of the intramolecular rearrangement because of evidence provided by the previous work (La Mar et al., 1984), and the extremely small dissociation constant of heme from the protein matrix ($K_d \sim 10^{-12}$ M). The only reason that argues against this mechanism is the compactness of the heme crevice from X-ray crystal structure (Takano, 1977). The compatibility of the activation energy parameters (ΔG^\ddagger 's are within the estimated experimental uncertainty of $\sim 10\%$) of this work with those of the heme-insertion pathway envisions a highly disrupted transient state of Mb to allow for the redistribution of the heme isomers within the heme pocket; the extent of the perturbation is apparently on the order of the complete heme dissociation postulate.

CONCLUSIONS

This work does not rule out the completely dissociative pathway of heme reorientational disorder, but shows that there would be substantial structural stress for the intramolecular rearrangement model. There are numerous other reasons in favor of this intramolecular model. The identification of a stable, low pH intermediate apoMb by ^1H NMR (Hughson et al., 1990) and modeling by molecular dynamics simulation (Brooks III, 1992) dictated that F-helix in apoMb is partially unfolded and therefore is highly flexible. Optical spectroscopy and electron paramagnetic resonance studies on the reconstitution of heme A, which replaces the 4-vinyl and 8- CH_3 of protohemin IX by a long hydrocarbon

chain and formyl group, respectively, with apoEqMb showed evidence of binding but disruption of the globin matrix (Larsen et al., 1992). The detection of the insertion of Sn-protoporphyrin IX dimer (Deeb & Peyton, 1992) in apoEqMb further reflects the ability for the protein matrix to accommodate sizable, hydrophobic prosthetic groups. These studies show that it is highly conceivable for the heme-binding cavity to overcome steric hindrance, given the flexibility of F-helix which is responsible for embracing heme in place after initial bimolecular reaction. This accommodation results at the expense of inevitable globin disruption, evident from the enormous entropic change accompanied by the activated complex.

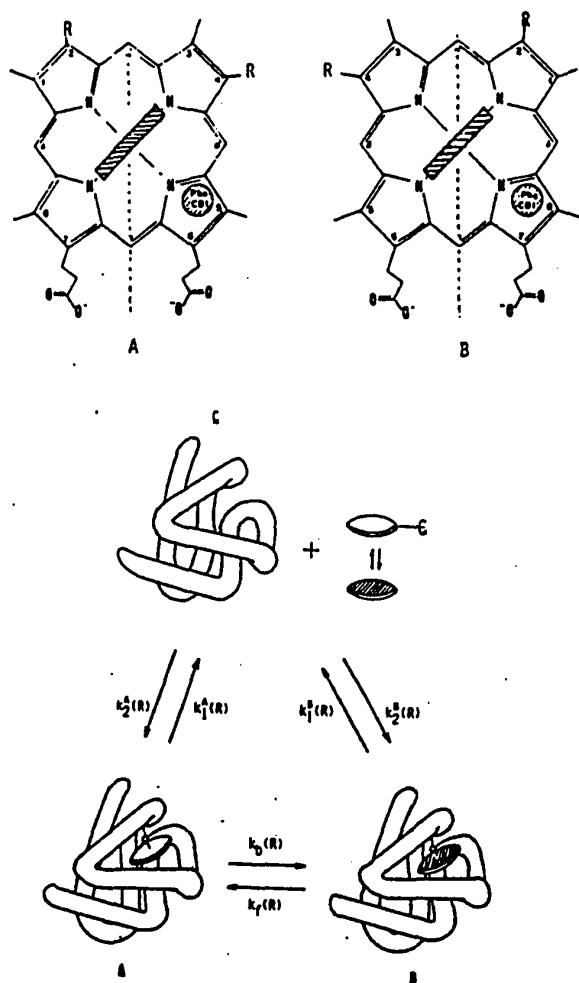


Figure 53. **TOP.** The top-down view of the major, and minor insertion-isomers on the right and left, respectively. **BOTTOM.** Schematic representation of the reconstitution processes between apoMb and heme. A and B are the holoproteins formed from the relative isomers from top, which are represented here as the open and shaded disks, respectively.

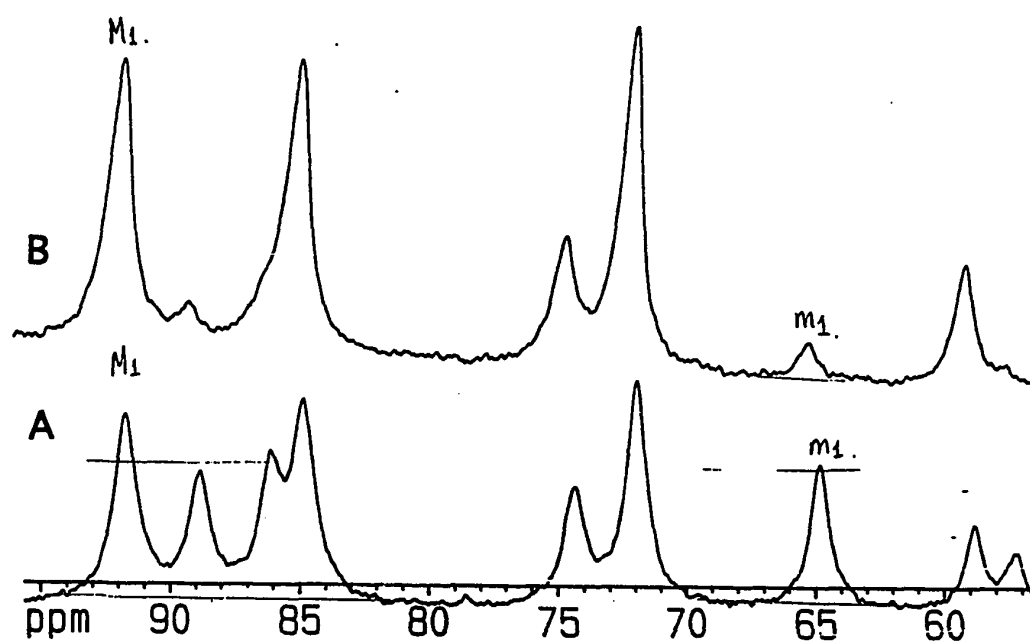


Figure 54. Low field portion of the 400-MHz ^1H NMR spectrum of the reaction product immediately after the reconstitution of 1 equivalence each of apoEqMb and heme at pH 6.72 and 25°C , with the use of column chromatography. M_1 and m_1 are the peaks corresponding to the major and minor form, respectively, used for calculation of k_{obsd} . A. 145 min after reconstitution; B. 1461 min after reconstitution.

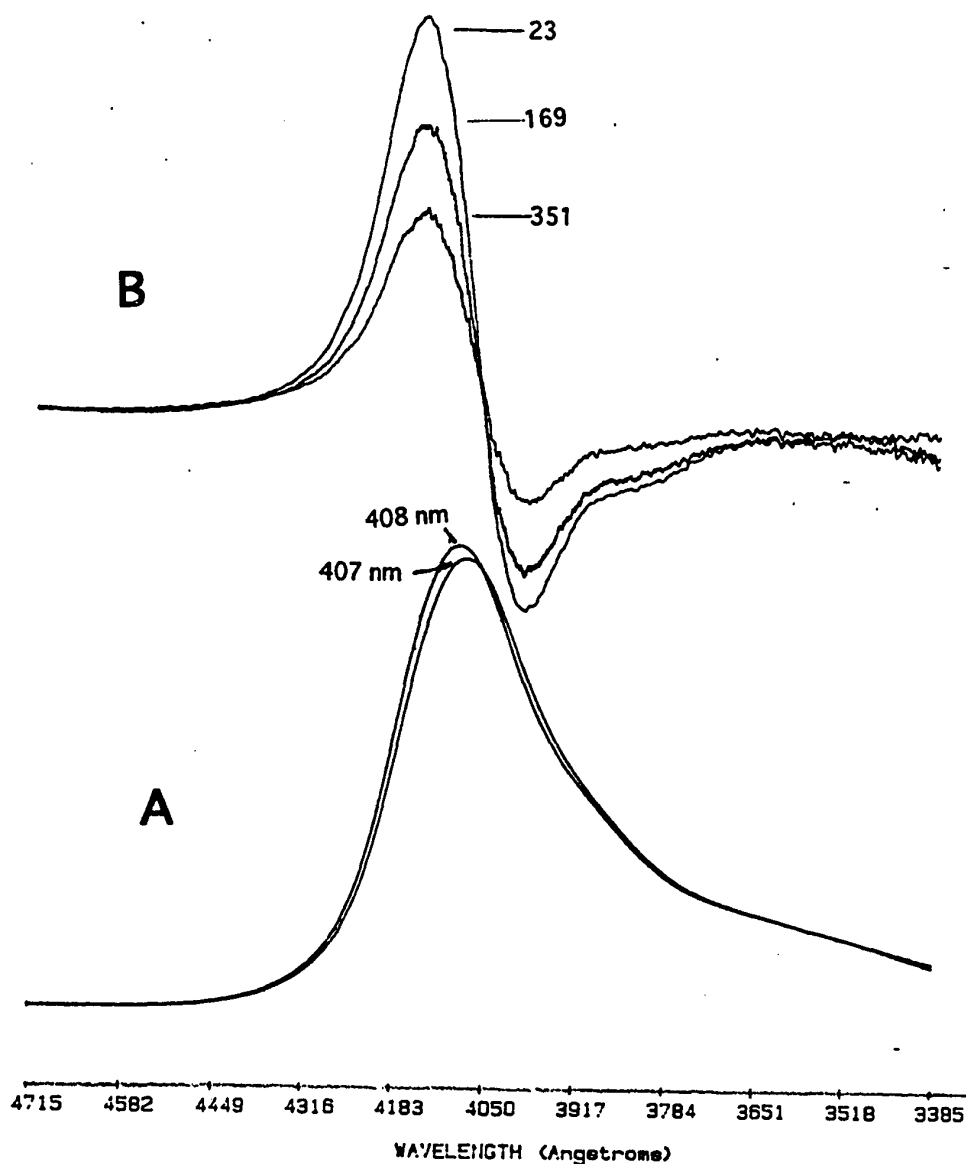


Figure 55. UV-VIS spectrum of the Soret region of reconstituted EqMb at pH 6.71 and 26.5°C. **A.** Absorbance tracing at 23 minutes and 2096 minutes, λ_{max} 's on each Soret band are marked, the absorbance of each is ~ 0.3 OD, **B.** Difference spectra of Soret region obtained by subtracting the spectra at 23 minutes, 157 minutes, and 361 from that at 2096 minutes. Times are as marked correspondingly. The vertical line labels the isosbestic point on the difference spectra.

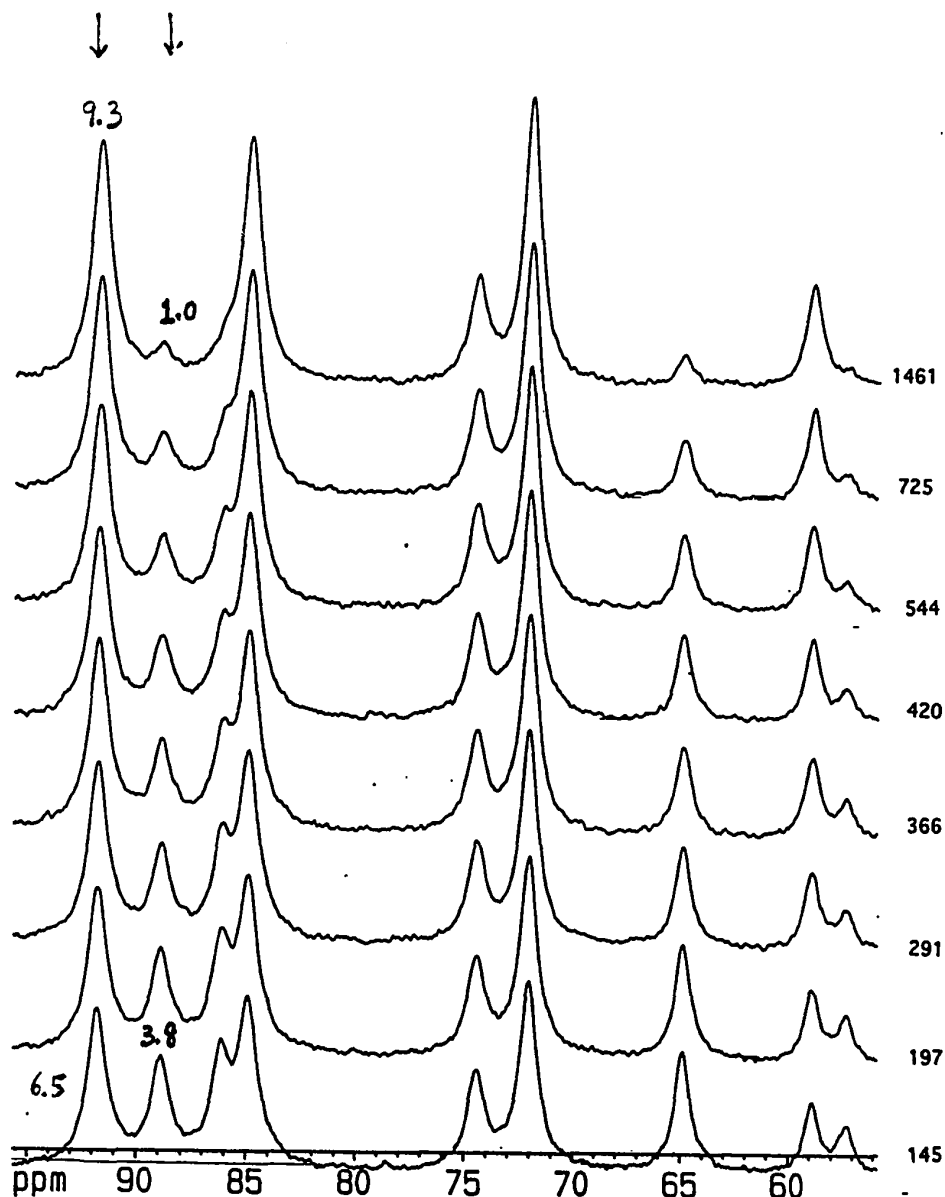


Figure 56. Low-field portions of the 400-MHz ^1H NMR spectra of the reconstitution of 1 equivalence each of apoEgMb and heme at pH 6.72 in $^2\text{H}_2\text{O}$ with the use of chromatography; the elapsed times are indicated at the right. Intensity ratios of the designated heme insertion-isomers were marked on the initial and final spectra. The sum of the ratio remained constant throughout the course of reconstitution.

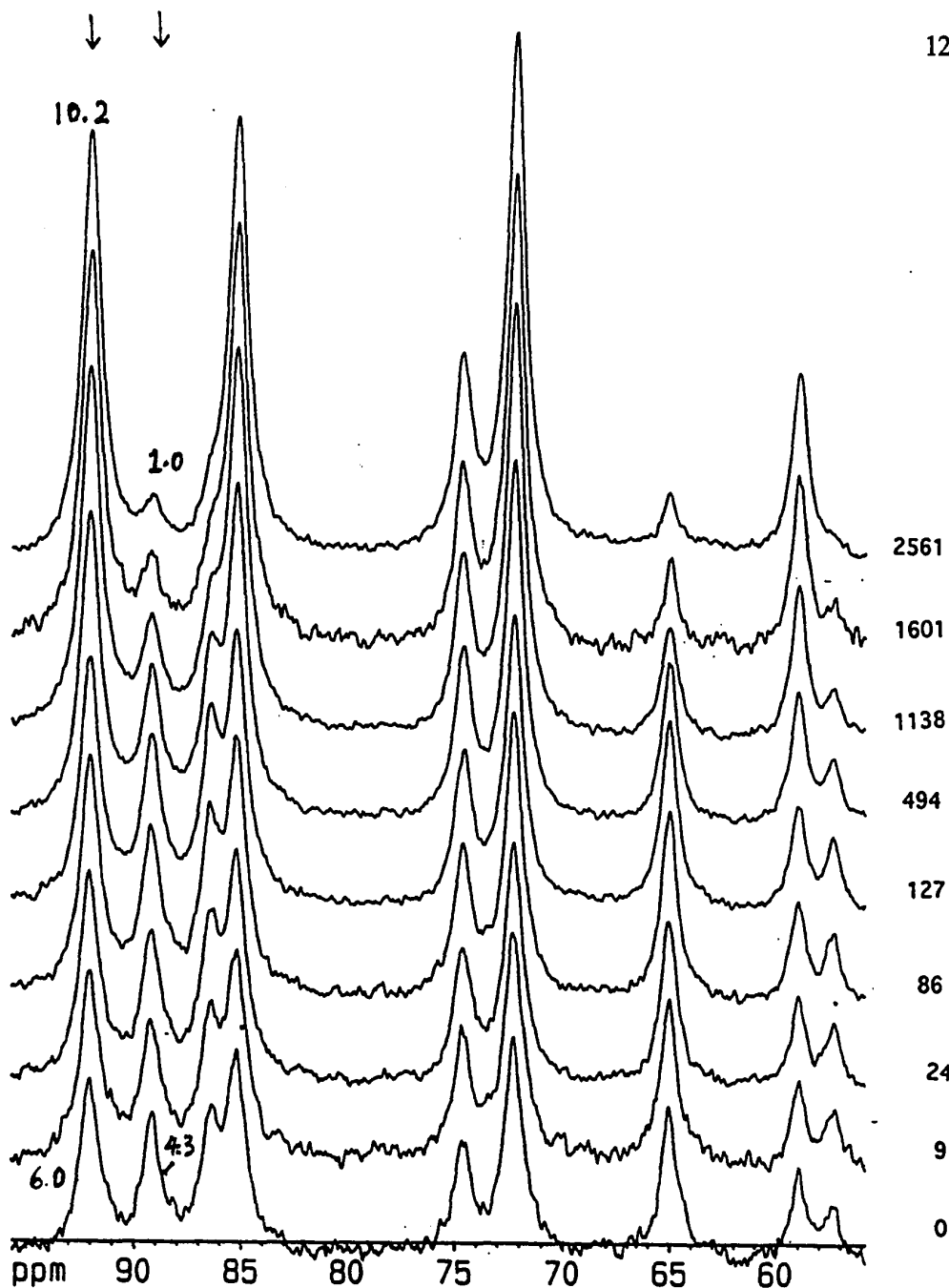


Figure 57 Low-field portions of the 400-MHz ^1H NMR spectra of the reconstitution of 1 equivalence each of apoEgMb and heme at pH 6.72 in $^2\text{H}_2\text{O}$ without the use of chromatography; the elapsed times are indicated on the right. Intensity ratios of the designated heme insertion-isomers were marked on the initial and final spectra. The sum of the ratio increased throughout the course of reconstitution.

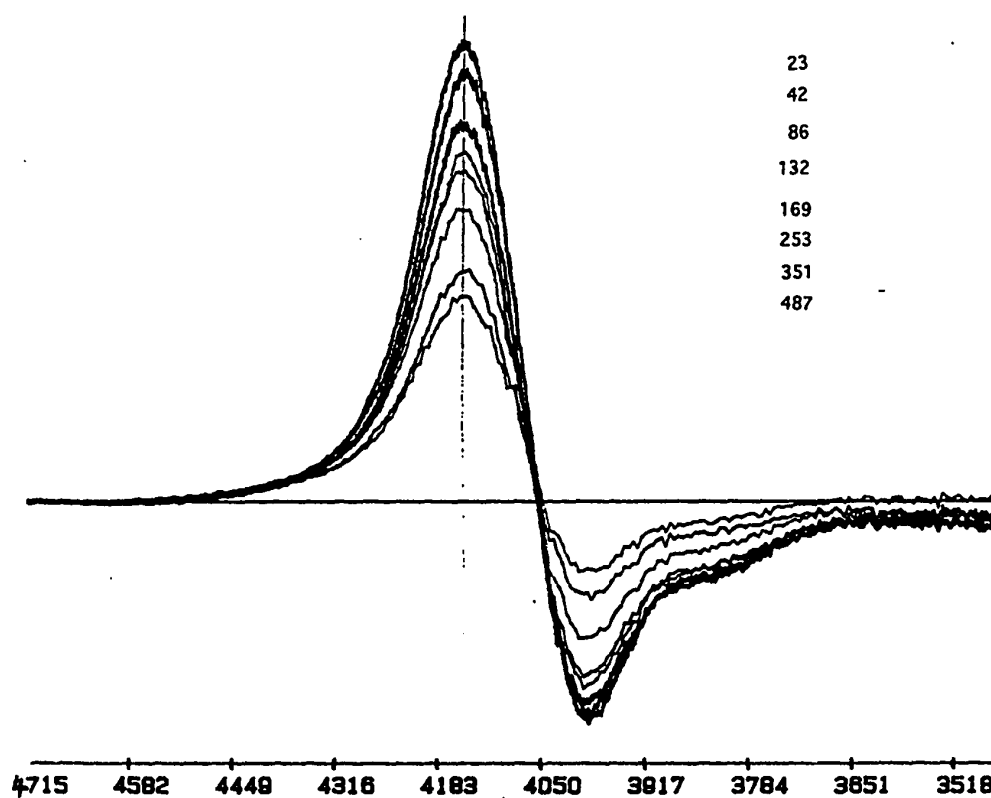


Figure 58 Optical spectroscopy difference spectra of the reconstitution of 1 equivalence each of apoEgMb and heme at pH 6.72 in $^2\text{H}_2\text{O}$ with the use of chromatography; the elapsed times are indicated on the right

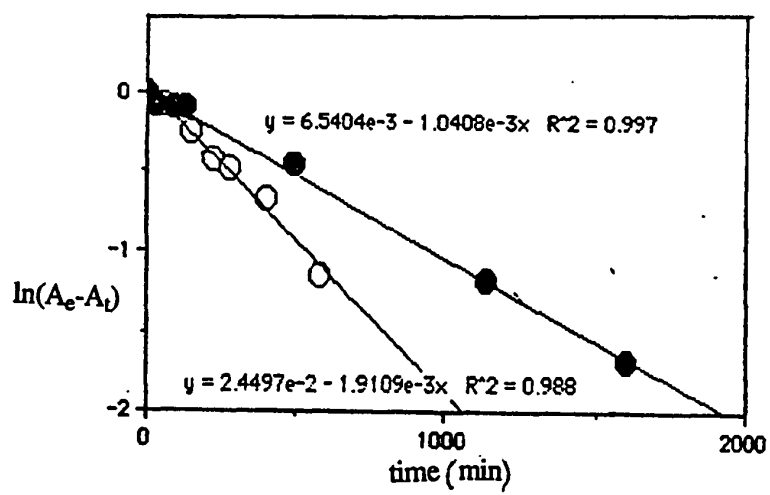


Figure 59. Plots of $\ln(A_e - A_t)$ vs. time for the equilibration of metEqMbH₂O. Right: by optical spectroscopy with column chromatography at 26.5°C and pH 6.71, and left: by ¹H NMR spectroscopy, with (○) and without (●) chromatography at 25°C and pH 6.71.

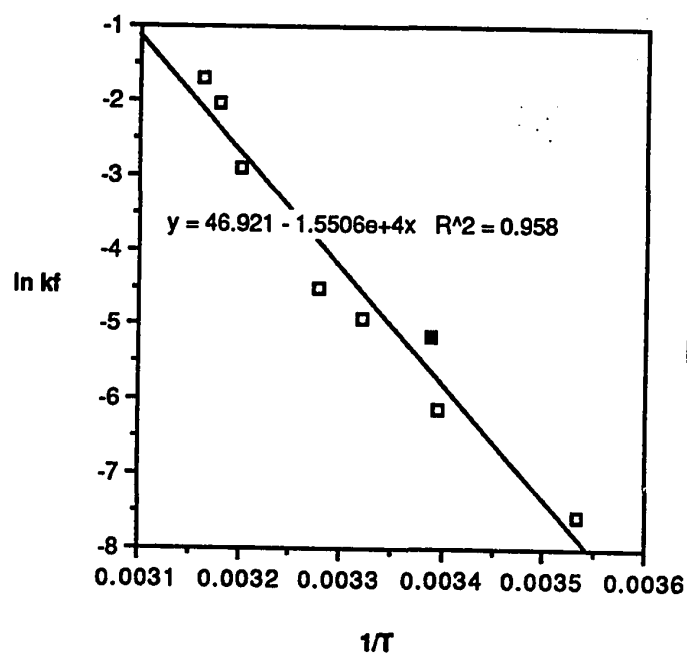


Figure 60. Arrhenius plot for heme redistribution process. All but one data point are collected at 5:1 apoMb:heme concentration ratio. The solid square point represents k_f at 1:1 apoMb:heme concentration ratio.

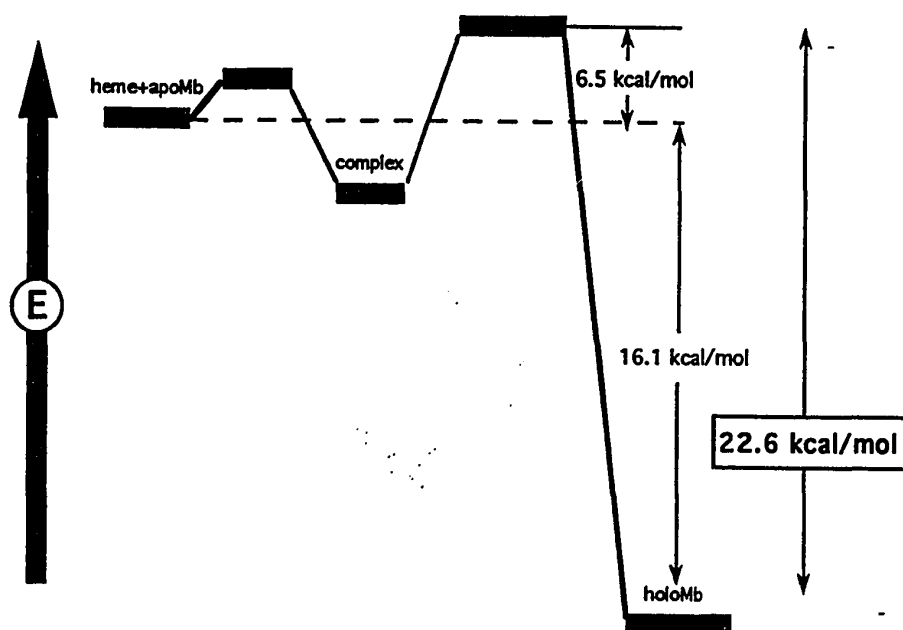


Figure 61. Free energy diagram of the reversibly, completely dissociative pathway for the reorientation of metMbH₂O based on the mechanism by Gibson and Antonini (1960). Activation free energies are labeled correspondingly. The total activation free energy of 22.6 kcal/mol obtained from this mechanism is used to compare with 20.7 kcal/mol from this work. Only one heme-insertion isomer is depicted here. The transition state, heme-apo complex, is obtained by the assumption that heme is completely dissociated from the binding crevice.

CHAPTER VII

LABILITIES OF THE EXCHANGEABLE PROTONS OF IMIDAZOLE AND AZIDO MYOGLOBINS

GENERAL

Structural, kinetic, spectroscopic, and site-directed mutagenesis studies of myoglobin have provided a wealth of information on the mechanics of heme binding. The conventional wisdom on this subject follows the proposal by Case and Karplus (1979) from theoretical molecular dynamics calculations. The ligand enters from the solvent-exposed distal side of the heme through the trajectory between Val E11 and His E7. To accommodate ligand entry, the imidazole ring of His E7 swings away from the iron toward the solvent, and in doing so disrupts a number of electrostatic interactions involving Arg CD3, heme 6-propionate, His E7 itself, and Asp E3. In support of this model, the X-ray crystal structure of metphenylMb (Ringe, 1984), and more recently that of metMbIm (Lionetti et al., 1990), have revealed some structural differences, as compared to metMbH₂O (Takano, 1977), that shed light on the mechanism by which ligand enters the protein matrix. The differences involve mainly orientation of the distal residues in the proposed ligand entry pathway. It was suggested that the displacement of these residues in this "open" conformation provides a possible passageway for ligand to the iron. Any disruption of the native structure can transiently expose buried labile protons to solvent; thus, studying the labilities of the exchangeable protons in the heme vicinity allows one to assess the extent of the structural fluctuation of globin. This chapter shows two

approaches, pH titration behavior and solvent isotope effects, to probe the kinetics of exchangeable protons by means of proton NMR spectroscopy.

pH Titration Behavior

Chemical exchange of labile protons in the protein interior can be followed by NMR spectroscopy. This is especially true for paramagnetic species, in which labile protons in the heme cavity can be assigned based on their relaxation behaviors, chemical shifts, and NOEs. In vertebrate Mbs and Hbs, proton exchange behaviors adopt an EX₂ mechanism, which is verified by the pH dependence of the exchange rates (Cutnell et al., 1981, Lecomte & La Mar, 1985). Two types of model have been characterized for the process that exposes internal regions of proteins to solvent species and thereby allows hydrogen exchange (Woodward et al., 1982; Woodward & Hilton, 1979). The first of these involve the reversible and localized unfolding of the protein, which allows the exposure of the internal protein segment transiently to solvent. Another model describes the penetration of the solvent species toward the exchange sites in the interior of the protein. For a buried proton, when the site exposure step is not limiting for both cases, EX₂ depicts a mechanism in which the rate of exchange is retarded by the probability, for the solvent species, of finding the exposed site.

In an effort to contribute to the database of heme pocket accessibility, the exchange behaviors of EqMb and PSwMb labile protons in various ligated states is investigated. The assignments of the labile protons are first made through relaxation behavior, extent of hyperfine shift, and saturation transfer experiments. A series of pH titrations is then performed on each species. Exchange rates of the resonances are obtained by monitoring their intensities throughout the titrations, with and without water presaturation, and determining their intrinsic spin-lattice relaxation rates, as in Equation (5) in Chapter II (Cutnell et al., 1981).

The exchange behaviors of His E7 and FG3 ring protons are particularly informative of the mechanism because there are two sites of attack on the imidazolium ring that require different catalyses. Acid catalysis would occur on the free nitrogens, N₁, of His E7 and His FG3; while base would attack their N₃Hs. Proximal His F8, which is attached to iron through its N₃, would experience only base catalysis. The crystal structure (Takano, 1977) and solvent isotope effects by ¹H NMR (Lecomte & La Mar, 1987) of metSwMbH₂O suggested hydrogen bonding interactions between N₁ of His E7 and H₂O in metSwMbH₂O, and that between N₃H of His E7 and CN in metSwMbCN, respectively (Figure 62). Therefore, ring NH of His E7 should only experience base or acid catalysis in the former and latter complex, respectively. While ring NH of His E7 is too fast-relaxed to be detected in metMbH₂O, metMbCN provided answers to the postulate (Cutnell et al., 1981). Expected similar exchange patterns of His FG3 and F8 have been observed for metSwMbCN, metEqMbCN, as well as metCAMbCN (Lecomte & La Mar, 1985), indicative of relatively conserved proximal moiety among the three Mbs. On the other hand, an anomaly in the His E7 exchange behavior is observed--His E7 ring protons of metEqMbCN and metCAMbCN are both acid- and base-catalysed, although metSwMbCN conforms to the expected acid catalysis hypothesis. A distal histidine trap door model was postulated to interpret this peculiarity (Lecomte & La Mar, 1985). In solution, myoglobins exist in a structural equilibrium between the closed (as in metMbH₂O) and open (as in metMbphenyl) orientations. This equilibrium is influenced by a structural difference in a single amino acid residue substitution Arg CD3 --> Lys CD3 at the distal side in horse and dog Mbs. This substitution encourages the open orientation in horse and dog Mbs, hence creating a higher probability for His E7 existing in the 'out' conformation, which dictates the base-catalyzed exchange as in a free histidine.

Solvent isotope effects

Hydrogen-bonding interactions are essential factors in hemoproteins because they not only maintain the usual interactions between the side-chains and backbones that stabilize tertiary structure, but also play important roles in regulating directly the reactivity of heme. La Mar and coworkers (La Mar et al., 1988, Lecomte & La Mar, 1987) have developed an NMR method to probe the exchange of bulk solvent with distal His E7. This approach is possible for paramagnetic systems because of the large hyperfine shift of the heme methyl resonances. Because ^2H and ^1H exhibit different hydrogen-bonding strengths, they can lead to different chemical shifts of heme protons.

Therefore, with $^2\text{H}/^1\text{H}$ substitution, existence of hydrogen bonding interaction is evident from either line broadening or splitting of heme resonances in the 50/50 mixture of $^2\text{H}_2\text{O}/^1\text{H}_2\text{O}$ of metMbs. La Mar and his group (La Mar et al., 1988) have demonstrated that in various high-spin metaquo hemoproteins, water is capable of hydrogen-bonding with any nearby distal H-donor/acceptor residue; low-spin metcyano hemoproteins have also been observed to express such interaction (La Mar et al., 1988). They suggested that the source of the isotope-generated line broadening is the distal His E7 hydrogen bond to the ligand, which in their case is water. One of the findings that lends support to their rationales is that hemoproteins such as ferricytochrome *c'* and *Aplysia* Mb, which are known to penta-coordinate and lack bound water at the sixth axial site, do not have this isotope effect.

X-ray crystal structures of metMbN₃ and metMbIm have implicated the existence of hydrogen bonding interaction between the exogenous ligand and His E7 (Lionetti et al., 1991; Stryer et al., 1964). However, greater flexibility is present in solution, so it would not be surprising to find a solvent-based isotope effect absent from these complexes in solution. On the other hand, one advantage of studying the imidazole complexes is that 1-methyl imidazole Mb can be used to verify the identity of the source of solvent isotope

effect. With one nitrogen involved in coordination to the iron and the other methylated, 1-methyl imidazole is not available for H-bonding to His E7 (see Figure 63). So it seemed worth looking for an isotope effect in the imidazole systems.

RESULTS AND DISCUSSION

Assignments of the Exchangeable Protons in MetEqMbN₃

pH titrations were performed on metEqMbN₃ (see Figures 66 and 67 for examples). Assignments for proximal His F8 ring and peptide NHs as well as His FG3 ring NH are made as listed in Table XI. Details of how these assignments were made as follow.

TABLE XI
ASSIGNMENTS OF THE EXCHANGEABLE PROTONS FOR
metEqMbN₃ AT 298 K

<u>Assignments</u>	<u>Chemical Shifts (ppm)</u>
His F8 ring NH (P1)	31.5
His F8 peptide NH (P2)	10.2
His FG3 ring NH (G1)	13.7
His FG3 ring C ₂ H (G2)	6.8
His FG3 C _β H (Gy-tentative)	7.6

The broad downfield peak in Figures 66 and 67 is assigned to His F8 ring NH, P1, because its position is comparable to that found in metCTTN₃ (La Mar et al., 1983) and metHbAN₃ (Yamamoto & La Mar, 1989). A variable temperature experiment also confirms this assignment. Because of the contact interaction with iron, His F8 experiences paramagnetic shift mediated through spin density of the porphyrin ring; increasing temperature induces more high-spin character to iron, thus increases the electron density. Therefore, larger (more downfield) shift results, as is observed for this resonance. A

downfield shift of 0.16 ppm/°C was evident from 298K to 318K. Saturation-transfer with jump-return selective excitation of His F8 NH shows an NOE to another exchangeable proton at 10.2 ppm, denoted **P2** (Figure 64), which is most likely the peptide NH of His F8. Although **P2** does not show reciprocal NOE to **P1** (Figure 65), which is not surprising because ring NH of His F8 (**P1**) is closer to the paramagnetic Fe and has a very much shorter relaxation time than peptide NH, it does show an NOE to ~6.7 ppm, which can be correlated to either C β H' of His F8 (as identified in Chapter VIII at 6.22 ppm at pH 6.8 and 308 K); or the ring C $_4$ H of His FG3. An NOE from His F8 peptidyl NH to ring CH of His FG3 is possible because this region of Mb engages in α -helical formation; and F8 and FG3 are 4 residues apart, one turn of an α helix which brings the protons close in space (Wüthrich, 1986). **P2** also exhibits a pH profile that resembles His F8 peptidyl NH of metSwCN (compare Figure 68 with Lecomte & La Mar, 1986), and its chemical shift is highly dependent on pH. The pH dependence of paramagnetic shift suggests strong electron-nuclear interaction with Fe, through dipolar or contact means. Given that the labile proton is relatively sharp, its position cannot be as close to the Fe as ring NHs of His FG3 and His E7 (based on their linewidths in metMbCN in Cutnell et al., 1981, and distances to Fe from X-ray coordinated in Kuriyan, 1986), the only other exchangeable proton that is sufficiently close to Fe to experience such a strong paramagnetic shift, and exerts a sizable influence on the electron density of the heme, is the coordinated His F8; therefore, the NOE and lability patterns of **P2** strongly support its identity to be the peptidyl NH of His F8. Figure 68 displays the pH profile for **P2**.

The pH titrations in Figures 66 and 67 show a distinctive labile proton, marked **G1** on the spectra. Initially, this resonance was thought to be His E7 ring NH because its titration behavior is similar to those of His E7 ring NH and His FG3 ring NH in metSwMbCN, i.e. both acid- and base- catalyzed as demonstrated in Figure 68 (compare with Cutnell et al., 1981). Nevertheless, as shown below, the chemical shift of this

resonance is pH- and ligand-independent, which argue against this earlier assignment. His E7 ring is suggested to mediate the pathway of ligand entry (Ringe, 1984; Case & Karplus, 1979; Elber, 1990) based on the size of, as well as the possibility of hydrogen-exchange with the incoming ligand, hence its exchange behavior and chemical shift should be influenced by the ligated state. The invariance of chemical shift to different ligated states and Mbs, when compared among metPSwMbN₃, metPSwMbIm, and metEqMbIm, dictates that this exchangeable proton is from the proximal side of the heme crevice. Figure 69 shows two dipolar connectivities at 6.8 ppm and 7.6 ppm, labeled **G2** and **Gy**, respectively, in the diamagnetic envelope upon saturating **G1**. This NOE pattern is characteristic of a histidine ring system, from the ring NH to the C₂H and C₄H (or C_βH). Furthermore, **G1** exhibits minimal temperature-dependence, which implies slight paramagnetic contribution -- which may be attributed to either distance to the paramagnetic Fe, or the (**G1**-Fe) vector being close to the magic angle of 54.7° (La Mar, 1979). The broad linewidth and downfield chemical shift of **G1** argues against large proton to Fe distance, which not only limits the choice for the resonance, but also suggests that the (**G1** to Fe) vector is the determining factor in the spatial orientation of the residue relative to Fe. There is only one proximal histidine other than His F8 within the vicinity of Fe on the proximal side, namely His FG3. Therefore, **G1** is assigned to ring NH of His FG3; the two NOEs induced from **G1** (Figure 69) are most likely those of the ring C₂H and C₄H, or C_βH of His FG3. Crystal coordinates of metSwMbH₂O (Takano, 1977) found the distances from Fe to the ring C₂H and C₄H of His FG3 at 7.25 Å and 4.45 Å, respectively. At 4.45 Å to the paramagnetic center, C₄H should experience sizable dipolar interaction which would induce hyperfine shift and/or efficient relaxation. The non-hyperfine shifted protons and the sharp linewidths of **G2** and **Gy** do not completely fulfill the distance criteria of the His FG3 ring being close to Fe. Figure 70 presents 1D NOE profile of **G2**, which shows reciprocal NOE to **G1**, but none to **Gy**. Because ring C₂H of

His FG3 is closer to G1 than to ring C₄H, it is expected to have greater NOE to G1 than Gy (assuming Gy is C₄H); furthermore, ring C₂H is sufficiently further from Fe to be influenced by the unpaired electrons, which explains its chemical shift and linewidth. Therefore, G2 is assigned to the ring C₂H of His FG3 .

There are few possibilities for the identity of Gy. The temperature-independence of G1 implies that His FG3 may be located directly on the edge of the (G1-Fe) vector caused by magic angle rotation, in which case His FG3 experiences minimal hyperfine interaction because of the canceling effect from both sides of the vector (see Figure 71) (Satterlee, 1990a, b). This postulate explains the sharpness and diamagnetic chemical shift of Gy (should it be C₄H), given its proximity to Fe. This scenario is further supported by the long T₁ (238 ms) of G1. X-ray coordinates place G1 at 5.39 Å to the Fe, hence according to Equation (11), its T₁ of ~15 ms is expected of a usual nuclear-electronic interaction. The experimental T₁ of almost 20 fold larger is indicative of the insensitive hyperfine interaction from Fe to His FG3. Another likely candidate for the identity of Gy is the C_βH of His FG3. From the inset in Figure 69, although C₂H is too far to induce NOE to C_βH, G1 is spatially close to C₂H and C_βH, causing NOEs to both. Moreover, C_βH is also relatively distant to the Fe from the crystal coordinates (~6 Å) to explain the minimal hyperfine interaction. Finally, the possibility that Gy may belong to a nearby proximal pocket residue which experiences dipolar interaction from G2 cannot be discounted. Upon saturation of G1, spin-diffusion causes indirect connectivity to Gy; although given the relatively short saturation time (100 ms) employed, spin-diffusion is unlikely. Citing similar NOE profiles for this exchangeable proton in metSwMbCN (Lecomte & La Mar, 1986), and the assignments of pocket residues in metSwMbCN (Emerson & La Mar, 1990), likely candidates which reside close enough to receive spin-diffusion are heme 6H_α and His F8 C_αH. Since heme 6-propionate system is identified in metEqMbN₃ (see Chapter III), and none of its protons is close to 7.6 ppm, Gy may be His F8 C_αH.

However, no NOE was found from His F8 C β H to Gy, when His F8 C β H of metEqMbIm was irradiated at 308K (not shown); therefore, this possibility is discounted. This experiment was done on metEqMbIm, instead of metEqMbN₃ because the His F8 C β H is identified in metEqMbIm. The result obtained is applicable to metEqMbN₃ because the saturation profiles of the labile proton at ~13.7 ppm are highly compatible in both cases (compare Figure 75 with 69). After exploration of all possible candidates, it appears that Gy is most likely the C β H of His FG3, especially from the size of the NOE from saturating G1 (see Figure 69). From the relatively longer distance of C α H, as compared to G2 (C α H), to G1, it is inconceivable to have NOE of comparable size. On the other hand, C β H is equidistant to G1 as C α H.

Assignments of the Exchangeable Protons in MetEqMbIm

Figures 72 and 73 are examples of pH behavior and the pH profiles for the corresponding resonances of metEqMbIm. Two exchangeable protons, at 13.7 ppm and 10.5 ppm, are prominent. The peak at 13.7 ppm is assigned to ring NH of His FG3 based on similar pH profile, pH-, temperature-, and species-independence characteristics to G1 of metEqMbN₃. Saturation of this peak also gives rise to identical NOEs to 6.8 ppm and 7.6 ppm (Figure 74), further supporting this assignment. The exchangeable proton at 10.5 ppm is identified as the peptidyl NH of His F8 for the following reasons. Figure 75 compares the connectivities from saturating the C β H of His F8 (which has been assigned in Chapter III) at 308K, a temperature at which this resonance is resolved from heme 6H α , with those from saturating the solvent resonance and observing the exchangeable proton at similar conditions. Most notable was that there is an NOE to an exchangeable proton resonance at ~10.8 ppm from saturating C β H of His F8. The corresponding pH titration (Figure 75C, D) shows that the NOE at 10.8 ppm correlates with the proposed peptidyl NH of His F8 at 298K. Furthermore, the pH profile of this peak at 10.5 ppm (at 298K)

resembles that of P2 in metEqMbN₃ (compare the pH profile of P2 in metEqMbN₃ in Figure 68 to that of 10.5 ppm of metEqMbIm in Figure 73). Comparison of crystal structures of metEqMbH₂O (Takano, 1977) and metSwMbIm (Lionetti et al., 1991) contends that although drastic changes in the distal pocket are evident, the proximal side of both species are similar, i.e., the proximal side of the heme pocket is insensitive to the ligated states. Therefore, comparison of pH profiles among different ligated Mbs should be valid.

Assignments of the Exchangeable Protons in metEqMbXIm, where X=1CH₃, 4CH₃

Figure 76 and 77 are representative of pH titrations for metEqMb1CH₃Im and metEqMb4CH₃Im, respectively. The characteristics of the exchangeable protons are identical to those of metEqMbIm. The same conclusions as that for metEqMbIm are drawn as to the identities of the labile protons at 13.7 ppm and 10.5 ppm.

Assignments of the exchangeables in metPSwMbN₃ and metPSwMbIm are identical to their EqMb counterparts, judging from their pH profiles (Figure 78A, B, respectively). The peptidyl NH of His F8 in metPSwMbN₃ was identified by its similar pH dependence to metEqMbN₃. Although the assignments of the exchangeables are approximately indifferent to various ligated states and species, the rate at which the ring NH of His FG3 exchanges with the bulk solvent is very much species-dependent from the differential saturation factors obtained at the pH with the slowest exchange for various species. Data is presented in Table XII.

The pHs for the species in Table XII were read before and after the experiment, and were always within 0.01-0.05 of a unit difference. The uncertainty for the calculation of saturation factors, from independent pH titrations at the same pH, is ~0.01. It is apparent from the saturation factors in Table XII that in both ligated states, PSwMb has more

TABLE XII

SATURATION FACTORS FOR G1 (RING NH OF His FG3) AT THE SLOWEST-EXCHANGED pH FOR VARIOUS MbS IN DIFFERENT LIGATED STATES

<u>Species</u>	<u>Saturation Factors</u> (= $\text{int}_{\text{hif}}/\text{int}_{\text{miss}}$)
metEqMbN ₃ (pH 9.10)	0.098
metPSwMbN ₃ (pH 8.95)	0.16
metEqMbIm (pH 8.45)	0.090
metPSwMbIm (pH 8.68)	0.12

restricted access of the proximal side to solvent, although the small saturation factors in all cases signify facile exchange of His FG3 with the bulk solvent. The restricted exposure of PSwMb relative to EqMb may be a result of the unique substitution of Lys CD3 --> Arg CD3 in PSwMb, supporting the pivotal role assumed by the CD3 residue in modulating the accessibility of heme pocket to incoming ligands, including the solvent H₂O. Figure 79 illustrates the movements of the residues necessitated in gating this process. Reference to Figure 47 in Chapter IV reinforces this postulate by demonstrating the more dramatic increase in linewidths of the 5- and 1- CH₃s in metPSwMbIm upon raising pH. Although FG3 is not on the ligand entry/exit route, it is a surface residue, which is shown to be affected here by the more compactness of the binding crevice in PSwMb.

Table XII also revealed that the size and orientation of exogenous ligand is influential in controlling the extent of exposure in the heme proximal pocket, as evidenced by the larger saturation factor in metMbN₃. The smaller size, the hydrogen-bonding interaction of N₃⁻ with His E7, and the optimal coordination angle with the Fe (Stryer & Kendrew, 1964, suggested possible σ interaction between N₃⁻ and Fe) slowed the solvent exchange rate in metMbN₃ so as to allow the better detection of the the labile His FG3 ring NH, despite the larger high-spin character of metMbN₃ relative to metMbIm. With the

saturation factor and Equation (5), k_{exch} is derivable if T_1 of the exchangeable can be obtained by an independent experiment. Non-selective inversion recovery with jump-return experiment was performed (the pulse-sequence is a combination of Equations (6) and (7), but without the selective saturation in Equation (7)) to extract T_1 of 333 ms and 238 ms for ring NH of FG3 in metPSwMbN₃ and metEqMbN₃, respectively. Because the experiment employs no saturation of the solvent signal, which is in exchange with the labile proton in concern, T_1 obtained is the intrinsic one. When a conventional non-selective inversion recovery experiment (Equation (6)) was performed with saturation of water signal on metPSwMbN₃, T_1 was found to be 172 ms. Therefore, caution must be taken when determining intrinsic T_1 s of labile protons. Equation (5) then allows the determination of k_{exch} for this labile proton at $\sim 16 \text{ s}^{-1}$ and 38 s^{-1} for metPSwMbN₃ and metEqMbN₃, respectively. This two-fold faster exchange rate in metPSwMbN₃, once again, reinforces the difference between the proteins in the heme crevice.

Solvent Isotope Effects

Line-broadening of the methyl resonances in various ratios of $^1\text{H}_2\text{O}/^2\text{H}_2\text{O}$ solvent is clearly manifested in metEqMbN₃ (see Figures 80 and 81). The extent of line-broadening is dependent on the ratio of the $^1\text{H}/^2\text{H}$, which implies solvent isotope contribution (La Mar et al., 1988), instead of merely artifacts from processing or experimental conditions. The broadening is apparent on all four methyls (although Figures 80 and 81 shows only three, a similar effect was detected for 3CH₃), albeit the effect is variably distributed, and is dependent on pH. The fact that all methyls are affected reflects an axial perturbation, which most likely arises from axial hydrogen-bonding with either the labile protons of proximal His F8 or ring NH of distal His E7. Two factors, the respective hydrogen exchange rates and pH dependence, allow the distinction between these interactions. The detection of ring NH of His F8 on metMbN₃ demands that its exchange

rate be slower than the NMR time-scale, i.e. $< 10^4 \text{ s}^{-1}$. On the other hand, the detection of splittings for all methyls at non-coalescence pH, i.e. $\text{pH} > 4.28$ (Figure 82) dictates that the solvent isotopes are in slow exchange on the NMR time scale, and therefore must be $< 50 \text{ s}^{-1}$ —equivalent to the splitting of the 5CH_3 . This exchange rate is in apparent disagreement with that of His F8 ring NH, and hence rules out the involvement of His F8. Figure 82 also demonstrates acid-catalysis of the isotopic exchange, showing the slowest exchange (the broadest methyl resonances) at $\sim \text{pH} 9$; base-catalysis of the exchange was unobtainable without denaturing the protein at too high a pH, because the 5- and 8CH_3 resonances remained split at as high a pH as 11.0, while 1CH_3 converges at $\text{pH} > 7$ (not shown). This acid-catalysis pattern argues against His F8 ring or peptidyl NHs as possible source of the isotope-effect because the labile protons of His F8 exhibit only base catalysis (Cutnell et al. 1981; Lecomte & La Mar, 1987; previous section in this chapter). Although this pH dependence fits the pH profiles of both ring NH of His FG3 and His E7, His FG3 is unlikely to be the source of this isotope effect because it maintains similar salt-bridge interaction, if any, with heme 6-propionate in all the species being studied, and results from this work demonstrate that the isotope effect is species-dependent—which contradicts the effect coming from the invariant salt-bridge interaction. Other isotope studies done on proteins without a distal His showed the lack of such broadening effect (La Mar et al., 1988), which further supported the source of such effect being the distal His E7. Among the four methyls, 5CH_3 and 8CH_3 are the most severely affected, which is attributed to differential distribution of spin density on the heme.

Neither the metMbIm nor metMb1CH₃Im (and presumably metMb4CH₃Im) species displays the solvent isotope effect (Figures 83-85). Based on the many-fold faster exchange of heme pocket labile protons of metMbIm (from comparison of His FG3 ring NH in Table XII) as compared to metEqMbN₃, the isotope effect on the heme methyl resonances must be too rapid to be observed on NMR time-scale. Furthermore, the

hydrogen-bonding effect may be either too weak to be detected due to the distance and the vector of hydrogen-bond, if any, from the iron paramagnetic center. The crystal structures of metHbIm (Bell et al., 1981) and metSwMbIm (Lionetti, 1991) implicated the possibility of hydrogen-bonding interaction between His E7 ring NH and the Im ring NH. The discrepancy detected for the different findings on the involvement of His E7 in hydrogen-bonding interaction merely reflects the different nature of X-ray crystallography and solution state NMR spectroscopy, in that NMR offers the ability to study dynamics. This is not without precedent, as revealed in the case of involvement of distal His E7 in the binding pocket of metCTTMbCN (compare work in Steigemann & Weber, 1979 with that in Peyton et al., 1991)

Although severe phase-shifted sine bell apodization of the isotope-broadened peaks (parameters as shown in the legend of Figure 82) of metEqMbN₃ helps deconvolute the splitting effect, the linewidths are too broad and close to the coalescence limit to allow accurate fit by CBS method, which depends on variables such as T_2 (linewidth parameter), T_1 (peak intensity parameter), population of each of the species, and so on. The uncertainties in more than one of the variables, such as the case here, vastly decreases the sensitivity of this method, rendering tremendous errors in the k_{exch} obtained. Therefore, only an upper boundary can be ascertained to the exchange rate of His E7 ring NH at $\sim 50 \text{ s}^{-1}$ based on the isotope splitting of 5CH_3 .

The compatible exchange rates of His E7 ring NHs in metMbN₃, as compared to metMbCN (Cutnell et al., 1981; Lecomte & La Mar, 1985) give rise to interesting conclusion about the role played by the exogenous ligand in modulating the lability of the heme cavity. Stryer, Kendrew, and coworkers (1964) suggested from the crystal structure of metSwMbN₃ that the coordination of N₃⁻ to Fe is close to the strength of a σ bond, and that Fe-N₃⁻-H (from His E7 ring NH) forms a trigonal planar that gets stabilized by the donation of electron density from N₃⁻ to Fe (see also discussion in Chapter III). Such

model dictates that the hydrogen bond strength of His E7 ring NH-N₃⁻ must be considerable, therefore slowing the exchange rate. This strong hydrogen bond also explains the this solvent isotope effect is not based-catalyzed at pH as high as 11, although His E7 of metEqMbCN has been shown to exhibit base catalyzed hydrogen exchange behavior (Cutnell et al., 1981).

Comparable k_{exch} 's were also obtained for the His FG3 ring NHs of metMbN₃ and metMbCN (Lecomte & La Mar, 1985) at 40°C. The compatibility of the is not surprising because His FG3 ring NH exhibits similar facile exchange as in all cases (by comparison of saturation factors in Table XII with the results of Cutnell et al., 1981, in which saturation factor was unobtainable because this peak was completely saturated at 40°C). k_{exch} for the His FG3 ring NH of metMbCN was determined by linewidth fit. The linewidth fit method for such relatively broad peak is expected to be less accurate than from saturation factors, as formulated in Equation (5), due to the same reasons mentioned earlier in Solvent Isotope Effect section.

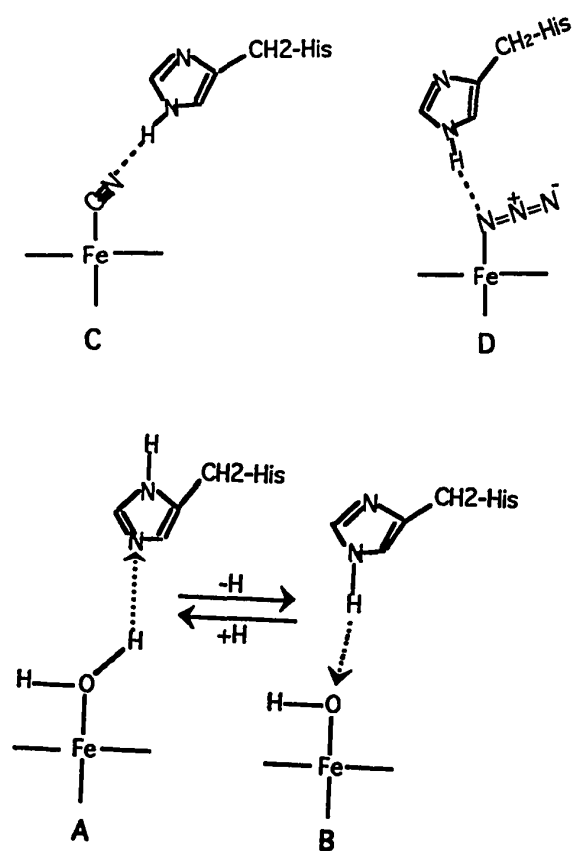


Figure 62. Proposed H-bonding between an **A.** iron-bound H₂O and His E7 at acidic pH, where a neutral H₂O acts as a H-donor to the imidazole. **B** at alkaline pH, where the imidazole acts as a H-donor to the bound hydroxide ion (La Mar et al., 1988). **C**, and **D**, H-bonding interactions in metMbCN (Cutnell et al., 1981), and metMbN₃ (Stryer et al., 1964), respectively.

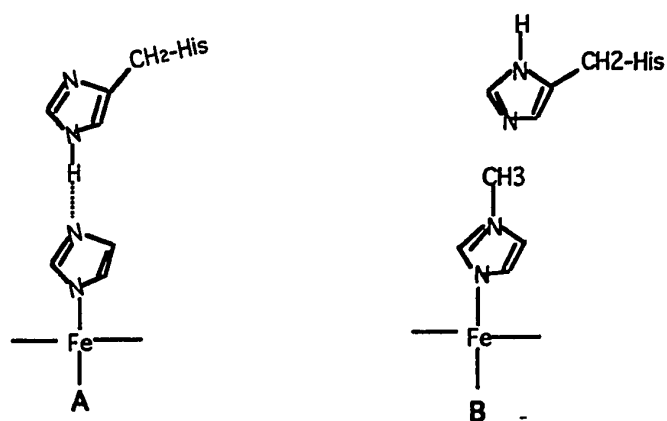


Figure 63. Presented here is one of the possible protonation scheme; other schemes have also been proposed. In (a), H-bonding interaction between H₁ of imidazole and N_c of His E7; whereas in (B), no H-bonding is available.

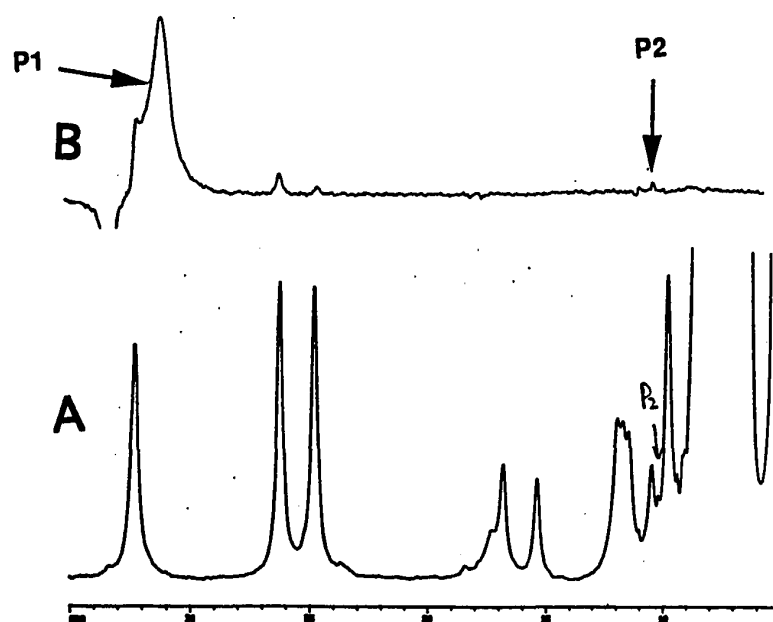


Figure 64. Selective excitation (p11 or jump-return) saturation-transfer spectra of met EqMbN₃ in 10% ²H₂O at 25°C and pH 7.4. A. Reference spectra; B. difference trace from saturating P1. Peaks are as labeled.

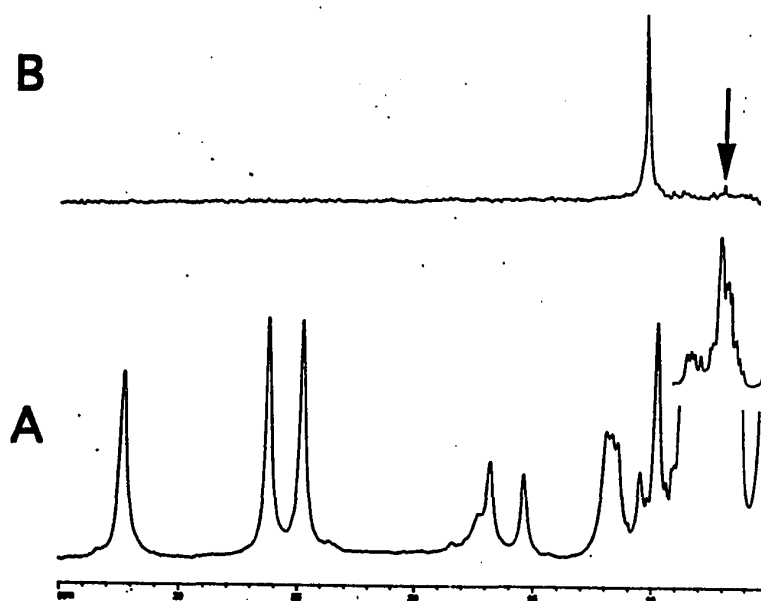


Figure 65. Selective excitation (p11 or jump-return) saturation-transfer spectra of P2 of met EqMbN₃ in 10% ²H₂O at 25°C and pH 7.3. A-B: spectra with and without saturation of P2, respectively, peaks are as labeled. The *inset* in A shows the expanded diamagnetic region. Note the NOE to ~6.7 ppm, possibly ring C₂H of His FG3, or C_βH' of His F8, which will be elaborated in Chapter VIII.

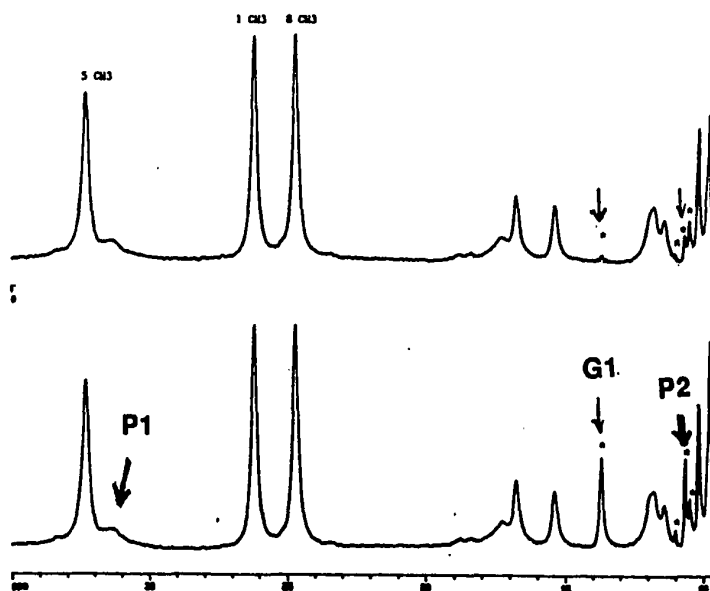


Figure 66. Selective excitation (p11 or jump-return) saturation-transfer spectra of met EqMbN₃ in 10% ²H₂O at 25°C and pH 8. Top and bottom: with and without saturation of the water resonance, respectively, asterisks denote resonances that exchange on the time-scale of the saturation rate.

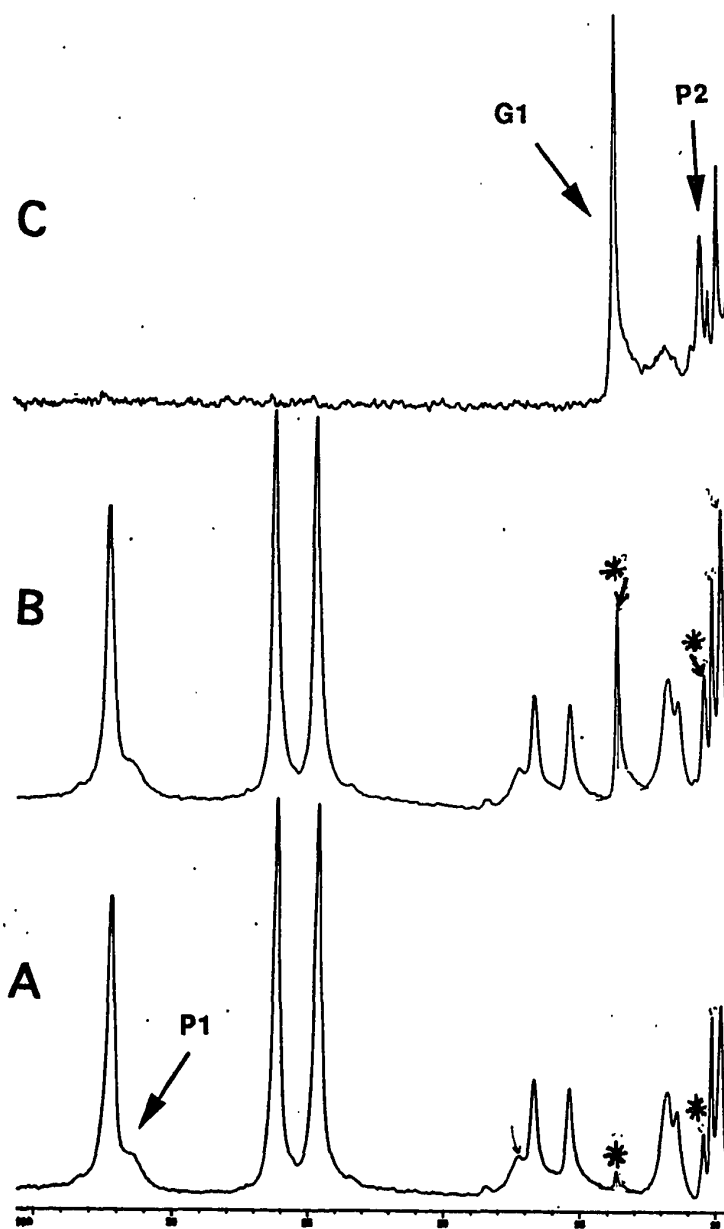


Figure 67. Selective excitation (p11 or jump-return) saturation-transfer spectra of met EqMbN₃ in 10% ²H₂O at 25°C and pH 9. A-C: spectra with and without saturation of the water resonance, and difference between them, respectively, asterisks denote resonances that exchange on the time-scale of the saturation rate.

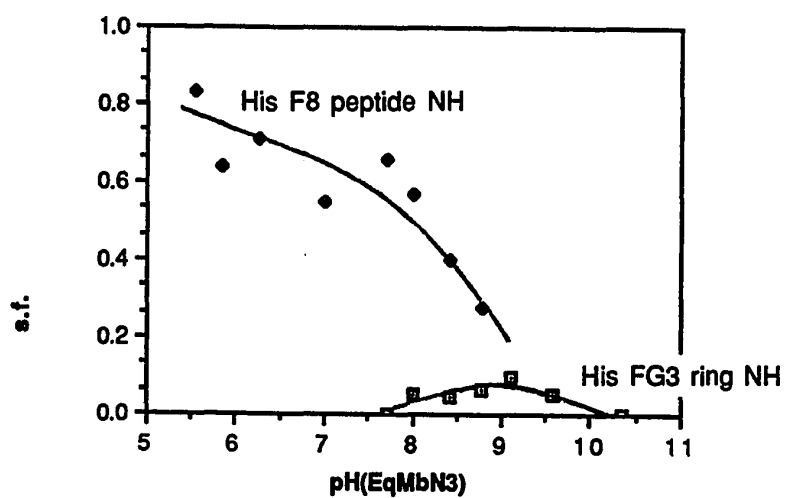


Figure 68. pH profiles of metEqMbN₃ at 298K. The solid line has no theoretical significance but merely serves to show the trend of the data points. Each data represents saturation factor determined at the corresponding pH. The assignments are as labeled on the individual traces.

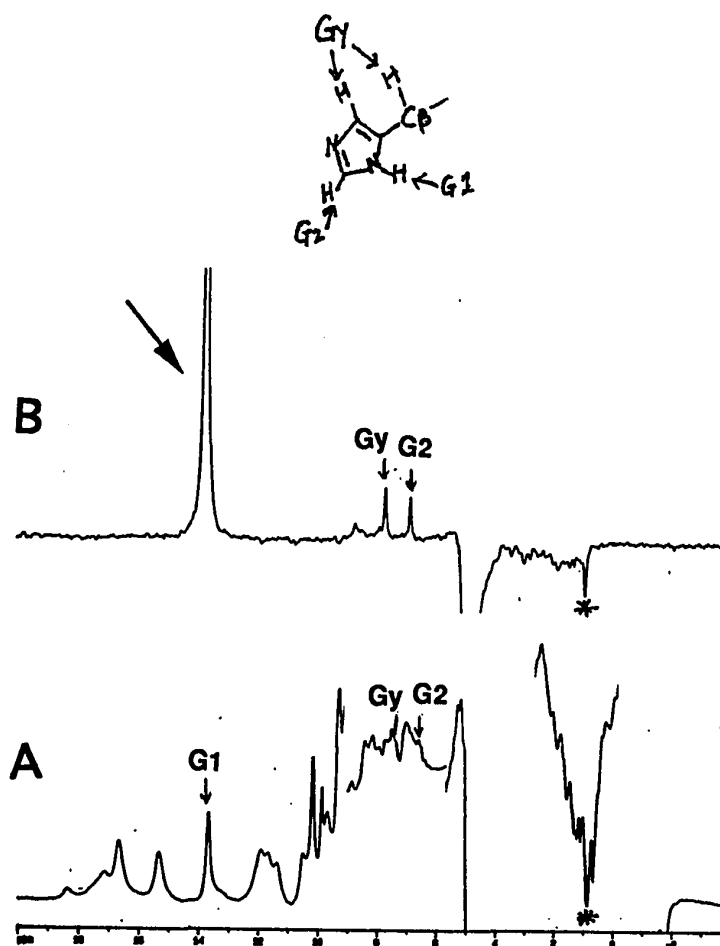


Figure 69. Selective excitation (p11 or jump-return) saturation-transfer spectra of saturating **G1** of metEqMbN₃ at pH 9.02 and 298K in 10% ²H₂O. The acquisition parameters used are d20=300ms, d10=54, d1=100ms, and d19=50μs. **A.** Reference spectrum with the transmitter off **G1**; **B.** difference trace. The *inset* shows the expanded diamagnetic region corresponding to NOEs to **G2** and **Gy**, and an upfield NOE. *Top* shows the structure and assignments of His FG3.

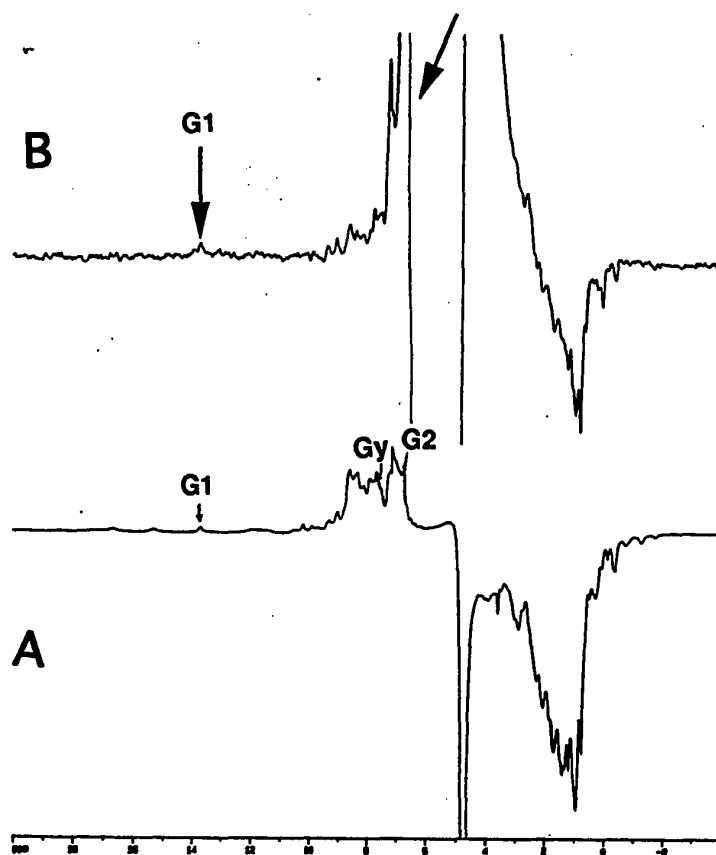


Figure 70. Selective excitation (p11 or jump-return) saturation-transfer spectra of saturating G2 of metEgMbN₃ at pH 9.02 and 298K in 10% ²H₂O. The acquisition parameters used are d20=500ms, d10=54, d1=100ms, and d19=50μs. The NOE to G1 is indicated by the arrow. A. Reference spectrum; B. difference trace.

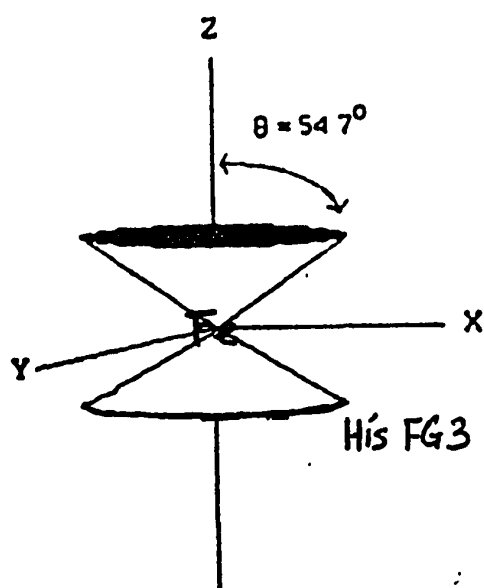


Figure 71. Magic angle rotation diagram. r is the distance between Fe and the nucleus H, and θ signifies the angle made between the vector Fe-H and the normal to the heme plane. When $\theta = 54.7^\circ$, the magic angle, no or minimal electron-nuclear interaction is experienced by H because the Hamiltonian for dipolar interaction between two point dipoles is calculated to be zero at that angle (Satterlee, 1991b).

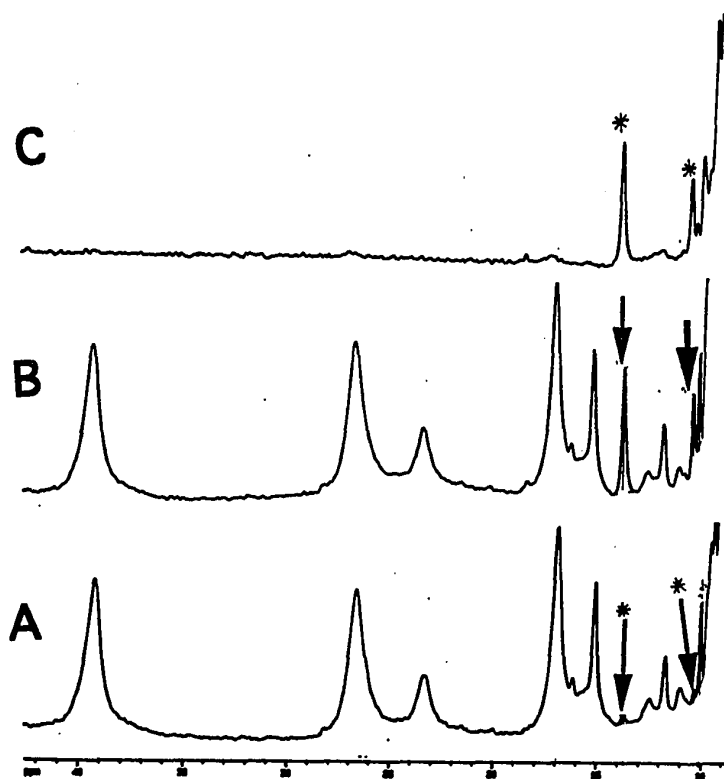


Figure 72. Selective excitation (p11 or jump-return) saturation-transfer spectra of metEqMbIm at pH 9.02 and 298K in 10% $^2\text{H}_2\text{O}$. A-C: spectra with and without saturation of water resonance, and the difference between them, respectively, arrows and labels denote exchangeable protons. The acquisition parameters used are $d10=40$, $d1=100\text{ms}$, $d20=100\text{ms}$, and $d19=30\mu\text{s}$.

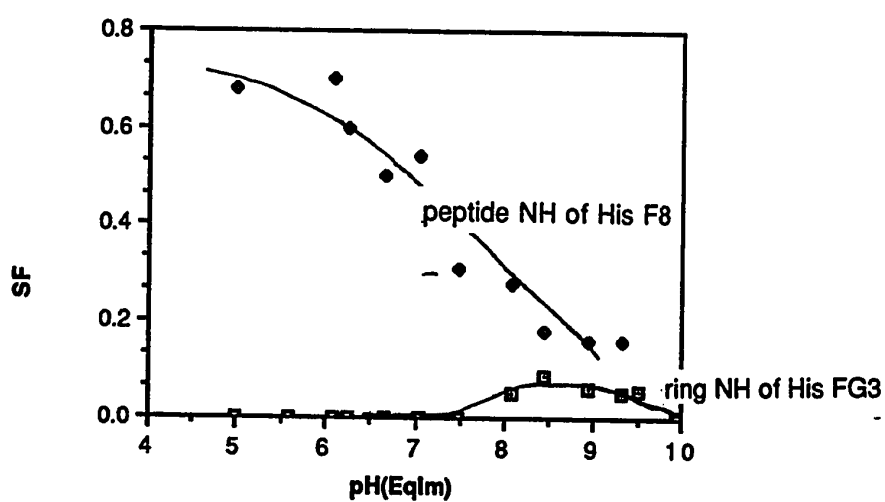


Figure 73. pH profiles of metEqMbIm at 298K. The solid line has no theoretical significance but merely serves to show the trend of the data points. Each data represents saturation factor determined at the corresponding pH. The assignments are as labeled on the individual traces.

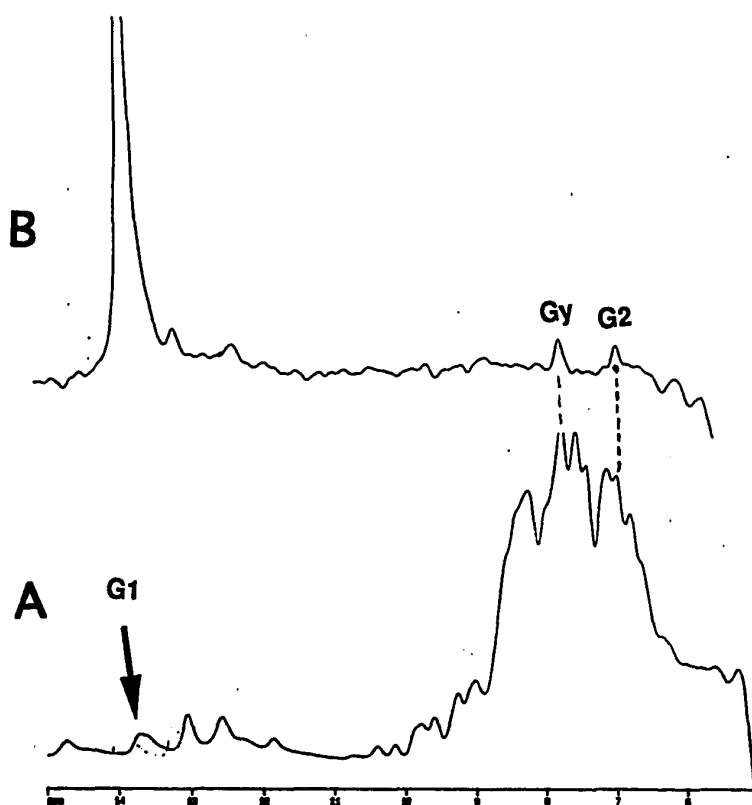


Figure 74. Selective excitation with jump-return saturation of **G1** of metEqMb4CH₃Im at pH 9 and 298 K in 10% ²H₂O. The acquisition parameters are d20=300ms, d10=54, d1=100ms, and d19=50μs. Peaks are as labeled. A. Reference spectrum with the transmitter off G1; B. Difference trace.

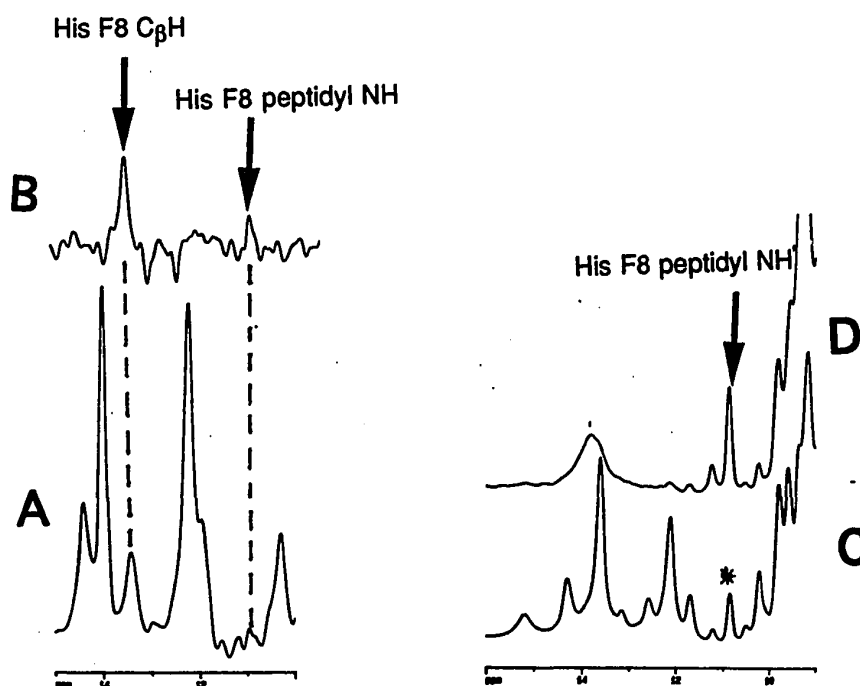


Figure 75. Comparison of pH titration with the NOE from saturating the $C_{\beta}H$ His F8 of metMb4CH₃Im. **A.** Reference spectrum of metPSwMb4CH₃Im at 308K and pH 7.24 in 100% ²H₂O, the intensity of the His F8 peptidyl NH is greatly reduced because of exchange with the solvent, **B.** Difference spectrum from saturating $C_{\beta}H$ His F8, the dashed lines connect the corresponding resonances. **C.** Reference spectrum of metEqMb4CH₃Im at 308K and pH 7.30 in 10% ²H₂O, the asterisk designates the labile proton; **D.** Difference spectrum from saturating the solvent H₂O. The assignments are labeled on the spectra.

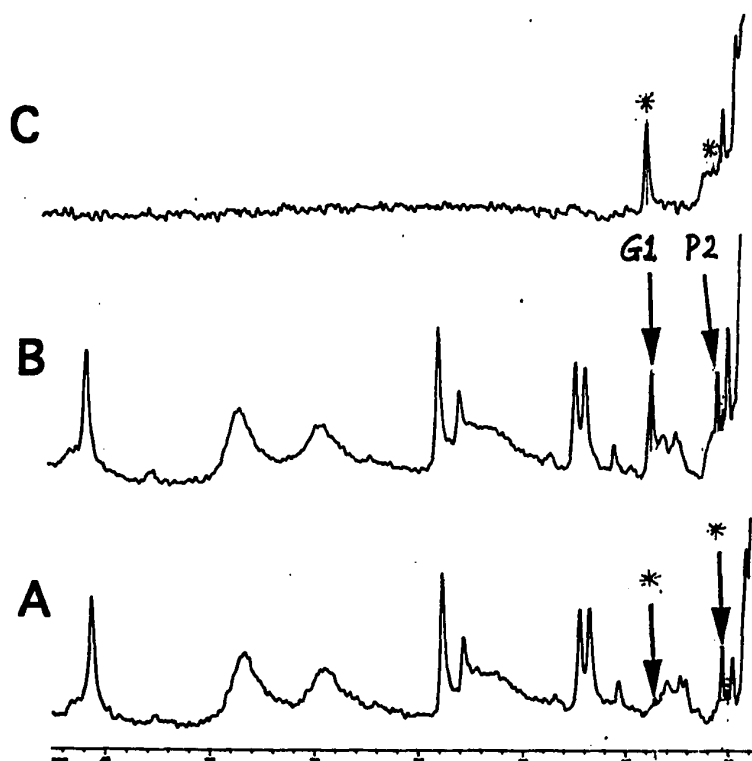


Figure 76. pH titration of metEqMb1CH₃Im at pH 9.32 and 298K. A-C: spectra with and without saturation of water resonance, and the difference between them, respectively, arrows and asterisks denote exchangeable protons. The acquisition parameters used are d10=40, d1=100ms, d20=100ms, and d19=30 μ s. Note that P2 is not very labile at this pH because it is acid-catalyzed.

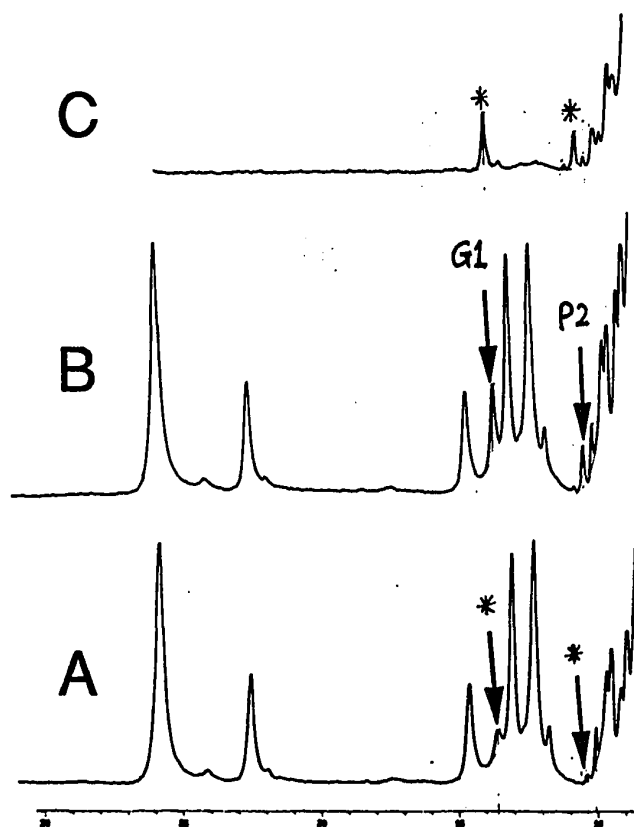


Figure 77. pH titration of metEqMb4CH₃Im at pH 8.30 and 298K. A-C. Spectra with and without saturation of the solvent H₂O, and the difference between them, respectively. Arrows and labels denote exchange protons. The acquisition parameters used are d10=40, d1=100ms, d20=100ms, and d19=30μs.

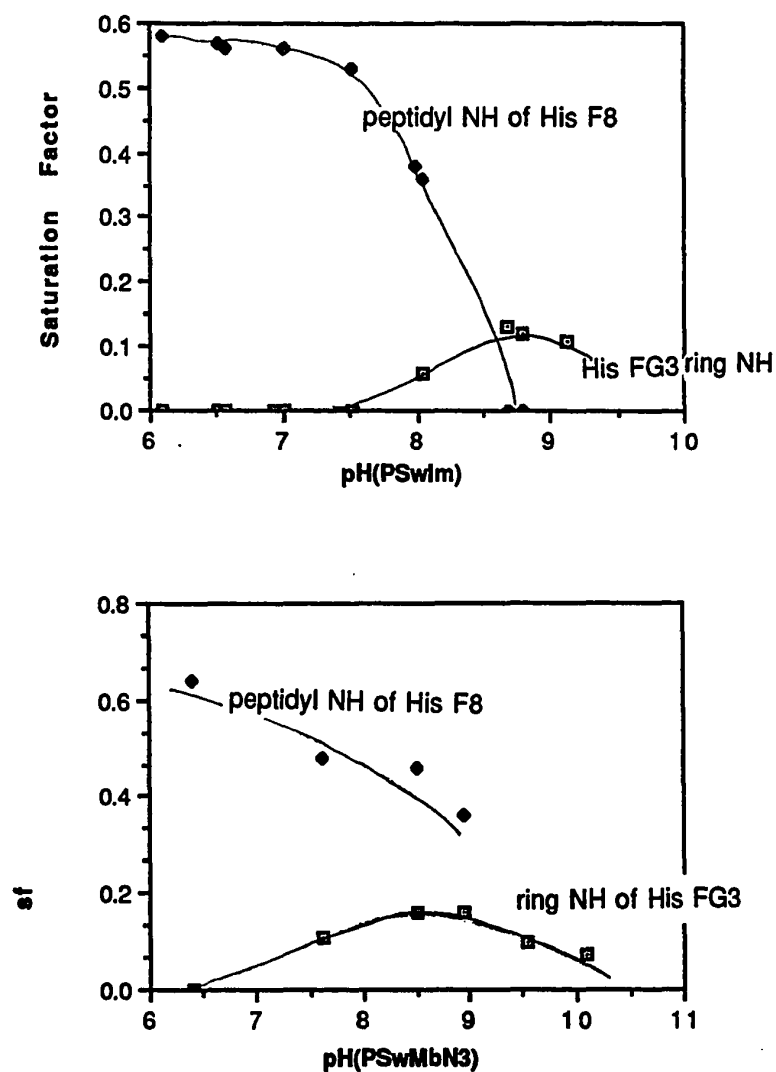


Figure 78. A, B. pH profiles of metPSwMbN₃, and metPSwMbIm, respectively at 298K. The solid line has no theoretical significance but merely serves to show the trend of the data points. Each data represents saturation factor determined at the corresponding pH. The assignments are as labeled on the individual traces.

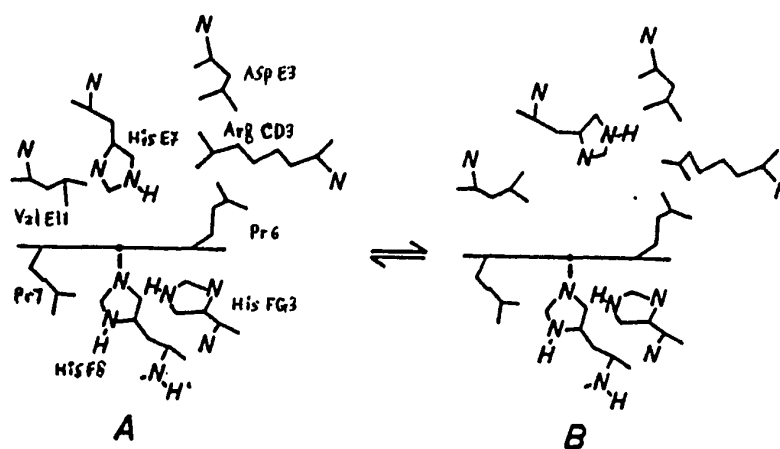


Figure 79. Movement involved in modulating ligand entry into the heme pocket. As shown is the heme environment in SwMb. A. Ligand channel closed by the 'in' conformation of the triads Val E11, His E7 and Arg CD3 (Lys CD3 in EqMb) (Case & Karplus, 1979); B. Ligand channel open when the triads swing towards the solvent. Only the residues of interest are represented.

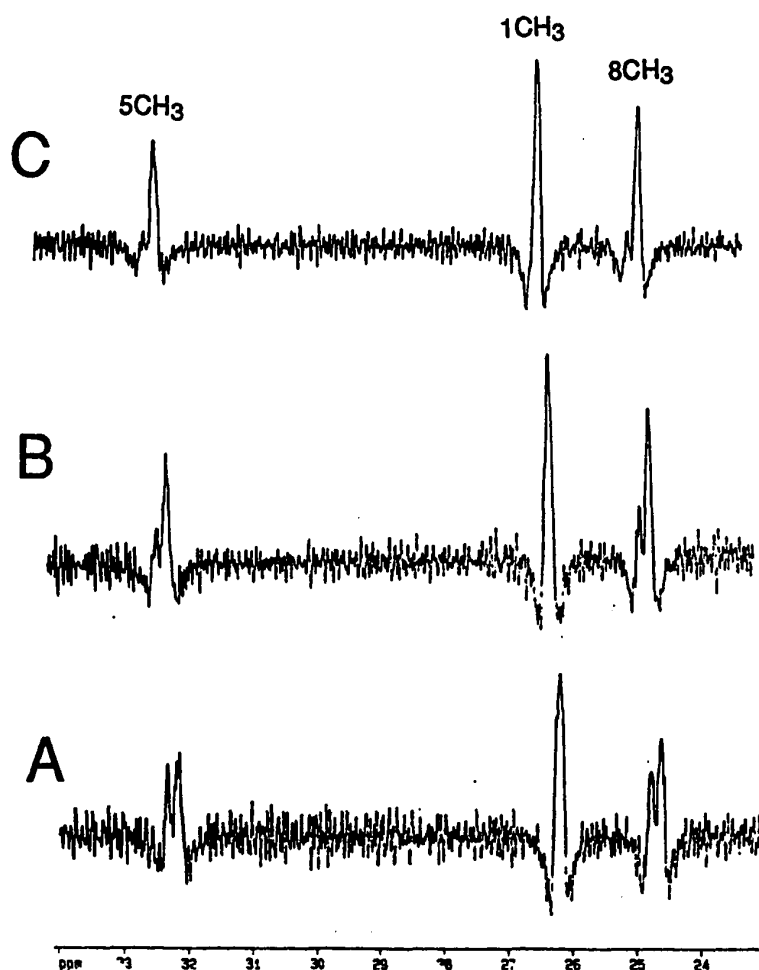


Figure 80. Comparison among the methyl linewidths of metEqMbN₃ at 298K and pH 9 in different ratios of ²H₂O:¹H₂O. A. 6:4; B. 7:3; C. 8:2. The phased-shifted sine bell function used here is SSB=1. Peak identities are as indicated.

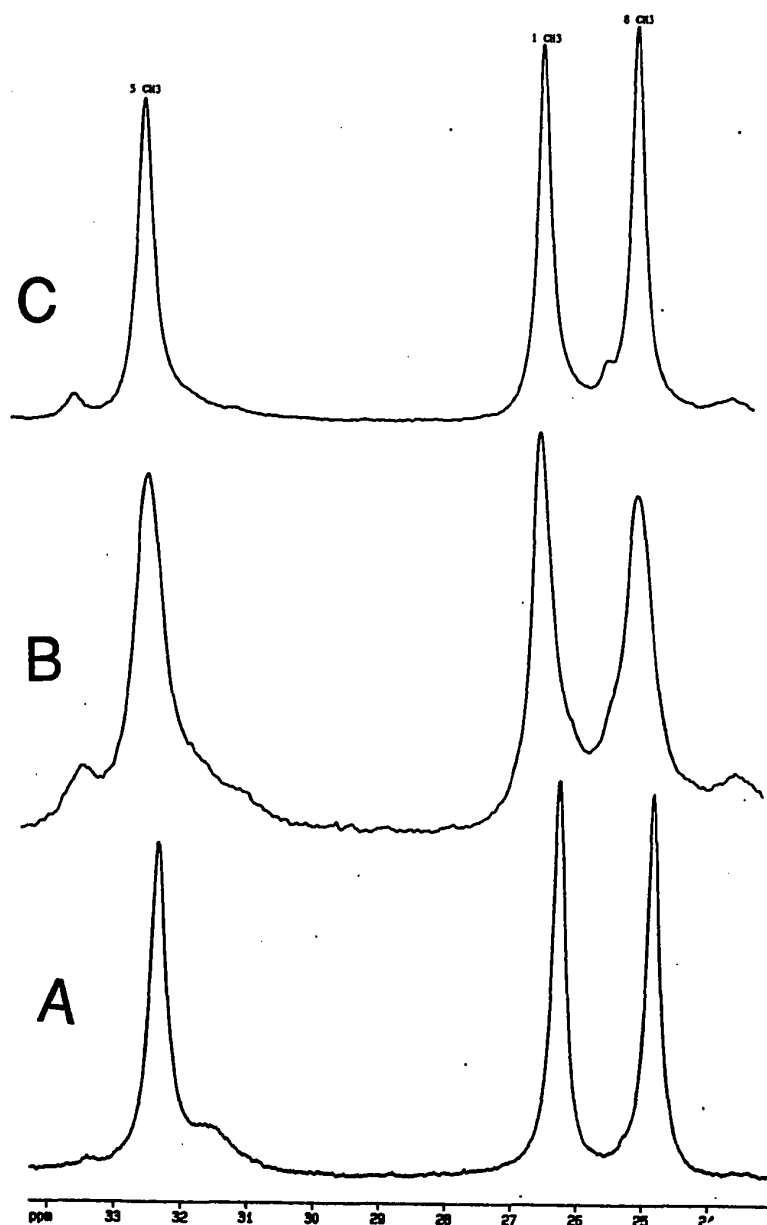


Figure 81. Comparison among the methyl linewidths of metEqMbN₃ at 298K and pH 6.2 in different ratios of $^1\text{H}_2\text{O}$: $^2\text{H}_2\text{O}$. A. 9:1; B. 1:1; C. 0:100. No phase-shifted sine bell apodization function is used.

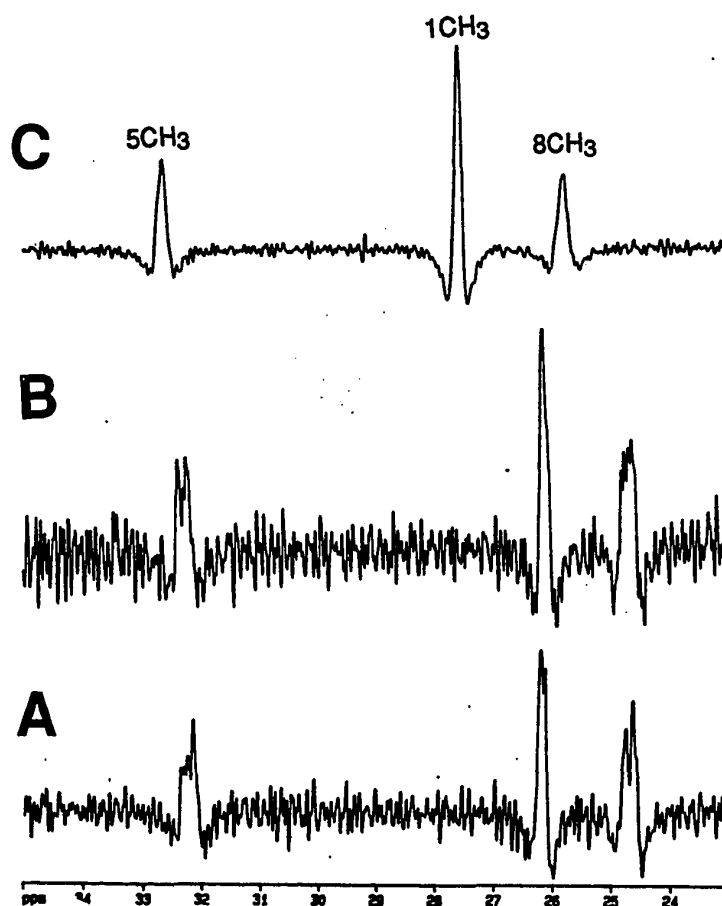


Figure 82. Comparison among the methyl linewidths of metEqMbN₃ at 298K and different pHs in 1:1 ratio of ¹H₂O:²H₂O. A. pH 9.02; B. pH 7.05; C. pH 4.28. Phase-shifted sine bell apodization function is SSB=1. Peaks are as identified. Note the convergence of the isotopely-split peaks at pH 4.28.

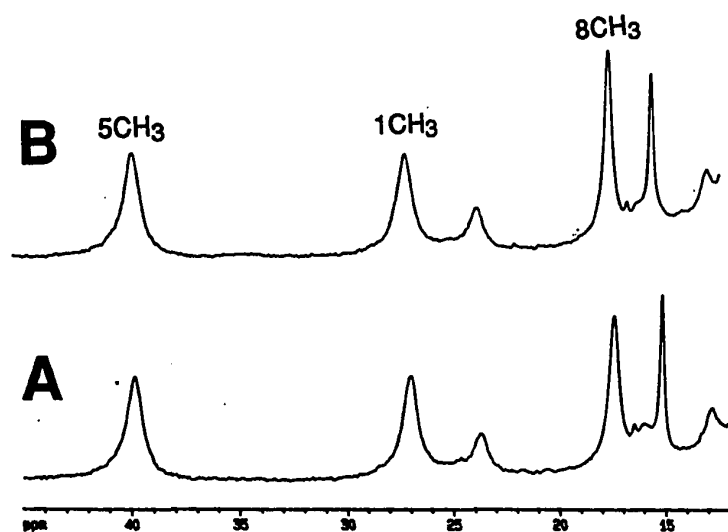


Figure 83. Comparison of metEqMbIm in different ratio of $^2\text{H}_2\text{O}$: $^1\text{H}_2\text{O}$ at pH 9.12. A. 100:0; B. 1:1. They are virtually superimposable.

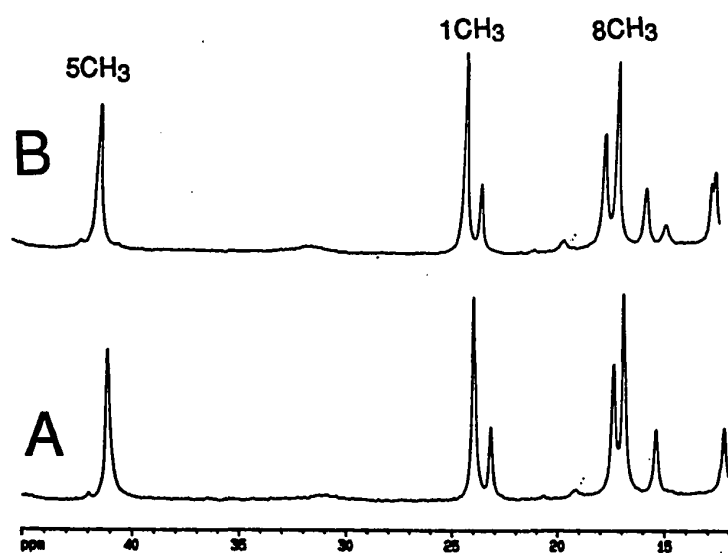


Figure 84. Comparison of metEqMb1CH₃Im in different ratio of $^2\text{H}_2\text{O}$: $^1\text{H}_2\text{O}$ at pH 7. A. 100:0; B. 1:1. They are virtually superimposable. Peaks are as identified on the spectra.

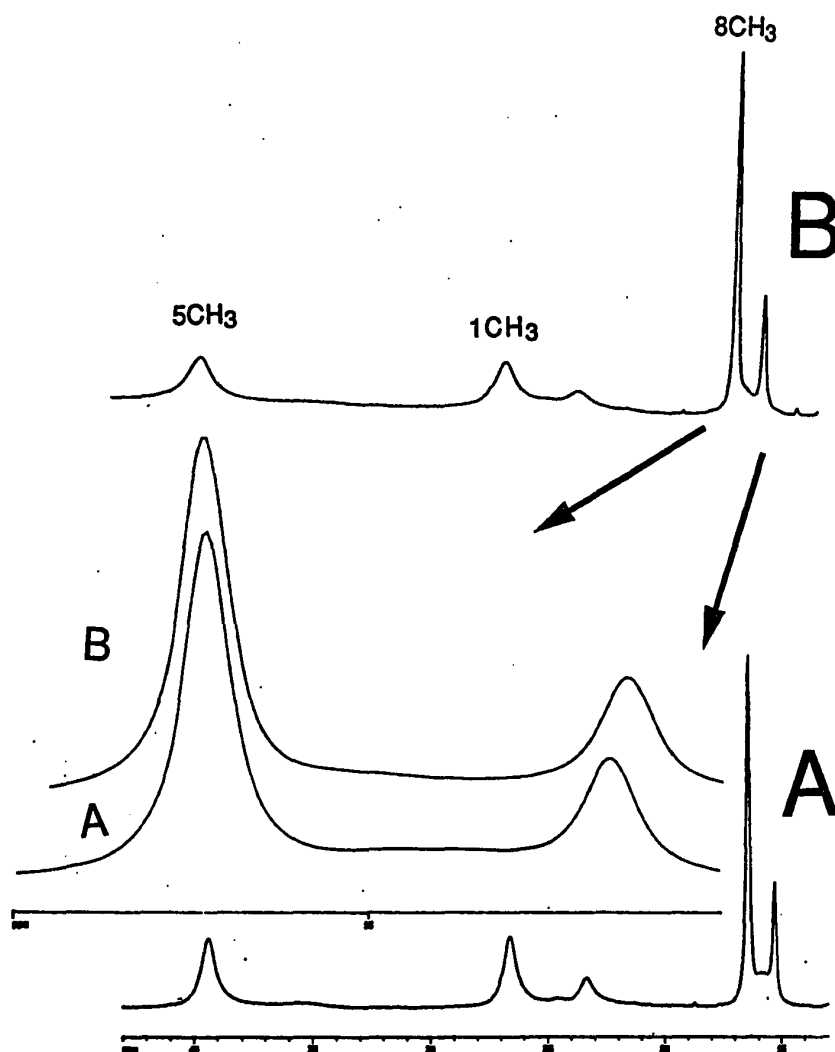


Figure 85. Comparison of metPSwMbIm in different ratio of $^2\text{H}_2\text{O}:\text{}^1\text{H}_2\text{O}$ at pH 9 and 298K. A. 100:0; B. 1:1. Peaks are as identified on the spectra. *Inset* overlays the expanded $8\text{CH}_3\text{s}$.

CHAPTER VIII

ASSIGNMENTS OF THE HEME POCKET RESIDUES IN IMIDAZOLE HORSE HEART MYOGLOBIN

Chapter III introduced the utility of saturation transfer from metEqMbH₂O to assign unresolved heme peripheral protons in metEqMbIm. Very few heme pocket residues in the high-spin metEqMbH₂O, however, have been assigned because of the broadness and extremely fast relaxation of protons from residues close to the paramagnetic Fe. A compelling reason to assign as many resonances as possible in metEqMbH₂O is that they can help formulate electronic and magnetic models for the pure high-spin system, which contributes to the global efforts of understanding paramagnetic NMR.

MetEqMbIm is relatively low spin and analogous to the metMbCN system based on the similar T₁s of their heme methyls (compare Table VI in Chapter III with Emerson & La Mar, 1990). The complete solution structural elucidation of the heme pocket residues in metSwMbCN (Emerson & La Mar, 1990) allows not only comparison of its heme crevice dynamics with that of metEqMbIm, hence verifies the finding from X-ray crystallography of dramatic change in the heme distal side, but also, in theory, enables the assignments of corresponding heme cavity residues in metEqMbH₂O by saturation transfer.

Characterization of the heme cavity residues in metEqMbIm is itself significant because it constitutes a basis for studying metalloproteins that exist only in paramagnetic functional states (for instance, hemopexin, peroxidases, and iron-sulfur proteins like ferredoxin to name a few). Until recently, the major source for assignments in intact paramagnetic proteins originated from the respective heme models (La Mar & Walker, 1979; La Mar, 1979). Although the iron-porphyrin and iron-axial ligand bonding are often

compatible between models and proteins, the protein environment reflects large heme in-plane asymmetry that cannot be predicted from models (Shulman et al., 1971; Satterlee, 1986).

The assignment strategies employed here are comparison of the highly shifted and/or relaxed protons with those of metSwMbCN (Emerson & La Mar, 1990), characterization of the spin systems of the corresponding residues, and comparison of their connectivities with those expected from X-ray coordinates of MbCO (Kuriyan et al., 1986). Figure 86 shows the schematic representation of the spatial dispositions of some heme pocket amino acid residues based on the X-ray structure.

RESULTS AND DISCUSSION

Assignments of the Strongly Relaxed heme pocket residues of metEqMbIm

Figures 87 and 88 show the 2D NOESY and COSY maps, respectively, of metEqMbIm at pH 7 and 308 K. Included at the top of Figure 86 are the amino acid spin systems of interest, from His, Ile and Val. All cross peaks are numerically labeled on the spectra, with the key to the labels included in the corresponding spectrum, as well as in the text.

His F8. $C_{\beta}H$ of His F8 at 14.64 ppm, as labeled in Figure 87, was assigned in Chapter III by means of saturation transfer from the same proton in metEqMbH₂O. Strong cross peaks in NOESY [1] and COSY [4] (Figure 88C) from this peak were observed to a peak at 6.22 ppm, which was assigned to $C_{\beta}H'$ of His F8 because geminal pairs (with dihedral angle $\sim 108^\circ$) are most likely to exert both strong through-space and through-bond interactions. $C_{\beta}H'$ has a possible COSY [5] cross peaks to a peak at 8.10 ppm. A 1D slice from 2D COSY of $C_{\beta}H'$ confirmed its COSY interactions to [4] and [5], as illustrated in Figure 88A. This peak at 8.10 ppm was tentatively identified as $C_{\alpha}H$ His F8 because there is no other resonance that is scalar coupled to $C_{\beta}H'$ (see His structure on Figure 86).

Although the expected NOEs were not observed from $C_{\alpha}H$ to $C_{\beta}H$ and $C_{\beta}H'$, as a result of weak dipolar coupling due to the orientation, COSY cross peak [2] was observed in the 1D slice of $C_{\beta}H$ from 2D COSY (Figure 88B). Comparison of [2] with Figure 88A verifies the $C_{\alpha}H \leftrightarrow C_{\beta}H$ COSY cross peak. The detection of weak scalar coupling between $C_{\beta}H$, $C_{\beta}H'$ and $C_{\alpha}H$ (i.e. [2] and [5]) is consistent with the 2D NOESY profile. The weak spatial and through-bond interactions dictate that they adopt one of a specific set of orientations. Consistent with this spatial orientation of this vicinal pair is that, as opposed to strong $C_{\beta}H' \leftrightarrow C_{\alpha}H$, only weak dipolar and scalar couplings of $C_{\beta}H \leftrightarrow C_{\alpha}H$ was observed in metSwMbCN (Emerson & La Mar, 1990).

Ile FG5. The upfield resonance at -5.2 ppm has relatively broad linewidth (~400 Hz) that integrates to one proton, is highly shifted, and exhibits extended COSY and NOESY connectivities. Few amino acids, for instance Ile, Val, and Leu, have extensive dipolar and scalar coupling patterns. One of the cross peaks to this peak (in both NOESY and COSY) yields dipolar connectivity to $5CH_3$, and comparison of the X-ray coordinates (Figure 86) with the T_1 -derived r_{H-Fe} (see below) identifies it as a proton from Ile FG5. There are four single-proton resonances, $C_{\alpha}H$, $C_{\beta}H$, $C_{\gamma}H$, and $C_{\gamma}H'$, on Ile FG5 (as illustrated on top of Figure 86). $C_{\gamma}H$ is singled out because of its short T_1 , which places it ~4.7 Å from Fe -- identical to that determined from X-ray coordinates. Expected NOESY/COSY patterns of Ile are referenced in Figure 5 of Chapter III. Here, most of the expected NOESY and COSY cross peaks were observed (as marked on Figures 87 and 88), including NOESY connectivities $C_{\gamma}H \leftrightarrow C_{\delta}H_3$ [6], $C_{\gamma}H \leftrightarrow C_{\beta}H$ [9], $C_{\gamma}H \leftrightarrow C_{\gamma}H'$ [8], $C_{\gamma}H \leftrightarrow C_{\gamma}H_3'$ [7], $C_{\gamma}H' \leftrightarrow C_{\delta}H_3$ [10], $C_{\gamma}H' \leftrightarrow C_{\gamma}H_3'$ [11], $C_{\gamma}H_3' \leftrightarrow C_{\beta}H$ [28], $C_{\delta}H_3 \leftrightarrow \beta\text{-meso}$ [12], $C_{\delta}H_3 \leftrightarrow 4H_{\alpha}$ [13]; $\beta\text{-meso}$ was further verified by its NOE to $5CH_3$ [14], and $4H_{\alpha}$ was identified both by saturation transfer from metEqMbH₂O (Chapter III) and $4H_{\alpha} \leftrightarrow 5CH_3$ NOE [15]. In addition, $5CH_3$ also has dipolar connectivity with $C_{\delta}H_3$ of FG5 [16]. These specific spatial interactions between

the heme peripheral protons and Ile FG5 place Ile in a unique orientation as illustrated in Figure 86. COSY cross peaks consistent with Ile spin-system include: $C_{\gamma}H \leftrightarrow C_{\delta}H_3$ [17], $C_{\gamma}H \leftrightarrow C_{\gamma}H'$ [18], and $C_{\gamma}H' \leftrightarrow C_{\delta}H_3$ [19], and $C_{\gamma}H_3' \leftrightarrow C_{\beta}H$ [20].

Other dipolar connectivities among the heme peripheral resonances that may help future assignments of pocket residues are shown in Figure 87 as: $1CH_3 \leftrightarrow \delta\text{-meso}$ [21], which is verified by the presence of expected NOE $8CH_3 \leftrightarrow \delta\text{-meso}$ [22]. The assignment of $\delta\text{-meso}$ is further confirmed by variable temperature NOESY experiments, which show that $\delta\text{-meso}$ is highly sensitive to temperature, characteristic of heme *meso* due to proximity as well as contact interaction with the paramagnetic center. A common NOESY cross peak occurs between a peak at 7.70 ppm and $5CH_3$ [23], $2H_{\alpha}$ [24]. The peak is also relatively invariant to variable temperatures. Inspection of the crystal structure for residues in the vicinity of the pyrrole I (Figure 86), as well as comparison with metSwMbCN profile tentatively assigns the resonance at 7.70 ppm to aromatic proton of Phe H15. The aromatic Phe H15 protons are $> 8 \text{ \AA}$ from the Fe center, thus not resolved from the diamagnetic envelope.

Val E11. Assignment of Val E11 was attempted by irradiation of the assigned $C_{\gamma}H_3$ of Val E11 in metEqMbH₂O by mutated Mbs at the E11 position (Rajaratnam et al., 1991). Figure 89 shows that 1D NOE irradiation of $C_{\gamma}H_3$ in a pure metEqMbH₂O sample induces possible dipolar connectivity to a methyl peak at -3.4 ppm, which has a T_1 of 8.8 ms. The relatively long T_1 , as compared to $\sim 1 \text{ ms}$ for $C_{\gamma}H_3$ of E11, suggests that the possible NOE observed (the asterisked peak in Figure 89) may have arisen from off-resonance effect. In addition, the T_1 places this peak at 6.8 \AA from the Fe center, which is further than the expected $r_{Fe-C_{\gamma}H_3}$ Val E11 (determined to be 5.10 \AA from the X-ray structure of MbCO (Kuriyan et al., 1986)). Therefore, no conclusive assignment can be made for Val E11 in metEqMbIm from saturation transfer to metEqMbH₂O.

Saturation Transfer to Identify Heme Pocket Residues in MetEqMbH₂O

As a prototype for the versatility of saturation transfer methodology, assignments in the high-spin metEqMbH₂O was made from metEqMbIm. The extreme usefulness of this technique lies in the fact that dipolar and scalar connectivities in the pure high-spin system are difficult to detect because of the large linewidths and fast relaxation, rendering rapid loss of coherence, even in steady-state 1D NOE experiments. As shown in Figure 89, resolved upfield resonances in metEqMbH₂O were not identifiable from 1D NOE, but were assigned through saturation transfer from metEqMbIm.

Leu G5. The methyl peak at ~-5.1 ppm in metEqMbH₂O at 308 K (Figure 90) compares with that at ~-3.4 ppm in Figure 89. Figure 90 shows a saturation transfer peak [25] was observed to metEqMbIm at ~-1.55 ppm. This methyl peak was shown not to be those of Val E11 and Ile FG5 because of its long T₁ and that its saturation transferred peak in metEqMbIm does not correspond to any of the Ile FG5 methyls, respectively. Its T₁ places it ~6.1 Å from the Fe. By virtue of elimination, r_{Fe-H}, and comparison with the assignments in metSwMbCN (Emerson & La Mar, 1990), this peak is tentatively assigned to the C₅H₃ of Leu G5. This assignment is also supported by the dipolar and scalar connectivities observed to its C_γH in Figures 87 and 88, [26] and [27], respectively.

Other MetEqMbH₂O Resonance Assignments. Resolved upfield peak at -7.4 ppm was previously assigned to heme 2-β -vinyl proton (Rajaratnam et al., 1991). However, without selective isotope labelling of the H_{βc,t}, no specific assignment was available. Figure 90, on the other hand, shows a strong EXSY cross peak to the 2H_{βt} of metEqMbIm [32], which immediately assigned the peak. As is apparent from Figure 90, there are numerous EXSY cross peaks that can be readily identifiable, given further assignments in the mixed-spin metEqMbIm system. The above examples clearly illustrate that the utility of saturation transfer between these two systems is not only theoretically amusing, but more importantly practically possible.

Table XIII lists all the assignments included here for both systems.

TABLE XIII

ASSIGNMENTS FOR SOME HEME POCKET RESIDUES IN
MetEqMbIm AND MetEqMbH₂O, AS INDICATED AT pH 6.8-7.0, 308
K. THE NUMBERS AFTER THE RESIDUES INDICATE THE
CORRESPONDING POSITIONS ON THE HELIX OF PROTEIN.

<u>Residue</u>	<u>Position</u>	<u>Chemical Shift (ppm)</u>
<u>MetEqMbIm</u>		
His F8/93	C _β H	14.64
	C _β H'	6.22
	C _α H	8.10
Ile FG5/99	C _β H	-1.60
	C _γ H ₃	-2.25
	C _γ H	-5.55
	C _γ H'	-0.33
	C _γ H ₃	1.25
Leu G5/104	C _{δ2} H ₃	-1.55
	C _γ H	1.75
(other)		
Heme <i>meso</i>	δ- <i>meso</i>	1.22
Phe H15	aromatic H	7.07
<u>MetEqMb- H₂O</u>		
Leu G5/104	C _{δ2} H ₃	-5.10
Heme 2- vinyl	2-H _{βt}	-7.55

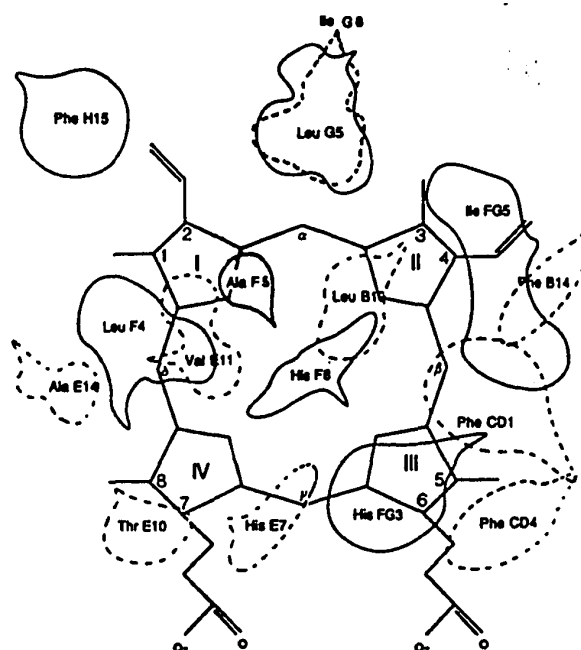
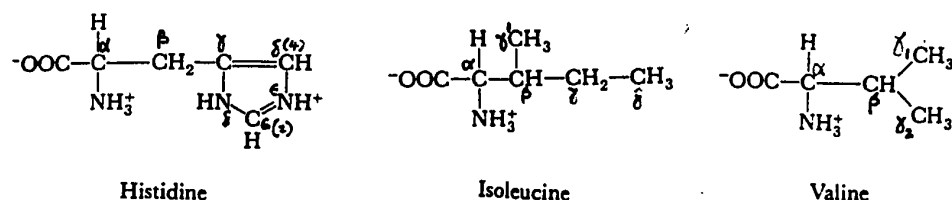


Figure 86. Schematic representation of the spatial disposition of amino acid side chains in the heme pocket of SwMb, from its X-ray coordinates in CO form (Kuriyan et al, 1986), as viewed face-on the heme from the proximal side. Solid and dotted lines represent the residues on the proximal and distal sides, respectively. The pointed end of each residue indicates the location of C_αH correspondingly. Top shows the structures of amino acids His, Ile, and Val, whose spin systems are elaborated.

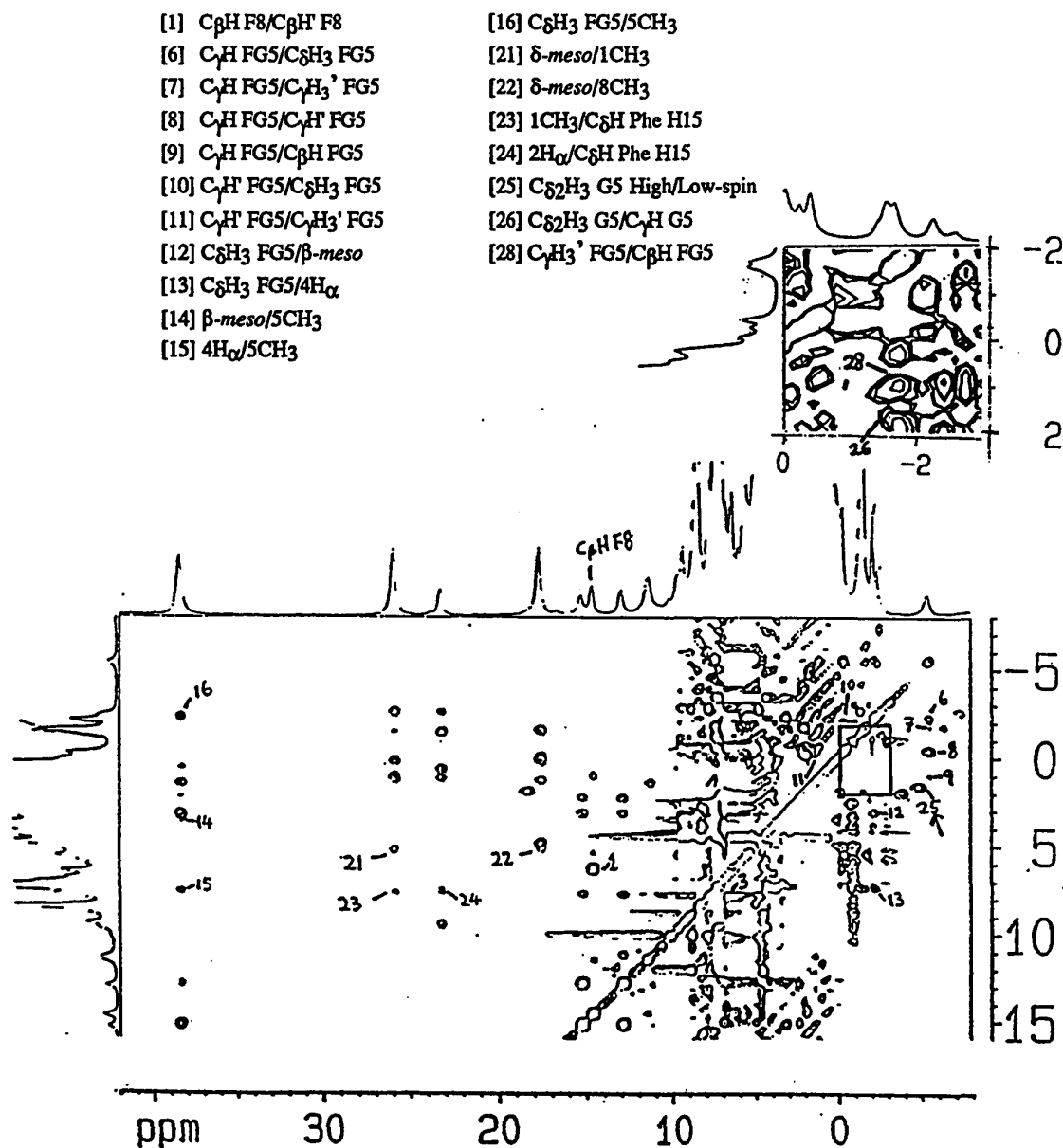


Figure 87. 400 MHz 2D ^1H phase-sensitive NOESY spectrum of metEqMbIm in $^2\text{H}_2\text{O}$ at pH 7.0, 308 K. Parameters include mixing time of 25 ms, relaxation delay of 20 ms, with 512 data points in both dimensions over a spectral window of 42 kHz. The diagonal corresponds to the reference spectra on both axes. Correlations are numbered on the cross peaks, as well as elaborated in the text. Key to the correlations are listed on top. An expansion of the squared region of an independently acquired and processed 2D NOESY of metEqMbIm (under identical conditions) to higher resolution is shown at the top.

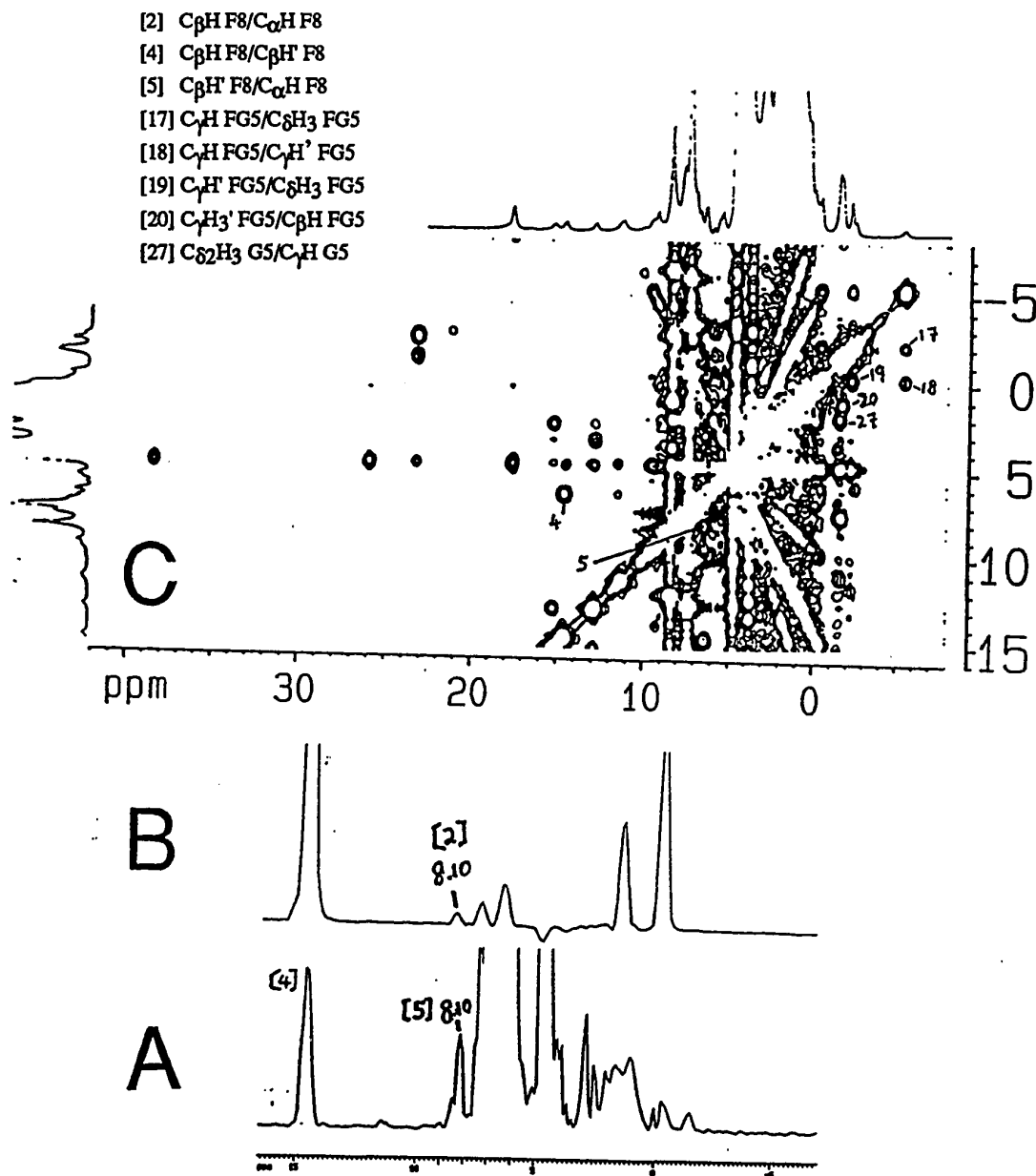


Figure 88. C. 400-MHz 2D 1H magnitude COSY spectrum of metEqMblm at pH 7.0, and 308 K. Parameters include relaxation delay of 20 ms, 450 and 1024 data points in the f1 and f2 dimensions, respectively over a spectral window of 42 kHz. The diagonal corresponds to the reference spectra on both axes. Correlations are numbered on the cross peaks, as well as elaborated in the text. Key to the correlations are listed on top. B.- A., 1D f1 slices from 2D COSY (C) of the resonances at 14.64 ppm and 6.22 ppm, respectively. Relative correlations are labeled correspondingly.

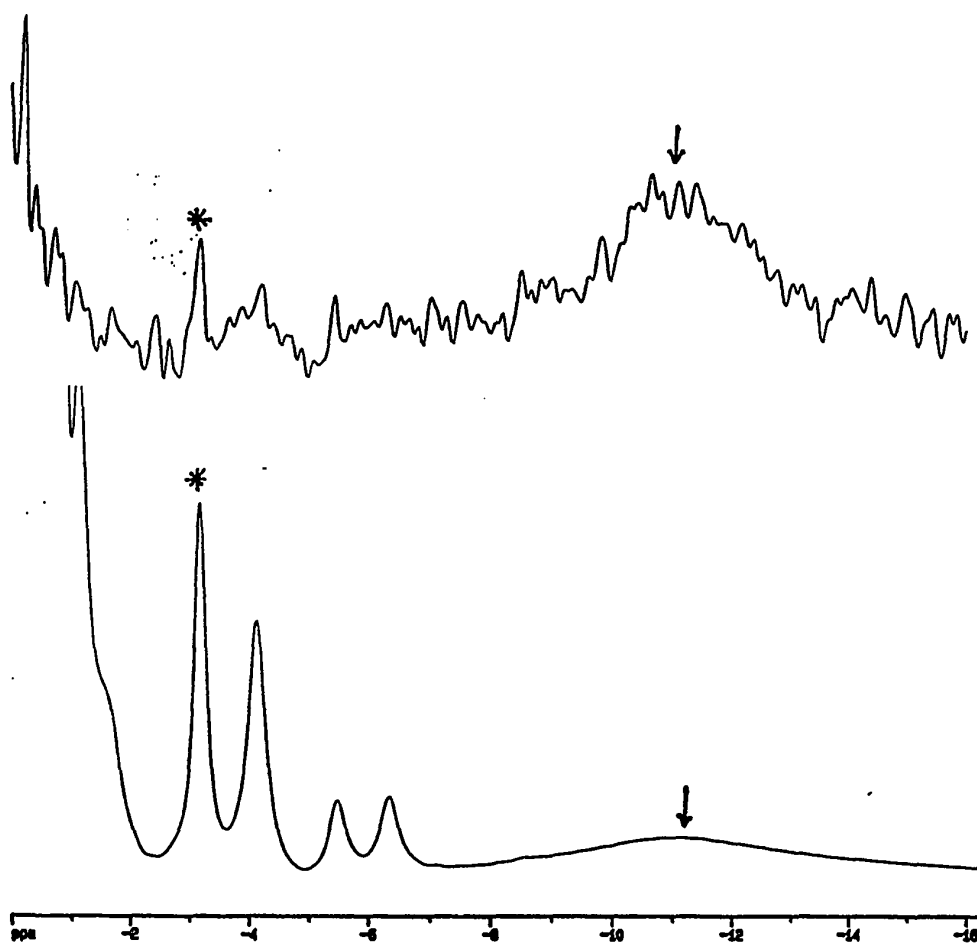


Figure 89. 1D NOE saturation of C₂H₃ Val E11 (marked by arrows) in metEqMbH₂O at pH 6.8 and 323 K. Parameters employed were d10=33, d1=40 ms, and d20=100 ms. The asterisk marks the off-resonance effect from the irradiated peak due to the long T₁ of the asterisked peak and the high irradiation power used.

[25] C₅₂H₃ G5 metEqMbIm/High-spin
 [31] Not assigned
 [32] Heme 2H_β metEqMbIm/High-spin

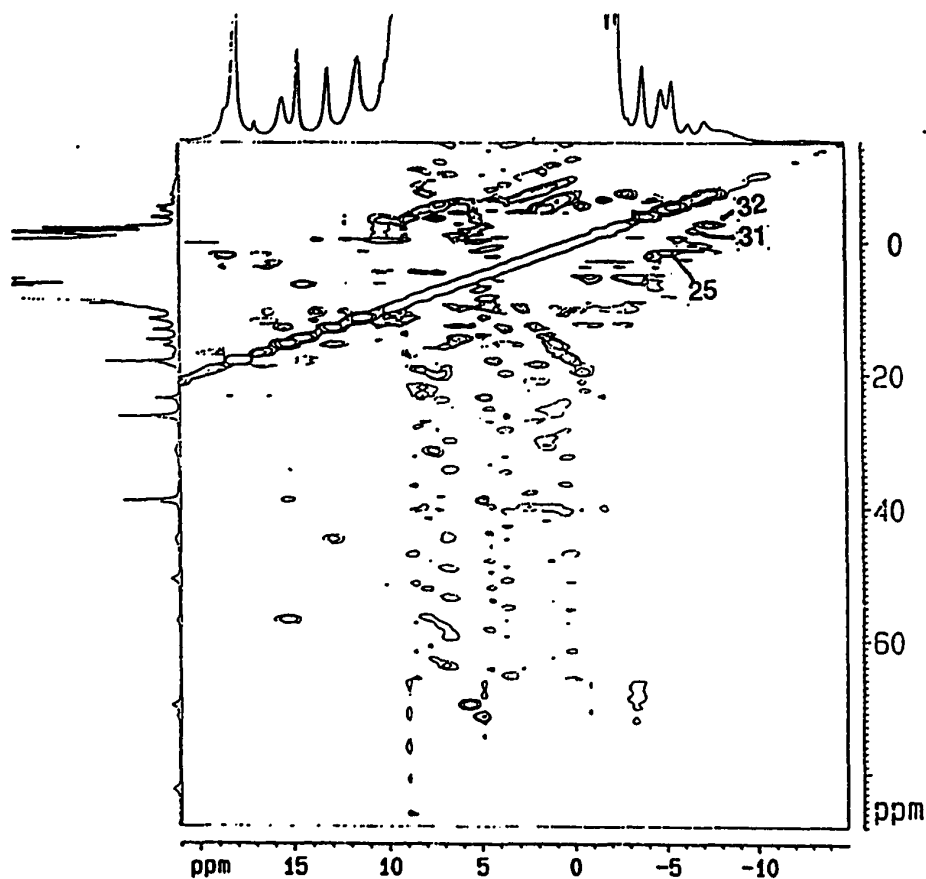


Figure 90. 400-MHz 2D ^1H phase-sensitive EXSY spectrum of metEqMbH₂O:Im at pH 6.8 and 308 K, compared with NOESY spectrum of metEqMbIm in Figure 87. EXSY was collected with 4 ms mixing time, 40 ms relaxation delay, and over a spectral window of 83 kHz. 512 data points were used in both dimensions. Note that in Figure 87, the sample was mostly metEqMbIm, with residual metEqMbH₂O components, as evidenced from the small saturation transfer observed. Correlations between the species are listed on top.

CHAPTER IX

CONCLUSIONS

This research accomplished the goal of depicting the dynamics of ligand binding in Mbs with solution-state ^1H NMR spectroscopy, and developing paramagnetic NMR methodology. The findings reinforce the complementary nature of crystallography and NMR spectroscopy.

The pioneering work on two-dimensional ^1H NMR studies of mixed-spin Mb system by Peyton (1991) paved the path for characterization of imidazole and azido Mbs in Chapter III. Spectral and T_1 comparisons between the two systems foreshadowed different interactions between the ligands and the heme Fe. The longer methyl T_1 s in metMbIm than in metMbN₃ contrasted the implication of more high-spin character of metMbIm by the larger hyperfine-shift of its 5CH₃ and its facile exchange with the high-spin metMbH₂O. The covalency of the N₃--heme Fe bond and its H-bonding pattern compensated for its weak ligand field character, thus exhibiting sharper linewidths and low ligand off-rate (suggested by its inability to exchange with metMbH₂O) than metMbIm. On the other hand, although Im is capable of stabilizing the heme Fe by better π electron back-bonding, steric hindrance imposed by its size results in its facile exchange with H₂O.

The broadness of heme methyl resonances in metMbIm is not merely a consequence of the mixed-spin characteristics, but is attributed to bound Im ring-equilibration between conformational isomers, and this is a function of pH and heme pocket residue variance (Chapter IV). Until the ban on sperm-whaling in the mid 1980's, SwMb has been the species most extensively studied (and still is in Japan). Comparison of metPSwMbIm with

metEqMbIm revealed striking spectral differences, most notably the much broader methyl linewidths in the former species, especially at basic pH. The unique heme crevice residue substitution Lys CD3 --> Arg CD3 in PSwMb is judged to be responsible for this. Mutations at the CD3 position of Mbs with ligand recombination and X-ray crystallographic studies asserted that this residue is crucial in providing energy barrier for the ligand escape trajectory through a concerted motions by His E7, Lys/Arg CD3, and Asp E3. A higher energy barrier was found for PSwMb, with Arg CD3, than for EqMbs, Lys CD3. ^1H NMR results promptly verified those findings by saturation-transfer profiles which implicated ring-flip between conformational isomers of the bound Im, and more importantly, the splitting of methyls at low temperature, characterizing two distinct conformations. CBS analysis allows the determination of energetics that shed light on differences involved in the ring equilibration between the species. The fact that this equilibration is acid-catalyzed suggests possible hydrogen-bonding interactions between the ligand and a nearby proton donor at basic pH to stabilize the minor conformation, therefore slowing interconversion of the two at high pH.

The unique role of residue CD3 is also demonstrated in Chapter V, when heme(CN)₂ was used as a probe to compare the heme cavity integrity among EqMb, SwMb, and PSwMb. The efficacy of heme(CN)₂ lies in its ability to insert in the dicyano-coordinated form into the heme pocket. The ratio of the heme-insertion isomers in metMbCN was monitored following the reconstitution with heme(CN)₂. This species is ultimately formed after the breakage of one of the CN-Fe bond and the formation of His F8-Fe bond. While metPSwMbCN and metSwMbCN showed identical an ratio of 2.5:1 of the major:minor isomers, metEqMbCN exhibited a 5:1 ratio. The closer to the equilibrium 9:1 ratio in metEqMbCN dictates different energetics in the heme pocket of EqMb than PSwMb and SwMb. This difference in ratios may be explained by the occurrence of the transiently-tense active site to accommodate the reorientation of

heme(CN)₂ within the pocket is facilitated by the swinging motion of His E7 toward the surface, which is then stabilized by the positively-charged, longer side chain of Arg CD3 in the two latter Mbs. Therefore, the more destabilized minor isomer in EqMb favored the major orientation in a more timely fashion, reflected by its ratio.

The conclusion from Chapter V is made on the premise that heme reorientation occurs within the protein heme crevice, instead of by way of a completely dissociative pathway. This is compatible with evidence from other work in this group that showed the ability of apoMb to accommodate Sn-dimer. Chapter VI examined the complete-dissociative pathway by free energy analysis of the heme redistributional disorder by optical spectroscopy. The analysis found that the activation free energy for dissociation would be somewhat larger than the measured heme-rotation. This supports a non-dissociative mechanism.

The abundance of protons in biological systems present valuable lessons to be learned on the dynamics of biological macromolecules by studying the labilities of exchangeable protons. Chapter VII focuses on the exchange kinetics of the labile protons in the vicinity of heme, namely His E7, His F8, and His FG3. Hydrogen-bonding interactions were found in the metMbN₃, but not in the metMbIm complexes, between the ring NH of His E7 and exogenous ligand, confirming the steric hindrance of Im in metMbIm that forces the His E7 to swing out partially. Implications of the modulation of exchange rate by exogenous ligand were made based on the approximately equal hydrogen exchange rate in metMbN₃ as compared to metSwMbCN. Strong hydrogen bond strength between ring NH of His E7 and N₃⁻ was postulated based on possible covalent bonding interaction in the trigonal planar formed by heme Fe--N₃--H (His E7). The failure to detect isotope splitting of the heme methyls from this interaction at basic pH supported this postulate, reminiscent that such interaction in metSwMbCN was observed to be both acid- and base-catalyzed. Comparison of the protons from the proximal His F8 lability among

the species (metMb- CN, N₃, and Im) provided evidence that the heme proximal side is relatively insensitive to exogenous ligand.

Novel NMR methodology of assigning the heme pocket residues in the pure high-spin metMbH₂O was proposed in Chapter VIII. The ability of the metMbIm to exchange readily with H₂O formulated the bulk of this exciting technique. While the few proton assignments in metMbH₂O reflect a history of laborious selective isotope-labelings and mutagenesis, this work identified C α H of Val E11, and the heme 2H β _t in metEqMbH₂O, unambiguously and painlessly.

REFERENCES

- Aojula, H.S., Wilson, M.T. & Drake, A. (1986) *Biochem. J.* 237, 613-616
- Augusto, O., Kunze, K.L., Ortiz de Montellano, P.R. (1982) *J. Biol. Chem.* 257, 6231-6241.
- Balasubramanian, S., Lambright, D.G., Marden, M.C., and Boxer, S.G., (1993) *J. Am. Chem. Soc.* 32, 2202-2212.
- Bell, J.A., Korszun, Z.R., and Moffat, K. (1980) *Biochim. Biophys. Acta* 622, 210-218.
- Braughler, J.M., Duncan, L.A., and Chase, R.L. (1986) *J. Biol. Chem.* 261, 10282-10289.
- Brooks III, M.R. (1992) *J. Mol. Biol.* 227, 375-380.
- Budd, D.L., La Mar, G.N., Langry, K.L., Smith, K.M., and Nayyir-Mazhir, R. (1979) *J. Am. Chem. Soc.* 101, 6091-6096.
- Burke, T.R., Jr, Martin, J.L., George, J.W., and Pohl, L.R. (1980) *Biochem. Pharm.* 29, 1623-1626.
- Cantoni, L., Gibbs, A.H., and De Matteis, F. (1981) *Int. J. Biochem.* 13, 823-830.
- Carver, T.E., Olson, J.S., Smerdon, S.J., Krzywda, S., Wilkinson, A.J., Gibson, R.H., Blackmore, R.S., Ropp, J.D., and Sligar, S.G. (1990) *Biochem.* 30, 4697-4705.
- Case, P.A., and Karplus, M. (1979) *J. Mol. Biol.* 132, 343-368.
- Cutnell, J., La Mar, G.N., & Kong, S. (1981) *J. Am. Chem. Soc.* 103, 3567-3572
- Dalvitt, C., & Wright, P.E. (1987) *J. Mol. Biol.* 194, 313-327.
- Dayhoff, M.O. (1972) Atlas of Protein Sequence and Structure Nat. Biomed. Res. Found., Washington, D.C.
- Deeb, R.S. (1993) Ph.D Dissertation, Portland State University, in progress.
- Deeb, R.S., & Peyton, D.H. (1991) *Biol. Chem.* 266, 3728-3783.

- Elber, R (1990) Simulation of Ligand Diffusion in Myoglobins and Myoglobin Mutants in *Research Summaries for Kinetics of Myoglobin and Hemoglobin* (Brunori, M., Eaton, W.A., Gibson, Q.H., & Karplus, M., Eds) June 25-27, P23. National Institutes of Health, Bethesda, MD.
- Emerson, S.D., & La Mar, G.N. (1990) *Biochemistry* 29, 1545-1556
- Figueiredo, E.A., Marcus, V.G., Heneine, I.F., Santos, I.C., and Hargreaves, F.B. (1973) *Comp. Biochem. Physiol.* 443, 481.
- Freeman, R., Hill, H.D.W. (1971) *J. Chem. Phys.* 54, 3367.
- French, J.K., Winterbourn, C.C., Carrell, R.W. (1978) *Biochem. J.* 173, 19-26.
- Galaris, D., Eddy, L., Arduini, A., Cadenas, E, and Hichstein, P. (1989a) *Biochem. Biophys. Res. Commun.* 160, 1162-1168.
- Galaris, M., Cadenas, E, and Hochstein, P. (1989b) *Arch. Biochem. Biophys.* 273, 497-504.
- Gebe, J.H., Peyton, D.H., and Peyton, J.A. (1989) *Biophys. Biochem. Res. Commun.* 161, 290-294.
- Gibson, Q.H. & Antonini, E. (1960) *Biochem. J.* 77, 328-341.
- Goldberg, B., Stern, A., Peisach, J. (1976) *J. Biol. Chem.* 251, 3045-3051.
- Harris, C.E., and Teller, D.C. (1973) *J. Theoret. Biol.* 38, 347-362.
- Harris, R.K. "NMR Spectroscopy--A Physicochemical View" (1989) Longman Group (F.E.) Ltd, H.K.
- Hauksson, J.B., La Mar, G.N., Pandey, R.K., Rezzano, I.N., and Smith, K.M. (1990) *J. Am. Chem. Soc.* 112, 6198-6205.
- Hughes, E.W. (1935) *J. Chem. Phys.* 3, 1.
- Ingram, V. (1963) "The Hemoglobins in Genetics and Evolution", Columbia University Press, N.Y.
- Jue, T., Krishnamoorthi, R., & La Mar, G.N. (1983) *J. Am. Chem. Soc.* 109, 5701-5703.
- Kanner, J, Harel, S (1985) *Lipids* 20, 625-628.
- Kawamura-Konishi, Y., Kihara, H., & Suzuki, H. (1988) *Eur. J. Biochem.* 170, 589-595
- Kendrew, J.C., Dickerson, R.E., Strandberg, B.E., Hart, R.G., Davies, D.R., Phillips, D.C., and Shore, V.C. (1960) *Nature* 185, 422-427.
- Ko, K.M., and Godin, D.V. (1990) *Mol. and Cell. Biochem.* 95, 125-131.

- Ko, K.M., and Godin, D.V. (1991) *Mol. and Cell. Biochem.* 101, 23-29.
- Krishnakumar, R., La Mar, G.N., Chiu, M.L., Sligar, S.G., Singh, J.P., and Smith, K.M. (1991) *J. Am. Chem. Soc.* 113, 7886-7892.
- Kuriyan, J., Wilz, S., Karplus, M., and Petsko, G.A. (1986) *J. Mol. Biol.* 192, 133-154.
- La Mar, G.N., Hauksson, J.B., Dugad, L.B., Liddell, P.A., Venkataramana, N., and Smith, K.M. (1991) *J. Am. Chem. Soc.* 113, 1544-1552.
- La Mar, G.N. (1973) in *NMR of Paramagnetic Molecules* (La Mar, G.N., Horrocks, W.D., Jr. & Holm, R.H., eds), Academic Press, New York.
- La Mar, G.N. (1979) in "Biological Application of Magnetic Resonance" Ed. Shulman, R.G., pp 305-343, Academic Press, N.Y.
- La Mar, G.N., and Walker-Jensen, F.A. (1978) in "The Porphyrins" Ed. Dolphin, D., Vol. IV, Part C, Academic Press, N.Y.
- La Mar, G.N., Budd, D.L., Smith, K.M., & Langry, K.C. (1980) *J. Am. Chem. Soc.* 102, 1822-1827.
- La Mar, G.N., Chatfield, M.J., Peyton, D.H., de Ropp, J.S., Smith, W.S., Krishnamoorthi, R. Satterlee, J.D. & Erman, J.E. (1988) *Biochim. Biophys. Acta* 956, 267-276.
- La Mar, G.N., Hauksson, J.B., Dugad, L.B., Liddell, P.A., Venkataramana, N. & Smith, K.M. (1991) *J. Am. Chem. Soc.* 113, 1544-1550.
- La Mar, G.N., Krishnamoorthi, R., Smith, K.M., Gersonde, K., and Sick, H. (1983) *Biochem.* 22, 6239-6246.
- La Mar, G.N., Lecomte, J., and Unger, S.W. (1991) *J. Mag. Res.* 94, 112-122.
- La Mar, G.N., Toi, H., & Krishnamoorthi, R. (1984) *J. Am. Chem. Soc.* 106, 6393-6401.
- La Mar, G.N., Viscio, D.B., Smith, K.M., Caughey, W.S., and Smith, M.L. (1978) *J. Am. Chem. Soc.* 100, 8085-8092.
- Lambright, D.G., Balasubramian, S., & Boxer, S.G. (1989) *J. Mol. Biol.* 207, 289-299.
- Larsen, R.W., Nunez, D.J., Macleod, J., Shiemke, A.K., Musser, S.M., Nguyen, H.H., Ondrias, M.R., and Chan, S.I. (1992) *J. Inorg. Biochem.* 48, 21-31.
- Lecomte, J., & La Mar, G.N. (1985) *Biochemistry* 24, 7388-7395.
- Lecomte, J., & La Mar, G.N. (1987) *J. Am. Chem. Soc.* 109, 7219-7222.
- Lecomte, J., Johnson, R.D. & La Mar, G.N. (1985) *Biochim. Biophys. Acta* 829, 268-274.

- Levin, W. Jacobson, M., Kuntzman, R. (1972) Arch. Biochem. Biophys. 148 262-269.
- Light, W.R., Rohlf, R.J., Palmer, G., and Drake, A. (1986) J. Biol. Chem. 262, 46-52.
- Lionetti, C., Guanziroli, M.G., Frigerio, F., Ascenzi, P., & Bolognesi, M. (1991) J. Mol. Biol. 217, 409-419.
- Mabbutt, B., & Wright, P.E. (1985) Biochim. Biophys. Acta 832, 175-185.
- McGrath, T.M., and La Mar, G.N. (1978) Biochim. Biophys. Acta 534, 99-111.
- Metzler, M., and McLachlan, J.A. (1978) Biochem. Biophys. Res. Commun. 85, 874-884.
- Noggled, J.H., and Shirmer, R.E. (1971) "The Nuclear Overhauser Effect" Academic Press, N.Y.
- Oldfield, T.J., Smerdon, S.J., Dauter, Z., Petratos, K. Wilson, K.S., and Wilkinson, A.J. (1992) Biochemistry 31, 8732-8739.
- Olson, J., Mathews, A.J., Rohlf, R.J., Springer, K.D., Ederberg, K.D., Sligar, S.G., Tame, J., Renaud, J.P. & Nagai, K. (1988) Nature 336, 265-266.
- Osawa, Y., and Pohl, L.R. (1989) Chem. Res. Toxicol. 2, 131-141.
- Osawa, Y., and Korzekwa, K. (1991) Proc. Natl. Acad. Sci. 88, 7081-7085.
- Osawa, Y., Highet, R.J., and Pohl, L.R. (1992) Xenobiotica 22, 1147-1156.
- Osawa, Y., Highet, R.L., Bax, A., and Pohl, L.R. (1991) J. Biol. Chem. 266, 3208-3214.
- Osawa, Y., Highet, R.L., Murphy, C.M., Cotter, R.J., and Pohl, L.R. (1989) J. Am. Chem. Soc. 111, 4462-4467.
- Pauling, L. (1960) "The Nature of Chemical Bond", 3rd ed., pp271, Ithaca, N.Y., Cornell University Press.
- Pauling, L., and Brockway, L.O. (1937) J. Am. Chem. Soc. 59, 13.
- Perutz, M.F., and Matthews, F.S. (1966) J. Mol. Biol. 21, 199.
- Peyton, D.P., La Mar, G.N., Pande, U., Ascoli, F., Smith, K.M., and Brunori, M. (1989) Biochemistry 28, 4880-4887.
- Peyton, D.H. (1991) Biochem. Biophys. Res. Comm. 175, 515-519
- Peyton, D.H., La Mar, G.N., Ramaprasad, S., Unger, S.W., Sankar, S., and Gersonde, K. (1991) J. Mol. Biol. 221, 1015-1026.
- Phillips, S.E.V. (1978) Nature 273, 247-248.

- Phillips, S.E.V., & Schoenborn, B.P. (1981) *Nature* 292, 81-82.
- Prasad, M.R., Engelman, R.M., Jones, R.M., and Das, D.K. (1989) *Biochem. J.* 263, 731-736.
- Rajaratnam, K., La Mar, G.N., Chiu, M.L., and Sligar, S.G. (1992) *J. Am. Chem. Soc.* 114, 9048-9058.
- Read, K.R.H. (1966) in *Physiology of Mollusca* "Molluscan hemoglobin and myoglobin", ed. Wilbur, K.M., and Yonge, C.M. Vol 2. Academic Press, N.Y.
- Rice, R.H., Lee, Y.M., and Brown, W.D. (1983) *Arch. Biochem. Biophys.* 221, 417-427.
- Ringe, D., Petsko, G.E., Kerr, D.E. & Ortiz de Montellano, P.R.O. (1984) *Biochemistry* 23, 2-4.
- Riordan, J.F. (1979) *Mol. & Cell. Biochem.* 26, 71-89.
- Rogan, E.G., Katomski, P.A., Roth, R.W., and Cavalieri, E.L. (1979) *J. Biol. Chem.* 254, 7055-7059.
- Rossi-Bernardi, L., and Chiancone, E. "Methods in Enzymology" (1981) 76, Eds. Antonini, E., Academic Press.
- Sanders, J.K.M., and Hunter, B.K. (1988) in "Modern NMR Spectroscopy: A Guide For Chemists." Oxford University Press, Great Britain.
- Sanström, J. (1982) "Dynamic NMR Spectroscopy" Academic Press, London.
- Satoh, Y., and Shikima, K. (1981) *J. Biol. Chem.* 256, 10270-10275.
- Satterlee, J.D. (1985) *Annu. Rep. NMR Spec.* 17, 79-178.
- Satterlee, J.D. (1990a) *Concepts Magn. Res.* 2, 69-79.
- Satterlee, J.D. (1990b) *Concepts Magn. Res.* 2, 119-129.
- Shikima, K. (1984) *Biochem. J.* 223, 279-280.
- Shulman, R.G., Glarum, S.H., and Karplus, M. (1971) *J. Mol. Biol.* 57, 93-115.
- Smith, M.B., & Millett, F. (1980) *Biochim. Biophys. Acta* 626, 64-72.
- Soltis, S.M., and Strousse, C.E. (1988) *J. Am. Chem. Soc.* 110, 2824-2829.
- Steigemann, W., Weber, E. (1979) *J. Mol. Biol.* 127, 309-338.
- Stryer, L., Kendrew, J.C. & Watson, H.C. (1964) *J. Mol. Biol.* 8, 96-104.
- Svedberg, T. (1933) *J. Biol. Chem.* 103, 311.

- Tajima, G., and Shikama, K. (1987) *J. Biol. Chem.* 262, 12603-12606.
- Takano, T. (1977) *J. Mol. Biol.* 110, 537-568.
- Teale, F. (1959) *Biochim. Biophys. Acta* 35, 543.
- Terwilliger, N.B., Terwilliger, R.C., and Schabtach, E. (1976) *Biochim. Biophys. Acta* 453, 101.
- Terwilliger, R.C. (1980) *Amer. Zool.*, 20, 53.
- Terwilliger, R.C., and Terwilliger, N.B. (1977) *Comp. Biochem. Physiol.* 50B, 283-287.
- Unger, S.W., Lecomte, J., & La Mar, G.N. (1985) *J. Magn. Res.* 64, 521-526.
- Vaughan, J., Mughrabi, Z., and Wu, E. (1970) *J. Org. Chem.* 35, 1141-1145.
- Vincent, S.H., Grady, R.W., Shaklai, N., Snider, J.M., and Muller-Eberhard, U. (1988) *Arch. Biochem. Biophys.* 265, 539-550.
- Wallace, W.J., Houtchens, R.A., Maxwell, J.C., and Caughey, W.S. (1982) *J. Biol. Chem.* 257, 4966-4977.
- Wood, E., and Gullick, W.J. (1979) *Biochim. Biophys. Acta* 576, 456-465.
- Woodward, C.K., and Hilton, B.D. (1979) *Annu. Rev. Biophys. Bioenerg.* 8, 99-127.
- Woodward, C.K., Simon, E., and Tuchsén, E. (1982) *Mol. Cell. Biochem.* 48, 135-160.
- Wüthrich (1986) *NMR of Proteins and Nucleic Acids*. Wiley, New York .
- Yamamoto, Y., & La Mar, G.N. (1986) *Biochem.* 25, 5288-5297.
- Yamamoto, Y., and La Mar, G.N. (1989) *Biochim. Biophys. Acta* 996, 189-194.
- Yamazaki, I., Yokota, K-N., & Shikama, K. (1964) *Biol. Chem.* 239, 4151-4153.
- Yee, S., & Peyton, D.H. (1991) *FEBS Lett.* 290, 119-122.
- Yu, L.P., La Mar, G.N., & Rajarathnam, K. (1990) *J. Am. Chem. Soc.* 112, 9527-9534.
-

APPENDIX A

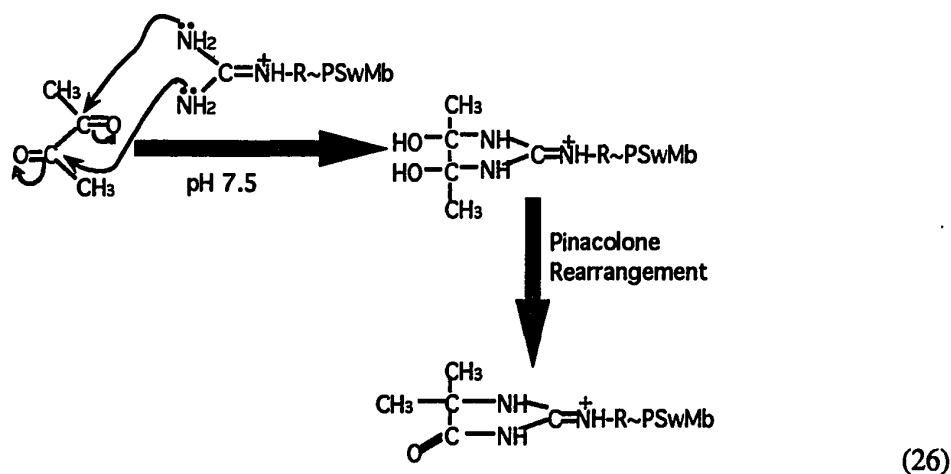
CHEMICAL MODIFICATIONS OF PIGMY SPERM WHALE MYOGLOBIN

APPENDIX

CHEMICAL MODIFICATIONS OF PIGMY SPERM WHALE MYOGLOBIN

Ever since the 1940's, the reaction conditions and specificities of chemical reagents toward amino acids have been widely explored (Herriott, 1947; Olcott & Fraenkel-Conrat, 1947), largely to gain better understanding of the chemical composition of proteins. By 1950's, this approach was used extensively to study protein functions (Boyer, 1959; Hartley, 1960). In this work, the CD3 residue in the heme pockets of two different Mbs is modified. In an attempt to characterize the contribution of CD3 residue to the ligand entry pathway as proposed by Case and Karplus (1979), and to supplement the results obtained from X-ray crystal structures (Oldfield et al., 1992) and geminate recombinations of diatomic molecules in various CD3 mutated Mbs (Balasubramanian et al., 1993; Carver et al., 1991).

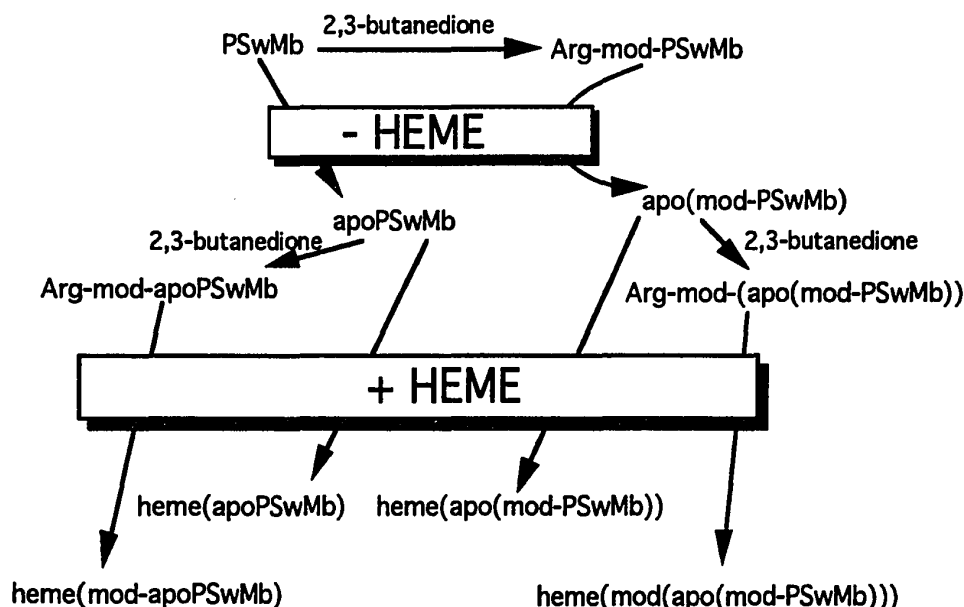
Arginine modification is performed on PSwMb. Distal Arg CD3 plays pivotal role in modulating the passageway of ligand entry by stabilizing the 'closed-door' orientation through hydrogen bonding to heme 6-propionate and Asp E3 (Hauksson et al., 1990) and increases both the inner and outer barriers to ligand escape (Balasubramanian et al., 1993) by restricting the swinging motion of His E7. The reagent 2,3-butanedione can modify arginine as shown in Equation (26) (Riordan, 1979), to remove the interactions which stabilize the 'closed' conformation. The two methyls resulted from this modification induce conformational changes to the heme 6-propionate which are evident in the ^1H NMR spectrum, thus serve to monitor the extent of reaction.



The most notable difficulty encountered by chemical modification of Mb lies in the isolation step. Most proteins, by nature, are sensitive to organic reagents. The folding patterns of tertiary structures of proteins are such that hydrophilic and hydrophobic residues face the exterior and interior, respectively. Hence, organic reagents can easily denature proteins. As a result, a modified Mb may be highly unstable, and thus has to be isolated as soon as it is made. While excess reagent is readily removed by size-exclusion column chromatography, the isolation of completely modified Mb from the partially or totally unmodified material by ion-exchange column chromatography proved to be challenging. For example in numerous Lys modification preparations of EqMb (not shown here), because there are 19 Lys residues, complete modification would cause a drastic increase in its pI, rendering the use of ion exchange futile.

METHODS

The original attempts to modify the Mbs are shown in flow-chart depicted in Equation (27).



(27)

Although complete compliance with this scheme is theoretically feasible, it is impossible practically, given the vulnerability of Mb to denaturation upon a series of chemical treatments. All steps were carried out at 5°C when possible, and dialysis instead of chromatography was employed to get rid of the excess reagent.

RESULTS AND DISCUSSION

Arginine Modification of PSwMb

Initial amino acid analysis results (not shown) revealed the expected trend, with fewer Arg in heme(mod-apoPSwMb) and heme(mod(mod(apo(mod-PSwMb)))) than in heme(apo(mod-PSwMb)). However, there was residual Arg's in all cases. Anion-exchange chromatography was then attempted to isolate the completely Arg-modified apoPSwMb based on the differential protein charges, which depend on the extent of modification. From Equation (26), the bulky group on the modified Arg potentially decreases the basicities of the attached nitrogens, thus, at pH 7.5, the more modified

fraction will be less positively-charged, and so elute at a slower rate from an anion exchanger. Figure 91 shows the DEAE-Cellulose chromatogram at the indicated salt gradient and pH 7.5 for the Arg-modified apoPSwMb. Three bands were apparent, as marked. The elution patterns of Bands I-III from DEAE-Cellulose are consistent among independent modification trials. Because there are four Arg's in PSwMb, one possibility could be that the bands correspond to four progressively modified apoPSwMb. Amino acid analysis showed Band III to be completely modified apoPSwMb (Table XIV).

Kinetics of reconstitution of native apoPSwMb and Band III by optical spectroscopy at pH 7.5 and 298 K determined a four-fold higher rate constant for the modified PSwMb as opposed to the native one, which has a k_f of $1.6 \times 10^{-1} \text{ min}^{-1}$. This finding satisfies the conventional wisdom that removal of the salt bridge between heme 6-propionate and Arg CD3 increases the rotational disorder. However, the recent revelation that the absence of positively-charged CD3 residue increases both the inner and outer energy barriers to ligand escape (Balasubramanian et al., 1993) due to destabilization of the swung-out His E7 casts doubt onto this result. The modified guanidinium group may lower its pK sufficiently significant, rendering no protonation at the nitrogens. Both the Soret and the long wavelength regions of Band III were distinctively uncharacteristic of Mb (not shown). The Soret band has a λ_{max} around 400 nm, as opposed to 408 nm for the freshly reconstituted PSwMb; another distinguishing anomaly is that the freshly reconstituted Band III with heme showed stronger Soret intensity than when it is equilibrated. The equilibrated reconstituted Band III was analyzed by ^1H NMR in the cyano form to determine its tertiary integrity. Unfortunately, because of the diluted concentration of the sample, partial denaturation, and/or exchange among various folding forms of the protein, no paramagnetically shifted peaks were observed, although the diamagnetic region suggested some extent of integrity (not shown). NMR is inherently a more sensitive technique than optical spectroscopy as to the detection of exchanging species

by line-broadening effect depending on the rate. Other work in this group on the observation of heme binding to renatured hemopexin (Deeb, 1993) showed similar discrepancy between the techniques, which implied that the rate constant determined optically for the reconstitution of modified-apoPSwMb may still be valid for comparison with the native PSwMb.

TABLE XIV
AMINO ACID ANALYSIS OF BAND III (FIGURE 91) AS COMPARED
TO THAT OF NATIVE PSwMb

Amino Acids	ApoPSwMb	Arg-mod ApoPSwMb
Asp	9	7
Thr	6	5
Ser	7	15
Glu	23	13
Gly	12	31
Ala	21	16
Val	7	6
Met	2	-
Ile	8	5
Leu	21	10
Tyr	3	-
Phe	6	-
His	15	5
Lys	23	11
Arg	3	-

ACKNOWLEDGEMENT

I wish to thank Professor Esther Breslow (Cornell Medical School) for the amino acid analyses work.

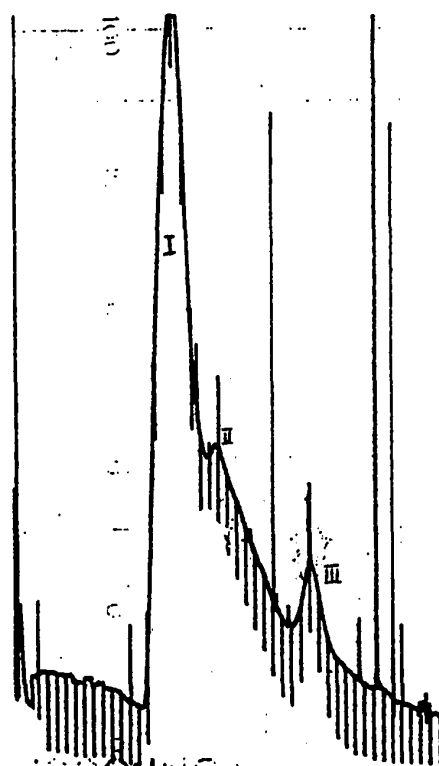


Figure 91. DEAE-Cellulose anion exchange chromatogram, expanded at 0.1 absorbance scale, of Arg-modified apoPSwMb, detected at 254 nm and 298 K on ISCO monitor, with pump speed set at 18. The buffer used was 50 mM Borate at pH 7.50. Salt gradient of 130 mL of 10 mM NaCl to 130 mL of 1 M NaCl was applied as soon as the sample was loaded. Bands are as labeled on the chromatogram. Bands I-III are reproducible among independent preparations, and Band III has been analysed to have no Arg left.

APPENDIX B

**PRELIMINARY STUDIES ON THE MYOGLOBIN AND HEMOGLOBIN OF
*BIOMPHALARIA GLABRATA***

APPENDIX

PRELIMINARY STUDIES ON THE MYOGLOBIN AND HEMOGLOBIN OF
BIOMPHALARIA GLABRATA

Preliminary ^1H NMR studies were performed on the polymeric extracellular Hb of a mollusca planorbidae -- *Biomphalaria glabrata* (Bg). To evaluate the compatibility of Bg with vertebrate, qualitative comparison of BgMb with EqMb was also established. Amino acid sequencing (Dayhoff, 1972) and X-ray crystallographic studies (Ingram, 1963) lend strong support to the postulate that all globins evolved from a common polypeptide ancestor, most possibly through a myoglobin-like precursor. There are reasons for studying invertebrate Hbs other than cost and availability. Human Hb variants usually show impairment of functional parameters ranging from reduced cooperativity to reduced Bohr effects; yet very rarely do we find total inhibition of the functions, which implies that all the functional parameters must be combinations of complex interactions of various binding sites, and they may be highly dependent on one another. Primitive species like the molluscs often have hemoglobins of high molecular weights with numerous interacting components. The idea that their development falls on the intermediate stage of the evolutionary track (Terwilliger, 1980) could be interpreted in the following way: their structures may be less complicated to study; and in the correlation of structures with functions, these primitive Hbs may reflect intermediate stage in the development of complex functional properties of HbA.

Hemoglobin exists as one of the two major extracellular respiratory proteins in molluscs; the other one being the copper-containing hemocyanin. The molecular weight of BgHb ranges from $1.7 - 2.0 \times 10^6$ Daltons (Figueiredo et al., 1973; Terwilliger & Terwilliger, 1977; Svedberg, 1933), and appear to be aggregates of ten 175-200 kDa subunits, each of which is circularly arranged, with a ring diameter of 200 Å (Terwilliger et

al., 1976). Because the planorbid Hbs were found to contain one heme per 15 - 17 kDa, each subunit must then consist of 10 - 12 oxygen binding domains (Figueirido et al., 1973).

The absence of pH dependence and cooperativity of the oxygen binding domains in the intact BgHb implies that none of the major components is sensitive to pH, which lead to the possibility that they lack the residues, possibly His, responsible for the famous Bohr effects. O₂-binding curves are strikingly similar between HbA and BgHb, with P₅₀ of ~ 0.68 (Figueirido et al., 1973). O₂-binding studies of a closely related planorbid Hb of *Helisoma trivolvis* revealed that the isolated multiples of Hb fragment bind oxygen reversibly like their intact Hb. None of the fragments displays evidence of cooperativity or a Bohr effect (Terwilliger et al., 1977), supporting the assertion of pH-independent subunits in BgHb. Merely a hindrance in the oxy-deoxy conformational transitions and lack of any significant pocket residue cannot account for this discrepancy. Rather, there must exist structural maneuvering of the amino acid residues around the individual binding sites upon aggregation. The unique quaternary structure of the planorbid Hbs has also triggered other interesting questions: (1) Planorbid Hbs have as high helical content as their vertebrate counterparts at 60 - 70% (Wood & Gullick, 1979); do their oxygen binding domains fold in a similar manner? (2) What is the linkage between the domains? (3) How are the domains arranged within each subunit? (4) Given that some conformational constraints must exist to favor against aggregation, is there any functional advantage to the polymeric structure of these Hbs?

Some of these questions can presumably be solved with better understanding of the oxygen binding site of the planorbid Hbs. To begin with, the monomeric and nonallosteric BgMb will be analyzed as a model for its more complicated Hb.

EXPERIMENTAL

Biomphalaria glabrata was donated by Dr. D.T Clark, from the Portland State University Biology Department. Myoglobin was isolated according Rossi-Bernardi & Chiancone (1981); while BgHb was isolated based on the methods in Terwilliger & Terwilliger (1977) with a few changes as follows. Polyethylene glycol (MW~8000) was used for the precipitation of BgHb, and separation of Hb from other hemolymphs was done on a 2 cm X 60 cm column of Sepharose CL-6B.

RESULTS

Qualitative Comparison Between MetBgMbN₃, MetBgMbCN, and the MetEqMb Counterparts.

Figure 92 compares ¹H NMR spectra of metBgMbN₃ with metEqMbN₃. The resolution of the protein diamagnetic envelope (not shown) and the well-resolved hyperfine-shifted peaks suggest the integrity of BgMb as a folded protein. There are a few striking differences between the two. The ratio of the major to minor heme-insertion isomers in metBgMbN₃ is lower than in metEqMbN₃, as evidenced by the relatively stronger intensities of the minor forms in the former (labeled by asterisks in the Figure). The possibility of the minor resonances arising from a second, weaker heme binding site is unlikely because the structure of BgMb should be similar to those of vertebrate Mbs, based on homology studies on a number of planorbic Mbs (Harris & Teller, 1973; Read, 1966). Another feature of metBgMbN₃ is the presence of four methyl peaks below 10 ppm, instead of three in metEqMbN₃ (marked by arrows in Figure 92). Assuming all four are heme methyls, the average methyl hyperfine shift is larger than in metEqMbN₃, suggesting either more high-spin character, or different magnetic axis. Given that both Mbs are in the azido forms, magnetic axis variance seems the likely candidate.

Furthermore, the absence of the broad upfield peak (present in metEqMbN₃) supports the postulate. Without sufficient material to map out the connectivities from 2D NOESY and COSY, no further information is inferred.

Qualitative Comparison of the Cyano Forms.

Figure 93 compares metEqMbCN with metBgMbCN. MetBgMbCN was prepared from metBgMbN₃, followed by the anion exchange chromatography to remove any denatured metBgMbN₃. Only one methyl peak was observed in the paramagnetic region. Variable temperature studies (Figure 93B-D) shows Curie behaviors for the upfield resonances, i.e. resonances are shifted towards the diamagnetic region at higher temperature, although not much movement was observed for the downfield methyl peak. If the metBgMbCN was intact, this disparity of the spread of methyl peaks from vertebrate metMbCNs, and deviation from the Curie behavior as compared to its EqMb (Satterlee, 1990a) counterpart dictate that a truly distinctive magnetic axis must present in metBgMbCN. This is consistent with the comparison of the azido forms in the previous section. Different magnetic axis has been found for the Mb of an invertebrate, *Aplysia limucina*, in which the absence of a distal His results in distinctive hypershift pattern of the heme peripheral and pocket residue protons (Rajaratnam et al., 1992). Nevertheless, preparation of a large amount of metBgMbCN and physical characterization to prove it has an intact native structure intact metBgMbCN is necessary before detailed investigation.

Investigation of MetBgHb in Various Ligated Forms.

Figure 94 presents metBgHb in various ligated forms. Two interesting features on this figure are the temperature and pH effects. At 298 K and neutral pH, when metBgHb is coordinated to H₂O (assuming the 6-coordinate aquo species), no visible peaks were observed (not shown); presumably because the Hb is sufficiently heterogeneous that the exchange among the species, on top of the large-size and the high-spin effects (i.e. broad

lines), produce extremely broad peaks that blend into the baseline. At pH 11.2, when a slightly stronger-field ligand, OH^- , predominates, a broad 'hump' is evident, suggesting that the heme subunits do coordinate to OH^- . As is apparent from Figure 94, more resolution, with the sharpest peaks in metBgHbCN, is observed when stronger-field ligands are employed at higher temperature, providing more evidence that the heme subunits in BgHb binds to all these ligands. Not shown in this figure is that metBgHbCN at neutral pH and 298 K does not exhibit the same features as in Figure 95C, implying that deprotonation of the protein plays a role in breaking the bridging between the subunits. The breakage of the inter-subunit bridge causes a decrease in size of the protein, and possibly eliminate some exchanging species, both of which would help resolve the peaks.

Future Prospects

Although results presented here are preliminary, they are sufficient to demonstrate the utility of solution state ^1H NMR on macromolecules of such large size. Analysis of the individual subunits is the next logical step in order to understand the change(s) involved in the aggregation process. Subtilisin has been shown to be effective in cleaving of the intact BgHb into its individual subunits (Terwilliger et al., 1977). Also, because of the suggestion of the unusual magnetic axis in BgMb, comprehensive assignments of metBgMbH₂O and metBgMbCN could provide additional parameters for understanding paramagnetic NMR of heme proteins.

ACKNOWLEDGEMENTS

I am most thankful to Professor David Clark (Portland State University Biology Department) for the supply of *Biomphalaria Glabrata*, Sepharose CL-6B, glassware, literature references, and helpful discussion.

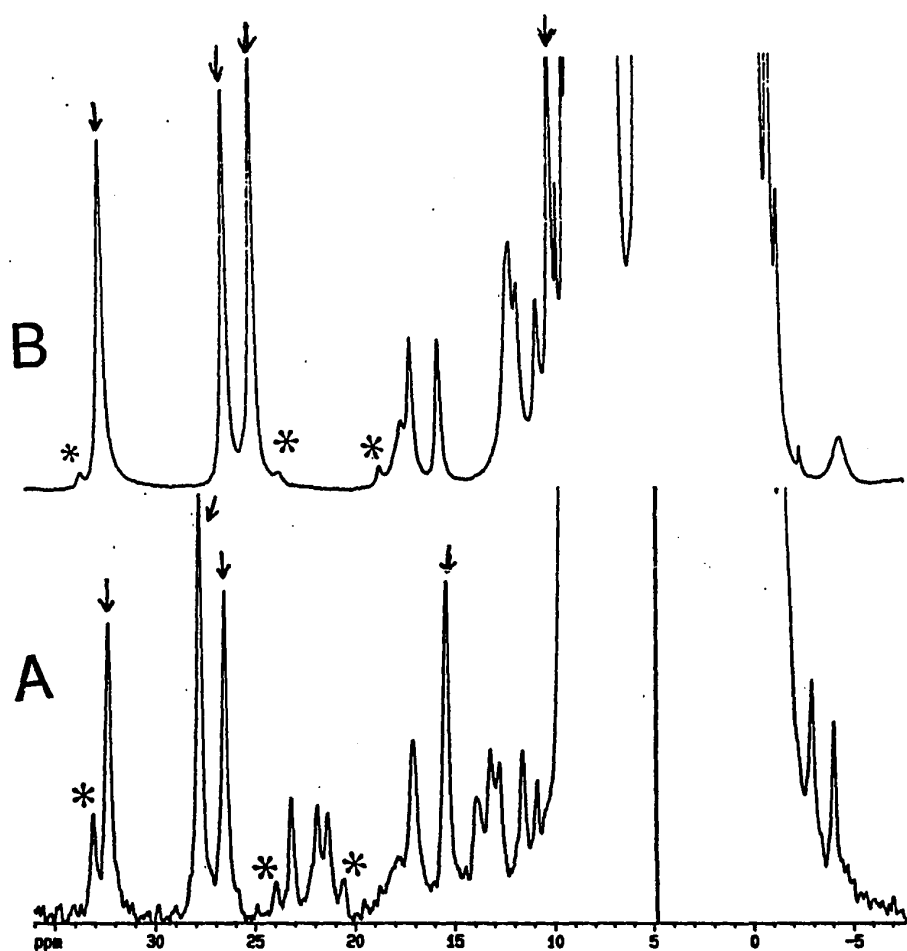


Figure 92. ^1H NMR spectral comparison of metBgMbN₃ at pH 7.5 (A) with metEqMbN₃ (B) at pH 7.0 and 298 K. Asterisks label the minor heme-insertion isomers; while arrows mark the heme methyls.

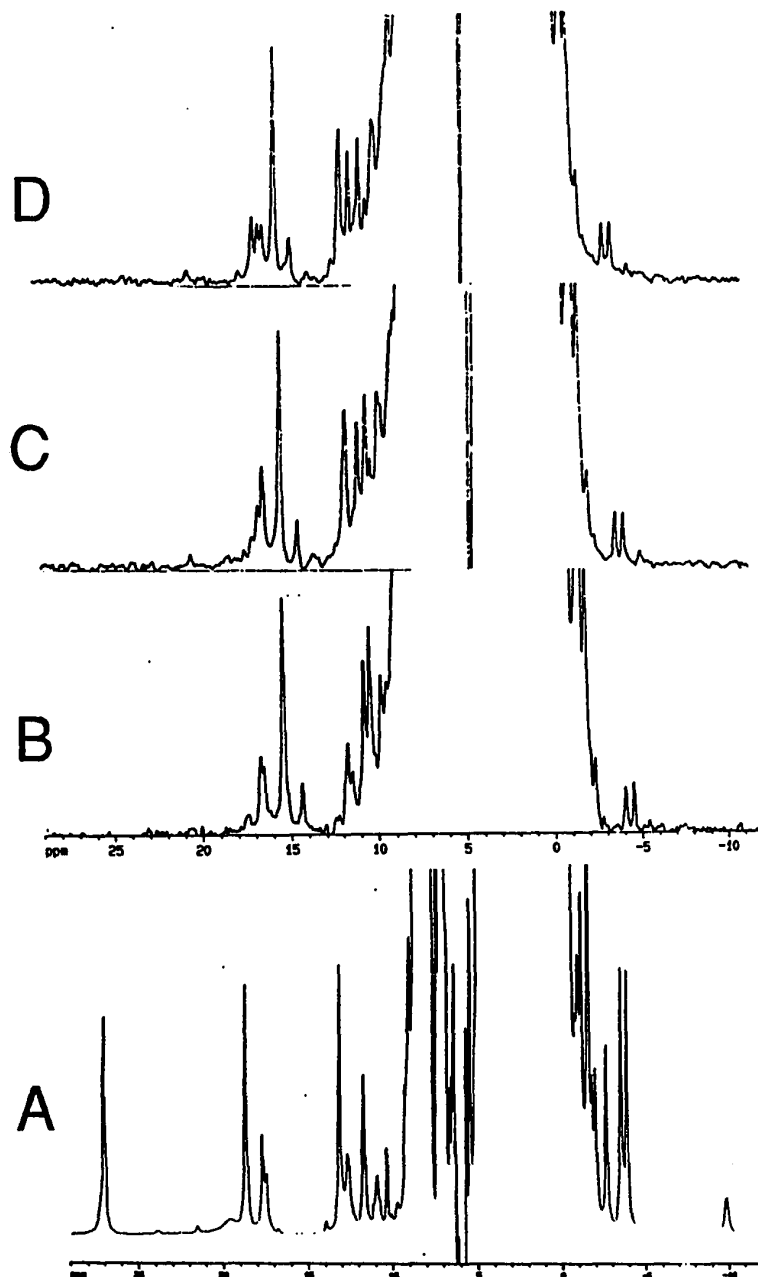


Figure 93. ^1H NMR spectral comparison of metEqMbCN at pH 9 (A) with metBgMbCN (B) at 298 K and pH 8.1. C-D. Variable temperature spectra of metBgMbCN at pH 8.1 and 303 K, and 308 K, respectively.

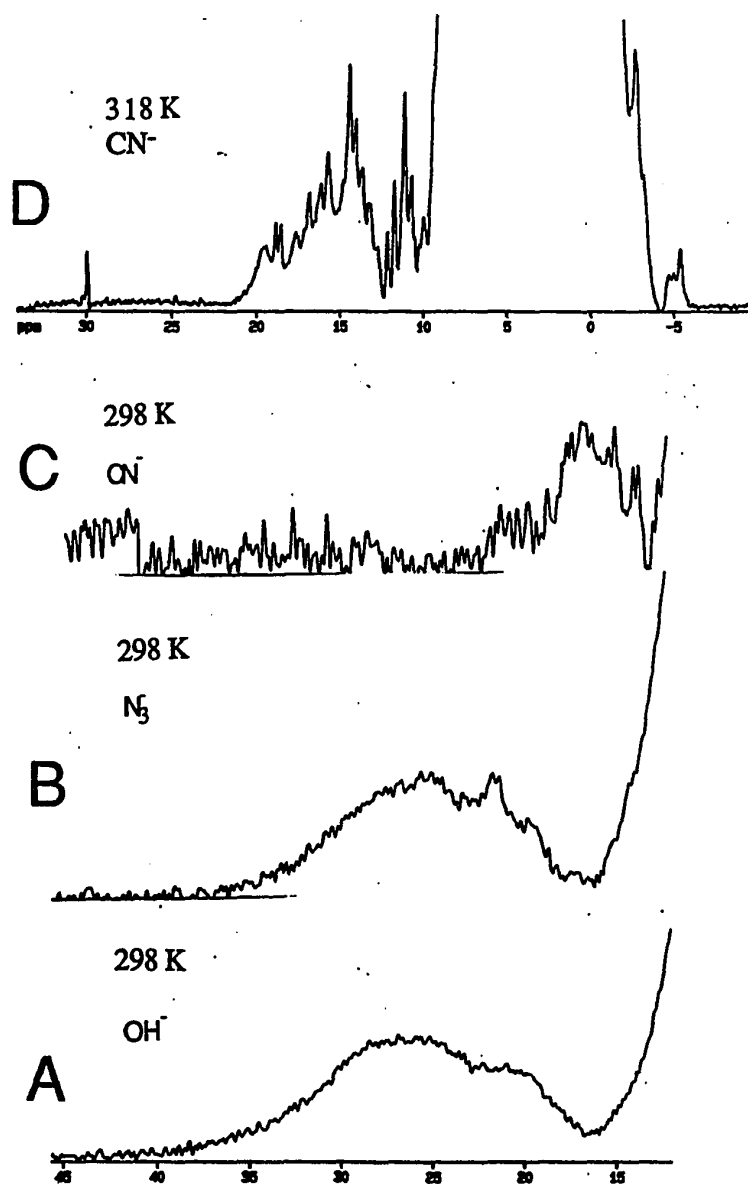


Figure 94. ^1H NMR spectra of metBgHb in various ligated states and temperatures at pH 11.20, as indicated on respective traces.